Ignition systems for lean-burn gas engines

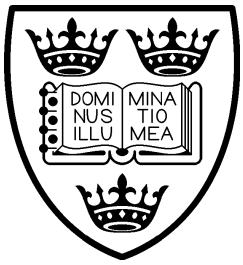

Nicholas C. Pashley
Exeter College
Oxford

A thesis submitted to the University of Oxford for the degree of Doctor of Philosophy

Department of Engineering Science
University of Oxford

Michaelmas Term 1997

Declaration

No portion of the work referred to in this thesis has been submitted in support of an application for another degree or qualification in this or any other institution of learning.

Ignition systems for lean-burn gas engines

Nicholas C Pashley **British Gas Research Scholar**
Department of Engineering Science **Exeter College Oxford**

A thesis submitted in partial fulfilment of the requirements of the Degree of Doctor of Philosophy at the University of Oxford, Michaelmas term 1997.

Abstract

This thesis describes an experimental investigation into ignition systems, their effects on the combustion process, and how the discharge is affected by the prevailing pressure, temperature and flow. The work is divided into four main areas, a comprehensive literature review, engine testing for ignition system suitability, non-flow rig testing (including erosion) and flow rig testing.

The literature review concluded that the most practical ignition system for lean burn gas engines will continue to be based on the spark plug, but in the medium to long term, laser ignition may become viable.

The measurement of the HT voltage and current is not straightforward, and appropriate methods have been identified.

Capacitive and inductive ignition system types were compared in lean and diluted conditions on a single cylinder research engine of modern design at different engine loads and speeds. It was found that the most beneficial ignition system was an inductive ignition system, although that for some conditions, capacitive systems induced better engine performance with a fraction of the stored energy of the inductive alternative.

Non flow tests showed that the early part of the spark discharge is sensitive to pressure and temperature effects, and as a consequence, the latter stages of the discharge are also affected. A correlation has been developed, for use with conventional nickel electrode spark plugs, to predict breakdown voltage as a function of pressure, temperature and gap.

Experiments were carried out at elevated pressures in a stream of flowing air with capacitive and inductive ignition systems. Different electrode designs and orientations were also compared. It was shown that when exposed to a flow field, the discharge can be stretched which results in a shortened spark duration; in some cases the electrode can shield the discharge from flow field effects.

This work showed that flow through the spark gap is a hindrance to the spark process, especially for longer duration systems. However for flame kernel growth, the literature review identified that flow is beneficial, serving to convect the kernel away from the electrodes, reducing the heat transfer from the flame.

Analysis of the glow voltage history in the pressurised flow rig has been used to develop a correlation relating the voltage, current, flow velocity, pressure and time. This correlation was used to analyse the velocity records from the spark plug in a firing engine. The predicted velocities and turbulence intensity were in agreement with independent measurements.

Acknowledgements

I would like to thank BG Plc (formerly British Gas R and T) for the generous financial support over the last three years and three months, and also my Industrial Supervisors, of whom there were many; Dr Rachel Palmer (now at Enerco NZ), Mehdi Daragheh (now at Perkins Technology), Dr Shang-you Duan (now at Rover), Dr Kay Kerbyson (now at Rover), John Parsons and Graham Roberts.

I would like to express my gratitude to my supervisor, Dr Richard Stone, for invaluable advice, guidance and encouragement throughout this study, and also my father for steering me into this area and proof reading the manuscript.

This work has also been enhanced as a consequence of discussions with Dr Peter Howson and Mr Simon Walters (University of Brighton), regarding the electrical aspects of ignition, and Mr David Latham (Champion Spark Plugs), who also helped with the provision of spark plug and ignition coil samples.

I must express gratitude to Major Jeff Ball (USAF) who had the misfortune to share an office with me for the final two years of this work, and provided the benefit of a fighter pilot's perspective to life and work. Thanks also to the departmental Electronics Workshop, and to Doug Hamilton, for help with electrical and electronic problems throughout the project, and to the Maintenance Workshop for making things happen in the lab.

I am indebted to the following people for making life in the department generally more bearable; Chris Waddup, John Hastings, Ken Howson, Maurice Keble-Smith, John Gills, Toby Miller, John Barton, Ken Dunford, Harry (CWP) Fearnley, Geoff Jones, Don Hollaway, Karl Smith, Richard Duffin, Brian Busby, Heather Burrage and Dominic Harris.

A big mention to all my friends at Oxford University Cycling Club; Jim Henderson, Digby Symons, Steve Morse, Jony Hudson, Veit Schenk and more, the naming of whom would send this thesis over the page limit.

Thanks also to Dr Brenda Allen for her help, encouragement and general good company

Nomenclature

ABDC	After bottom dead centre
AC	Alternating current
AFR	Air-fuel ratio
ATDC	After top dead centre
BBDC	Before bottom dead centre
BDC	Bottom dead centre
BMEP	Brake mean effective pressure
BTDC	Before top dead centre
BDV	Breakdown voltage
CDI	Capacitor discharge ignition
CHP	Combined heat and power
CI	Coil ignition
CNG	Compressed natural gas
DSO	Digital storage oscilloscope
DC	Direct current
E	Electric field strength
ECU	Electronic control unit
EGR	Exhaust gas recirculation
EMI	Electromagnetic interference
FID	Flame ionisation detector
HC	Hydrocarbon
I	Current
IMEP	Indicated mean effective pressure
LDA	Laser doppler anemometry
LED	Light emitting diode
LML	Lean mixture limit
LPG	Liquefied petroleum gas
LT	Low tension
MABT	Minimum advance for best torque
MBT	Maximum brake torque
P	Pressure
PIV	Particle image velocimetry
R	Resistance
RFI	Radio frequency interference
RPM	Revolutions per minute (engine rotational speed)

SI	Spark ignition
T	Temperature
t	Time
TCI	Transistorised coil ignition
TDC	Top dead centre
V	Voltage
VRA	Voltage rise anemometry
°	Degrees crank angle
λ	Excess air ratio (non dimensional air-fuel ratio
κ	Ratio of specific heats

Contents

DECLARATION 2
ABSTRACT 3
ACKNOWLEDGEMENTS 4
NOMENCLATURE 5
CONTENTS 7

1. INTRODUCTION AND REVIEW OF RELEVANT LITERATURE 11

1.1 INTRODUCTION 11
1.2 REVIEW OF IGNITION MECHANISMS 11
1.3 AUTOIGNITION 13
1.4 OPEN FLAME 15
1.5 SURFACE IGNITION METHODS 16
1.5.1 Hot tube 16
1.5.2 Glow plug 16
1.6 PILOT FUEL 17
1.7 RAPID COMPRESSION MACHINE 18
1.8 CATALYTIC IGNITION 18
1.9 BULK PLASMA GENERATION 19
1.9.1 Thermodynamic expansion methods - Pulsed plasma jets 19
1.9.2 Electromagnetic plasma injection - Rail methods 21
1.10 LASER BASED TECHNIQUES 23
1.11 SPARKING PLUGS 24
1.11.1 History 24
1.11.2 Construction 24
1.12 ALTERNATIVE SPARK IGNITION STRATEGIES 25
1.12.1 Pre-chamber spark plug methods 25
1.12.2 Puff-jet methods 26
1.13 CONCLUSIONS 26

2. SPARKING PLUG IGNITION TYPES 27

2.1 TREMBLER COIL 27
2.2 MAGNETO 27
2.3 COIL AND BATTERY IGNITION (KETTERING) 28
2.4 TRANSISTORISED COIL IGNITION (TCI) 30
2.5 CAPACITOR DISCHARGE IGNITION (CDI) 31
2.6 BREAKDOWN SYSTEMS (VFZ) 34
2.7 BRIGHTON PHOTOCONDUCTIVE SWITCH IGNITION SYSTEM 35
2.7.1 LED activated photoconductive switch circuit 36
2.7.2 Xenon flash switched circuit 36
2.8 COIL DESIGN 37
2.9 SPARKING PLUGS 40
2.9.1 Heat range 40
2.9.2 Electrode material and type 41
2.9.3 Spark plug fouling and methods of reduction 44
2.9.4 Wear mechanisms 46
2.10 IGNITION SYSTEM AND SPARK PLUG EFFICIENCY 49
2.11 SPARK PLUGS AS DIAGNOSTIC INSTRUMENTS 52
2.12 ELECTRICAL CHARACTERISTICS OF ARCS 54
2.12.1 Pre-breakdown mode 55
2.12.2 Breakdown mode 56
2.12.3 Arc discharge mode 57
2.12.4 Glow discharge mode 57
2.12.5 Voltage drops across the gap in the Arc and Glow discharge regimes 57
2.13 THE IGNITION PROCESS 59
2.13.1 Flow field effects 59

2.13.2 Heat transfer effects *63*
2.13.3 Effects of ignition power *63*
2.13.4 Effects of spark duration *64*
2.13.5 Multiple ignition sources *67*
2.13.6 Ignition process enhancement *68*
2.14 CHAPTER SUMMARY 69

3. CORE APPARATUS AND MEASUREMENT PROCEDURES 72

3.1 CORE APPARATUS 72
3.1.1 Lucas AB13 transistorised coil ignition system *72*
3.1.2 Oxford Capacitor Discharge Ignition System *72*
3.1.3 Bosch TCI system *73*
3.1.4 Digital storage oscilloscope *74*
3.2 VOLTAGE MEASUREMENT 74
3.2.1 Apparatus and utilisation *74*
3.2.2 Effects of plug to voltage divider lead length *75*
3.2.3 Justification of use *76*
3.3 CURRENT MEASUREMENT 77
3.3.2 Experimental apparatus *78*
3.3.3 Method of investigation *80*
3.3.4 Discussion of results *80*
3.3.5 Positioning for current measurement *83*
3.3.6 Conclusions *84*
3.4 DATA POST-PROCESSING 89
3.4.1 Waveform smoothing *89*
3.4.2 Waveform differentiation *90*
3.4.3 Application to acquired data *90*

4. ENGINE TESTING 95

4.1 EXPERIMENTAL APPARATUS 95
4.2 METHOD OF INVESTIGATION 99
4.2.1 Combustion analysis *100*
4.2.2 Influence of atmospheric conditions *100*
4.2.3 Energy storage *101*
4.2.4 Calculation of stored energy *101*
4.2.5 Producing the spark *101*
4.3 DISCUSSION OF RESULTS 102
4.3.1 Effects of reduction in energy (test site 1) *102*
4.3.2 Effects of different ignition transformer (test site 1) *102*
4.3.3 Effects of higher engine speeds (test site 2) *103*
4.3.4 Effects of higher IMEPs (test site 3) *104*
4.3.5 Effects of EGR (test site 3) *104*
4.4 GENERAL DISCUSSION 104
4.5 CHAPTER CONCLUSIONS 105

5. NON-FLOW RIG TESTING 120

5.1 HEATED PRESSURE VESSEL TESTING 120
5.2 RESULTS 121
5.2.1 Effects of increasing the pressure and temperature on the breakdown process *121*
5.2.2 Effects of increasing electrode gap on the breakdown process *122*
5.2.3 Effects of increasing the pressure and temperature on the glow discharge *122*
5.2.4 The validity of Paschen's Law *122*
5.2.5 A linear fit for voltage prediction *123*
5.3 HEATED RIG SUMMARY 123
5.4 EROSION TESTING 130
5.4.1 Introduction *130*
5.4.2 Required breakdown voltage *130*
5.4.3 Loss of electrode mass *130*

5.4.4 Electrode gap growth *131*
5.4.5 Method of investigation *131*
5.5 DISCUSSION 134
5.6 EROSION SUMMARY 134

6. FLOW RIG TESTING 137

6.1 APPARATUS 137
6.1.1 Blockage caused by spark plug protrusion *138*
6.2 THE EFFECTS OF FLOW ON AN ELECTRICAL DISCHARGE 139
6.2.1 Factors to consider *139*
6.3 FLOW EFFECTS ON AN INDUCTIVE IGNITION SYSTEM 139
6.4 FLOW EFFECTS ON A CAPACITIVE IGNITION SYSTEM 140
6.5 EFFECTS OF ELECTRODE TYPE AND ORIENTATION ON INDUCTIVE IGNITION PERFORMANCE 140
6.5.1 J type electrode *140*
6.5.2 Double electrode *140*
6.5.3 Triple electrode *141*
6.5.4 Surface discharge *142*
6.6 CONCLUSIONS 142
6.7 FLOW VELOCITY DETERMINATION 147
6.8 COLUMN FIELD SENSITIVITY 149
6.8.1 Column field strength as function of measuring time and current for a conventional coil ignition system *149*
6.8.2 Column strength as a function of pressure *149*
6.8.3 Column strength as a function of temperature *150*
6.8.4 The calculation of column field strength at any point in a discharge *150*
6.8.5 The graphical user interface (GUI) for data analysis *150*
6.8.6 Curve fitting *150*
6.9 ESTIMATES OF THE FLOW VELOCITY IN THE PRESSURISED FLOW RIG FOR THE GLOW VOLTAGE 152
6.10 APPLICATION TO ENGINE MEASUREMENTS 153
6.11 CONCLUSIONS 153

7. CONCLUSIONS AND RECOMMENDATIONS FOR FURTHER WORK 163

7.1 REVIEW OF GOALS 163
7.1.1 Ignitability experiments *163*
7.1.2 Erosion Experiments *163*
7.1.3 Flow rig testing *163*
7.1.4 Effects of ambient conditions upon the spark discharge process *164*
7.2 SUGGESTIONS FOR FURTHER WORK 165
7.2.1 Erosion testing *165*
7.2.2 Engine testing - Electrode orientation and electrode type *165*
7.2.3 Further velocity predictions in a running engine *165*

8. REFERENCES AND BIBLIOGRAPHY 166

APPENDIX A EQUIVALENT CIRCUIT FOR AUTOMOTIVE IGNITION SYSTEM 179

APPENDIX B CURRENT MEASURING SYSTEM SPECIFICATIONS 180

APPENDIX C IGNITION SYSTEM SPECIFICATIONS 181

ENGINE TESTING 181
RIG TESTING 181
TCI system 181
CDI system 123

APPENDIX D ADDITIONAL RESULTS WITH DISCUSSION (CHAPTER 3) 184

APPENDIX E CD IGNITION SOURCES 198

APPENDIX F COILS USED FOR EXPERIMENTS 199

APPENDIX G PIN CONNECTIONS FOR IGNITION SYSTEMS USED 200

APPENDIX H FUEL INJECTOR TECHNICAL NOTE 202

APPENDIX I INSTRUMENTATION FOR AIRFLOW METER 213

APPENDIX J CALCULATIONS FOR AIR-FUEL RATIO 215

APPENDIX K EQUIVALENT ELECTRODE GAPS FOR NON J ELECTRODE PLUGS 224

APPENDIX L CALCULATION OF AIR VELOCITY FOR FLOW RIG EXPERIMENTS ...226

APPENDIX M THREE TERM LEAST SQUARES FITTING 227

1. Introduction and review of relevant literature

1.1 Introduction

Original Aims
Gas engine development at the British Gas Research and Technology centre had highlighted three areas concerning ignition where knowledge should be stronger.
Ignition system suitability to Natural Gas Vehicles
There are two main types of natural gas vehicle, those with converted gasoline engines and those with converted diesel engines. In the past, converted gasoline engines have retained the original ignition system, but was this the optimal system ? Converted diesel engines required the selection of a system, and capacitor discharge or high energy inductive systems had been used as alternatives with no science behind the selection.
Reduction of electrode erosion
Gas engines, developed from compression ignition engines, are increasingly being used for stationary power generation, often in co-generation applications. Advantages over diesel engines include a lower cost of fuel and a piped supply. The gas engine's weak point, however, is spark plug erosion. In a car, spark plugs may last 10,000 miles, but this equates to only around 200 hours, or 8 days use. In addition to the downtime of equipment, the cost of the technician to change the plugs is incurred, normally charged by the hour, perhaps with a callout fee.
Investigation into the interaction of flow with the spark
As mentioned previously, a proportion of gas engines are developed from heavy duty diesel engines. Diesel engine combustion systems are normally designed to use 'swirl' to improve mixing and combustion. This mechanism of high velocity can disrupt the arc and result in a shortened spark duration which can decrease ignition reliability. This leads to the possibility of using the discharge of an inductive ignition system as an indication of the flow regime and indeed whether the spark plug is in the appropriate location.

1.2 Review of ignition mechanisms

To induce a self sustaining oxidation process there must be enough energy input to cause chain initiation reactions, and the release of radicals to start chain propagation reactions. Ignition is the transition from a non-reactive state to a reactive one by external stimuli. This is normally done using a heat source which results in the formation of highly reactive radicals in areas of high local dissociation.
The magnitude of ignition energy is a minimum at around stoichiometric conditions for methane and rises sharply as the mixture becomes richer or leaner, as shown in Figure 1.1.

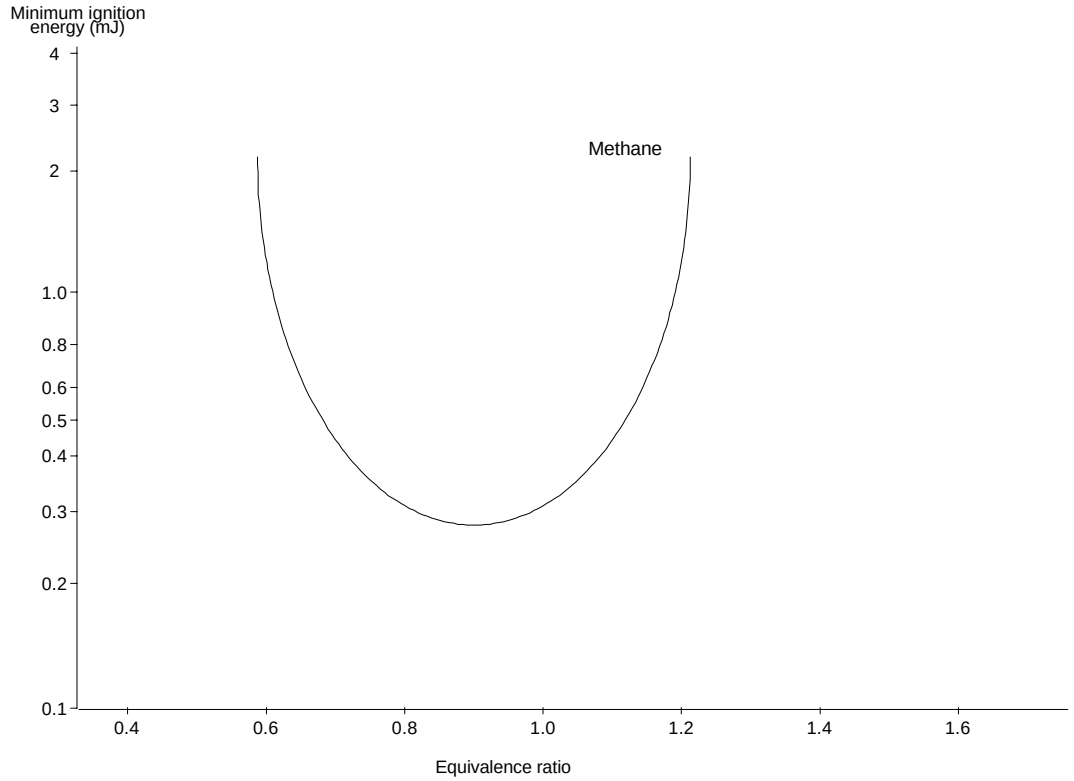

Figure 1.1 Minimum ignition energy of methane against fuel-air equivalence ratio (Adapted from Lewis and Von Elbe 1951)

Once combustion has been initiated flame propagation will only occur if the mixture is between the flammability limits, if the mixture is too lean or too rich the flame will be quenched since energy is wasted heating oxidants or fuel which are merely spectators. This will result in rapid termination of the combustion process. The general rule for flame propagation is that the energy released by the combustion process must be greater than that transferred to the surroundings.

For ignition to occur, the three T rule (Kuo 1986) must apply to the conditions:

Temperature	Must be high enough to form highly reactive radicals
Time	Must have enough residence time for the fuel-oxidant mixture to reach the desired temperature
Turbulence	Must be high enough to allow good mixing between fuel and oxidant and allow good heat transfer between reacted and unreacted medium

The above list is far from complete and must include other parameters such as mixture strength, pressure and combustion chamber shape.

Three types of external stimuli exist (Kuo 1986):

Thermal energy stimuli	Heat transfer to the reactants by conduction or convection or a combination thereof.
Chemical stimuli	Introduction of reactive agents or catalysts.
Mechanical stimuli	Mechanical impact, friction or shock waves - these stimuli result in thermal sources.

Review of igniter types with reference to IC engines To enable work to be done, on the expansion stroke, in a two-stroke or four-stroke cycle, fuel must be burned to give a rise in

pressure. Ignition is needed to initiate the combustion process, Figure 1.2 shows a taxonomy of IC engine ignition systems.

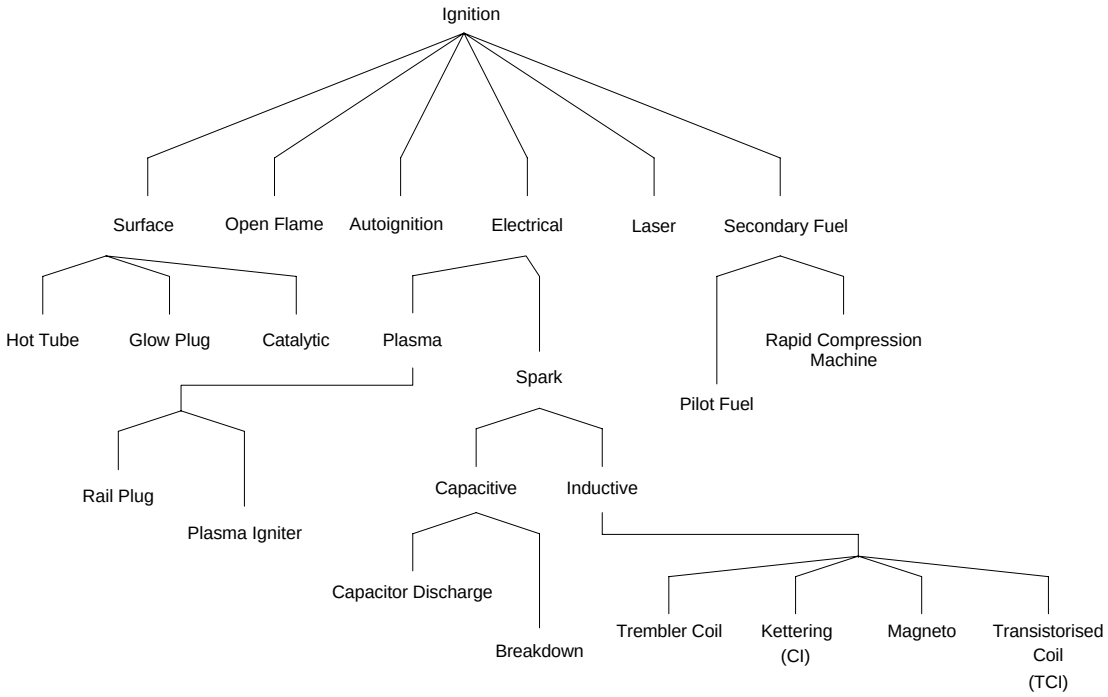

Figure 1.2 IC engine ignition taxonomy

1.3 Autoignition

Diesel engines exploit fuel autoignition for initiation of the initial flame kernels. The compression ratio required to allow ignition to take place is between 12 and 24:1 and is usually determined according to cold start requirements (Stone 1992). Air is drawn into the cylinder on the induction stroke and compressed on the compression stroke. During compression, fuel is atomised and injected into the combustion chamber at high velocity. Portions of the mixture then spontaneously combust because the mixture temperature and pressure are above the ignition temperature of the fuel-air mixture. As rapid mixing occurs, flame fronts propagate and the fuel is eventually consumed. Knock, as associated with spark ignition engines, does not occur with diesel engines since the fuel-air mixture is stratified, and there is essentially no end gas which can be heated by the cylinder walls for the necessary residence time. Ignition timing is controlled by the fuel injection timing, in-cylinder conditions and the fuel *cetane number*.

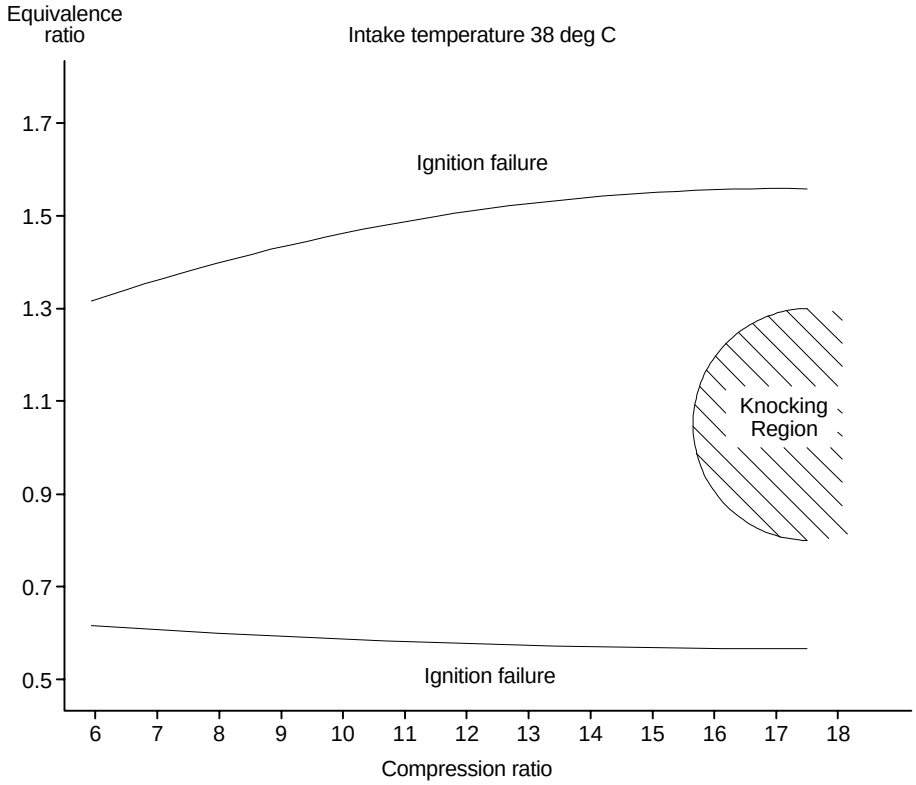

Figure 1.3 Ignition behaviour of methane preheated to 38°C (Karim 1983)

If the compression ratio is high enough, in a premixed charge engine, and the mixture composition is favourable then knocking will occur, this is induced by the wall temperature adding energy to the end gas. Knock is a product of uncontrollable autoignition in a spark ignition engine. End gases in the cylinder are heated, by a combination of the cylinder wall and the pressure rise due to the expanding flame front, for the necessary residence time, for spontaneous combustion to occur. The knocking noise is the result of intense pressure waves in the charge which force the cylinder walls to vibrate and thus communicate the sound to the atmosphere (Taylor 1985). Knock, or *detonation*, can erode the combustion chamber and piston crown due to the very high local temperatures. Knock is a performance constraint restricting the maximum cylinder pressure and ignition timing advance.
Karim (1983) argues that it is possible for methane-air mixtures to be self-ignited in a controlled way. When the inlet temperature is increased, it is not necessarily the end gas which is ignited first, so provided the compression ratio is between certain limits and the mixture strength is lean of stoichiometric, a controlled autoignition mechanism may be exploited. The in-coming charge temperature being similar to, if not higher than, the cylinder wall temperature results in no energy being transferred to the end gas, and hence a vastly reduced chance of knock occurring.

As the compression ratio is increased further or the mixture is enriched, knocking can be seen to occur as well as the controlled ignition. As can be seen from Figure 1.3 and Figure 1.4, a homogenous methane-air mixture will only auto-ignite controllably when the charge is preheated to over 150°C. Even with this aid, control is difficult due to the narrow range between knock and ignition failure. Because of this, all practical applications of methane as a fuel require an auxiliary ignition source.

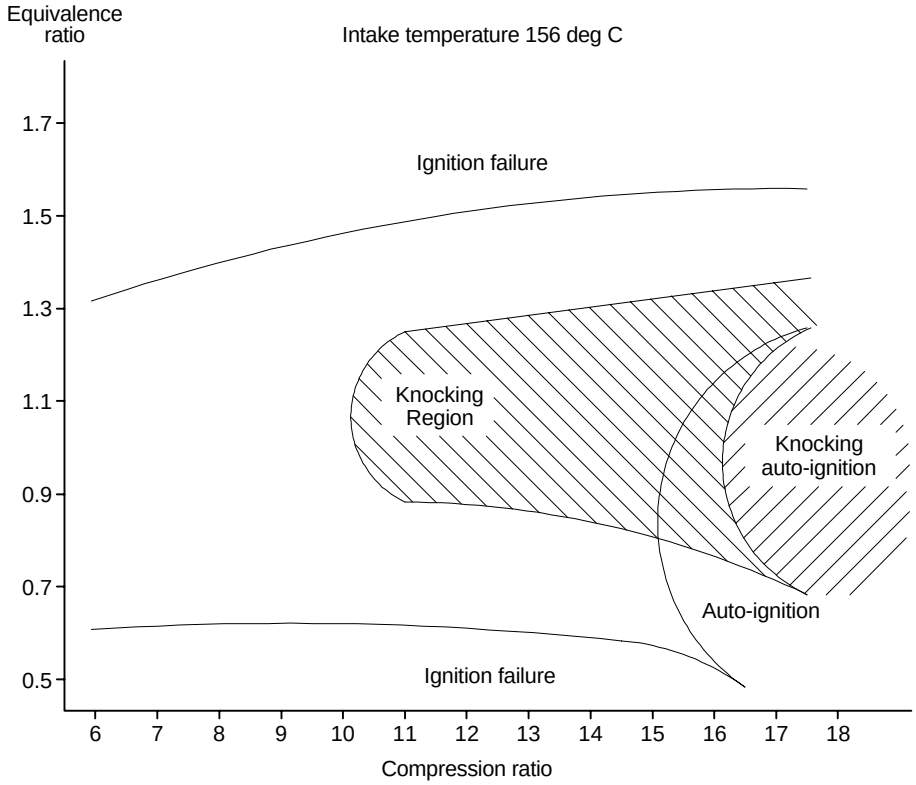

Figure 1.4 Ignition behaviour of methane preheated to 156°C (Karim 1983)

1.4 Open flame

Ignition by open flame was first implemented in 1838 by William Barnett, an early gas engineer (Kennedy 1913).

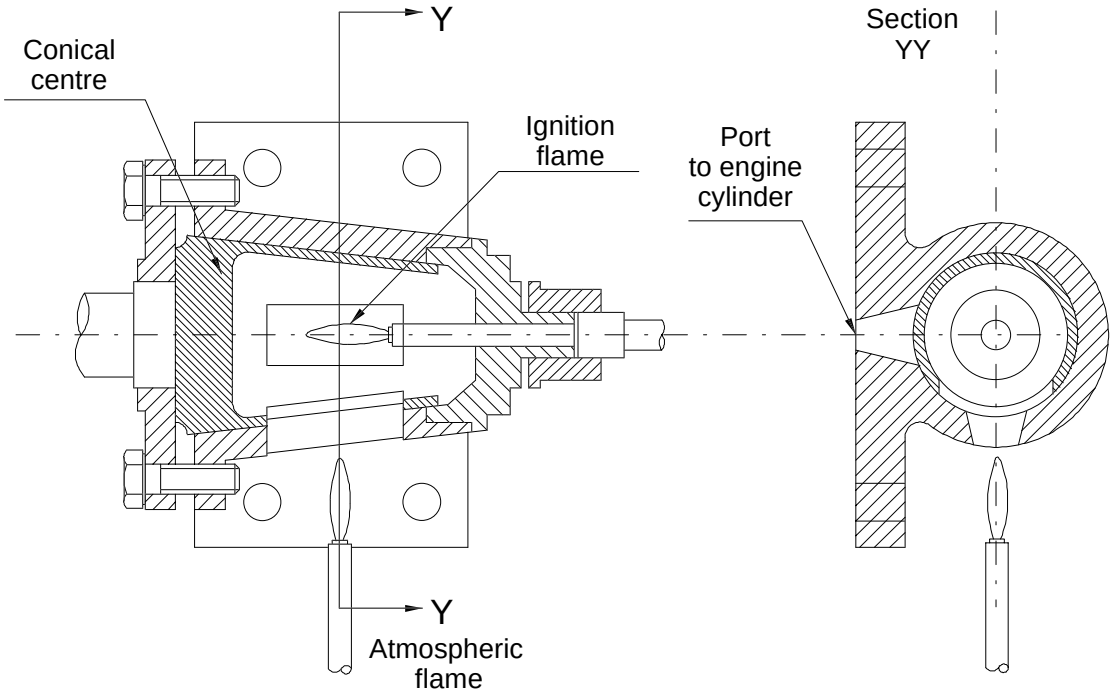

Figure 1.5 The flame cock method of ignition used by William Barnett

The flame was drawn into the cylinder by means of a cock key or rotary valve which is shown in Figure 1.5. The cock had a single port in the rotating conical centre section and two ports in an outer casting, one leading to a continuously burning atmospheric flame, the other to the engine combustion chamber.
A set of gears would drive the rotating centre. The ignition flame inside the conical centre was re-lit each cycle by the external atmospheric flame on port opening. The ignition flame then ignited the charge in the combustion chamber at the desired time when the cock was rotated to open into the combustion chamber. The Otto and Langen atmospheric engines also used an open flame method of ignition in approximately 1880, but with a sliding valve arrangement. This method of ignition was restricted to engines with little or no compression running at very slow speeds (Lichty 1967).

1.5 Surface ignition methods

1.5.1 Hot tube

In 1843, Alfred Drake from Philadelphia, USA, used a glowing tube as a source of ignition (Day 1980). The hot tube became a useful ignition source after the open flame system had been abandoned. The tube was manufactured from a ceramic or a precious metal after it was found that iron was unsuitable due to thermal fatigue. It was passed through the cylinder wall and heated till red hot from the outside of the engine by a petrol or gas flame for starting purposes. The ignition timing was then varied by altering the position of the external flame, thereby changing the temperature profile of the tube. Daimler adopted this ignition source in 1887 for use with their engines (Setright 1988), but changed to magneto systems in 1899 (Amann 1990). The idea was developed further by using valves to control the exposure of the internal hot surface. Although this was an improvement in operation, the valves were a source of unreliability and the concept was discarded in favour of other methods.
Hot-tube ignition is only satisfactory for a limited speed and load range. Furthermore, the surface ignition of gaseous fuels relied on the presence of hydrogen: methane is not susceptible to surface ignition.

1.5.2 Glow plug

Glow plugs are used to induce surface ignition. They are commonly used in very small two-stroke engines fitted to model aircraft. The plug is initially electrically heated to a temperature which will induce autoignition of the fuel. After starting, the temperatures induced by the combustion processes will then allow the plug to be maintained at a sufficient temperature to auto-ignite the fuel with no further electrical input. The type of fuel used is critical as it has to allow controlled ignition at the glow plug temperature. The ignition timing is controlled by the plug temperature, but this cannot be readily controlled under engine operation. Reducing the thermal path, and hence the heat transfer from the plug to the cylinder head would result in a more advanced timing. Glow plugs are normally made from a precious metal such as platinum, so as to exploit catalytic ignition.
A extension to the glow plug method is to combine it with a timed fuel injection system. Fuels which were normally associated with spark ignition engines can be used in a glow plug assisted compression ignition engine. The glow plug is heated to a constant temperature, the fuel is injected in a stratified manner and ignites after the required residence time. In this mode, the system is able to work with a controllable ignition timing, and an adaptive controller could be used to alter the time of injection to suit the residence time, speed and load.

1.6 Pilot fuel

Pilot fuel ignition can be traced back to the start of the century, being used in dual fuel engines. This type of engine is essentially a diesel engine fitted with a carburettor or mixer, for the introduction of a secondary fuel; as with a diesel, the engine remains unthrottled. The secondary fuel is usually a fluctuating supply of methane or natural gas providing a cheap source of energy. Methane or natural gases are ideal fuels for use in a dual fuel engine, because of their high knock resistance and tolerance to high compression ratios (which are needed to ignite the pilot fuel). The engine can run predominantly on gas, or wholly on diesel when the gas supply diminishes. The type of engines exploiting this technology are mainly stationary, but vehicular use is common in some parts of the world.

This powerful and voluminous ignition source is suited to lean homogeneous mixtures. The low flame speed of methane is improved by the large ignition energy, the multiplicity of ignition sites and the high compression ratio. A reduction in cyclic variation resulting in smoother combustion is also noted when using this ignition method, caused by the averaging effect of many ignition sites.

The gaseous fuel is introduced using a simple carburettor or in certain circumstances is injected directly into the induction manifold. Control systems are more complicated than either a spark ignition or compression ignition engine, which means higher capital and operational costs.

Pilot ignition engines suffer from poor light load performance and idling, due to an increase in the delay angle of the charge with very little gaseous fuel addition, this phenomenon is shown in Figure 1.6. The delay angle then reduces with the addition of further fuel. This effect is believed to be a consequence of the pilot fuel and gas competing for radicals (Karim 1983). Increasing the amount of gas admitted generates significant amounts of energy which aids ignition and reduces ignition delay. Light load running also results in substantial concentrations of unreacted gaseous fuel and carbon monoxide in the exhaust, when in-cylinder temperatures are inadequate to induce full oxidation of the very lean gaseous fuel mixture. It is also postulated that the flame fronts initiated by the sprays do not reach all parts of the combustion chamber. This can itself result in increased unburned hydrocarbon emissions compared to both a diesel or spark ignition gas engine.

When running at higher loads the pilot fuelled gas engine can be seen to be more efficient than the full diesel equivalent, and the oxides of nitrogen emission levels are also reduced. They can be reduced further by reducing the amount of pilot fuel injected which also influences the engine efficiency and performance, and can be cut to a very small amount at high load (indeed below the quantity of fuel required to enable the engine to idle as a diesel).

Lower peak cylinder pressures occur when using a dual fuel engine compared to that of a purely diesel fuelled alternative, but knock can be a problem when very high power outputs are required, or where high inlet temperatures or large bore cylinders are used.

Performance can be seen to suffer when gaseous fuels containing inert gases are used, although the oxides of nitrogen are substantially reduced and the effective octane number of the mixture is increased.

Pilot ignition engines are reliable, since there is no electrical ignition system which is likely to cause problems. The reliability of diesel engines applies to dual fuel engines, with the bonus of cleaner oil due to the gaseous nature of the major fuel; this leads to fewer oil and filter changes. The characteristic diesel smoke is eliminated and injector fouling is reduced (Karim 1983).

The attraction of using a pilot injection system instead of a full diesel engine is purely economic, since the cost of natural gas is lower than the pilot fuel and has a far greater availability.

The main drawback with this method of ignition is in the pilot fuel itself, the engine requiring two types of fuel which results in increased complexity and an increase in weight, which is a drawback for vehicle applications, although it can give a good drive-home facility on an empty CNG tank.

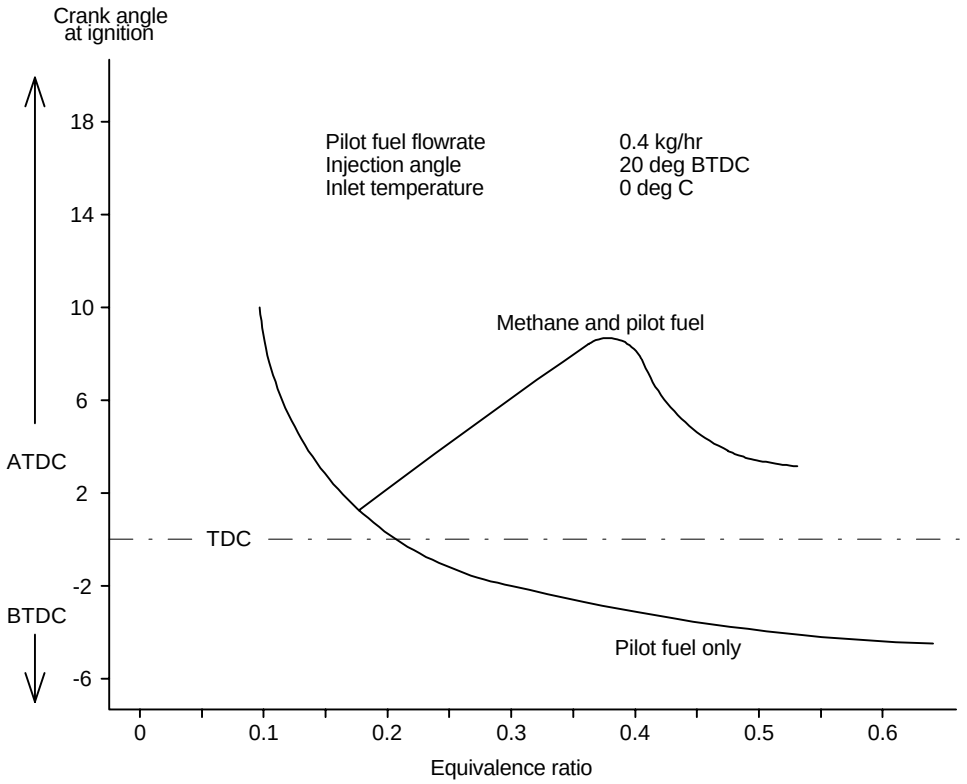

Figure 1.6 Variation of ignition point for pilot fuelled engine (Karim 1983)

1.7 Rapid compression machine

Rapid compression machines have been used to initiate combustion in gas engines (Khassaf 1972) using a pilot oil as fuel. This type of ignition has been shown to reduce cyclic variations through inducing fast initial burn rates, but has the drawback of additional complexities and the requirement for a secondary fuel.

The rapid compression machine runs at the same speed as the engine and injects burning mixture into the combustion chamber as the source of ignition. The machine used by Khassaf was basically a two stroke engine with the exhaust directed into the engine combustion chamber. The machine was run successfully using propane as the fuel, but it was found to be unsuitable to use a gas mixture of predominantly methane.

1.8 Catalytic ignition

Catalytic ignition can be traced to the days of Sir Humphrey Davy when he discovered that hot platinum wires were able to promote reactions in ignitable mixtures. Maximum temperatures exist for the use of this method, due to the physical properties of the catalyst itself, so applications which use a lot of excess-air are favoured. These include stationary gas turbines and exhaust after-treatment in spark ignition engines.

Work by Krylov et al. (1995) concerned the use of oxide catalysts, using manganese, to react carbon dioxide with hydrocarbons and alcohols. The experiments were carried out in laboratory conditions. Although not aimed at engine usage, this method could exploit the presence of residuals in the cylinder to provide an ignition source. The reactions with a wide range of hydrocarbons resulted in the formation of CO due to the lack of oxygen. With a lean burn strategy, where excess air is available, the CO could be converted to CO_2 during the expansion stroke reducing the chemical energy lost to the exhaust.

Again the initiation of combustion is not controllable and is therefore unsuitable for ignition in the narrow window of timing required to give best torque and emissions characteristics.

1.9 Bulk plasma generation

1.9.1 Thermodynamic expansion methods - Pulsed plasma jets

Plasma jets were originally used as propulsion devices, but with a move to improve the efficiency and reduce the emissions of automobile engines the technology was developed as an ignition source. The first documented use as an ignition source was by Waterson (1973), where a modified spark plug was used, but it was not till much later that plasma igniters were used to study radical production.

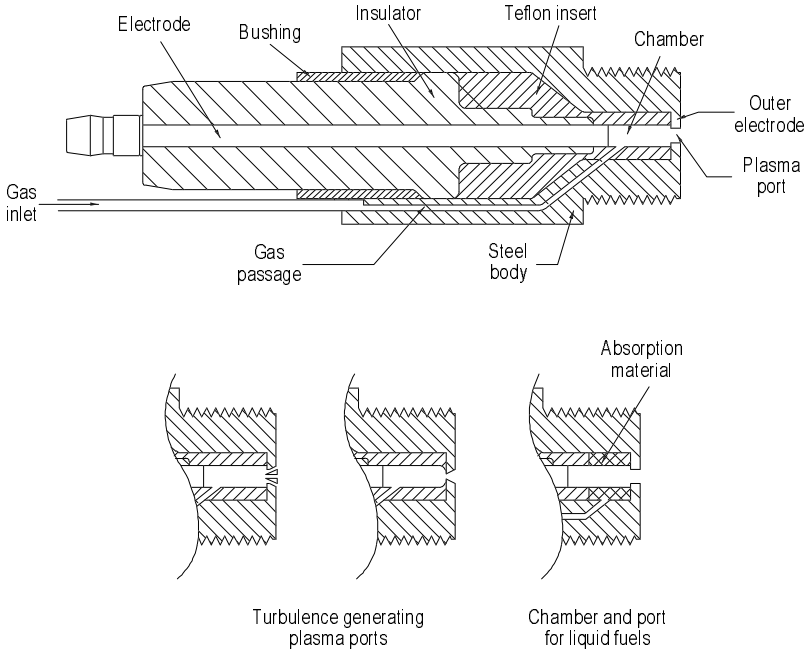

Figure 1.7 Plasma igniters (Weinberg 1986)

Plasma jet igniters use a high power spark discharge to form a plasma. Unlike a conventional spark plug, this occurs in a small cavity surrounding the electrodes (shown in Figure 1.7), which is able to communicate with the combustion chamber through a small orifice. The medium flows into the cavity either by a feed from outside the igniter, or from the combustion chamber on the compression stroke; it is changed to a high temperature plasma very rapidly. The rapid expansion results in the flow of a supersonic jet of dissociated products into the combustion chamber from the orifice (Heywood 1988) single atoms and radicals. The cavity and orifice size dictates the plasma temperature, velocity, turbulence and the species generated. The type of medium used for formation of plasma is relatively unimportant, as successful use is reported of nitrogen, argon and oxygen, although hydrocarbons give the best results where hydrogen atoms are generated, aiding combustion. If oxygen is present with the hydrocarbon, then oxygen atoms and hydroxyl radicals can also be formed. On the compression stroke the

medium stored in the cavity may become diluted or displaced, liquids can be used, being absorbed in the cavity, the medium then remains relatively incompressible on the compression stroke; this has the added benefit of the latent heat of evaporation removing heat from the electrodes.

It has been shown that plasma jets are efficient for sustaining combustion in very lean air-fuel mixtures. Comparisons have been made with conventional ignition systems, and it has been shown that there is a very large extension to the lean limit. Specific fuel consumption and power output are improved at the expense of an increase in NOx emissions, unburned hydrocarbons and carbon monoxide remain unchanged. Although the NOx is increased, the mixture may be weakened off further, whilst maintaining similar levels of ignitability to those of a richer mixture in an engine with conventional spark ignition.

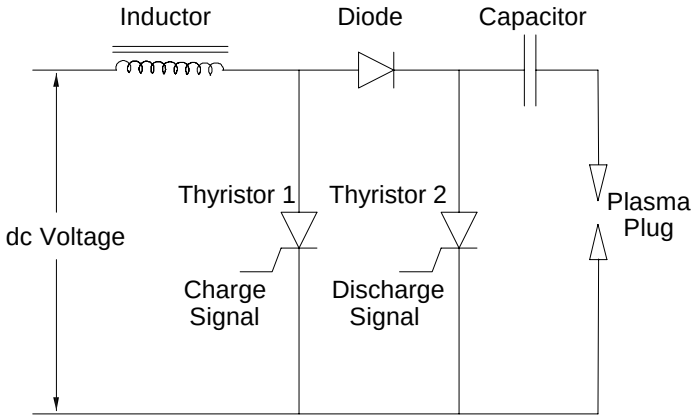

Figure 1.8 Typical plasma igniter drive circuit

The igniter drive circuit is shown in Figure 1.8. An inductor is charged by a DC voltage source, once charged a signal is applied to the first thyristor which breaks the circuit. The current then flows through the diode to charge the capacitor, when fully charged a signal is applied to the second thyristor and the capacitor is discharged across the plasma plug.

The energy input is usually a lot higher than with a conventional spark plug ignition system, typically 1J compared to 50mJ, and is discharged in approximately 20μs (Heywood 1988) compared to 1-2ms for a spark plug. Burn duration is reduced when compared to a conventional ignition system, especially during the early (laminar flame development) stages of combustion (Kupe et al. 1987). Plasma igniters have been measured to be no more than 10% efficient, measured using a calorimeter, when compared to the energy stored in the capacitor. Losses along the system include: the transition from stored energy to the arc, the high tension

leads, the condition of the igniter, and the heat transfer from the plasma to the igniter body (Smy et al. 1983).

It has been shown (Weinberg 1986) that when using a plasma jet the ignition timing becomes less critical, this means that a timing change for optimum efficiency is not needed with a change in fuel, e.g. from petrol to methane. The fast burn time can also result in an extension of the knock limit, since the end-gas residence time is reduced.
If all the fuel is injected through the igniter, a heterogeneous charge results which has the advantages of a reduced tendency to knock, and lower crevice storage of hydrocarbons. With only air being inducted, a more efficient scavenging process can be used without the possibility of the carryover of unburned fuel into the exhaust, the engine is now fuel limited and therefore does not need a throttle, low load efficiency is then improved.
The main disadvantage of the plasma jet igniter is the very fast wear rate of the orifice (which is also one of the electrodes), due to the high currents: a typical life is between 1 hour (Tozzi and Dabora 1982) and 40 hours (Kupe et al. 1987). Smy et al. (1983) have shown that a low capacity and high voltage supplied by the drive circuit results in a low efficiency and a lower wear rate.

Because of the limited service life, plasma igniters are currently unsuitable for use in stationary, continuous running, engine applications, since a change in igniter would be needed approximately once every two days. With the fast wear rate in mind, this type of igniter would lend itself to a situation where intermittent use is desired such as a starting mechanism for diesel or spark ignition engines (perhaps utilising another system as the primary ignition source).

1.9.2 Electromagnetic plasma injection - Rail methods

The rail gun is a device which is said to force ionised gas down a *barrel* purely by Lorentz forces, in a similar manner to the action of a solenoid, and differs from a plasma igniter where the motion of the ionised gas is induced purely by thermodynamic expansion. Industrial rail guns produce very high temperature plasmas (10,000 to 50,000 K) which are *fired* from the barrel at 10 to 100 km/s, this is accomplished with currents of millions of amperes over a time duration of milliseconds, the power consumption can be measured in gigawatts.
The Rail plug (Figure 1.9) is a miniature rail gun and was developed by Hall et al. (1991, 1992). Electromagnetic forces are said to accelerate the plasma into the combustion chamber, but thermodynamic expansion could appear to be a more realistic explanation.
The plasma injection mechanism induces a jet of turbulent radicals which promote combustion in highly diluted mixtures. This makes them ideal as ignition sources for conditions of high dilution, e.g. heavy EGR, throttled conditions and lean burn strategies. They also lend themselves to use for the cold starting of diesel and alcohol fuelled engines (Dawe et al.), ignition assistance in dual fuel engines, and the relighting of aircraft gas turbines at high altitude.

The initial ionisation is carried out by striking an arc at the rail plug breech, in a similar manner to conventional spark ignition. Once the arc is struck, it does not remain stationary, and this non-stationary arc, unlike pulsed plasma injection and conventional spark plugs, gives greatly reduced wear, since erosion occurs along the total rail length. Energy is dissipated along the whole rail length and as the arc is accelerated along the length of the barrel, erosion time is therefore substantially reduced. At the breech, where the arc is struck, a higher erosion rate is expected, but this can be compensated for by the choice of a more wear resistant material. The lack of rail cooling however will result in higher erosion levels.

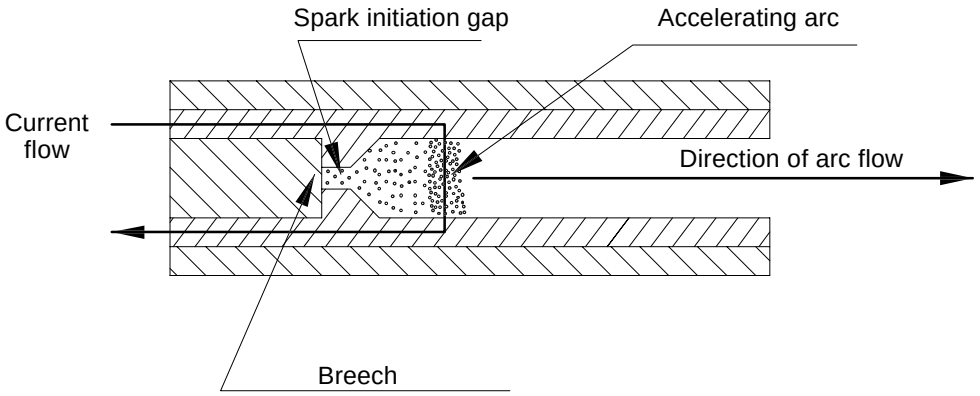

Figure 1.9 Typical rail plug schematic

Although not documented, the rail plug could act as the fuel injector, this would result in a cooling effect for the rails, and a plasma consisting of a higher proportion of hydrogen atoms which (as discussed earlier) promote better ignition characteristics. As with plasma jet methods, the barrel does not necessarily need to be purged or filled with a specific medium, as the plasma can be generated with whatever molecules are present.

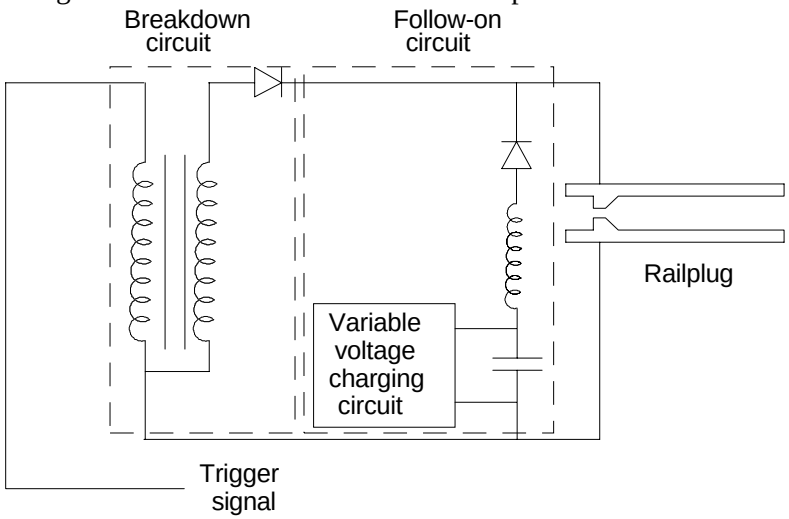

Figure 1.10 Rail plug ignition driver circuit (based on Hall 1992)

The drive circuit is similar in operation to a pulsed plasma igniter, in that a system is needed for initial breakdown and for maintaining the arc. A conventional coil ignition circuit causes breakdown, and a bank of charged capacitors discharge to sustain the arc. Stored energies are in the region of 1 to 6 joules, and the arc duration is approximately 500μs; a similar energy level to a plasma igniter, but with an arc duration falling between CDI and (T)CI systems.

Photographic evidence shows plasma movement, and the importance of the correct firing energy. Deficiency in energy results in eddy currents being set up in the plasma as momentum allows molecular motion to continue after the current ceases. In this case the plasma operates as part of a *generator* instead of a *motor*.

Both photographic evidence and pressure-time histories, carried out in a constant volume bomb, confirm that combustion time is reduced when compared to a conventional spark plug, notably in the early flame development period. Engine tests were performed (Hall 1992) and

showed a reduction in COV, near to the lean limit, when compared to a conventional spark ignition system.

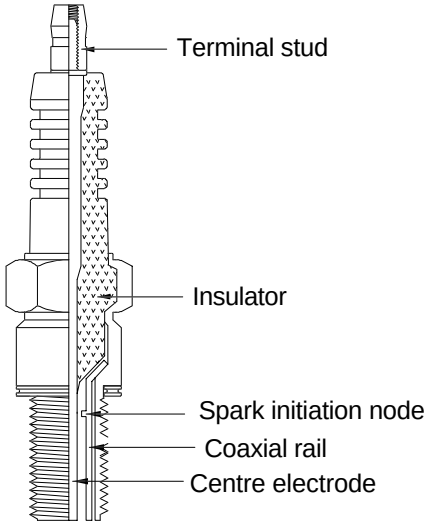

Figure 1.11 Prototype rail plug igniter (based on Hall et al. 1992)

Champion Spark Plugs Ltd have produced at least two types of rail plug, model numbers 689 and 705. The 689 has a tungsten centre electrode, the 705 a high nickel (95.5%) alloy. The high nickel alloy plug was found to last twenty five times as long as the tungsten electrode type. The actual life with a 0.5J energy input was measured to be 4.5 hours; the power input is still an order of magnitude greater than that associated with spark plug systems. Discussions with Champion Spark Plugs Ltd (1995a) have revealed that the co-axial rail plug ignition systems are currently not in production due to the very short life span of the electrodes.

1.10 Laser based techniques

Six different ignition mechanisms may be exploited by using laser technology, these are listed by Hills et al. (1992) as:

Direct thermal ignition	particles may be heated sufficiently to ionise molecules locally
Photochemical excitation	photo-dissociation of molecular oxygen
Explosion by thermal ignition	enough energy to cause rapid ignition through heating only
Direct laser ignition	formation of a plasma
Laser spark ignition of particle	optical breakdown occurring due to a thermal explosion of a particle
Radiative heating of particle	absorption of radiation

The most widespread use of laser ignition, is ignition initiated by the vibration of molecules causing bonds to break bonds. This causes both highly reactive radicals and heat generation, and is done with an absorption method at the correct frequency. This process is termed direct laser ignition.

The ignition source may be focused in the optimum position in the combustion chamber for flame initiation, and the constraint for fitting the ignition source around other engine component constraints is removed. There is also scope for splitting the laser beam and focusing it at

multiple points in the combustion chamber. A chopper and mirror arrangement could be used to split the beam and allow the laser to ignite the charge in multiple cylinder engines.

Heat transfer to the ignition provider is eliminated, and all energy is available for radical formation and hence flame initiation and propagation. Sher et al. (1991) postulated that the heat transfer effect is a cause of misfire, in conventional ignition systems. In this respect, the chance of misfire with laser ignition is significantly reduced and the lean limit may be extended with laser ignition. The major shortcoming of laser ignition is that optical access is needed to the combustion chamber, and these optics may be fouled by combustion deposits masking the source, this may occur in as little as one hour. A model for laser ignition of a gaseous medium was developed by Adler (1992), but this centred around the particle heating mechanism.

1.11 Sparking plugs

1.11.1 History

The history of the spark plug can be traced back to the days of Lebon, when in 1801 he put forward an idea for the operation of a gas fired engine working on a steam cycle. The mixtures were to be ignited by an electric spark. The engine was never built, but the ideas were used by Isaac de Rivaz in his internal combustion engined vehicles built in 1805 and 1813 (Day 1980). Lenoir and Hugon also used an electric spark to ignite gas and air mixtures in adaptations of steam engines. Some years later electric ignition was rejected due to the complexity and unreliability of the ignition circuitry. There were also problems with the rapid discharge of the battery cells, which at the time were the only sources of electric current.

The spark plug has remained virtually unchanged since that of Lenoir in 1860, i.e. a hollow body with an insulating core cemented inside, an earth electrode fixed to the body and a live electrode passing through the insulator (Day 1980). Since then there have been many technical advances.

1.11.2 Construction

The spark plug comprises three main components; the shell or body, the electrodes and insulator, and is shown in Figure 1.12. The plug body is usually nickel (or cadmium - depending upon manufacturer) plated to deter corrosion and to prevent thread seizure (which can be a particular problem with aluminium alloy cylinder heads). The insulator is inserted into the shell and then swaged and heat shrunk into position (Tranter 1993).

The electrodes are produced from a material which will prevent chemical corrosion and will withstand the high in-cylinder temperatures. The centre electrode is inserted in the insulator and held in place by a thermally conducting solid glass seal (Bosch 1985) or powdered glass seal (NGK 1976). The usual material for electrodes is a nickel alloy, and some manufacturers use a core of copper which assists heat transfer (Tranter 1993) (Lenk and Podiak 1977) and leads to a reduction in electrode wear. Other materials used for the centre electrodes include precious metals which are normally smaller in diameter (allowed by lower corrosion rates) than nickel types, this results in a more effective discharge with a much higher voltage density (Bosch 1988). On high performance engines silver was favoured for superior heat transfer characteristics, but now even racing engines are returning to copper centre electrodes, albeit covered by another material where the arc is struck (Arkless 1992).

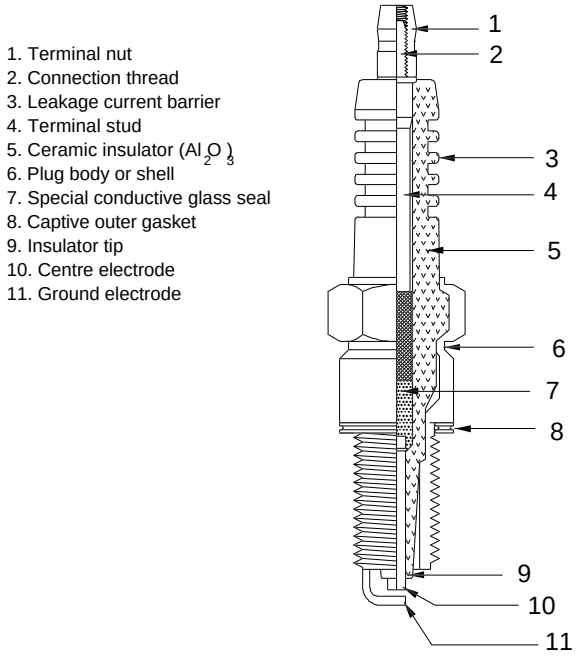

Figure 1.12 Construction of a spark plug (Bosch 1988)

Originally the insulator was produced from mica but this was superseded by alumina (Al_2O_3), when in 1926 ethyl-lead anti-knock compounds were introduced into gasoline. The insulator separates the anode and cathode so must therefore be of very high electrical resistance. It must also have very good heat transfer properties and be resistant to thermal shock and chemical corrosion. The ribbed section of the insulation, labelled 3 in Figure 1.12, is intended to reduce external *corona discharge*, a phenomenon induced by high local atmospheric ionisation which allows a *leakage* current to flow along the insulator. This occurs mostly in conditions of humidity and rain, and where dirt is present on the insulator (NGK 1976).

1.12 Alternative spark ignition strategies

1.12.1 Pre-chamber spark plug methods

Larger spark ignition engines use a pre-chamber arrangement to initiate combustion (Wattam et al. 1993). The pre-chamber receives a pre-carburetted mixture or pure fuel, by way of an additional valve or injector, and the cylinder inducts a weaker mixture.

When the mixture in the pre-chamber is ignited, the initial flame front penetrates deep into the mixture causing a voluminous ignition source. This type of strategy is referred to as a *divided chamber, stratified charge* system (Dale and Oppenheim 1981). Effective stratification can be achieved at the expense of a more complex mixture admission system. Fuel consumption can be reduced and the lean limit can be extended. The charge stratification can also allow lower knock resistant fuels to be used at the same compression ratio. The slower burning of the lean mixture results in lower combustion temperatures and hence low NOx emissions.

Torch cells work on a similar principle but the mixture for the pre-combustion chamber is supplied from the main charge in the cylinder. Ignition results in the initiation of a turbulent jet which can lead to an extension of the lean mixture limit (LML). This type of chamber can lead to an increased quenching area which itself may lead to higher hydrocarbon emissions.

The addition of an orifice of reduced area at the exit from the pre-combustion chamber leads to deeper penetration, and systems of this type are referred to as *flame jet igniters*. The pre-chambers in this case are usually of lower volume due to a higher risk of quenching. The exiting jet leads to shear flows that induce turbulence, causing multiple flame kernels throughout the mixture. The LML has been extended as far as 33:1 with this type of strategy.

1.12.2 Puff-jet methods

Although not strictly a pre-chamber method, the puff-jet ignition system has been deemed to be useful at decreasing burn time in a similar manner to pre-chamber and plasma igniters. The puff-jet ignition system operates by directly injecting gaseous fuels into the combustion chamber. A pair of electrodes are positioned in the path of the induced plume, and ignition is initiated by striking an arc when the plume has mixed sufficiently to create a flammable mixture. Experiments by Dawe et al. (1994) used 1% of the bulk charge as the plume, which was injected at 7bar. The remainder of the charge was inducted using a conventional carburettor, in a very lean mixture. The ignition system had a power of 150mJ and used a gap of 4mm, both parameters being higher than a conventional system. In operation, the kernel was seen to be similar to that obtained using a plasma igniter. The puff-jet system was found to reduce ignition delay and burn duration when compared to a conventional spark plug, with a marked improvement in combustion of lean burn engines. Increased power output was experienced, and this was due in part to a faster burn time coupled with the more retarded ignition timing. Cyclic dispersions were reduced due to the voluminous source of ignition for the majority of the charge, and the convection of the kernel away from the relatively cold electrodes.

1.13 Conclusions

Currently the only viable ignition system for production homogeneous charge engines is by use of a spark. Other systems may become of use as new materials develop, plasma ignition can form a deep penetration during ignition but is dogged by the electrode life, which may only be a few hours. Laser ignition can be used to supply multiple ignition sites and is free from heat transfer effects normally associated with spark plug electrodes, but is dependent upon reliable optical access.

2. Sparking plug ignition types

2.1 Trembler coil

The trembler coil was the first type of commercially available electrical ignition system to use an ignition transformer. It was designed by De la Rive and Heinrich Daniel Rühmkorff, and was first used by Barsanti and Mattcucci in 1855 (Day (1980)).

The trembler system, shown in Figure 2.1, utilised an early ignition transformer consisting of a primary and secondary winding which were wrapped around an iron core. The primary winding was made from thick wire and had only a few turns; the secondary had many more turns of smaller diameter wire. The low tension (LT) contact breaker consisted of a blade spring mounted above the transformer core which was attracted when the core was energised. On attraction the LT contact was broken and the magnetic field collapsed. This process would continue, the speed of which was governed by the spring characteristics and the gap between the transformer and the LT contact breaker.

The fluctuating primary current induced a fluctuating high voltage in the secondary winding great enough to provide a spark at the plug electrodes when the HT contact breakers were opened. A condenser or ignition capacitor was fitted to the LT contact breakers to store current, induced by the back EMF, and prevented it from arcing between the opening contacts. The condenser also reduces erosion of the contact breaker surfaces caused by spark discharges.

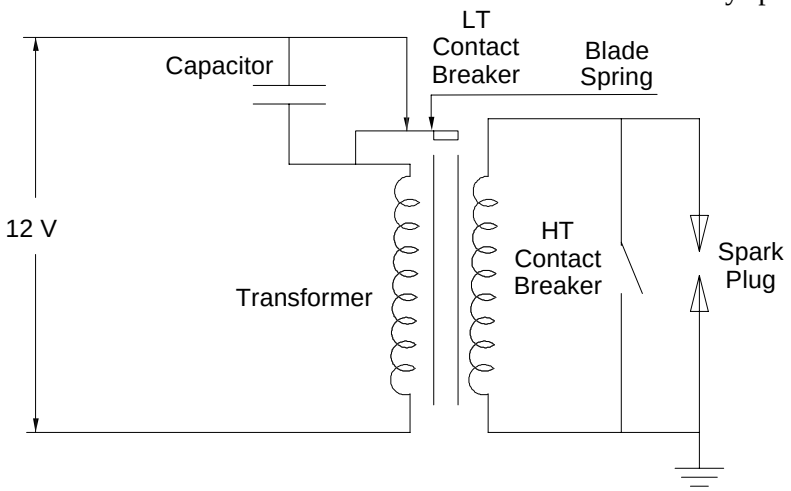

Figure 2.1 Trembler coil ignition circuit

The trembler coil circuit resulted in a multiple-strike ignition system with the timing being controlled by the distributor. Battery life was the main drawback for the trembler coil, if it were a dry cell it would require replacement after 300 - 400 hours, or if a storage cell, it would need to be recharged after 25 to 30 hours because at this time there were no engine driven charging systems (Amann 1990). This form of ignition was last used on the model T Ford which ceased production in 1927.

2.2 Magneto

The magneto was born when the need for an electrical ignition system which did not rely on unreliable battery energy arose. Originally this was a self generating low tension system which was used successfully to produce pulse voltages at specific times during the engine rotation.

These pulse voltages were sufficient to provide ignition sparks at one or more plugs. Three types of magneto system have been used:

i. **The rotating armature** - in this case the armature rotated and the high tension output was obtained through brass slip rings. As speeds increased the coils held within the armature were subjected to increasing strain and coil fracture became a problem.
ii. **The rotating magnet** - the magnet rotates within the stator primary and secondary windings eliminating the need for moving electrical parts.
iii. **The flywheel magneto** -With small engines the flywheel could be used as the rotating part of the ignition generation system. The rotor rotated over the source coil, the increase in radius increased the rotor inertia and allowed it to be used as the flywheel for the engine. The output is then fed to an external ignition transformer.

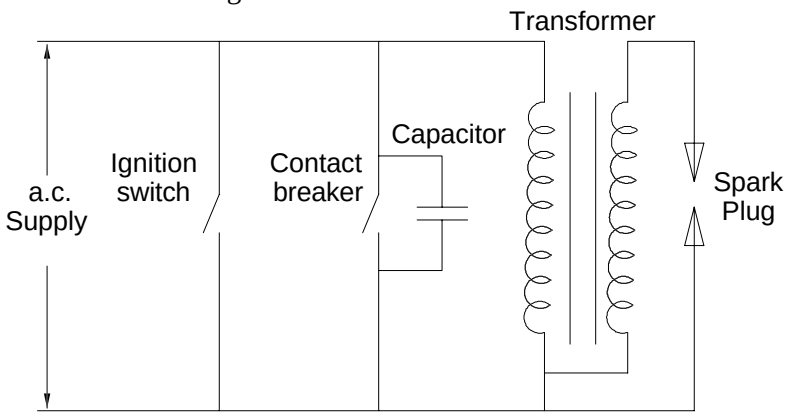

Figure 2.2 Magneto ignition circuit

A typical circuit for the high tension system is shown in Figure 2.2. The contact breakers allow the transformer to charge when they are opened. When closed a short circuit arises. The capacitor is used to eliminate arcing across the contact breaker gap on opening. The system is unlike the trembler coil arrangement as it receives current in alternating form. The voltage output of the magneto is dependant upon the rotational speed of the generator which leads to a low power output when running slowly, although mechanisms have been implemented to induce faster motion of the generator stator when starting.

Magneto systems are now only found on small engines such as chain saws, lawn mowers and mopeds the circuit existing in the flywheel guise. The technology of the magneto system has developed into the self generating CDI system which is discussed in 2.5.

2.3 Coil and battery ignition (Kettering)

The coil and battery type of ignition dates back to 1908 and was first suggested by Kettering who later became the head of research and development at General Motors. The circuit has changed very little over 85 years and is shown in Figure 2.3.

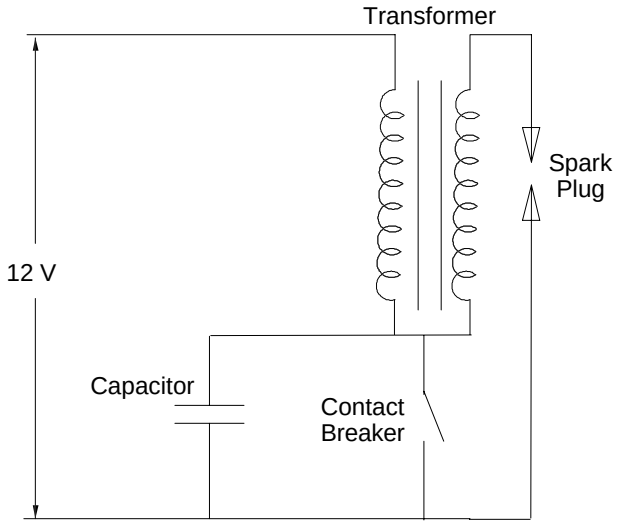

Figure 2.3 Coil and battery ignition system - points and condenser

The ignition energy is stored in the ignition coil until the contact breakers are opened, at which point the magnetic field collapses and induces an EMF in the secondary winding. As with all contact breaker systems, at high engine speeds the contact breakers may suffer from bounce when the mechanical switching device approaches a resonant frequency. Methods are available for the reduction of this phenomenon and include the use of a stronger spring to maintain closure, but this leads to an increase in wear to both the ignition cam and the contact breakers themselves.

The battery was re-adopted as the power for the ignition circuit after vehicles began to be fitted with electric lamps and storage battery technology improved. There was no reduction in ignition power output at low speeds (the main drawback of the magneto system) although at higher speeds there was insufficient energy stored in the coil. Some older vehicles, such as those produced by Rolls Royce, used two plugs per cylinder, one fired by a magneto system and the other fired by a Kettering circuit.

Modern CI coils are designed with both the primary and secondary windings connected in series which results in the sum of the primary and secondary voltages occurring at the spark plug. This also results in the primary current flowing through the battery, to earth, on the collapse of the magnetic field.

The coil and battery system suffers from low power output at high engine speeds, due to the finite time needed for the coil to charge up; the use of a ballast resistor was adopted to relieve this problem. The ballast resistor improves the coil charge at high engine speeds. When the resistor is cool due to lower power dissipation caused by shorter dwell times, (i.e. at high speeds), a higher voltage is allowed to reach the ignition coil. When the resistor is hot due to an increased dwell time (at lower speeds), less voltage is available, typically 8V. A lower voltage coil can then be used and, with the careful choice of resistor, will not become damaged. For starting purposes the ballast resistor can be bypassed, since the battery voltage is substantially reduced during the cranking period and permanent damage will not occur. Coil ignition can supply approximately 20000 sparks per minute (Bosch 1976) with a 10 to 25kV secondary voltage.

2.4 Transistorised coil ignition (TCI)

Transistorised coil ignition is the most widely used type of internal combustion flame initiation, being used on the majority of automobile engines. The system evolved from the basic coil and battery type (Kettering) of system where there was a need to reduce the current carried by the contact breakers. This was accomplished by using the points purely as a signal generator to supply a transistorised ignition amplifier. As the technology evolved the contact breakers were replaced by inductive or hall effect transducers which improved operation and reliability, and resulted in a maintenance free system.

As with battery and coil ignition there is a deficiency in energy stored at high engine speeds, since the coil is allowed less time for charging. This does not cause a great problem for many modern engines since at high speeds and loads there are very few residuals in the cylinder making an easily ignitable mixture (Bosch 1976). Semiconductor devices can control the dwell period in units of time, rather than in units of crank angle as with the coil and battery system, optimising the coil charging process. Even so, this time period is reduced when the engine runs at high speed. The use of a low inductance coil and a transistor amplifier results in a low voltage drop over the engine speed range. Low bounce contact breakers can allow up to 24000 sparks per minute, since when bouncing begins to occur, a loss in dwell time is experienced (Bosch 1976). Inductive, hall effect or optical pulsing can increase the sparking rate to 30000 sparks per minute. Coil charging can be increased by the use (or more correctly the bypass) of a ballast resistor described in the previous section, additionally, the transistor can be used to restrict the current to a lower resistance coil, thereby achieving the same effect.

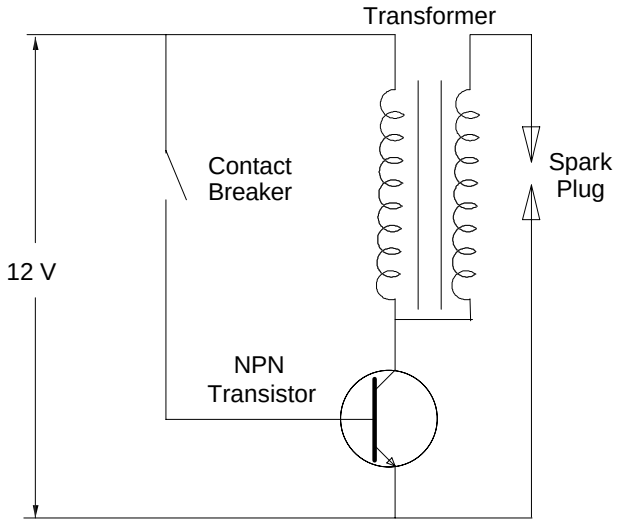

Figure 2.4 Transistorised coil ignition

When charging the coil, the transistor amplifier can allow currents of up to 16A to flow for an accurately controlled time. This is an improvement over the maximum of about 5A allowed by contact breaker systems before overheating occurs. Since there are no moving parts, the switching mechanism does not wear, or erode, and can switch more rapidly.

TCI coil design differs slightly from that of CI because of the greater voltage drop over the switching mechanism, 1.5V (internal resistance) with the transistor compared to 0.2V over a set of contact breakers (Bosch 1976), TCI coils also have a lower resistance to enable faster charging. The system is characterised by a long spark duration of approximately 1.5ms (Bosch 1988). TCI systems are the most widely used, particularly in the automotive sector, Figure 2.5 shows a typical packaged system.

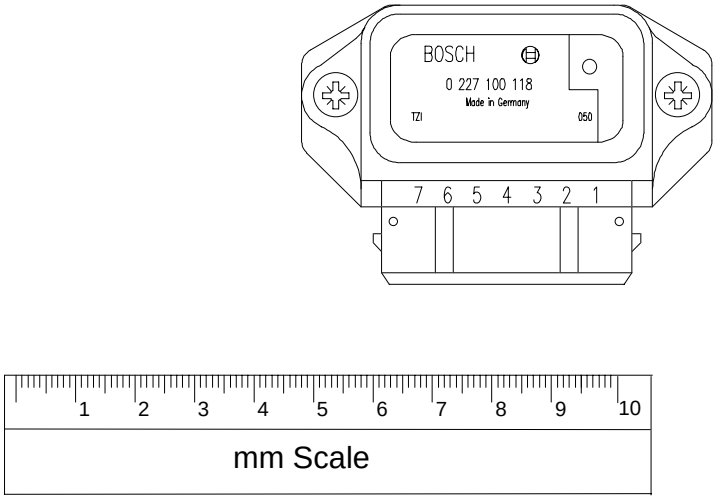

Figure 2.5 Typical packaged TCI driver unit

2.5 Capacitor discharge ignition (CDI)

The capacitor discharge ignition system was first used between 1805 and 1813 by Phillipe Lebon when he used a *Leyden Jar*, a type of condenser discovered by Allesandro Volta in 1776, to form the ignition system of his internal combustion vehicle engines.

With a capacitor discharge ignition system the energy for the ignition transformer (or coil) is stored in a capacitor, of approximate capacitance 1μF, which is discharged by activating a triac or thyristor at the required spark timing. The spark is induced by charging the ignition transformer, the opposite to a TCI or CI system which rely on discharge (collapse of the magnetic field). The rise in output voltage is accomplished very quickly, and the spark duration is very short, making it unsuitable for: non-homogenous mixtures, heavy EGR or very lean mixtures, where ignition probability is low. The capacitor is always fully charged before firing (Bosch 1976), whereas a conventional coil acting as the energy storage device may be left partially saturated at the point of ignition; the dwell period is also no longer a problem since system charging is much faster. The thyristor can switch and block far higher currents than a transistor, with CDI systems, surges of up to 100A are not uncommon (Bosch 1976), since the thyristor is 'closed' before the capacitor is fully discharged it must withstand the capacitor voltage until the next firing. Switching of the thyristor can be achieved by conventional contact breakers, but at high speeds misfire can occur when contact breaker 'bounce' results in undesired multiple switching. Inductive, hall-effect and optical switching are more reliable.

The transformer charge time results in no loss of spark energy at high engine speeds (Mears and Oxley 1989). CDI systems are used with surface gap spark plugs on racing engines and

are usually triggered with an electronic control unit (ECU) which holds the ignition timing map for optimum performance.

CDI systems are very tolerant of combustion deposits on the spark plug insulator, the very fast rise time associated with the capacitor discharge gives a very high initial energy which is able to 'break through' deposits or damaged system components, as the breakdown voltage is reached quickly before energy can escape along leakage paths. This makes this type of ignition driver ideal for use with two-stroke engines (running with total loss lubrication systems) where oil fouling can cause earth leakage.

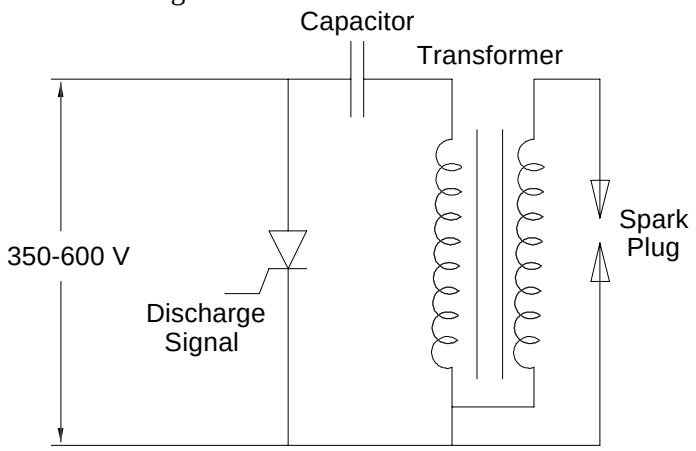

Figure 2.6 Capacitor discharge ignition system

There is confusion as to what type of coil is used with a CDI system, a standard TCI coil may be used (Weber 1994), but a special coil with a lower turns ratio may be needed (Teasel and Miller 1967). A special coil may be required since the CDI system may give a higher peak current (Zytec 1994). The lower turns ratio gives a lower inductance and hence a different voltage waveform and performance characteristic. Although other sources (Zytec 1994) disclose that the difference in coil turn ratio is to reduce losses in the system by lowering the transformer impedance, normally around 15kΩ. Reduction of the coil impedance can result in a 0.5A primary current and a 100-500mA secondary current. CDI ignition coils for use with racing engines may have a turns ratio of between 50:1 and 200:1 (Zytec 1994). The most comprehensive guide to coil and ignition system suitability is that provided by Bosch (1976). It states that if a conventional CI or TCI transformer is used with a CDI system, the generally higher inductance will result in a much lower voltage rise time and hence the loss of shunt insensitivity. The CDI coils are usually of a much lower primary inductance and dynamic internal resistance, typically 50kΩ, 10% of the resistance of a conventional ignition coil. The low inductance associated with CDI coils is to enable high re-striking rates to occur with low energy storage.

CDI systems can be powered by either a battery or a self-generating system. The self generating system is widely used with motorcycles but only works satisfactorily after the engine has reached 200 - 500 revs/min when enough power is produced at the generator. The battery system favoured on cars maintains the correct voltage and current regardless of engine operating parameters.

Variations on the CDI system include one developed by SAAB, known as the direct ignition system. The ignition procedure can take place with multiple sparks over a crank angle of approximately 20° which increases the ignition probability and lends itself to use with diluted and non-homogenous mixtures. The SAAB control strategy only uses this multiple strike capability during cranking and low speed throttled conditions. However, with multiple arcs struck, it would be expected that the sparking plug electrodes will suffer from increased wear rates, but this is not the case with spark plug life almost doubling that expected in a similar engine with a TCI system (Granlund 1986).

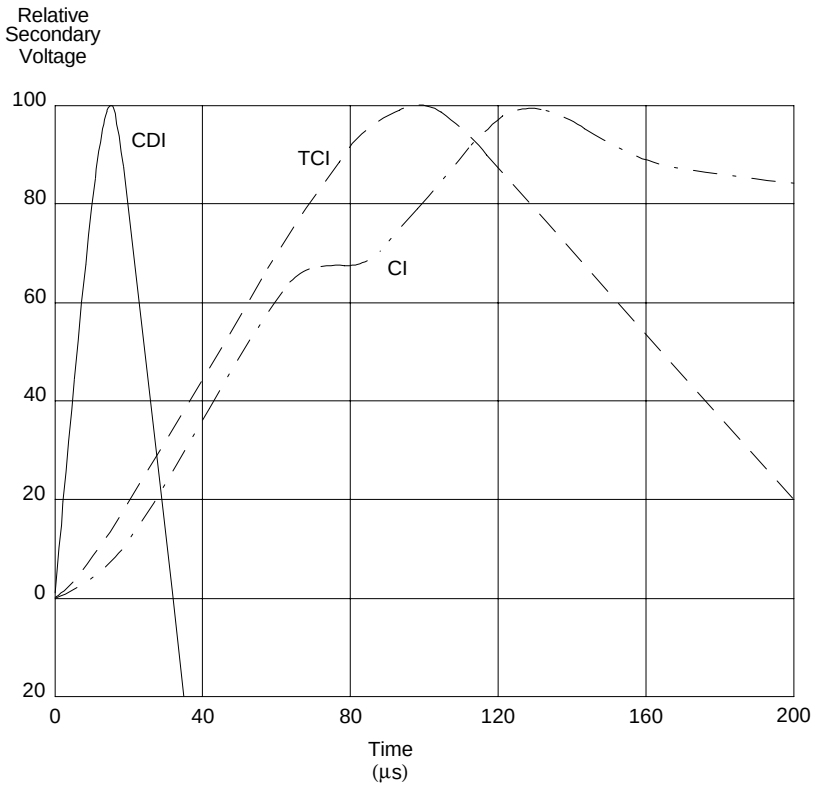

Figure 2.7 Variation of secondary voltage against time with change in ignition system (adapted from Bosch 1976)

The reasons behind this unexpected result is that automotive spark plugs do not necessarily reach the end of their service life by erosion only, the accumulation of fouling materials, especially with the use of leaded petrol, can determine the service interval. The very fast voltage rise time of the CDI system renders it insensitive to this plug life constraint. Figure 2.7 compares the voltage rise time to that of TCI and CI systems.

In service, the CDI system may become damaged if the secondary magnetic field is unable to discharge, if a plug lead were to become disconnected for instance. Some systems incorporate a safety system to prevent damage in these cases (Bell 1993).

2.6 Breakdown systems (VFZ)

This type of system is not commercially available but has been used extensively for research purposes by many workers such as Maly (1984), Anderson (1987), Cho et al. (1992) and Pischinger and Heywood (1988).

Breakdown ignition systems consist of modified CDI systems which give a faster voltage rise and a higher current flow than the parent circuit. Figure 2.8 shows the layout of this type of ignition system. The spark duration is very short, with all the energy concentrated in the first part of the spark discharge; this leads to very high ignition powers for a low energy. The system used by Cho uses no ignition transformer, instead the storage capacitor is charged by a high voltage power supply to a voltage of up to 50kV, and a mechanical switch is then used to discharge the capacitor. For systems based on the CDI circuit, LT charging is accomplished by a high voltage DC supply as before.

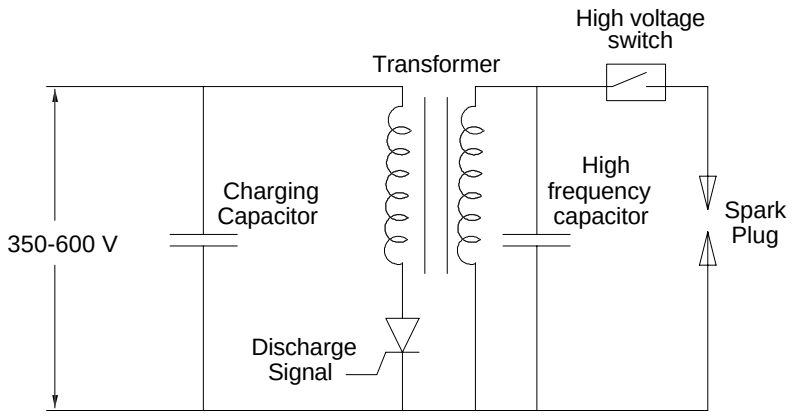

Figure 2.8 VFZ ignition circuit

More common systems charge a capacitor on the HT circuit through the ignition transformer and utilise a switch for discharging through the spark plug. The switch may take the form of a mechanical type (Maly 1984) or an auxiliary spark (booster) gap (Anderson 1987), see section 2.9.3. With the breakdown system there is an almost instantaneous voltage available for breakdown to occur, this is followed by a very high current. Increasing the energy storage results in a spark of the same duration but a higher breakdown current. A high voltage diode is

often used in the HT side as a simple rectifier to block any back EMF formed during the oscillation period where electric fields are created and destroyed.

Breakdown systems have been shown to extend the lean limit of combustion even though the spark duration is shorter than the CDI systems. This is believed to be because the total spark energy is deposited in the ignition zone in a very short time before any flow field effects can influence the transport of radicals and dissociated species.

Even though breakdown systems have been used for experimental work, as far as the literature can reveal, they have not been put into production as an ignition system.

2.7 Brighton Photoconductive Switch Ignition System

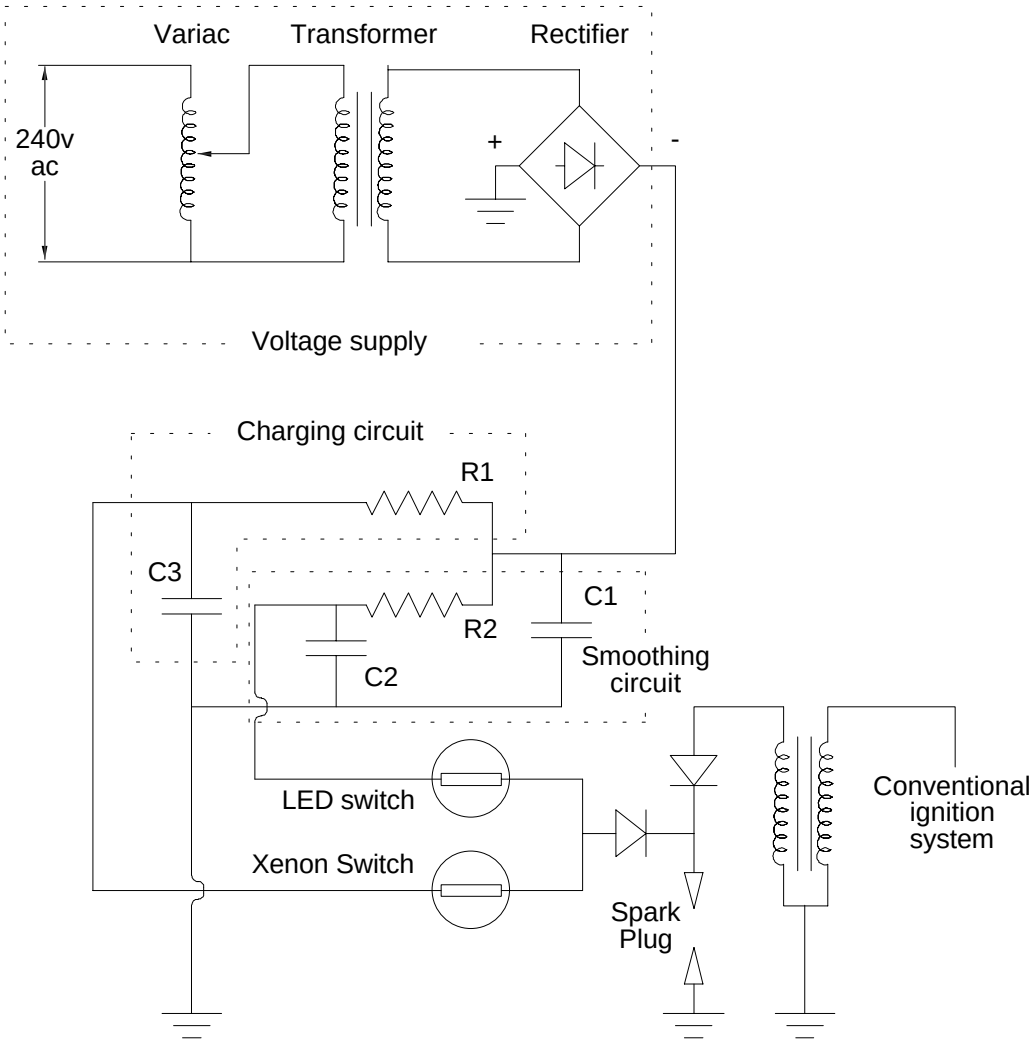

Figure 2.9 Brighton ignition system

The ignition system developed by the University of Brighton (Howson 1989, 1990a, 1990b, 1990c, 1991, 1992) uses two high voltage semiconductor devices to switch very high voltages.

These semiconductor devices are activated by a light source, which can be anything from an LED to a strobe type system, the voltage rise time being light source dependant. The system, shown in Figure 2.9, consists of four modules:

1. A conventional ignition system (transistorised) to create the initial breakdown.
2. A variable DC voltage supply (rectified AC).
3. A system based on timers to control the duration of the LED and Xenon flashtube.
4. An oil filled box housing the two photoconductive switches and light sources.

Typical component values:

R1	15kΩ
R2	44kΩ
C1	0.1mF
C2	0.1mF
C3	0.1mF

The use of photoconductive switches allows high voltages to be switched directly and hence the duration of voltage and current to the electrode gap can be controlled accurately.

2.7.1 LED activated photoconductive switch circuit

The LED activated photoconductive switch circuit directly switches the inverter voltage across the plug gap. This can only be achieved after the initial breakdown has taken place. In reality, the switch is operated before breakdown occurs causing a potential difference at the plug electrodes, no current flows since the necessary breakdown voltage is not exceeded. When breakdown does occur, the DC voltage from the inverter is sufficient to sustain the discharge indefinitely. The type of switch used has an impedance reducing from several MΩ to a value of 4-5kΩ when energised by LEDs, and it is used to control the duration of the glow phase (see section 2.12.4).

R1, R2, C1, C2 and C3 act as a model pi RC smoothing circuit to reduce the ripple associated with rectified DC voltage. The value of C2 is chosen so that it does not completely discharge prior to termination of the spark.

2.7.2 Xenon flash switched circuit

The Xenon flash switched circuit discharges capacitor C3 across the plug gap. During operation of the flash tube, the switch resistance drops to 100Ω for a few microseconds then exponentially recovers to a relatively high value, typically over a period of 100ms. This part of the circuit produces a pseudo arc phase.

2.8 Coil design

The link between the low voltage and high voltage sides of the ignition driver is the ignition transformer or coil. The design of the ignition coil has been briefly discussed in 2.5 with reasons for the choice of turns ratio.

The system favoured by a majority of engine and ignition manufacturers for many years is to use a single coil and a mechanical distributor. The coil is usually filled with oil for cooling purposes and has the primary and secondary windings connected together in series. This allows the HT voltage to be added to the LT voltage. A metal, commonly aluminium, cladding is used to cover the coil windings and reduce stray magnetic fields (Bosch 1988). This type of coil is capable of supplying 18000 full strength sparks per minute (Bell 1993).

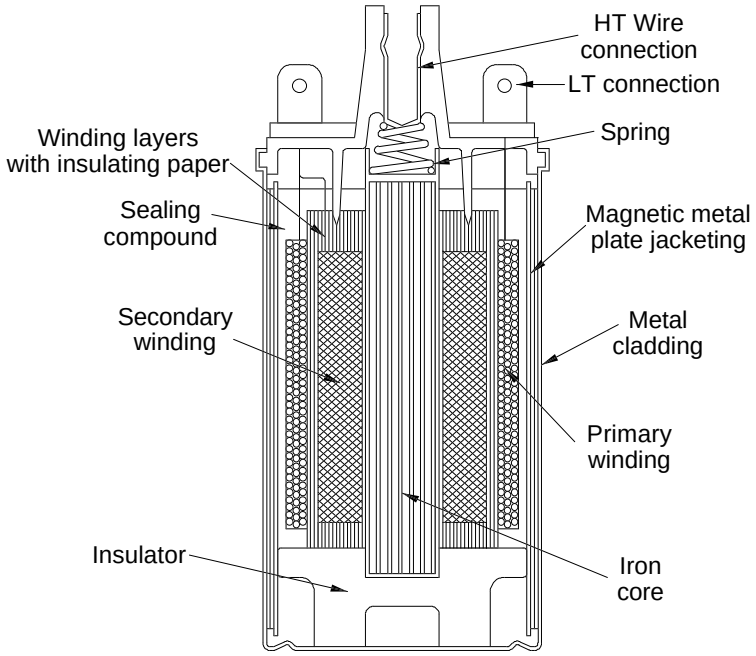

Figure 2.10 Conventional ignition coil (adapted from Bosch 1987)

With the unreliability of electro-mechanical devices the distributor is slowly being replaced by other purely electrical methods of HT distribution. HT leads normally use a powdered carbon core (to reduce EMI), which may break internally and increase the system resistance (Bell 1993). This problem is overcome by the use of one coil per cylinder interfacing directly with the spark plug. This method has been adopted by many high performance engines, and has been used to a great extent by SAAB. Other problems with HT leads include cross-firing, where closely grouped HT leads induce voltages in one another and result in misfire in cylinders where an arc is easily struck, e.g. at an early stage on the compression stroke. It is also clear that cross-firing can also interfere with ignition timing, especially where the angle between firings is small, such as common with eight and twelve cylinder engines. Cross-firing can be cured by keeping HT leads at least 75mm apart (Bell 1993) which makes for an untidy engine. The use of separate 'coil-on-spark' ignition transformers can resolve the problem completely, since only low voltage conductors are present outside of the engine structure and can be contained in a multi-core wiring harness.

The individual coil systems are susceptible to problems, being mounted within an enclosed space (usually in a recess in the cylinder head casting), results in virtually no cooling. This can reduce the performance of the coil by increasing its resistance. Also, without proper support, the coils may lead to fracture of the spark plug insulator under the extreme vibration synonymous with a running engine (Bamsey 1991). In twin-cam engines the head casting is usually deep enough for supporting these coils at the LT end, and insulator failures are virtually eliminated.

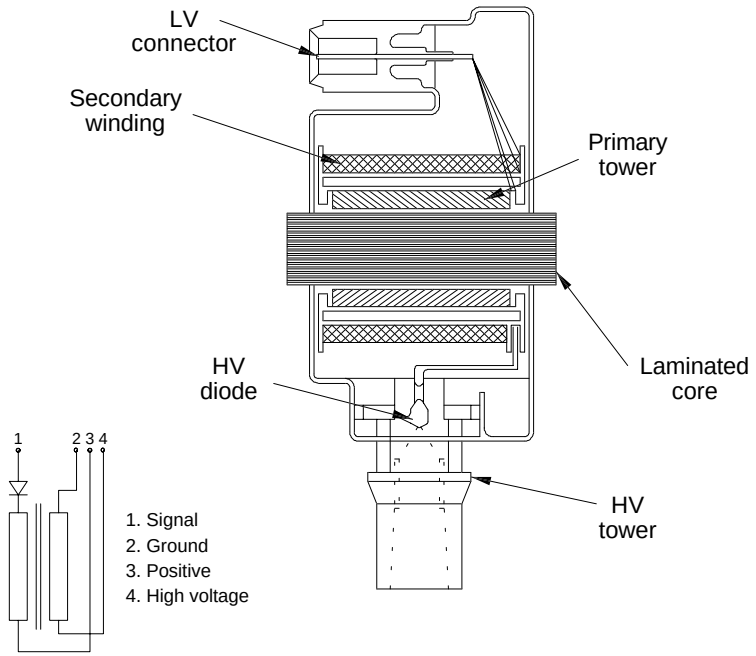

Figure 2.11 Individual coil system for direct mounting to spark plug (adapted from Magnetti Marelli)

Wasted spark systems use a double ended coil which fires two plugs at once. The two cylinders are normally both at TDC, one on the compression stroke, the other on the exhaust stroke. The spark plug exposed to the burned products sparks readily since the gas is at a lower pressure, the electrodes are hot and the gas is highly ionised. This plug acts as a *booster gap* which has been shown to decrease ignition sensitivity to electrical shunts caused by deposits (Bell 1993).

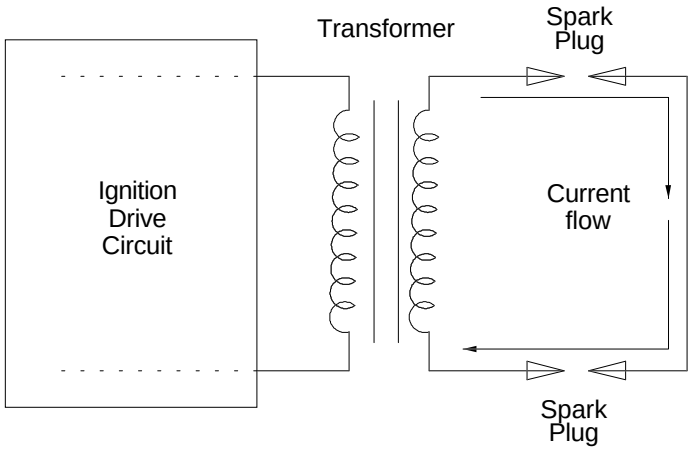

Figure 2.12 Waste spark system circuit

Wasted spark systems are advantageous since there are fewer HT connections, no rotating HT components, reduced noise, and no open sparks which may cause interference to electronic circuitry. The coils are usually packaged as plastic moulded items; cooling is achieved by the iron core which can be partially exposed from the casing (Bosch 1988). The plastic casing is more resistant to shocks and fatigue and allows a more compact design than metal clad conventional designs.

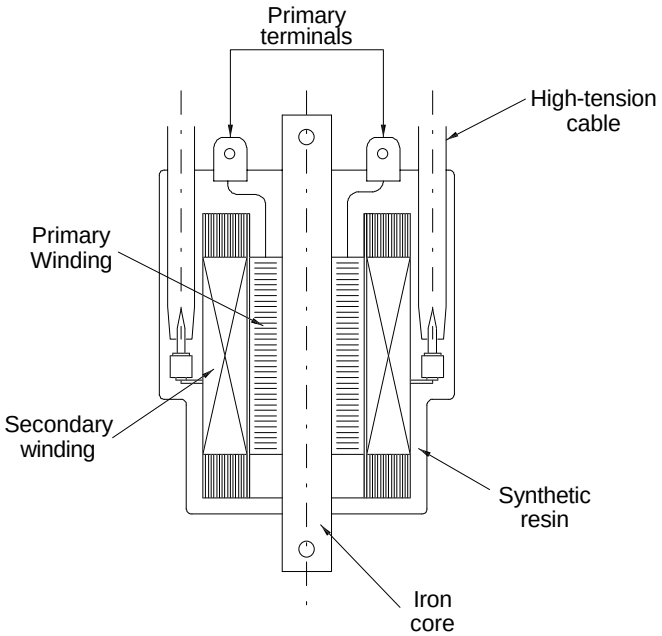

Figure 2.13 Double ended coil for use with a waste spark strategy (Adapted from Tranter)

A slightly higher voltage is required at the spark plug, this is due to additional energy being required for the spark to jump across two gaps, and also because one plug works with a reversed polarity and electrons being forced to migrate from a colder electrode. Wasted spark systems do not lend themselves to engines with odd numbers of cylinders, such as 3 or 5, or uneven firing intervals. In these applications of distributorless ignition, one or more wasted spark coils must be complemented by a single coil (Bosch 1988). Walker points out that the use of wasted spark and single coil systems can increase the number of sparks per unit time

since the coils have longer to charge, in the case of wasted spark systems, a factor equal to half the number of cylinders and in the case of single coils, a factor equal to the number of cylinders.

It should be noted that although the trend seems to be a move towards purely electrical systems high performance engines, such as those used in formula one racing, are not consistent on the system strategy. The Cosworth AC engine, of 1983 onwards, used a single distributor to fire eight cylinders, the Cosworth Zetec-R 3.5L V8 engine of 1994 used a waste spark system, the 3L V8 Cosworth ED of 1995 reverted to a double distributor but the 1992 Judd/Yamaha V10 engine was seen to use a *coil on plug* method. Meanwhile, in normal production engines, the Ford Zeta engine, found in Ford Escorts and the like in the early 1990s used a *wasted spark* system.

With high performance engines as an example, it should be noted that any benefits of a particular system may be offset by inherent disadvantages and that the spark distribution method is not seen as a constraint on performance.

The choice of an ignition transformer to suit the ignition system is considered by the author to be a critical factor in ignition system optimisation, although in practice the subject seems to lack the attention which it deserves. Many factors must be considered when making a coil choice, these include turns ratio, physical size, inductance and internal resistance.

2.9 Sparking plugs

2.9.1 Heat range

The working temperature of a spark plug is critical to the operation of the engine. The optimum temperature range for spark plug operation is between 400 and 800°C. If the spark plug tip is too hot then increased wear, increased oxide deposition and uncontrollable surface ignition will occur. If the spark plug is too cold, combustion products may become condensed on the plug electrodes, thereby shielding the surfaces, increasing the plug resistance and preventing the initiation of a plasma column. Surface ignition will lead to higher in-cylinder temperatures and possible engine damage as a consequence. The property of the spark plug which dictates the temperature is the heat range. A cold (or hard) sparking plug has a higher heat transfer rate to the surroundings, a hot (or soft) spark plug has a lower heat transfer rate. The heat range criterion is usually met by increasing the surface area of contact between the insulator and plug body and the length of the thermal path, shown in Figure 2.14.

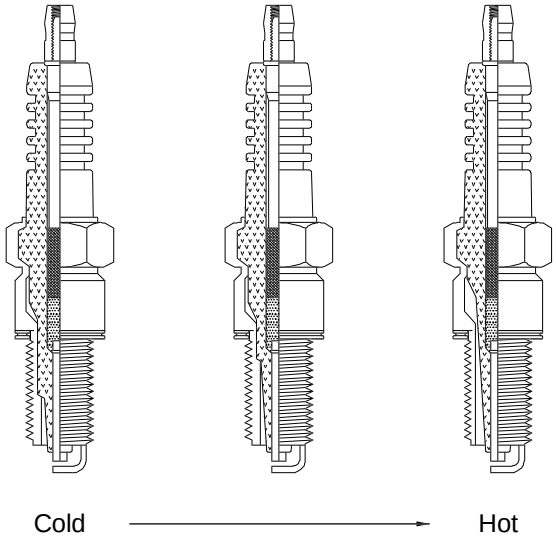

Figure 2.14 Examples of spark plug construction to achieve correct heat range (developed from Bosch (1988))

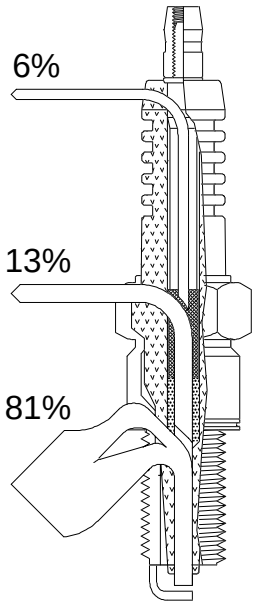

Figure 2.15 Thermal conduction in the spark plug (developed from Bosch (1988))

The heat conduction path can be seen from Figure 2.15, 81% of the heat is transferred by conduction to the cylinder head, through the close fitting spark threads. About 13% of the heat is transferred through the insulator to the shell and then to the atmosphere, the remaining 6% through the insulator and also to the atmosphere.

2.9.2 Electrode material and type

The electrode material, as discussed previously, is usually a nickel alloy and can be complemented with a copper core to enhance heat transfer properties. Other common materials for centre electrodes include platinum, gold, palladium and other precious metals which prove

to be more wear resistant and allow thinner electrodes for the same erosion characteristics. The precious electrode materials also resist oxidation and pick up fewer deposits (Arkless 1992). Currently, the best available material for electrodes is Iridium, with a high melting point and superior high temperature oxidation resistance (Nishio et al. 1993). This allows thinner centre electrodes to be used with an increased field intensity, which results in a lower breakdown voltage (Pischinger and Heywood 1990). Erosion resistance can be improved further by the dispersion of earth metal oxides in the electrode surface. It has been shown that reducing the length of the earth electrode results in a lower breakdown voltage (Bell 1983), this is due to an increase in field intensity, but a decrease in plug life is expected unless suitable materials have been chosen, such as those described above.

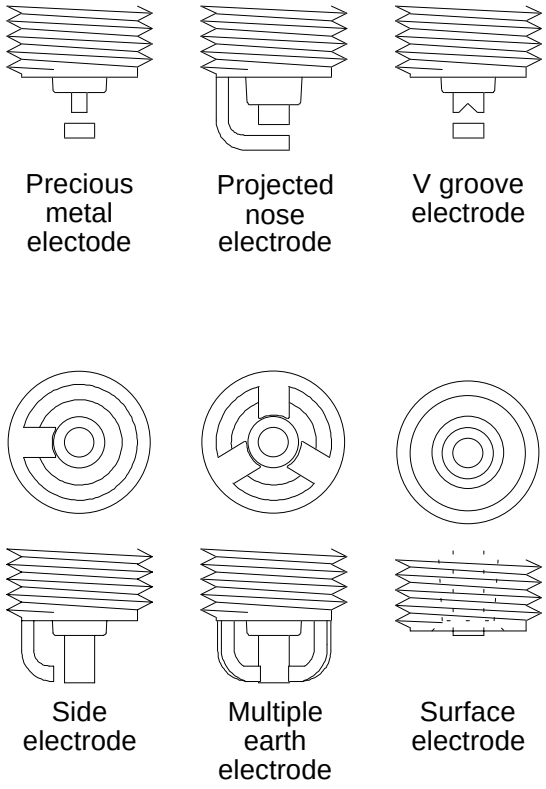

Figure 2.16 Spark plug electrode types (NGK)

The type and configuration of electrodes allow for different service conditions. Multiple earth and surface electrodes allow longer life, at the expense of cost, and are used in very high temperature situations such as rotary engines where electrode erosion is a problem. The surface electrode sparking plugs were designed to be used with CDI ignition systems, they concentrate the flame initiation at the cooler surfaces of the plug (Black 1986). Due to ignition taking place in a relatively calm atmosphere towards the edge of the combustion chamber, shielded from the majority of the turbulence, fuel and ash deposits collect readily and result in plug fouling (Bell 1983). Current formula one racing engines use semi-surface gap plugs, where the spark path is exposed to charge movement, which are powered by high energy CD ignition systems (approximately 75 mJ) (Arkless 1992).

The increase in the number of earth electrodes or plug volume interfering with the flame kernel development results in a higher probability of flame quenching at highly diluted conditions. This renders these types of plug unsuitable for lean mixture operation, even though longer life results from the increased electrode area.

V-grooved spark plugs are claimed to reduce the flame quenching effects of normal electrodes by initiating the spark at the edge of the electrode, and inducing flame growth away from the plug itself. This type of electrode has been claimed to reduce misfire in highly diluted mixtures allowing engine idle at substantially leaner air-fuel ratios than conventional electrode plugs for the same ignition probability (Hood 1990). The V-grooved plugs are also said to exhibit superior anti-fouling characteristics.

Thinner electrodes, as discussed above, allow breakdown to occur at a lower voltage due to the increase in field strength. When the plug is new and sharp edges are present on the electrodes, the breakdown voltage is less sensitive to electrode diameter (Nishio et al. 1993). As the plug erodes the thinner diameter can be beneficial to the breakdown process. Thinner electrodes have also been shown to extend the limit of lean operation (Pischinger and Heywood 1990a).

Projected nose plugs are characterised by a longer insulator and centre electrode. This allows a cooler centre electrode at high load due to the projection into the fresh incoming charge and an electrode which can reach its operating temperature quickly under conditions of high charge dilution. The drawback of this plug type is that the electrode is also more exposed to the hot gases and may be more prone to failure through thermal fatigue.

Experiments by Anderson and Asik (1983) on a running engine have shown that semi-surface gap and multiple ground electrode plugs can improve performance when running in the lean mixture region. The coefficient of variance (COV), in terms of peak pressure, was reduced by up to 19% and the 0-10% burn time was reduced by approximately 5%. This contradicts what one might suspect, since the multiple electrode plug has a higher obstructive volume which may interfere with the flame kernel growth. Anderson and Asik (1983) also found that a plug of correct reach, i.e. one that used the full length of the spark plug hole, was superior to one that was essentially recessed. The reasons for this were that the recession obstructed the early growth, and resulted in increased heat transfer, as will be discussed in section 2.13.2.

The size of the gap between the two electrodes can have a significant effect on engine performance. With an increased gap, the flame kernel is allowed to grow to a greater size

before the kernel contacts the electrodes and quenching occurs. The greater width also allows a larger volume of charge to be locally dissociated and hence increases the ignition probability.

2.9.3 Spark plug fouling and methods of reduction

Spark plugs are very susceptible to fouling, which will allow the ignition current to reach earth by means of a weak or shielded arc. The spark plug becomes most vulnerable to fouling as the heat range tends to the cold end. Cold spark plugs are favoured in two stroke engines, where twice as many combustion cycles take place with little cooling of the insulator nose; flexible fuel vehicles, where an engine may be expected to run on two types of fuel with the same ignition system; and higher compression ratio engines where combustion chamber temperatures are higher. Fouling is most likely to occur at low load and idle, especially in cold conditions. The deposits, normally of carbon, condense on the overcooled insulator and electrode, since in this case the plug is unable to attain its self cleaning temperature. Different electrode materials have been shown to have no effect on this process, which results in rough low load and idle performance.

The fouling mechanism is the consequence of accumulated carbon deposits on the insulator nose, these deposits allow the current to leak away before the breakdown voltage can be attained. Arcs have been observed to form in the cavity between the plug shell and the insulator nose, a pocket where ignitability is poor since the volume is occupied predominantly by residual gases.

The theory of fouled sparking plugs was investigated by Mogi et al. (1992) using an artificially fouled plug. Low load and transient performance were both seen to suffer. It was also observed that the spark duration was up to 25% shorter when mis-sparking occurred. The resistance along the insulator was measured and found to vary non-linearly, and a critical resistance was noted. As the fouling increased, the spark duration became shorter and eventually no spark would be seen - the current passing directly via the fouling to the plug shell. In this case, the effect of fouling can be reduced by decreasing the amount of carbon present, or increasing the cavity gap between the insulator and the plug shell. The latter cure will still result in the absence of a spark given enough deposition.

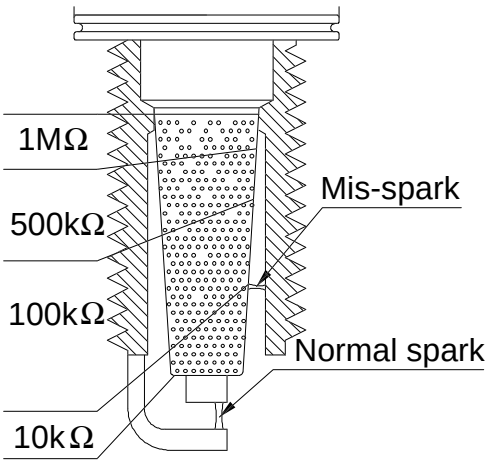

Figure 2.17 Fouled spark plug insulator showing representative electrode to insulator resistances and spark types (adapted from Mogi et al. (1992))

Whether or not fouling will prevent the occurrence of a spark, has been shown to be sensitive to the rate of change of spark voltage, but insensitive to the maximum spark voltage itself. A spark occurring in the cavity is the result of the voltage across the insulator and plug shell reaching breakdown conditions before that of the electrode gap. The CDI type of ignition system is characterised by its very fast voltage rise, and this allows breakdown conditions to be met at the electrode gap before current can leak away to the cavity, even though the breakdown voltage in the cavity may be a lot lower.

Currently the CDI system has the fastest voltage rise time (although the use of booster gaps can result in improvements), a factor which must be improved to reduce the effects of plug fouling. Mogi et al. (1992) investigated the use of a series gap in the HT side of the ignition system. The series gap was to act as a high speed switch which was activated when the characteristic breakdown voltage had been reached. The series gap was found to result in a very fast voltage rise at the spark plug electrodes, with a 15kV breakdown occurring within 50ns, this compared to 40μs with the same battery and coil system without the gap.

It was found that if the series gap voltage was too small then the electrode voltage would have a very high initial voltage rise, to the same level as the series voltage, but continue with a slow change. In this mode mis-sparking may still occur. The upper limit on the series gap voltage is that of the coil insulation, the breakdown gap is therefore constrained by these limits. The series gap should be designed to have the lowest energy loss possible, and have a low electrode erosion rate. For the latter constraint, the electrodes are best contained in an inert atmosphere where oxidation is eliminated. Mogi et al. also noted that the best results with a series gap were obtained when sited nearer to the plug. With this last factor in mind Toyota Motor Co produced a series gap, HT spark plug cap.

2.9.4 Wear mechanisms

Wear mechanisms of the spark plug lead to excessive electrode gap widening, this is the major cause of spark plug failure on natural gas engines (Klimstra and Overmars 1991). A survey of natural gas spark plug life in 3000 engines was conducted, and the findings showed plug failure occurring between 200 and 5000 hours, although the type of electrode material was not shown. Two types of wear mechanism are believed to exist, these are the erosion mechanism and the corrosion mechanism.

2.9.4.1 Erosion

Electrode erosion is caused by the initiation and interaction of the arc with the metallic surfaces. During the capacitive component of the discharge (the breakdown mode) erosion occurs at the electrode edge, whereas during the inductive component (the glow and arc discharges) erosion occurs at the centre producing a hollow. The capacitive component may be reduced by using a series resistance; this results in a slightly longer breakdown phase and less radio frequency interference (RFI). If the series resistance increases greater than a few MΩs the inductive component increases with a concomitant effect on the erosion volume.

Three theories of erosion are postulated, these are *particle ejection*, *oxide removal* (Young and Grimes 1978) and *sputtering* (Nishio et al. 1993). Particle ejection occurs when anions produced in the gas bombard the centre electrode with high kinetic energy, this is then converted to thermal energy and causes a local melting zone where particles are ejected (Nishio et al. 1993). Scanning electron microscope micrographs show craters and ejected particles; the craters being sub micron to 10 microns in size, and the particles ranging from sub micron to 5 microns in size. Ejected particles take the form of metallic particles or vapour (Young and Grimes 1978).

Oxide removal is the primary erosion mechanism when using leaded fuel. It concerns the removal of a layer of base metal oxides, of thickness 25-125μm, which are consistently found on eroded lips. Any oxide must be removed before any other erosion mechanism can exist. Copper cored electrodes have been shown to have a lower erosion rate, and this is believed to be because of the higher heat transfer properties, and hence lower electrode temperatures which result in less oxidation. Gold electrodes are not prone to erosion, even near to their melting point, since for inert metals oxidation is severely reduced if not eliminated. Even so, there is no recorded explanation for how the oxide is removed.

Sputtering occurs during the arc and glow discharge phases, when incident ions displace atoms out of the electrode surface. The kinetic energy from these accelerated gaseous anions is

changed to break the bond energies in target atoms during elastic or inelastic collisions. These target atoms are then ejected from the surface.

Nishio et al. (1993) showed that high melting point electrode materials exhibited lower erosion characteristics when rig tested at high pressures and room temperature. When the same test was carried out in an engine, erosion was increased due to the higher temperatures and oxidation properties of the material.

2.9.4.2 Corrosion

Corrosion effects are caused by the interaction of the gaseous medium with the electrode material at high temperatures. As discussed above, the effects of temperature on the electrode material increase the wear rate. This is due to oxidation of the material. Tungsten, a high melting point metal, was shown by Nishio et al. (1993) to exhibit superior erosion properties at room temperature, yet when tested in an engine environment its oxidation resistance was seen to be very poor. On the other hand, platinum has a high oxidation resistance but a low melting point, even so, the wear characteristics in an engine surpassed that of tungsten. High electrode thermal conductivity is desirable, so as to keep the electrode surfaces as cool as possible, thus reducing the amount of oxidation.

Young and Grimes (1978) suggested that electrode materials should be resistant to corrosion, have a high boiling point and have a high thermal conductivity, these factors should result in a long service life. They also showed that depending upon the electrode material, a different mechanism of erosion would be dominant. The platinum central electrode was found to erode at the centre, and therefore it was postulated that particle ejection was the more important mechanism. Nickel electrodes were found to be eroded by chemical reaction, with the formation of base metal oxides at the grain boundaries. This oxide then was thought to react with fuel residues to form a non-protective compound. In the absence of combustion, nickel electrodes were found to erode by the ejection of the oxide layer which was formed on the electrode surface. Interestingly, Young and Grimes (1978) noted that an automobile fitted with a CDI system displayed a significantly lower electrical erosion characteristic compared to a similar vehicle fitted with a TCI system. This is due to the differences in discharge modes, the TCI system energy manifesting itself in the glow phase, with the CDI system operating predominantly in the breakdown and arc phases. This erosion characteristic was also noted by SAAB (Granlund 1986) with the SAAB direct ignition system described in section 2.5.

For maximum spark plug life, thick cool electrodes are favoured, whereas for good ignition, minimum flame quenching, small hot electrodes with a high spark energy are favoured. The

use of lean burn combustion strategies requires a higher spark energy which leads to increased erosion.

Driver circuit	Gap length (mm)	Supplied energy (mJ)	Erosion per 10^6 discharges ($g \times 10^{-4}$)	($g/mJ \times 10^{-6}$)
TCI	0.5	33	0.89	2.7
	1.0	37	1.29	3.5
	2.0	41	1.43	3.5
CDI	0.5	1.6	0.25	15.6
	1.0	1.76	0.32	18.2
	2.0	1.17	0.29	24.8
CDI + arc	0.5	185	333	180
V_{arc} = 100V	1.0	115	242	210
τ_{arc} = 100µs	2.0	67	150	223
CDI + arc	0.5	278	467	168
V_{arc} = 200V	1.0	225	442	196
τ_{arc} = 100µs	2.0	236	483	204
VFZ	0.5	40	6.4	16
20kV	2.0	40	4.8	12
Breakdown	4.0	40	1.3	3.3

Table 2-1 Cathode wear rates for different ignition driver circuits (Maly 1984)

The wear rate of spark plugs in response to the gap width attracts conflicting views. As the gap grows, the breakdown voltage increases, causing more energy dissipation in the early part of the spark. The breakdown and arc energy is therefore increased, and the glow discharge period shortened, this should reduce electrode wear by using more efficient discharge modes (Klimstra and Overmars 1991). Maly (1984) shows this not to be true, although all work was carried out in atmospheric conditions. The relation of discharge efficiency to electrode wear is probably a misunderstanding in many authors' work, since the work of Maly (1984) shows that the most efficient discharge modes (breakdown and arc) result in higher erosion rates than for similar systems exploiting the longer glow discharge when using the same ignition energy.

2.10 Ignition system and spark plug efficiency

Due to a series of losses, only a fraction of the supplied electrical energy is transferred to the medium in the gap. Most of the energy loss in the igniter is dissipated in the electrodes where heating occurs, but a proportion is lost in the ignition driver circuit itself, especially the ignition transformer. At the igniter, the energy is transferred by three mechanisms: heating of the electrodes, radiative heat transfer, and deposition in the gas. The last mechanism can allow the heat to return to the electrodes after heat transfer to the gas. A study to evaluate the efficiencies of various ignition strategies could lead to reduced igniter wear, and hence reduce the need for preventative maintenance.

Calorimetry methods have been used to evaluate spark plug efficiencies, based upon pressure rise within a chamber compared to the energy input; other methods exist, such as a measure of igniter temperature after a course of firings. To try and emulate the conditions of an engine cylinder, the calorimetry tests are best carried out at high pressure and the resulting energy is measured in terms of the vessel pressure rise. Since this rise is very low (30μbar for an energy dissipation of 45mJ) a differential pressure transducer should be used in a two part chamber, one side being at the reference pressure, the other being subjected to the effects of the spark discharge. The energy dissipated in the capacitance (≈5pF) of the spark plug is normally neglected, being as low as 1% of the total value. The higher the calorimeter pressure, the more chance of leakage, which will cast doubt on the results.

From work done at atmospheric pressure, Stone and Steele (1989) found that the conversion efficiency from electrical energy to thermodynamic work was increased with the size of the spark gap. This was postulated to be a result of a lower heat transfer to the electrodes. The gap was increased in size up to 2.4mm at which point the gap became unrealistic as an ignition device, since the centre electrode coverage was reduced. The maximum efficiency with this gap size was found to be approximately 10%. It was also found that efficiency was increased by decreasing the dwell, or coil charging, period. In this case inefficiencies might be due to the discharge mode entering the *glow* regime where a cold cathode results in poor energy conversion. Electrical conversion efficiency of the transformer, or coil, was also seen to deteriorate with an increase in charging time, typical values being between 40 and 60%.

Engine tests by Stone and Steele showed that a 0.75mm spark gap was the optimum as far as cyclic dispersion and specific fuel consumption were concerned, increasing the gap beyond this figure yielded no increase in performance. The dwell time became important when the spark gap was reduced below 0.6mm where a longer period became beneficial. In practise the spark gap will be limited by the risk of an external breakdown inside the coil.

Teets and Sell (1988) used a similar calorimeter at elevated pressures and obtained similar results. Three different non-resistor commercial spark plugs, a platinum electrode plug, a thin titanium electrode plug and a plasma igniter were used for the study. For the spark plugs a coil was used with a stored energy of 50mJ.

The results of Teets and Sell (1988) showed that as the pressure increases, so too does the conversion efficiency, and a further increase can be gained at the higher pressures by using larger spark gaps, as noted by Stone and Steele (1989). A drop in efficiency was experienced with an increase in spark energy. Teets and Sell (1988) also noted that the conversion efficiency was independent of electrode material, although it was found that increasing the electrode surface area was more detrimental than using a higher thermally conductive material. Igniter efficiency increased when the working fluid was changed from air to methane, but was decreased when argon was used; the use of nitrogen yielded similar results to air. Previous work documented by Blair (1978) has shown that the breakdown voltage in argon is less than 33% of the figure when using air implying a complex relationship between gas composition and igniter efficiency. It is believed that the argon present in the air allows more effective breakdown characteristics (Motorcraft 1994).

The plasma igniter proved to be less than half as efficient as the conventional spark plug for the same stored energy; 12% compared to 24% at 500mJ and 1 bar pressure. The work showed no relation between efficiency and cavity size.

A breakdown ignition system was briefly tested by Teets and Sell (1988), and the efficiency was increased, since the glow discharge mode was not exploited, resulting in lower heat transfer to the electrodes. Further investigation was not documented with this system.

In a real engine situation the spark plug electrodes would be at a higher temperature, and hence a lower heat transfer to the electrodes would be expected. Therefore calorimetry studies bear a resemblance to engine starting conditions where the electrode temperature is low and the in-cylinder turbulence is low if not non-existent. The study has shown that when the pressure is low, the igniter efficiency is also lower. This factor could mean an increase in cyclic dispersion at low load, and hence low cylinder pressures, such as throttled running where the added handicap of mixture dilution is present.

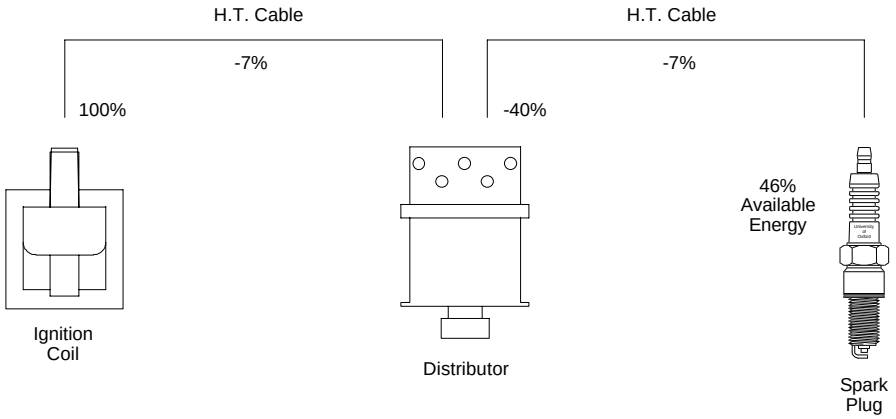

Figure 2.18 System losses using conventional HT ignition distributor system (Champion 1995b)

Higher efficiency igniters could allow inefficiencies to be tolerated elsewhere in the ignition system, for instance smaller and less efficient coils and driver circuits, for the same performance. System losses, according to Champion (1995b), can result in as little as 46% of the stored energy reaching the spark plug. The worst case is for a HT distributed system, shown in Figure 2.18, where two lengths of HT cable dissipate a total of 14% of the energy and the distributor a further 40%. With a wasted spark system, Figure 2.19, where two plugs are fired simultaneously in separate cylinders, one on the compression stroke, the other on the exhaust stroke, 61% of the stored energy is available for the ignition process. Up to 14% of the energy is dissipated in the HT cable and 25% is lost with the use of the additional spark gap.

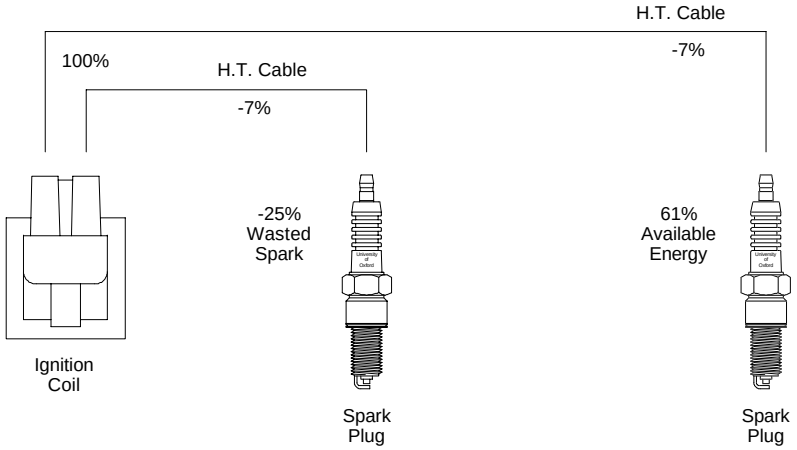

Figure 2.19 System losses using wasted spark ignition system (Champion 1995b)

The most efficient ignition distribution system is that of the coil-on-spark method, shown in Figure 2.20. In this situation, the electrical distribution is carried out at low voltage and the HT path is minimised by siting the coil as near to the spark plug as possible. This results in virtually a 100% energy transfer to the plug gap.

2.11 Spark plugs as diagnostic instruments

The use of a spark plug as a diagnostic instrument has been investigated, and in some cases commercially exploited, for use in engine control strategies (SAAB 1988). The plug is positioned at the theoretical centre of the flame kernel and is therefore a witness to the combustion process. With a suitable spark plug, many different measurements may be made without additional instruments which may influence the combustion process. The traditional method of combustion analysis is to use a pressure transducer mounted in the cylinder head. With new engine designs, the utilisation of such a transducer is prohibited by the lack of space with increases in valve area (this problem has led to the development of a smaller diameter spark plug (Kagawa and Kato 1989)). Pressure transducers for use with engine management systems have also been shown to be expensive and not very durable.

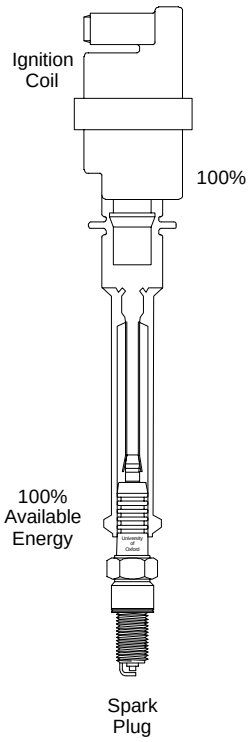

Figure 2.20 System losses using coil-on-spark ignition system (Champion 1995b)

The simplest measured quantity is that of HT voltage or current. The results of measurements may depict: the combustion history through the conductivity of ionised products, the state of insulator deposition through the measured leakage current, or other parameters through voltages and currents throughout the discharge modes.

Ionisation is generated by the oxidation of hydrocarbon fuels, due to small quantities of positive and negatively charged particles, and forms the basis of many hydrocarbon emissions

measurement strategies. Combustion derived ionisation is a function of many parameters, and the information gained cannot readily be interpreted except for the fact that combustion has occurred. Ionisation signals are at a maximum when burning a stoichiometric mixture. When running richer, a steady decrease occurs until the onset of sooting, at which point the signal falls very rapidly. The ionisation signal falls rapidly with time due to recombination of the charged particles, this suggests that measurements may be engine speed sensitive. The fuel type has also been seen to influence output signals. The degree of ionisation is measured by supplying an additional voltage source (DC) and measuring the current flow.

Leakage currents are a function of the insulator resistance and are used to measure plug fouling, and are again measured using the additional DC voltage source. Insulator resistance can decrease with deposition and fouling, especially when using leaded petrol. Fouling of the insulator has been seen to change the leakage current on a cycle by cycle basis. Leakage currents are best measured before combustion occurs, either at the start of each cycle on a time resolved basis or when the engine is stopped. Time resolved measurements can also yield information on knock (Blauhaut 1983), but with limited success.

Time resolved spark voltage and current measurements can be used to measure the breakdown voltage, which can give an indication of electrode spacing, and hence wear, and also characteristics in the later discharge modes can be used to predict flow parameters (Maly et al. 1983a) (Anderson and Kim 1995). The flow velocity has been shown to behave in a linear relationship with the measured glow or arc discharge voltage. This method of flow measurement is ideal for use on production engines, where the lack of optical access rules out the use of laser doppler velocimetry (LDV) (hot wire probes are limited to motored engine situations where temperatures do not exceed 600°C). The voltage measurement method of the flow field is known as Voltage Rise Anemometry (VRA) and is of use in both firing and motoring conditions. Nevertheless, problems do exist with changes in the in-cylinder gas composition and state, and this leads to uncertainties in the measurements.

Klimstra and Overmars (1991) used the electrical characteristics of the spark plug to estimate the spark gap during engine operation. The work showed that the gap length was linearly related to the breakdown voltage at constant conditions, i.e. constant air-fuel ratio and cylinder pressure at time of firing. For an operating engine it was concluded that a direct HT connection of any monitoring equipment was not feasible, due to the risk of connection failure. This led to the use of an induction coil positioned around the HT output, giving a voltage output corresponding to a change in current. A linear relationship was found to exist between the breakdown voltage and the induced voltage. Further tests showed the monitoring strategy was insensitive to mixture strength but was sensitive to cylinder pressure and therefore engine

load. A system was then designed to measure an average peak induced voltage at a reproducible condition, full load or idle.

Ion currents have also been successfully measured by using an additional spark plug electrode. Shimasaki et al. (1993) used these measurements to detect whether combustion had occurred. The data would then be used to measure the misfire frequency and alter fuelling or EGR to suit the engine condition. It was found that the ion current could only be measured after the spark had been initiated.

Optical spark plugs have been used for many years, such as the *colourtune system* used for setting the mixture at low load conditions on installed engines. Meyer et al. (1993) used an optical spark plug in association with a head gasket impregnated with ionisation probes. The system was applied directly to a production engine and was intended as a diagnostic tool for looking at the sources of unburned hydrocarbon emissions during engine warm up periods. The plug used 8 fibre optic cables mounted around the periphery of the centre electrode and insulator of an 8mm spark plug. This was then mounted in the body of a larger plug (14 or 18mm). In use, it was found that flame luminosity was very low at idle and highly diluted conditions, this needed an increase in the photo multiplier sensitivity, but this presented problems with the signal obtained during the initiation of the spark. The plug was used to look at the effects of tumble and swirl on flame growth for which data correlated well with the 0-2% heat release data.

Spark plugs may also be instrumented to measure temperature. Electrode and insulator temperature have been measured by spark plug manufacturers to determine plug suitability for continuous operation in the *self cleaning region*. The point at which measurement is carried out differs between manufacturers, Champion (1995a) measure the insulator tip temperature whereas NGK and Bosch measure the temperature at the tip of the centre electrode (NGK 1976)(Bosch 1985). Champion (1995a) argue that it is the insulator temperature that is important, since this is where the fouling occurs.

2.12 Electrical characteristics of arcs

An arc may only be formed in a gaseous medium if a sufficiently high voltage is applied. The electrical characteristics of an arc struck between two electrodes in a gaseous medium, can be described in four distinct modes. These are: the pre-breakdown mode, the breakdown mode, the arc-discharge mode and the glow-discharge mode. Work done by Maly (1984) has resulted in the following summary. Figure 2.21 depicts these modes with respect to time.

2.12.1 Pre-breakdown mode

Initially, the gas between the electrodes acts as a perfect insulator. As the potential difference increases across the gap to a high enough value, the gas becomes a conductor. The pre-breakdown phase is typically a few nanoseconds in duration (Maly 1984). As the spark pulse is applied, electrons existing in the gap are accelerated towards the anode. Once the voltage density has reached a high enough value, the free electrons have enough energy so that when they collide with gas molecules, they ionise the gas and create further free electrons.

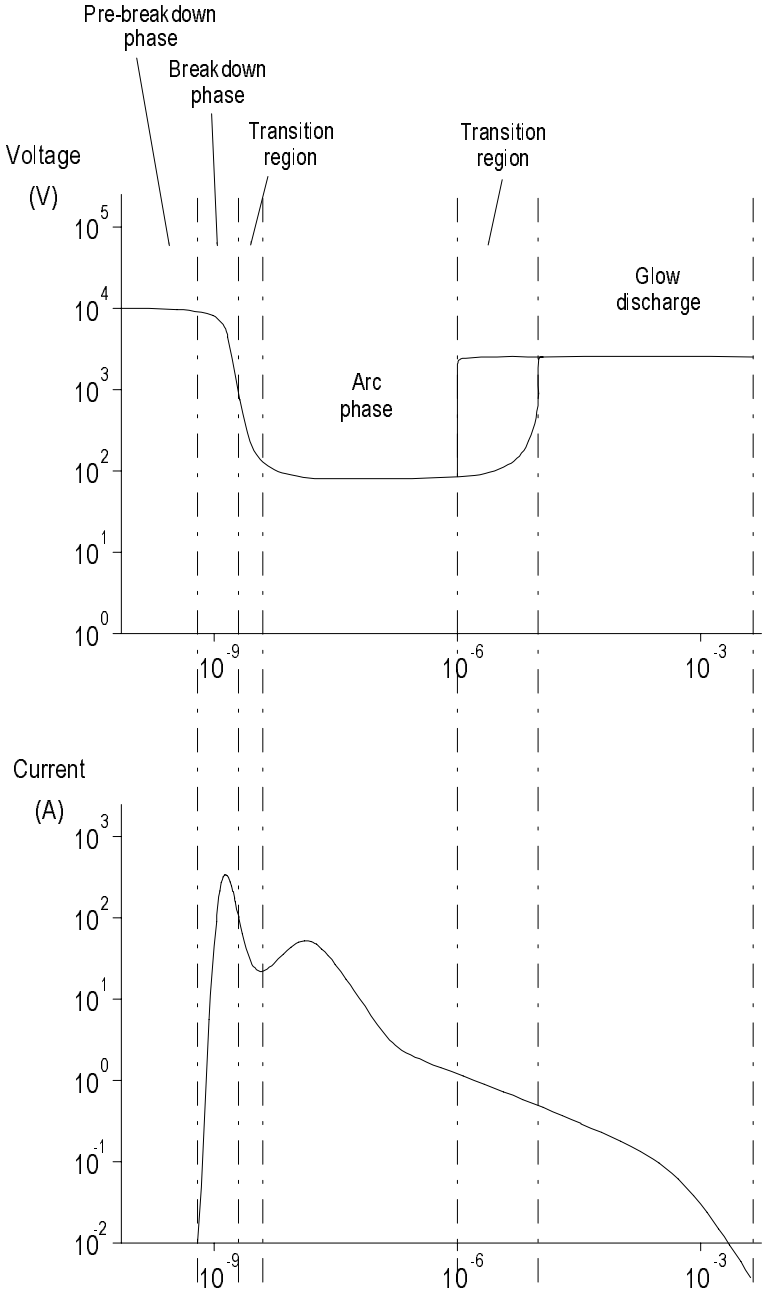

Figure 2.21 Electrical characteristics as a function of time during a spark discharge

Smaller electrode sparking plugs give a higher voltage density, allowing a more efficient breakdown. The newly formed electrons gain energy from the electric field and accelerate

towards the anode also. This mechanism continues and rapidly causes an electrode avalanche. As the anode collects the flowing electrons, new electrons at the cathode are generated, this is believed to occur by the action of UV radiation emitted from excited ions. At low pressures and small spark gaps, the UV radiation can reach the cathode directly to liberate electrons with minimal losses. As the gap size and pressure increases, the efficiency decreases since the UV radiation is absorbed by the surrounding gas.

The pre-breakdown phase is said to exist if fewer electrons are liberated than are needed to allow a self sustaining arc. This phase duration can last for minutes when systems with slow voltage rise times are used, very fast voltage rise systems with substantial over voltage capability, e.g. CDI systems, result in the phase being very short and very effective at ionising the gas. During this period, the gas temperatures within the spark gap are very close to the initial value and the high field strength is contained within an ionisation cloud.

2.12.2 Breakdown mode

The breakdown mode is said to occur when the gap voltage begins to reduce and the current begins to rise substantially. This occurs when enough feedback electrons are produced to facilitate an over exponential increase in current, which is assisted by the charge within the streamers. This type of discharge occurs at currents in excess of 10mA; the current is limited only by the impedance of the discharge and the immediate external circuit close to the gap, and can rise to 10-100A within a few nanoseconds. The voltage across the gap drops to around 100V with a field strength of 1kV/cm. The minimum energy needed to cause breakdown over a 1mm gap at atmospheric conditions is approximately 0.3mJ. Of all the streamers, the volume segment with slightly higher electrical conductivity becomes the major path for current. In this mode the ion density increases and the dominant energy loss from the accelerated electrons is the exchange of Coulomb forces between the electrons and ions.

A high degree of ionisation, electronic excitation and temperature rise occurs. A narrow cylindrical channel of approximately 40μm is formed in which all particles are fully dissociated and temperatures of around 60,000K exist. The channel pressure rises almost instantaneously to hundreds of bar and initiates a shock wave, which then expands at supersonic speed and begins to cool. All potential energy (that stored in the dissociation and ionisation of the gas) is gradually changed to thermal energy adding to the expansion.

Prolonged high current flow leads to thermionic emission from cathode hot spots. This characteristic signals the end of the breakdown phase; the end can also be signified by a drop in voltage to 10% of the breakdown voltage.

2.12.3 Arc discharge mode

An arc discharge requires high electrical conductivity to initiate it, currents of greater than 100mA are common, and are governed by external electrical impedances. This current rise is complemented by a fall in voltage to ≈100V, 30% of which is dissipated in sustaining the cathode hot spots. The arc cannot be sustained without these hot spots and these can lead to a loss of electrode material through evaporation. The erosion rates for arc discharges increase with electrode gap, since a higher voltage is required to allow electrical conduction. Prolonged contact of the plasma with the electrodes leads to serious heat losses by conduction

2.12.4 Glow discharge mode

Glow discharges are similar to arc discharges but exist with a cold cathode. Feedback electrons are liberated by ion impact which is a very inefficient method of supply. Due to the cold cathode, only low currents can be sustained. This type of discharge is common at low pressures, increased pressures compress the gas and will initiate the arc regime. If the current manages to increase above 100mA the arc regime will be initiated due to the formation of cathode hot spots. The voltage increases to allow an increase in electron emission.

Erosion rates are low in this mode since the cathode is cold, the dominant mechanism being sputtering (see section 2.9.4), the rate of which is determined by the product of the time and current flow. The efficiency of the discharge is listed as approximately 30%, the losses are due to heating of the electrodes. This low efficiency is believed to increase the wear rates of the electrodes (Klimstra and Overmars 1991) which contradicts the cold electrode theory.

Glow discharges are long and are very sensitive to flow field effects where the arc can be stretched or even swept away. More electrons can be generated to allow for the increase in channel length. Under high flow regimes the voltage needed to sustain a stretched arc may exceed that needed to initiate a fresh arc. In these cases the re-striking voltage is quite low, 2-3kV, since electrons and ions are available at the cathode surface. The original discharge is interrupted by the successive birth of new channels by lower breakdown voltages. These are similar in nature to the plasma formed in the breakdown/arc transition region and are less efficient than the ones they replace, because the energy is carried by many small conductors although most of the energy is still carried by the oldest stream. The discharge lengths may grow to twenty times the gap length before re-striking occurs (Maly 1984).

2.12.5 Voltage drops across the gap in the Arc and Glow discharge regimes

Although there are voltage drops throughout an ignition system due to resistances of the various components, the majority of the voltage drop is across the spark gap itself. Three discrete regions are considered to exist, shown in Figure 2.22, the cathode fall, the positive

column voltage and the anode fall (Cobine 1958) (although many other minor regions are present).

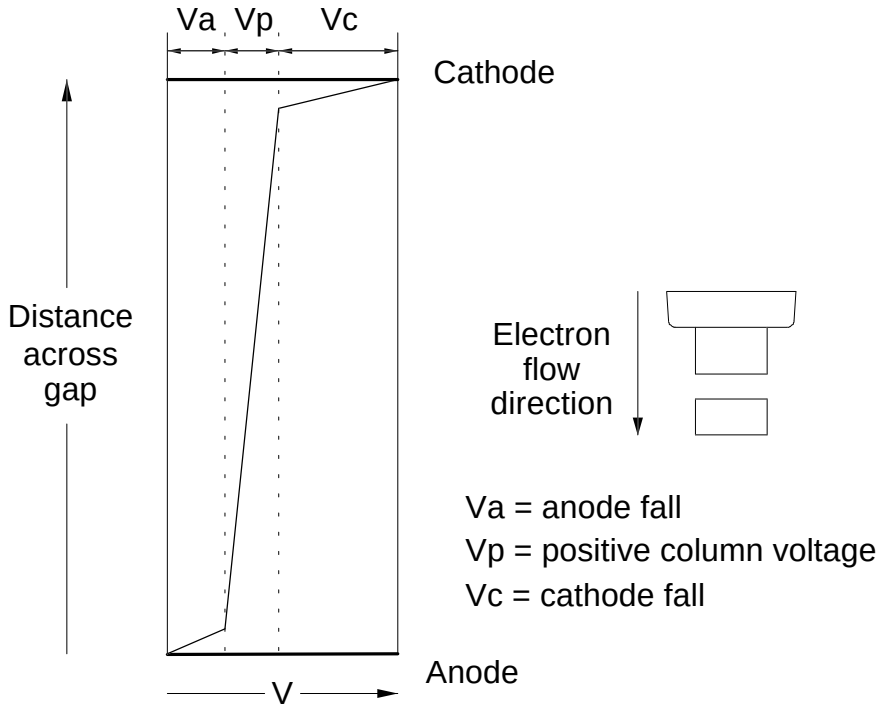

Figure 2.22 The three main voltage drops associated with a glow discharge

2.12.5.1 Cathode fall

The cathode fall is the highest voltage drop associated with the glow discharge since this is where the electrons are emitted. Cobine (1958) gives a relationship for the cathode fall for both arc and glow discharge modes.

For the cathode fall in a normal glow discharge:

$$V_c = \frac{3B}{A} \ln\left(1 + \frac{1}{\gamma}\right)$$

where	V_c is the cathode fall	(volts)
	B is a constant dependent upon the gas	(volts/cm/mmHg)
	A is a constant dependent upon the gas	(volts/cm/mmHg)
	γ is the electron emission constant	(dependent upon gas and electrode material)

It is interesting to note that Cobine (1958) uses two constants to describe the gas property (A and B), when one would suffice. The units of A and B cancel to make the cathode fall appear to be insensitive to pressure, although there seems to be no treatment of the effects of temperature.

For air and nickel electrodes in the normal glow discharge;
A=14.6
B=365
γ=0.036

this results in a cathode fall of 252 volts.

The cathode fall for the arc phase is very low, in the range of 8 to 12 volts. These values are small due to the temperature of the electrode surfaces, since the arc phase induces cathode hot spots and therefore lowers the voltage drop between the electrode and the gas, allowing electrons to be liberated through thermionic emission.

2.12.5.2 Anode fall

The anode fall in a normal glow discharge is similar to that in the arc phase, no relationships could be found by the author, although an estimate by Cobine places the value between 2 and 10 volts (although not documented for nickel electrodes, this value is similar for copper, carbon and iron electrodes) which is very much smaller than the cathode fall.

These results should be treated with caution, the term *normal glow discharge* refers to a glow discharge at a pressure close to atmospheric in air; this study is concerned with discharges at pressures as high as 12 bar and hence these relationships may fail to hold. Relationships such as those described by Cobine (1958) are perhaps more applicable to low pressure or vacuum applications.

Anderson and Kim (1995) used a different relationship for calculating the anode fall, referencing Cobine (1958), the relationship below was adopted:

$$V_a = V_1 + \phi$$

where V_1 is a constant (13.6V)
ϕ is the work function of the electrode material

2.12.5.3 Calculation of the positive column voltage

The positive column voltage is calculated by subtracting the cathode and anode falls from the measured voltage drop across the plug. The anode and cathode falls are considered to be constant throughout the glow discharge phase, this yields the following equation:

$$V_{pc} = V - (V_a + V_c)$$

or for nickel electrodes in air

$$V_{pc} = V - 262$$

If a resistive plug is used, the voltage drop across the internal resistance would also need to be considered.

2.13 The ignition process

2.13.1 Flow field effects

As discussed in section 5.4, as the flow field can be influential on the arc shape during long discharges. This characteristic forms the basis of the VRA system exploited by Maly et al. (1983a), where the flow field may be evaluated by the voltage history recorded during the glow discharge period.

In conditions of adverse flow, the ionised column of gas between the electrodes can be swept away, and as the required voltage to sustain the arc rises above that needed to initiate a fresh arc, re-striking occurs. In these situations the breakdown voltage is a lot lower since ions exist close to the electrode surfaces. It has been postulated that this phenomenon is responsible for severe electrode erosion occurring towards the edge of the electrodes.

Halldin (1992) conducted experiments using LDA techniques applied to a spark plug subjected to a flowing mixture in a perspex tube. Three flow conditions were investigated, each with the earth electrode positioned both upstream and downstream of the flow direction. The flow conditions consisted of a high mean velocity with a low turbulence intensity, a medium flow velocity and a medium turbulence intensity, and a low flow velocity with a high turbulence intensity. The third flow condition was believed to be representative of a fast burn combustion system, where the high turbulence is acknowledged to be instrumental during early flame kernel growth. It is also acknowledged that for the best ignition, and early flame kernel growth, the mean velocity should tend to zero, although other studies (Pischinger and Heywood 1990a, 1990b, Sher et al. 1991) show that to minimise heat transfer to electrodes a small flow must be present. In Halldin's work, the turbulence and mean flow velocities were altered by introducing a semi-circular obstruction upstream of the spark plug, the magnitudes of which were determined by the distance of the obstruction from the plug. All measurements were made at ambient conditions; these were argued to be representative of engine starting conditions where the probability of misfire is at a maximum.

All measurements of the flow velocity were made on a horizontal plane corresponding to the centre of the spark plug gap. Halldin (1992) concluded that the orientation of the spark plug electrode was important, when considering the flow field within a spark plug radius of the gap. Measurements across the width of the gap showed no large velocity gradients, therefore the boundary layer is believed to be much smaller than the gap itself.

Using a spark plug in a pressurised flow rig, Weyl (1993) showed that the spark duration was shortened by the presence of flow. This was thought to be because a small amount of re-striking had occurred, and therefore more energy had been wasted to provide additional breakdowns. The initial breakdown voltage, breakdown energy and peak current were found to be unchanged. This is due to the breakdown process occurring in a very short time compared to the subsequent discharge modes, and hence the flow of gas in the ion channel is less significant. The maximum voltage during the arc/glow phase was increased with increasing flow velocity, this is because the ionised gas column is stretched, and hence a longer and more resistive path, for the current to flow, exists. Weyl also noted that the use of increased spark

gaps, made the ignition system more susceptible to flow variations. The spark plug orientation was shown to be important, a crossflow position (see Figure 2.23) was more likely to be affected by flow velocity, since re-striking was seen to occur late in the discharge. The breakdown phase was however insensitive to plug orientation.

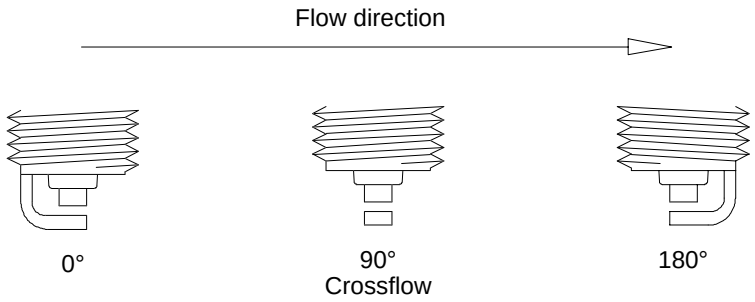

Figure 2.23 Electrode orientations with respect to flow direction

Zeigler et al. (1986) used a constant flow of flammable mixture to evaluate the early flame kernel growth with different spark plug electrode orientations. All tests were carried out at atmospheric pressure and high speed photography was used to monitor the flame growth. Three different spark plugs were used for the work, two types of Bosch and one type of Champion brand. One of the Bosch plugs was a platinum electrode type. The results showed that flame growth was fastest when the flow field acted across the central electrode, i.e. with the earth electrode at 90° to the flow. When the earth electrode is positioned at 180° to the flow, the flame growth was constrained due to quenching by the relatively cool metal. The spark characteristic was also shown and at an electrode orientation of 90°, multiple re-striking could be seen. This shows that flow fields are beneficial for flame growth but not for electrical discharges.

The 90° orientation of the earth electrode extended the lean limit, and the use of thin electrodes with this orientation made an additional small improvement. An optimum gas flow velocity was shown to exist at lean conditions for each of the electrode orientations. When positioned at 90°, the optimum flow velocity was found to be 5m/s, faster velocities than this increased turbulent heat transfer at the kernel surface and hampered flame growth. With the electrode in the 180° orientation, the flame growth was much less sensitive to the flow velocity.

Zeigler et al. (1986) continued the tests with an engine and this showed similar results to the previous tests at ambient conditions. The tests concluded that the ground electrode orientation is important to reduce quenching, and it was also found that the flow velocity is more important than the plug type when the lean limit is concerned.

Experiments by Anderson and Asik (1983) showed that the cyclic dispersion was reduced by up to 30%, when the ignition source was sited directly downstream from the inlet valve in the direction of swirl. A reduction in early burn time was also noticed. With the plug in the opposite position, i.e. directly upstream of the exhaust valve, it was postulated that the presence of residuals influenced the combustion process. It was also shown that exposing the electrode orientation in a crossflow manner to the swirl direction resulted in a minor improvement in combustion stability. This was thought to be mainly due to the reduction in turbulence caused by the earth electrode when positioned either upstream or downstream of the central electrode. It is well known that after the *ignition delay* or *flame development period* (the 0-10% burn time), the use of turbulence is beneficial for increasing flame propagation. The mechanism works by inducing a wrinkling effect to the flame front and therefore increasing the area. Turbulence can however result in increased heat transfer from an early developing flame front.

Arcoumanis and Bae (1992) showed that under turbulent conditions in a combustion bomb, the ignition process becomes insensitive to ignition circuit type, i.e. CDI and TCI systems give the same results concerning the lean misfire limit. This work showed the sensitivity of ignition to the spark plug orientation. With the earth electrode upstream to the flow direction, a wake is formed and acts as a flame holder, increasing the heat loss to the electrodes. This resulted in a slower 0-10% burn time. When higher flow velocities were used, with the earth electrode in this position, the lean limit was reduced due to an increase in the wake effect.

Ujiie (1994) used the upper cylinder of a motored engine to supply four nozzles, mounted radially in an optical access constant volume bomb. Turbulence was created by the collision of the four jets of gas, in this case a premixed propane-air mixture. The nozzle velocities were altered so as to achieve no mean velocity, and the turbulence was controlled by the engine motoring speed. The four jet velocities were measured by the use of LDA techniques. Using an ignition system based on a breakdown circuit, with additional supplementary spark duration circuitry, the minimum ignition energy, for 50% ignitability, was measured as a function of turbulence intensity. Stainless steel electrodes, of diameter 1mm, were used to provide the ignition source. High speed photography showed a stationary flame centre due to there being no mean velocity component. With a breakdown spark only, the early flame growth (up to 20μs) was seen to be insensitive to the mixture motion and followed the toroidal shape seen with ignition in quiescent conditions. After this initial period, the kernel diverged from the toroidal shape and showed increased surface distortion whilst expanding normal to the electrode axis. When the breakdown spark was complemented by a supplementary voltage supply, a healthier flame kernel was seen to develop. The minimum ignition energy was seen to increase with

increasing turbulence intensity, although the inclusion of a supplementary ignition component reduced the total minimum ignition energy.

2.13.2 Heat transfer effects

The electrodes of a spark plug may act as a heat sink, dissipating energy which could otherwise be used to generate reactive radicals.

Work by Pischinger and Heywood (1990a) attempted to measure the heat transfer to the spark plug electrodes by using high speed photography in the MIT square pistoned engine. Two types of spark plug were used, one was a standard Bosch W8DC item, the other a modified plug of the same type with thinner electrodes. A transistorised coil ignition system was used, of energy 160mJ, which was representative of current automotive trends. The high speed Schlieren film was used to enable tracing of the flame boundaries. Heat losses were calculated by measuring the contact area of the flame front with the electrodes. The results showed that the thinner electrodes gave a reduction in the MBT ignition timing and extended the lean limit. It was shown that the plug orientation was important, with the worst engine performance occurring when the flame kernel was blown onto the earth electrode. More slower burning cycles existed with the thick electrode spark plugs, and it was seen that faster burning cycles occurred when the flame kernel was swept away from the electrodes. When in contact with the electrodes, the flame kernel was reduced in volume, this happened to a lesser extent with the thin electrodes since the contact volume was reduced. Pischinger and Heywood (1990a, 1990b) went on to develop a model for the electrode heat transfer mechanism. Without any high speed film this model is of little use, since it relies upon detailed knowledge of flame boundaries. It was pointed out that the experimental thin electrode spark plug would have a far shorter service life for the same electrode material. A misfire criterion was developed which postulated that when the heat transferred by the spark plug electrodes increased beyond the heat liberated during the combustion reactions, the flame will be quenched. Work carried out by Sher et al. (1991) suggested that near to the ignition limit, heat losses can affect the flame growth significantly and hence the cyclic dispersion. Misfire was said to be minimised when the flame was convected away from the electrodes, because heat transfer was minimised.

2.13.3 Effects of ignition power

In a conventional ignition system, i.e. one where the coil acts as the energy storage facility, an increase in energy results in an increase in discharge time since it takes longer for the coil current to drop to a low value below which the arc cannot be sustained. With systems where the secondary voltage and current are formed by the establishment of a magnetic field, increases in the stored energy do not necessarily manifest themselves towards the end of the discharge. If the voltage rise is very fast, as with a CDI or breakdown system, the increase in

stored energy may result in an increase in the maximum voltage which is induced before breakdown is initiated. Using a booster gap, as described in section 2.9.3, the maximum voltage can be controlled by the external electrode gap. The induced voltage rise is then almost instantaneous at the spark plug electrodes and is complemented by a higher current.

For a shorter arc, with the same ignition energy, massive increases in spark power can be realised. In this respect breakdown systems are the most powerful (Cho et al. 1992). Anderson and Asik (1983) showed that increasing the ignition power needlessly resulted in no performance increase. The use of a supplementary spark energy unit, one where the arc is lengthened by superimposing a 2.5kV constant voltage supply on top of the coil discharge, resulted in a negligible decrease in cyclic dispersion.

It has been discussed that the ignition energy needed to ignite a flammable mixture increases as the mixture strength deviates from stoichiometric, refer to Fig 1.1.

2.13.4 Effects of spark duration

For an inductive ignition system, the duration of the spark is primarily governed by the energy stored in the ignition system. It has been shown that longer duration sparks, operating in the glow-discharge phase can increase the ignitability in conditions of high charge dilution. This is the main reason why TCI systems have won widespread use in the automotive market.

Weyl (1993) noted that a smaller plug gap was beneficial when used in a lean burn engine. The smaller gap redistributed the spark energy from the breakdown phase to the glow phase which resulted in an increased spark duration and therefore increased ignition probability.

The suitability of longer duration sparks to lean mixtures is challenged by Maly and Vogel (1978). Their work has shown that very high energy breakdown systems, containing the same total energy as the longer duration systems, are able to put all the energy into the inflammation zone. The work showed that a spark of minimum duration produces a larger initial flame kernel when compared to a longer duration spark of the same energy. It was also noted that the breakdown system resulted in a rougher flame-front whereas the high energy arc system produced a smooth flame-front. A multiple strike system is currently in use by SAAB, based upon a short duration CDI system. The multiple strike strategies exist for slow speed running and starting and serve to produce a longer effective spark duration.

A similar system developed by Ford was tested by Harrington et al. (1974). For the work a spark was initiated every 300μs for a total duration of 5ms. The engine speed was 1500rpm and this combined spark duration resulted in a crank angle duration of 45°, the fuel used was

indolene, a hydrocarbon blend representative of pump petrol. The CDI system used was not representative of current technology in that a capacitor was charged on the high voltage side of the circuit. This would result in a very fast voltage rise, since there would be no ignition transformer inductance and resistance in the system. When compared to a conventional TCI system, an extension of the lean limit was noticed. The effect was most pronounced at low loads where dilution due to residuals was high. When comparing the emissions results, the multistrike system decreased the unburned hydrocarbon figure in the lean range with no increase in NOx. The system was also found to be more tolerant of dilution by EGR, thus enabling a shift in the lean limit at a constant dilution rate. The extension of the lean limit allowed the engine to run leaner, exploiting the inherent reduction in NOx emissions without incurring a penalty in the hydrocarbon output. The system was documented as being very versatile with a variable effective spark length, attained by increasing the number of sparks, and a variable striking frequency. Ford produced another multiple strike system, again based upon the CDI system, this time exploiting ferro-resonance to give multi-strike capability. The system was documented by Asik and Bates (1976).

Nakai et al. (1975) compared two ignition systems, one with a 1.5ms spark duration, the other with a 6ms duration. Tests were carried out with a combustion bomb and an engine using high speed photography. In a quiescent mixture no difference in flame growth was detected, but when the same systems were tested in a turbulent mixture, the flame growth was much faster when the longer duration system was used. In the engine tests, the longer duration spark was found to increase performance when using EGR, and also to lead to a lower specific fuel consumption. It was argued that the optimum spark duration would equal the heat release delay. The longer spark reduced early combustion fluctuations but a penalty was paid by the need for increased ignition system energy, where the electrical supply may reduce the low speed fuel consumption due to the alternator load.

Arcoumanis and Bae (1992) compared TCI and CDI systems to study the relationship between electrical characteristics and flame development. The studies were performed in both quiescent and flowing mixtures. Three plug types were used, a standard type, a V-grooved type and a surface gap type. The gap was varied on the conventional plug from 0.6 to 1.9mm and the mixture pressure was set at 3, 6 and 9 bar. The instantaneous voltage and current, flame front travel, propagation speed, and pressure were measured. The flame characteristics were measured using a two beam diffraction method. Pre-ignition flow was measured using LDV techniques. For turbulent combustion, the mixture was introduced at a tangent to the combustion vessel and the mixture was allowed to settle for a predetermined residence time. Three orientations of the spark plug were used during testing.

The experiments showed that with a quiescent mixture, leaner running could be achieved using the TCI system, i.e. the mixture could be made leaner for the same misfire rate. With a turbulent mixture, the lean limit was the same for both the CDI system and TCI system. No further extension could be achieved by using the surface gap plug or the V grooved electrode plug, even though the latter had the lowest breakdown voltage of all the igniters tested. Arcoumanis and Bae (1992) also noted that the breakdown voltage was reduced at higher temperatures.

Modien et al. (1991) compared the performance of three ignition circuits, a conventional TCI system, a breakdown system and a plasma jet system. The plasma jet drive circuit was tested both with a plasma igniter and a surface gap spark plug, the other two systems were tested with the surface gap plug only. The plasma circuit consisted of a conventional TCI system to initiate the ionisation, and a constant 1kV supply to continue the discharge. The ignition circuits were tested in both quiescent and turbulent lean methane-air mixtures contained within a combustion bomb. The flame development was monitored by measuring the chamber pressure, signals from two ionisation probes, and high speed photography. A separate chamber was used for turbulent conditions, the mixture motion being induced by drawing a grid across the volume and allowing a pre-determined settling time before ignition. The turbulent chamber was fitted with a central pair of electrodes and therefore did not use the plasma igniter and the spark plug.

The experiments showed that in quiescent conditions, the burning velocities were highest for the plasma jet igniter (and circuit) throughout the mixture strength range. For mixtures close to the weak flammability limit, the breakdown system induced a slightly higher burning velocity than the plasma drive circuit connected to the surface gap plug. However, at stoichiometric the plasma drive circuit is slightly superior. The standard TCI system was worse at all conditions. Reasons for these results were postulated to be that the plasma igniter initiated combustion from a turbulent jet towards the centre of the chamber, whereas the surface gap plug initiated combustion at the periphery, where quenching was able to occur at the chamber surface. The higher energy systems were seen to induce higher burning velocities, and this was thought to be because of the induced motion of the ionised column. The kernel motion is determined by JxB, where J is the current density and B is the magnetic flux density. The use of higher energies can increase both these factors, and therefore result in the kernel being moved away from the electrodes and reducing the quenching effect. With heat release analysis, the 0-5% burn duration (termed the flame development period) was compared for each ignition strategy. The flame development time for the TCI system was two and a half times longer than the plasma jet circuit and plasma jet igniter. The flame development time for the plasma drive circuit and the breakdown system, both used with the surface gap plug, were 70% as long as the TCI system.

The burn duration, 5-95% of the total heat released, was also analysed. The plasma drive circuit and the breakdown circuit, both using the surface gap plug, were found to have a burn duration of 85% of the burn duration for the TCI system. The plasma igniter and the plasma drive circuit was found to have a burn duration of 65% of that of the TCI system.

Ujiie (1994) used a 10kV breakdown circuit with an additional 0.8kV component to increase the duration. A thyratron was used to switch the capacitor to discharge across the electrodes. It was found that a secondary component was able to reduce the total minimum ignition energy, therefore increasing ignition probability.

2.13.5 Multiple ignition sources

The use of multiple ignition sources has filtered through to mainstream ignition strategies. The most famous is the TSpark system used by Alfa Romeo (Curtess 1988). Work by Anderson and Asik (1983) has shown that this scheme is beneficial at reducing the COV by up to 26% and the 0-10% burn time by 14%. A double spark plug method was adopted by Nissan and is described by Kuroda et al. (1976). The system formed part of a fast burn combustion system which was designed to be tolerant of EGR in a bid to lower NOx emissions.

Meyer et al. (1992) used an engine which utilised a cylinder head with four spark plug holes. Two of the holes were on the periphery, the other two towards the centre of the disc shaped combustion chamber. Testing showed that the best engine performance, in terms of power and IMEP, was obtained, over the full air-fuel ratio range, with four sources of ignition. The results of these tests showed a ten percent increase in power and an increase in brake thermal efficiency, especially in lean mixture regions, over a centrally mounted plug case. A more retarded ignition timing for best torque was noted when all four plugs were used, this characterised the faster burn time. The lean limit was extended since the four sparks increased the probability of ignition. The emissions were increased with the four plug strategy, when compared to the central plug. The NOx increased as a consequence of the faster, and therefore hotter combustion process, the UHCs were increased also and this was postulated to be caused by the faster burn time and the flame front reaching the ring pack crevice at a higher cylinder pressure. In this case, more HC mass is stored, and then released when the cylinder pressure reduces, other reasons for the higher exhaust concentrations include increased crevice volumes in the additional plugs, and the slight increase in quenching area. When the exhaust species were calculated on a specific basis, the UHC emissions for the four plug combustion system were the lowest. This was due to the increase in power output due to lower misfire. Tests were carried out with two plugs mounted towards the periphery, but this configuration was found to have a worse performance due to a longer burn time.

Other methods for multiple ignition sources have been presented, including one where the cylinder head gasket contains four pairs of electrodes (Eureka 1993). However, the economics of replacing the cylinder head gasket at a similar service interval to a conventional spark plug renders the scheme unviable.

Nakamura et al. (1985) detailed the development of a multiple ignition source strategy where up to twelve spark gaps were connected in series. A special CDI system was used to initiate the sparks which were sited at the edge on opposite sides of the combustion chamber. The spark sources were collectively termed an ignition plate and this acted as the cylinder head gasket. A breakdown time of 1.5 ms for all gaps was measured and the breakdowns were considered to occur simultaneously. The use of twelve gaps resulted in a 5% reduction in fuel consumption and a shift of the lean misfire limit by up to three air-fuel ratios. Combustion duration was reduced by up to 50%. With the multiple ignition sources, the use of swirl made negligible difference to combustion performance.

In reality, multiple ignition sources are of use in disc chambers where combustion is slow. In an active chamber, with high turbulence, the multiple sources would only be used at low load. At high load, where the flame speed is high, the combustion would be too fast causing excessive noise and perhaps component damage.

2.13.6 Ignition process enhancement

Enhancements to the ignition process to aid early flame kernel growth have been documented. Hacohen et al. (1992) detail work carried out using a static high voltage DC electrode to supply 15kV to induce excess charge effects near to the spark source. The excess charge effects are believed to extend flammability limits (Sher et al. 1992). This additional electrical source was shown to have a slightly beneficial effect with respect to cyclic variability, but these trends were not shown to be conclusive.

Hacohen et al. (1992) were also involved in the testing of a spark plug which is able to create a high electric field, introducing momentum to ions and resulting in corona flow effects. When an electric field is applied between a sharply curved surface and a blunt surface, a voltage is reached where the gas near to the curved surface breaks down at a lower voltage than the spark breakdown voltage. A glow discharge then occurs and is known as a corona, gas movement can be observed to flow in the electrode gap towards the blunt surface, this is known as an ionic, electric or corona wind, the velocity of which is proportional to the square root of the initiating current. Although not tested in engine conditions, flow velocities from the igniter of over 10m/s were recorded in a high pressure chamber. The *corona wind* can result in a

constant flow through the igniter electrodes, until spark initiation, which it is said can minimise the heat transfer to the cooler igniter surfaces.

Sher et al. (1992) designed and tested a similar type of igniter on a flow rig in a constant volume combustion bomb, and a commercial automotive engine. With the use of high speed photography, it was found that the acceleration of the flame front was doubled within the first 2ms of combustion. When using the corona igniter, the production engine was found to display lower unburned hydrocarbon emissions at low loads when compared with the conventional ignition system.

Ofurum (1993) evaluated a spark enhancement unit and its effects upon combustion at the lean limit in a petrol fuelled engine. The unit was intended to be a retrofit to existing systems, fitting between the ignition coil and the spark plug on the HT electrical side. The HT signal is filtered by the unit with certain frequency components being removed, this is said by the manufacturer (Accelertron Automotive Ltd.) to *optimise the release of fuel sensitive coil energy*. The effect of the spark enhancement unit could be seen on the spark current wave form, the peak current was reduced by 10% and the spark duration was reduced by 30%, the ignition energy manifesting itself in the earlier part of the spark duration. When tested on a running engine it was noted that the average current flow through the spark plug was approximately 10% lower at all engine speeds and also that the spark duration remained approximately constant, albeit up to 40% shorter, when compared to the decrease in duration with speed when using a conventional ignition system. At full throttle it was found that the spark enhancement unit did not improve power output or carbon monoxide emissions at any speed, although a marked reduction in unburned hydrocarbon emissions was noted throughout the engine speed range. Brake specific fuel consumption was also improved, most notably at lower engine speeds. When the engine was running at part throttle the unburned hydrocarbon levels were again consistently lower with the use of the spark enhancement unit. It was found that the lean limit of the engine was extended somewhat, especially in the mid-range.

2.14 Chapter summary

This survey suggests that the best type of ignition circuit for lean burn strategies is either a high energy conventional system, resulting in a long duration, or a very short high current breakdown system. These two distinct systems are supported in the literature for improving ignition probability, a factor which will have to tend towards 100% to meet any emissions legislation. Multiple strike intermediate duration systems are also supported, in use these behave in a fashion similar to long duration systems, but have superior breakdown behaviour if based upon a CDI circuit.

Turbulence mechanisms in the combustion chamber can affect the ignition system in various ways. Turbulence can be beneficial in convecting away the early flame kernel from the relatively cool electrodes, and increasing the surface area through wrinkling. The increase in surface area can increase the flame speed due to the increase in exposed reactive species, and can also increase heat transfer to the surrounding gas. If the degree of heat transfer becomes high enough, quenching may occur and the flame front may expand slower than anticipated. For long duration sparks, such as those created using high energy conventional systems, the flow field may interfere with the arc. The ionised gas column may be swept away, resulting in further breakdown processes. If the energy in the coil is almost depleted, further breakdowns may not occur due to insufficient remaining energy; this is therefore a waste of energy. However, this phenomenon results in a *stream* of dissociated gas which if the mixture is poorly mixed, will improve the ignition probability. Breakdown systems are unaffected by flow field effects, since the spark occurs very quickly. The system relies on a higher degree of dissociation, in a concentrated volume, than conventional systems.

It is acknowledged that the weakness of the CDI system is the use of an ignition transformer. With a breakdown system, essentially a CDI system with a voltage step-up achieved before the storage device, the switching mechanism can be very costly and unreliable. It is therefore possible that lower inductance coils may increase CDI performance to a level attained by the breakdown systems, i.e. a greater voltage may be supplied to the plug gap before breakdown occurs. Special winding techniques with suitable core materials can reduce transformer inductance whilst remaining reliable for long life ignition usage. These effects can be enhanced further by the use of breaker or spark gaps.

To reduce system losses to a minimum, direct mounting single coils per spark plug are considered to be the current state of the art. These dispense with the losses associated with HT leads, distributors and wasted spark systems. For TCI systems, coil charging times are increased by a factor equal to the number of cylinders.

Spark plug fouling mechanisms do not pose a threat to lean burn gas engines (so long as lubricant consumption is negligible) since the fuel is in gaseous form. Because of this, the engine is less sensitive to spark plug heat range and therefore a colder plug may be selected, with the benefit of a cooler central electrode and hence a lower wear rate.

The life of the spark plug in a lean burn gas engine is limited by electrode erosion, but with the emergence of rare earth metal electrodes service lives are extended to as long as 5000 hours (Champion 1995b) which currently surpasses that of the lubricating oil. As oil technology improves, so too must that of the ignition system since these are the major causes of stoppages

for continuously running stationary engines. It is still unclear which ignition systems give the lowest electrode erosion characteristics, and whether the erosion rate increases with erosion itself.

3. Core apparatus and measurement procedures

This chapter compares and justifies the use of the electrical measurement equipment, techniques and core apparatus for the overall study.

3.1 Core apparatus

Two types of ignition system were used in testing, a Transistorised Coil Ignition (TCI) system and a Capacitive Discharge Ignition (CDI) system. A further system was used, due to its simplicity, for the evaluation of the measurement apparatus and techniques.

3.1.1 Lucas AB13 transistorised coil ignition system

The Lucas ignition system consisted of a coil and transistorised switch unit which is shown in Figure 3.1. The transistorised switch unit was of a simple type, the coil-on-time being controlled by the pulse width of the TTL input control signal, in this case from the Lucas Dial-a-Time system for the engine, or a function generator for the rig tests. This operation enabled the primary current to be controlled, and hence the stored energy to be varied, and the effects on the combustion process to be investigated. The maximum stored energy for this system, using a 12V DC supply, was 100mJ.

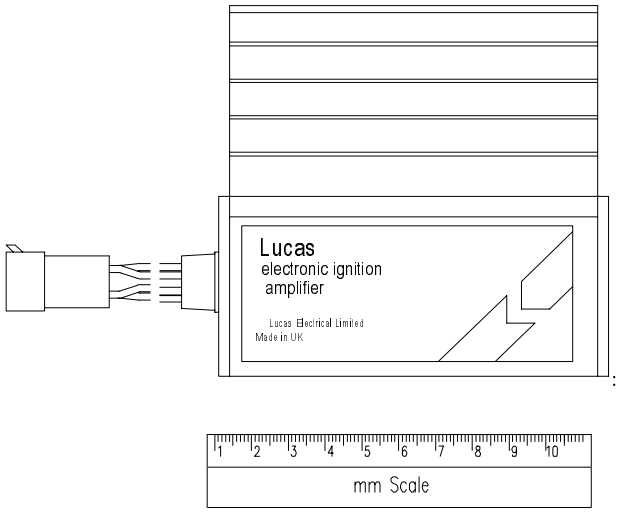

Figure 3.1 Lucas AB13 transistorised coil ignition system

3.1.2 Oxford Capacitor Discharge Ignition System

The Oxford CDI system, shown in Figure 3.2, is based upon a design by Wilkinson (1975) and uses an oscillator, inverter and step up transformer to convert the 12V DC supply voltage to 350V DC to charge the capacitors. The capacitors are discharged through the ignition transformer by the thyristor which is controlled, through an interface, by the Lucas Dial-a-Time ignition controller. The stored energy is controlled by switching additional capacitors into the circuit with relays. This gave a maximum capacitance of approximately 2μF and a minimum of 0.12μF, although the nominal capacitance (100%) was taken to be 1μF, resulting in a stored energy of 60mJ.

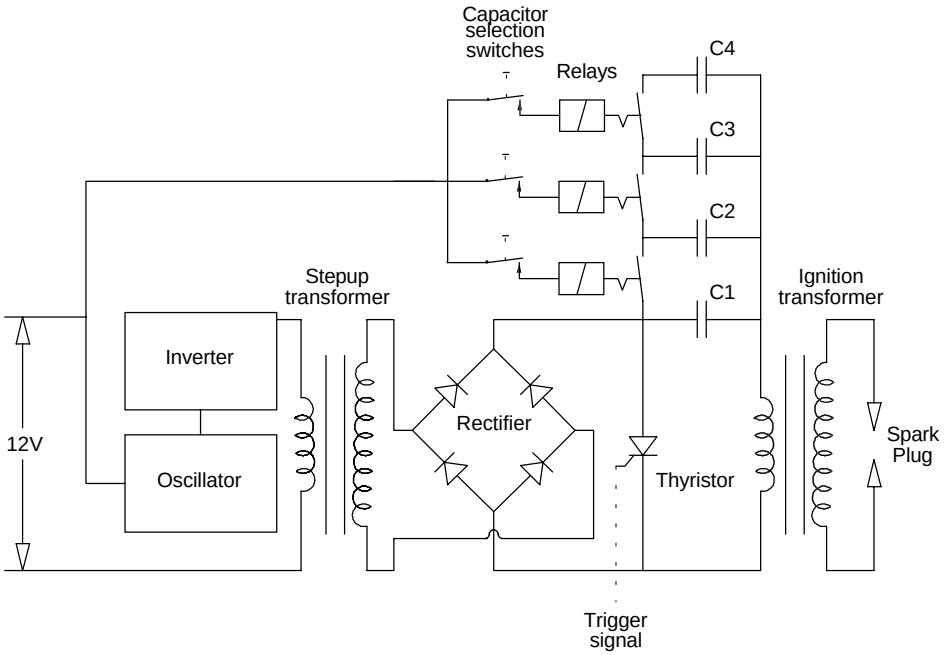

Figure 3.2 Oxford CDI system schematic showing capacitance selection

3.1.3 Bosch TCI system

The Bosch system is more advanced than the Lucas in that the dwell time, or coil-on-time, is controlled internally, its simplicity made it ideal for testing measurement apparatus and development of measurement methods. A coil with a very low primary resistance is used with the switch, this allows the maximum current to be achieved in a much shorter time than conventional TCI systems, such as the Lucas. The benefits of a system like the Bosch can be seen best on high speed multi-cylinder engines, utilising a single coil and distributor, where the coil-on-time becomes very short. The unit also features a current limiting function which ensures that the coil windings are not destroyed by overheating, this works by reducing the voltage at the coil from the nominal 12 volts when the desired current level has been reached. Since the coil is of very low resistance and the system incorporates a current limiting facility, a ballast resistor is no longer needed. The switch unit is shown in Figure 3.3.

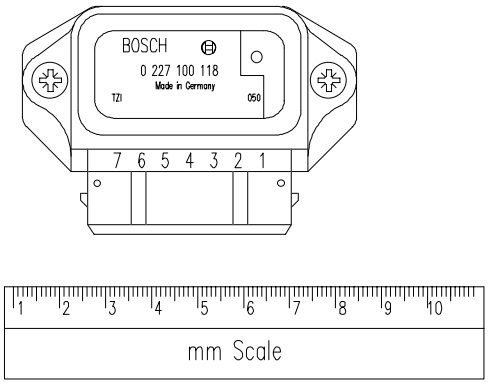

Figure 3.3 Bosch TCI switch unit

3.1.4 Digital storage oscilloscope

A Tektronix TDS 310 digital storage oscilloscope was used for data capture. The instrument had a bandwidth of 50Mhz and a maximum sampling rate of 200 mega samples per second. An RS232 compatible port on the rear of the instrument allowed interfacing to a PC and downloading of data in either numerical or graphical format. In numerical format, two channels were downloaded, each consisting of 1000 data points. The instrument was of 8 bit vertical resolution, hence the accuracy was 1/256 of the full scale deflection. The full scale deflection of the instrument can be calculated as the volts per division multiplied by the 10 scope divisions. For monitoring the breakdown process, on a 2 volt per division set-up (assuming the 1000:1 attenuation of the voltage divider), the error would be ±78 volts. When considering the glow phase, with the scope set for 0.5 volts per division (assuming the voltage divider calibration above), the error would be ±19.5 volts. The oscilloscope also had a self calibration facility which was carried out before measurements were taken.

3.2 Voltage measurement

3.2.1 Apparatus and utilisation

The measurement of ignition voltage was carried out using a high impedance voltage divider with an attenuation factor of 1000:1 (1V/kV). The type used throughout the study was a Ross Engineering Corp. VD50-4.1-AC-L-T-F with a maximum operating voltage of 30kV continuous or 50kV pulse. Figure 3.4 shows a schematic of the internal components of the device.

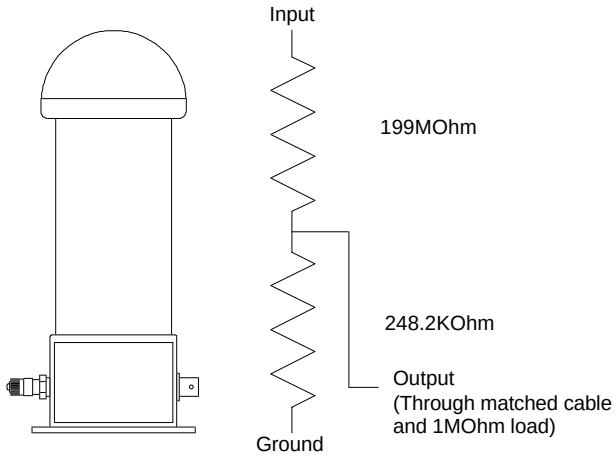

Figure 3.4 Voltage divider and equivalent internal circuit

The voltage divider was connected to the voltage measurement lead via a polished aluminium domed cap, accepting a screwed ring terminal. The use of the domed cap reduces the electrical field, normally high at sharp edges and points and hence reduces the risk of external breakdown. The instrument housing was constructed from a resin tube, housing the resistance network in an atmosphere of poorly conducting gas (Sulphur Hexafluoride), with the earth terminal being connected to the brass base of the device. The voltage divider was connected as close to the plug electrode (cathode) as possible since there were resistive losses along the system, which is shown in Figure 3.5. The closest point for measurement was at the spark plug terminal, a second HT lead was connected to the crimped ignition lead terminal with a piece of copper wire.

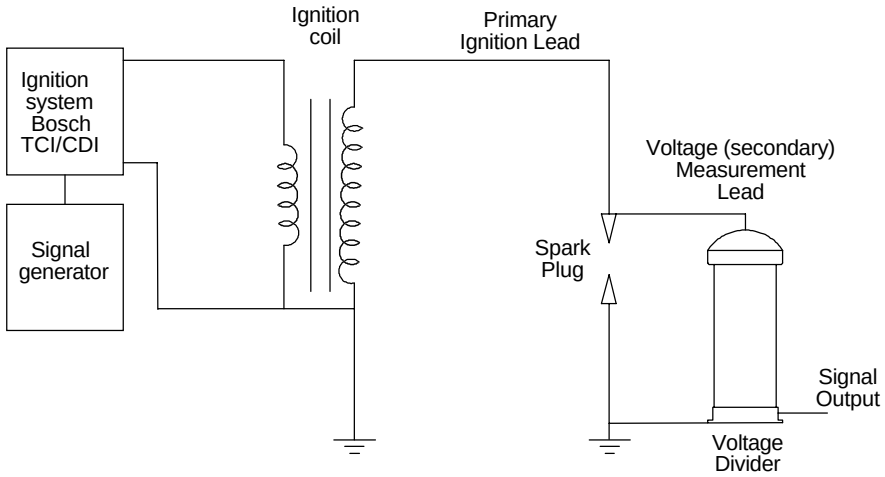

Figure 3.5 Voltage divider connection in typical ignition circuit

Resistive leads were used throughout, since interference from high ignition currents could corrupt the instrumentation. These resistive leads had little effect on the use of the voltage divider since the voltage measuring point was at the end of the primary lead and the current flowing in the secondary lead, from the plug to the voltage divider, was much lower and therefore had a much lower voltage drop, this is qualified later in this section. The voltage divider was connected by a BNC connector to the digital storage oscilloscope, through a matched cable.

3.2.2 Effects of plug to voltage divider lead length

It was thought that the length of the lead from the spark plug terminal to the voltage divider (voltage measurement lead) would influence the results by inducing a delay in the measurement of voltage. Three different length leads were tested, 0.25m, 0.5m and 1m in length. Figure 3.6 shows a screen image downloaded from the scope. This image shows the breakdown voltage measured at the same physical sparking conditions (air at ambient pressure, 1mm plug gap) for three different lead lengths.

The waveforms are so close that it is not worth labelling them, suffice to say, there is no change in breakdown voltage lag with an extension in the measuring lead from the spark plug

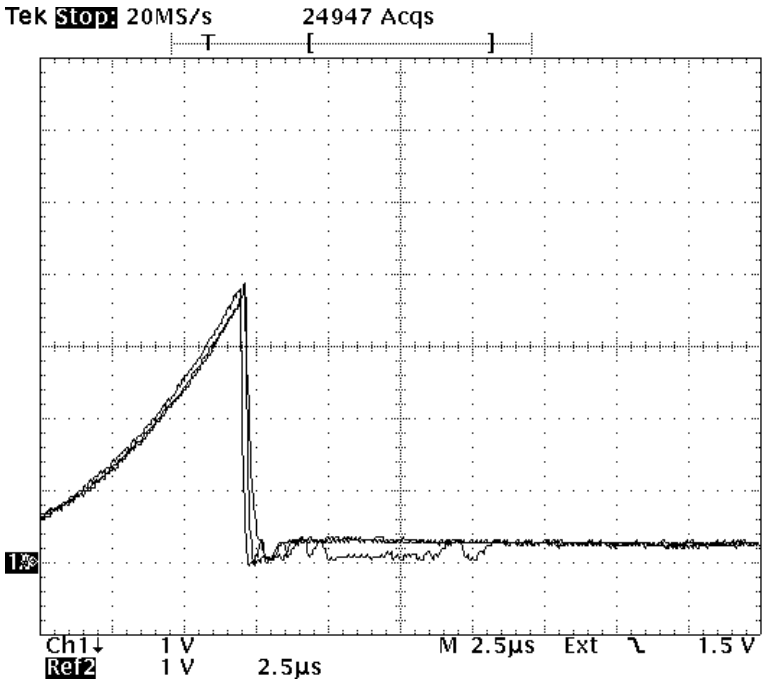

Figure 3.6 Comparison of voltage measuring lead length

terminal. We can conclude that, for the purposes of the overall study, the measurement of voltage is not sensitive to the plug to voltage divider lead length.

3.2.3 Justification of use

A resistive component in the ignition circuit, in parallel to the plug gap can result in a leakage of current, commonly known as a shunt. This current leakage has been calculated to be very low in comparison to that flowing in the gap, these calculations are shown below.
Overall resistance of the voltage divider:

$$R_{total} = R_1 + R_2$$

$$R_1 = 199M\Omega$$

$$R_2 = \frac{1}{\frac{1}{1M\Omega} + \frac{1}{248.2K\Omega}} = 199K\Omega$$

$$R_{total} = 199.199M\Omega$$

The voltage divider has an overall resistance of 199.199MΩ which with a breakdown voltage of 25kV, will result in 126µA of current flow. This equates to a current drain of 0.157%, of the measured value, with a current of 80mA flowing in the plug gap.

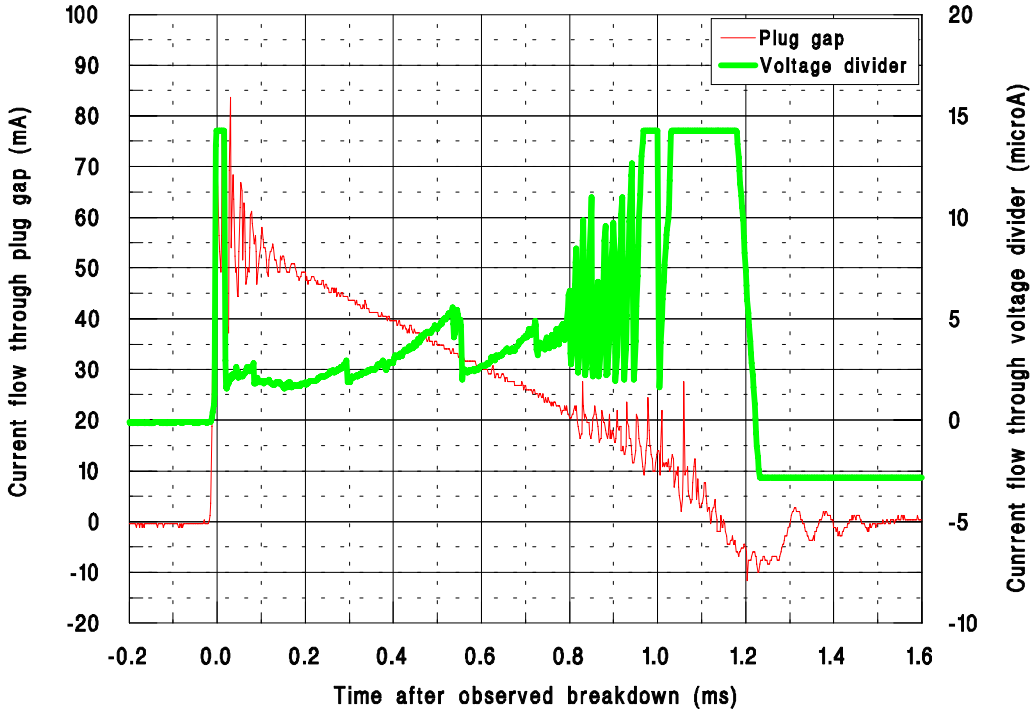

Figure 3.7 Comparison of current flowing through plug gap and current flowing through voltage divider

Figure 3.7 shows that the current flowing through the voltage divider is an order of magnitude smaller than that flowing through the plug gap, therefore we can neglect the effects of current leakage through the device.

3.3 Current measurement

The measurement of HT current presents a number of problems. The current is small (in the milliamp range), has a very fast rise time (in excess of 8000 amps per second) and the actual duration of flow is short (in the millisecond range). This section aims to compare five methods of measuring HT current on an ignition system. These methods are:

The HT resistor method
The Pearson 4100 current transformer
The Pearson 410 current transformer
The Pearson 411 current transformer
The Tektronix TM502A current measurement system.

The technical specifications of all five systems can be seen in Appendix B.

All three families of systems vary in price substantially, the resistor costing a few pence, the Pearson transformers costing £600 and the Tektronix costing £2800. Obviously, the cheapest system which would give adequate results should be adopted.

3.3.1.1 Resistive method

Using a resistor in the secondary circuit allows current to be measured by Ohms law, i.e.:

$$I = \frac{V}{R}$$

The SAE standard (SAE 1995) recommends a resistor of 100 ohms to be used, this is small compared to the resistance of the spark plug gap, or the HT winding, which is typically two orders of magnitude higher. A metal oxide resistor is the preferred choice due to its negligible inductance.

The method prescribed by the SAE, is to use a series resistor on the earth side of the secondary ignition circuit, this is not always possible. On three terminal coils, such as conventional automotive coils, the earth windings from both the primary and secondary circuits are connected together internally, this makes it impossible to add a series resistance without the coil being permanently switched on. Using the resistor on the high voltage side can result in very high voltages at the measuring equipment and hence damage occurring as well as danger to life. On a TCI system, the current flows through the battery, the battery voltage being added in series to the spark voltage. A resistor could not be placed in the 12V feed to the coil since the charging current would be severely reduced. Most commercial ignition systems do not utilise coils where access is available to both ends of the HT winding. The use of a double ended coil in this situation would allow the use of the resistance method but would change the manufacturers choice of components, and hence may upset the way the system was designed to work. Moreover, the use of more elaborate ignition systems, such as the use of the Brighton optically operated high voltage switch (Howson 1989, 1990a, 1990b, 1990c, 1991, 1992), will not allow the use of a series resistor. Additionally, it is advantageous to measure voltage and current at the same position in the circuit. A resistor on the earth side of the coil will result in a voltage lag if the voltage is measured at the plug terminal.

Therefore, when evaluating standard ignition systems, a current probe or transformer of some sort must be used.

3.3.1.2 Pearson Current Transformers

The Pearson current transformer is a solid core device and has to be placed on the ignition lead before any terminals are added.

Current transformers can only measure a change in current. The change in current, in the primary winding of the transformer, induces a voltage in the secondary (the measuring device). When a DC component is present, the ferromagnetic core of the device saturates (in the same way as an inductive ignition coil is charged). As saturation occurs, the output from the device droops from the true current value. A DC biasing current can be used to offset the saturation, this is achieved by passing a second conductor through the core with current flowing in the opposite direction to that being measured. The value of the DC current is chosen to nearly saturate the core in the negative sense allowing almost twice the saturation level of the standard system. The ferromagnetic core of the current transformer will always exhibit a droop characteristic, the extent of which will determine the useable frequency range of the device. The lower the droop, the lower the minimum frequency, the trade off for this being a lowered maximum frequency, which also restricts the measurable signal rise time. With lower droop, the device suffers a loss of sensitivity, the inductance being lowered by a reduction in secondary windings.

The Pearson current transformer has a specific bandwidth which results in a reliable output, but with the broad range of 'frequencies' which occur in a spark discharge, the transducer may not respond in the desired manner.
Other research groups and organisations have published material which includes details on the methods of current measurement utilised in the work. Both Arcoumanis (1992) and Anderson and Kim (1995) have used the Pearson 3464, which has a specification similar to the 411 used in this study.

3.3.1.3 Tektronix TM502A

The Tektronix TM502A is a contrast to the Pearson system consisting of a probe and an amplifier resulting in a more complicated device.

The TM502 system combines Hall Effect and inductive technology to measure current from a DC level up to a frequency of 50 MHz. When measuring low frequency current, the system uses a biasing current, inside the probe head, to prevent or minimise core saturation. This also allows AC current with a DC offset to be measured. The biasing current is controlled by the amplifier, its magnitude and direction being determined by the Hall device output. The amplifier also controls the signal attenuation before reaching the oscilloscope. This split core device allows the probe to be placed around a conductor, of up to 21mm diameter, without a disturbance to the connections.

3.3.2 Experimental apparatus

The resistor, the Tektronix, the Pearson 4100 and 411 current measuring systems were tested on the Rover K series engine, since this would highlight any problems, particularly noise, in an engine environment.

A double ended coil, originally intended for a wasted spark ignition system, was used with a 100 ohm resistor bridging the second output, of the high voltage winding, to earth. The Tektronix system was connected as close as possible to the resistor, with the Pearson current transformers being positioned over the resistor.

The HT cable used was of the resistive type, of typical resistance 15kΩ per metre. The cable measured 400mm from the coil to the distributor and 300mm from the distributor to the spark plug. With all leads in position, the capacitance of the ignition lead to the engine structure was measured as 46.3 pF. Ignition voltage was measured as described in section 3.2.1 with a 500mm length of resistive HT cable.

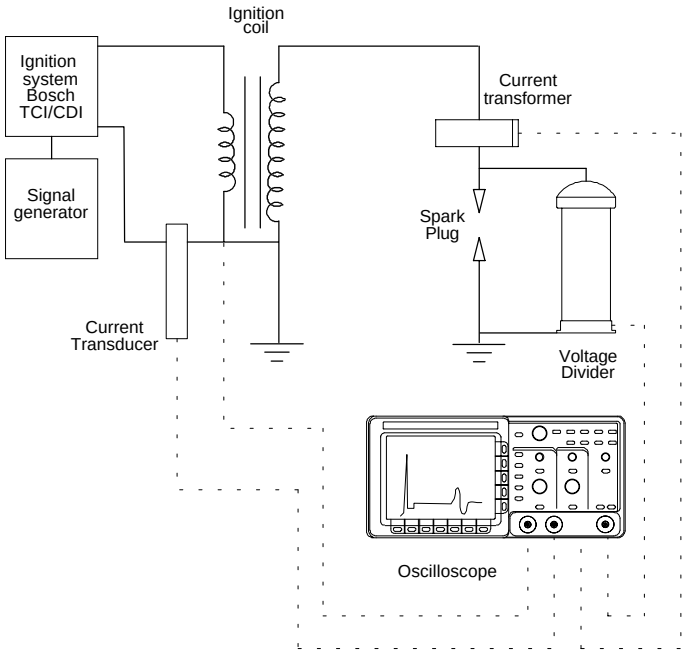

Figure 3.8 Experimental apparatus (rig tests)

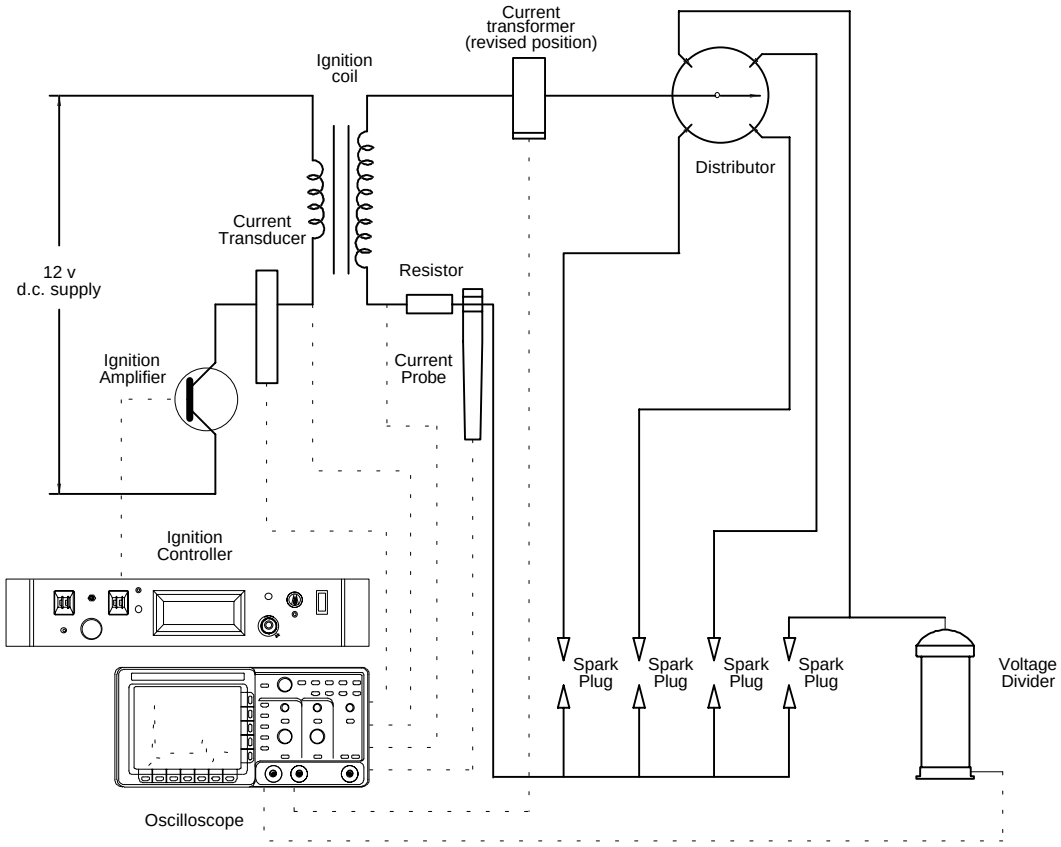

Figure 3.9 Experimental apparatus (on engine tests)

Additional tests were carried out, with the Pearson transformers, using standard Bosch components where current measurement using a resistor method was not possible. These systems were used off the engine and were of TCI and CDI type, on the CDI type the current transformers were used to measure the LT current also. The experimental apparatus is shown in Figure 3.8.

3.3.3 Method of investigation

3.3.3.1 On engine testing

The equipment was assembled on the engine as shown in Figure 3.9. The engine was then motored at 1200 revs/min with the throttle 2/3 open. The fuel injectors were not used since the tests did not need the engine to be firing. The ignition, however, was switched on, being timed at 10 degrees before TDC.

It was the intention to trigger the oscilloscope from the switched side of the coil, being pulled down to 0V when the coil is charged. The engine, being equipped with a distributor, meant that the triggering from the coil switch-off occurred on every spark at each plug. This method of triggering was found to be unsatisfactory, especially when trying to relate the measured current with the voltage at the spark plug. Instead, it was decided to trigger off the breakdown voltage.

A series of 25 acquisitions was made for each discharge, these discharges were not necessarily consecutive since a finite time was required by the oscilloscope to download each waveform. The files were saved in a comma delimited file format and loaded into a spreadsheet. The spreadsheet was used to apply calibration factors to the data.

3.3.3.2 Rig testing

As discussed in 3.3, a series of tests was carried out with standard Bosch systems where no provision was available for a resistive type measurement. These tests were carried out at ambient conditions, a series of 25 acquisitions were made using the scope which was again triggered from the breakdown of the high voltage measurement.

The measurement systems tested were the Pearson current transformer, types: 410, 411 and 4100. The Tektronix system was not used because the probe clamp was of too small a diameter to fit over the HT lead (it had previously been fitted over the series resistor on a double ended coil). No resistor method was used since the primary and secondary windings were connected together.

Tests were carried out with both TCI systems and CDI systems. On the TCI system, only complete discharges were considered. With the CDI system, the early discharge period, the complete discharge and the LT waveforms were measured. These waveforms were imported into a spreadsheet where calibration factors were applied and analysis was undertaken on a single discharge basis.

3.3.4 Discussion of results

A comprehensive set of results was obtained from the tests outlined in the previous section. The more important results are shown and discussed below, the less important results are presented in Appendix E.

All plotted results are for a single discharge only, the actual discharges do not lend themselves to averaging because of their non-repeatable nature and their discrete elements, thus any averaging would lead to a rounding of peak current flows etc.

3.3.4.1 On engine testing

Figure 3.10 shows the percentage charge dissipated in the spark gap, compared to the charge measured with the resistor tested on the same discharge. The charge is considered to be important because one function of measuring current is for the calculation of energy.

The energy dissipated in the spark plug gap is defined as:

$$E = \int_{t=0}^{t} VI \, dt$$

where V is the voltage in volts
I is the current in amps
t is the time in milliseconds

The charge is defined as:

$$q = \int_{t=0}^{t} I \, dt$$

where q is the charge in coulombs

The % charge is defined as:

$$\%q = \frac{\left(\int_{t=0}^{t} I\,dt \right)_{test}}{\max\left(\int_{t=0}^{t} I\,dt \right)_{resistor}}$$

where the subscripts test and resistor apply to the method, of measuring the current, under test and the resistor method.

Figure 3.10 shows the percentage charge as a function of time for the three non-resistive current measuring methods. The effects of the specified droop characteristics can be seen for the Pearson 4100, where the charge actually becomes negative. This could result in a calculated energy being negative, or at best very much lower than reality.

For the Tektronix and Pearson 411, the % charge never actually reaches 100%, therefore never equalling the maximum calculated charge of the resistor method. This is surprising since the Pearson 411 and the resistor method measurements were indistinguishable on the screen of the oscilloscope. However, the Pearson 411 does have a droop rate specified as 0.9% per millisecond, resulting in a droop of up to 2% towards the end of the discharge. These errors, although not appearing significant on the scope display, can accumulate in the integral of the waveform when the data is multiplied by the corresponding calibration factor.
There was also a slight DC offset on both the Tektronix and Pearson 411 measurements, although for different reasons. The Tektronix suffered from DC offset problems from discharge to discharge, the DC offset is governed by a Hall Effect transducer which measures the DC current level. The Pearson 411 does not suffer from DC offset problems directly, but a

DC offset is induced by the scope. The volts per division must be reduced to the minimum to enable the measurement to take place, and this allows any slight offset in the scope (perhaps due to temperature effects on the amplification circuits) to induce errors. A facility on the scope is available to set DC offsets to zero (signal path compensation), this can also be carried out in software post processing.

The % charge deficiency with Pearson 411 could be attributed to other more fundamental factors, the calibration of the current transformer may be invalid, no tolerance is specified for the models used although other models with similar specifications are listed as having a +/- 1% tolerance. The two current measuring systems were also used with different scaling factors on the scope and were amplified through different circuits.

Since the Pearson 411 is an inductive device, and is a transformer, with the measurand being the primary and the transducer as the secondary, a certain efficiency of conversion must be expected, although this will probably be compensated for by calibration factors. It is possible, however, that the efficiency may be a function of the air gap between the transducer and the wire which results in a magnetic flux loss.

From these tests, it would appear that the best system to adopt for TCI HT current measurement, on an engine, is the Pearson 411. The Tektronix system has a similar performance, but the cost of such a system is prohibitive, and the instrument would seem to require the DC offset to be adjusted for each discharge.

3.3.4.2 Rig testing

3.3.4.2.1 Bosch TCI system

Figure 3.11 shows the time resolved charge dissipated in the spark plug gap. Two traces of the 4100 characteristic are plotted, this is because the scope can only measure two traces at one time and therefore the 4100 was used as one channel and compared to both the 410 and 411. The two 4100 traces are almost identical and therefore the results can all be considered comparable. The coil used in this test was a standard Bosch unit in which the primary and secondary windings are connected together preventing a series resistor being installed. From previous tests, the Pearson 411 current transformer has been shown to be the most accurate, so this is taken as the standard.

With the long discharge, where less energy is dissipated in the breakdown period of the spark, the effects of droop become more significant. The charge measured with both the 410 and the 4100 becomes negative before the end of the discharge, but the 411 remains at a constant value as the discharge finishes.

These results were not compared with the resistor case because a conventional coil was used, and the Tektronix TM502A, since the current probe was not large enough to accommodate the 8mm diameter ignition lead. However, the TM502A which is owned by the University of Brighton, was compared to the Pearson 411 and was found to have similar performance when viewed on the scope screen.

It would appear that the best method of viewing the current waveform from a TCI system discharging at atmospheric conditions (with a coil that has no provision for a series resistor), is the Pearson 411 current transformer. When the pressure at the spark gap increases, the duration becomes shorter, decreasing the tendency to droop.

3.3.4.2.2 Bosch CDI system

Figure 3.12 shows the early discharge period for the Capacitive Discharge ignition system, it can be seen that the Pearson 410 and 411 exhibit substantial noise characteristics. This will not significantly affect the results, especially when calculating current, since the oscillations will have a cancelling out effect with each other (assuming no lag in measurement) and the majority of the noise occurs in the (short) early discharge region where current rise rates are at a maximum.

When considering the full discharge, as shown in Figure 3.13, the three Pearson current transducers exhibit similar characteristics, although the two lower gain transformers are more prone to electrical noise.

For the shorter discharge of the CD ignition system, the best current transformer to adopt would be the Pearson 4100 with its higher gain and better response to higher frequency pulses.

When considering the LT current for a CD ignition system, the results obtained by measuring with the Pearson current transformers are shown in Figure 3.14. The Pearson 410 and 411 show the same characteristics although the 4100 appears to decay abruptly. This is a function of the I.t Max parameter of the current transformer (two orders of magnitude lower than both the 410 and 411), which if exceeded will result in core saturation, and is discussed in the Pearson selection literature (Pearson (a), Pearson (b), Pearson (1991), Pearson (1994)). Figure 3.15 compares the HT and LT currents, and since current still flows in the HT circuit, current must also be flowing in the LT circuit, therefore the 411 and 410 are considered to measure correctly.

For LT current measurements on a CD ignition system, the most suitable current transformer is either the Pearson 410 or the Pearson 411.

3.3.5 Positioning for current measurement

When measuring ignition parameters, it is important to do so as close to the electrode surfaces as possible. However, this is not always possible. The closest position the voltage can be measured, without changing the characteristics of the spark plug design, is at the spark plug terminal. For measuring current, a different situation exists. The current measurement systems described in this chapter work by fitting over the ignition lead. Ideally the measurement systems would be positioned over the spark plug terminal, insulated by the rubber boot that covers the end of the ignition lead and the spark plug insulator. Under conditions of high pressure, where the required breakdown voltage is increased, external breakdown can occur with electrical conduction through the insulation of the rubber boot to the current measuring system. This problem is exaggerated by the addition of the voltage measuring lead which makes efficient insulation very difficult.

Tests were carried out by taking voltage and current measurements with the current transformer both close to the spark plug and close to the coil, the actual breakdown phase of both parameters was compared, since the steep drop in voltage would act as a datum from which to compare important current features. When considering the current waveform, Figure 3.16 and Figure 3.17, the difference in current measuring position is not great. The breakdown phase can be used as a datum for the steep rise in current. Interestingly, the arc phase can be seen quite clearly (low voltage, high current). The time scale on the two plots show the breakdown occurring at different times, this is thought to be a triggering problem with the scope. This has no effect on the interpretation of the results.

Another important feature of the two different measuring positions is that when measuring current closer to the coil, electrical noise is reduced considerably. The low gain of the current transformer (0.1V/A) renders the device susceptible to electromagnetic interference (EMI).

From the results included here, we can see that when using the flow rig, with a simplified ignition system (i.e. no distributor and capacitance induced effects from engine structures), it is acceptable to measure current close to the coil. This will reduce the risk of external breakdown which was found to occur from the voltage tapping, on the ignition lead, to the current transformer body.

3.3.6 Conclusions

From the results it has been seen that the most reliable way of measuring current is by measuring the voltage drop across a resistor. It has been discussed that this is not always possible, furthermore, if the current is to be used to calculate energy with a measured voltage, the two parameters must be measured as close to each other as possible. This is not possible with a resistor method since the current is measured at the earth side of the coil, and the voltage is measured at the plug to ensure that the voltage drop across the resistive HT cable is taken into account.

The alternative method is to use a current probe or a current transformer. It has been discussed that a current probe, such as the Tektronix TM502A does not give consistent results since the DC offset is unreliable. It has also been shown that the correct current transformer must be used to avoid unnecessary droop occurring, to catch high frequency peaks and to give a good noise free output.

From the study, the following recommendations are made:

Measurement	System
TCI HT current	Pearson 411
CDI HT current	Pearson 4100
CDI LT current	Pearson 411

It has been argued that the current measurement should be made as close to the voltage measuring source as possible, although it has been discussed that this is not always possible. Measuring the current closer to the coil has been shown to reduce electrical noise with a minimal penalty of measurement lag.

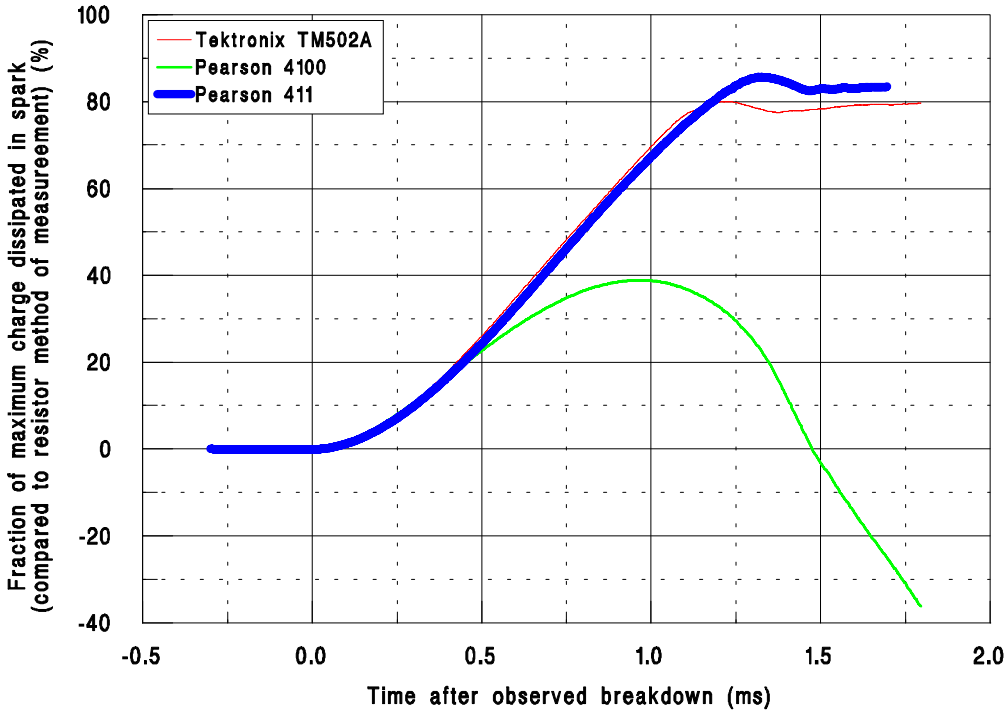

Figure 3.10 **Comparison of current measuring performance for relationship of percentage dissipated charge (compared to maximum resistance charge) with time.**

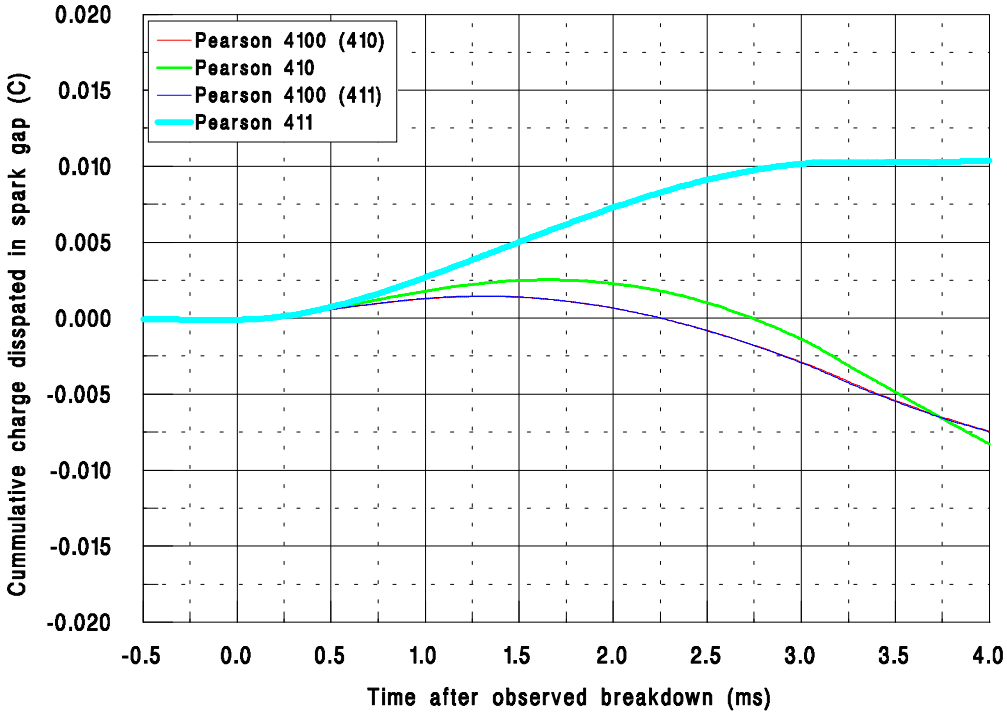

Figure 3.11 **Comparison of current measuring performance for relationship of dissipated charge with time (Bosch TCI system)**

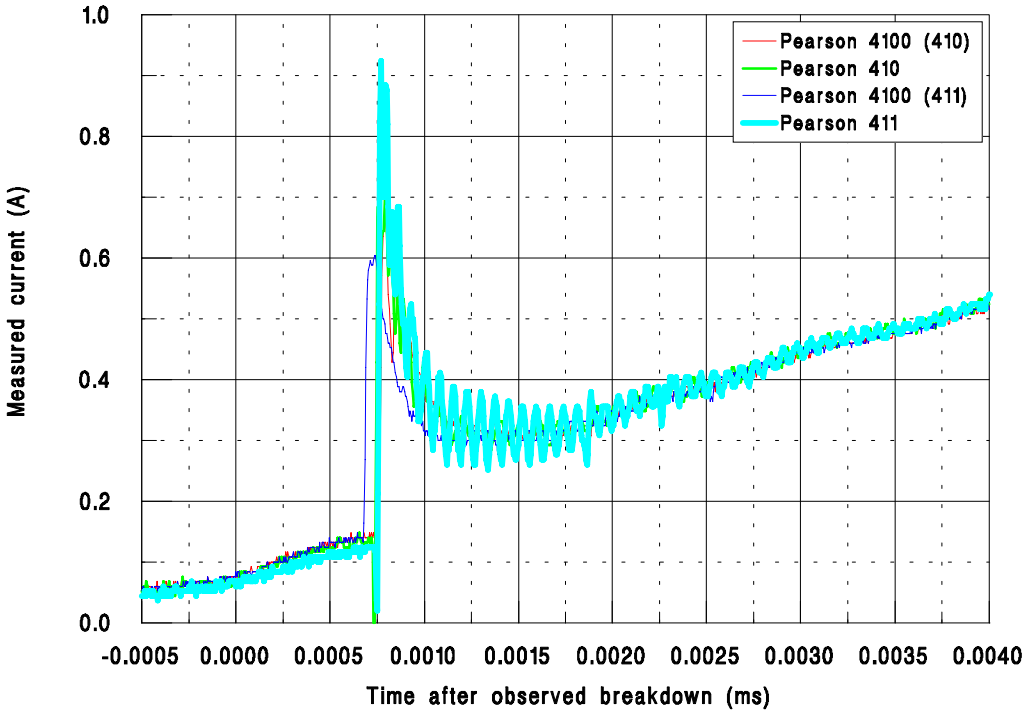

Figure 3.12 **Comparison of current measuring performance between Pearson 4100, Pearson 410 and Pearson 411 for early stages of single discharge (Bosch CDI system)**

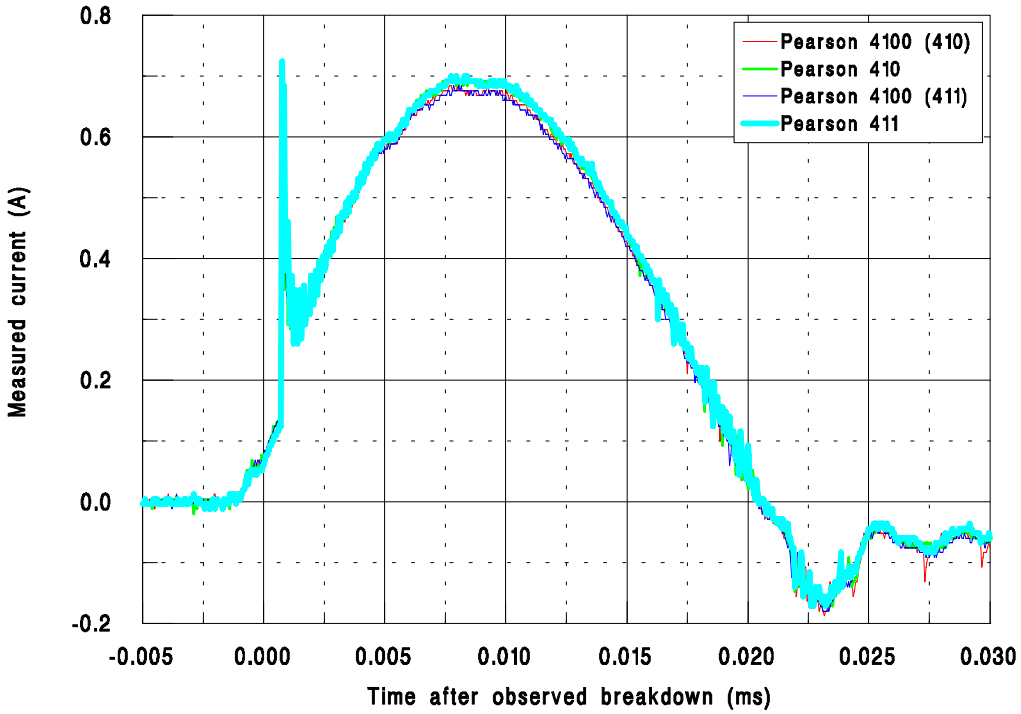

Figure 3.13 **Comparison of current measuring performance between Pearson 4100, Pearson 410 and Pearson 411 for complete single discharge (Bosch CDI system)**

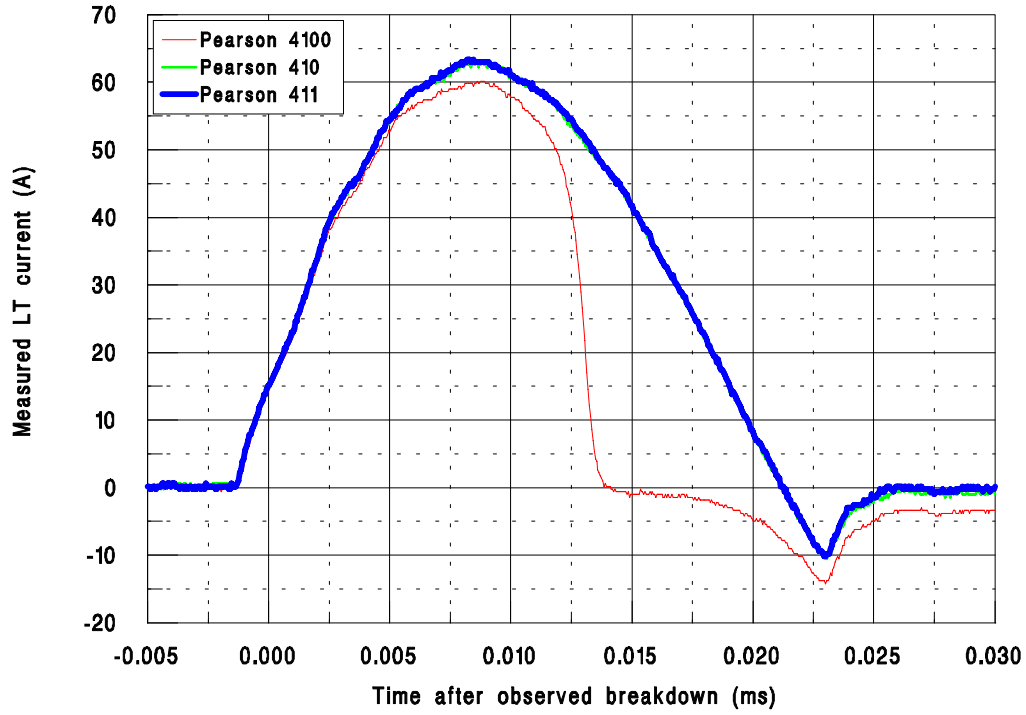

Figure 3.14 **Comparison of LT current measuring performance between Pearson 4100, Pearson 410 and Pearson 411 for complete single discharge (Bosch CDI system)**

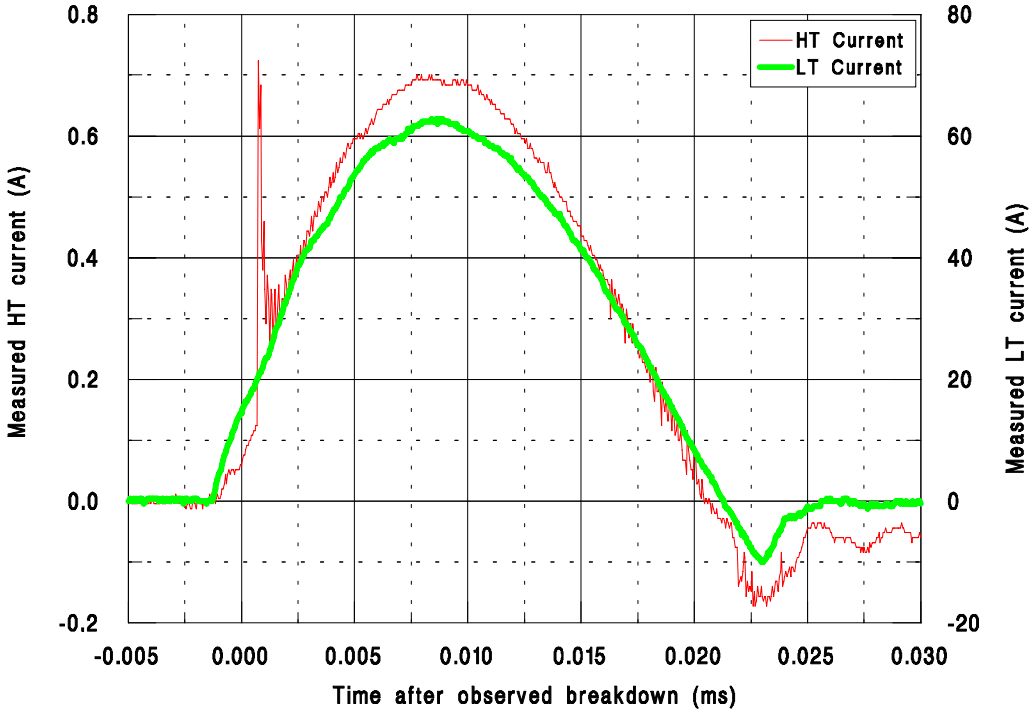

Figure 3.15 **Measured HT current and LT current events for complete single discharge (CDI system)**

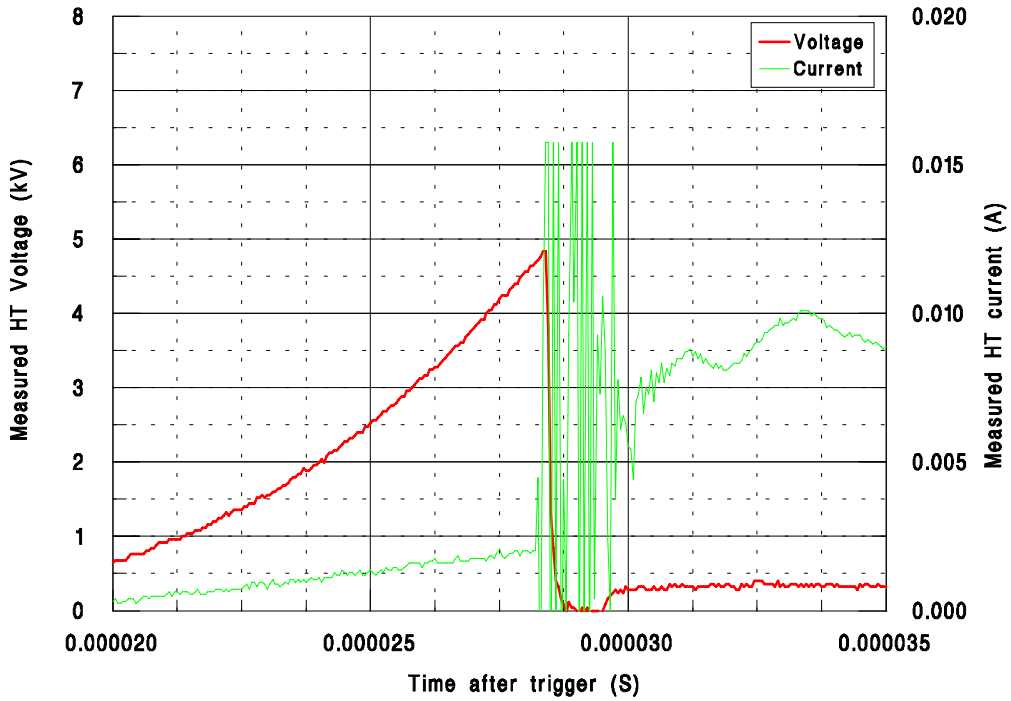

Figure 3.16 **Breakdown phase for voltage and current measured at the spark plug**

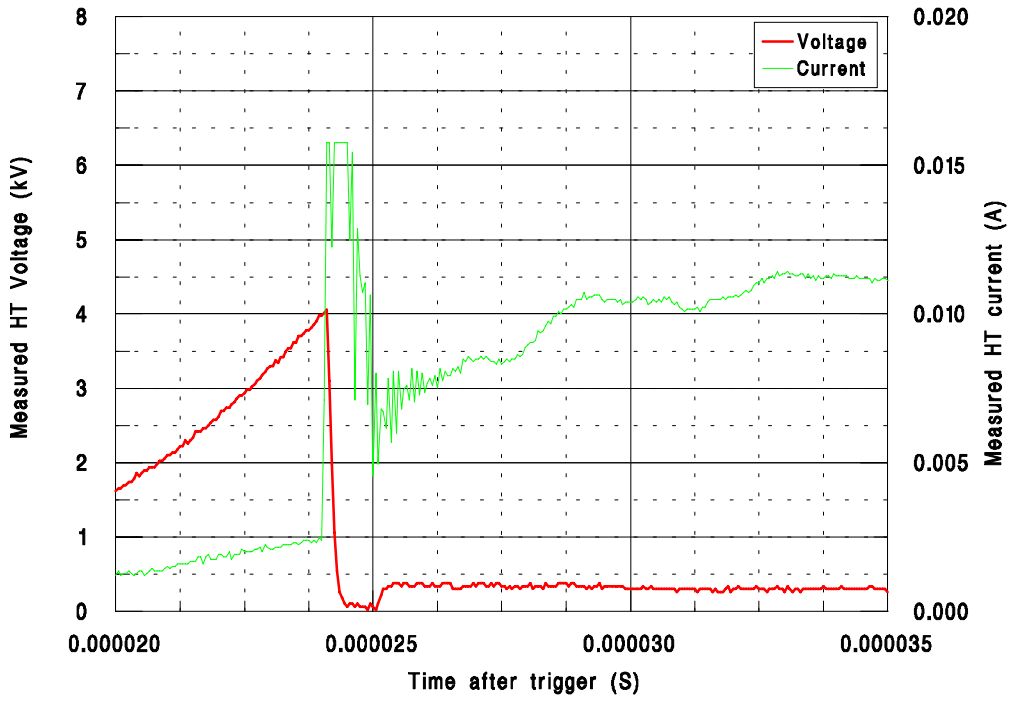

Figure 3.17 **Breakdown phase for voltage measured at the spark plug and current measured at the coil**

3.4 Data post-processing

3.4.1 Waveform smoothing

The following algorithm was adopted for smoothing data before analysis:

(3-1

$$a_n = \frac{1}{b^2}\left[a_{n-(b-1)} + 2a_{n-(b-2)} + 3a_{n-(b-3)} + \ldots + ba_n + \ldots + 3a_{n-(b+3)} + 2a_{n-(b+2)} + a_{n-(b+1)}\right]$$

where n is the data point number, in our case between 1 and 1000.
a is the data point.
b is the number of data points used for smoothing (actually 2b+1)

in a simple form, where b = 2

(3-2

$$a_n = \frac{(a_{n-1}) + 2(a_n) + (a_{n+1})}{4}$$

where n is the data point number, in our case between 1 and 1000.
a is the data value.

Sub *SMOOTHD*, below allows the number of points, used for smoothing, to be altered by changing one number only.

```
SMOOTHD:
      B% = 5
      N% = 1 + B%
      DO WHILE N% < (WFPOINTS% - B% / 2)
            SMOOTHD!(N%) = 0
            FOR J% = 1 TO B%
                  SMOOTHD!(N%) = SMOOTHD!(N%) + J% * (WFTEMP!(N% - B%
                  - J%) + WFTEMP!(N% - B% + J%))
            NEXT J%
            SMOOTHD!(N%) = (SMOOTHD!(N%) - WFTEMP!(N%)) / (B% * B%)
            N% = N% + 1
      LOOP
      FOR N% = 1 TO WFPOINTS%
            WFTEMP!(N%) = SMOOTHD!(N%)
      NEXT N%
RETURN
```

Two loops exist, the first loops through all the waveform points, the second inner loop loops through all the terms used in equation (3-1. The algorithm uses a looping addition function for each waveform point being smoothed. The second loop starts at 1 and adds the outermost pair of points to the function (one and its mirror image), this continues until b reaches its maximum (pre-set by the user). In actual fact, this looping addition function results in two ba_n values being added. On exiting the loop, one of these values is subtracted to correct the error and results in 1+2b points being used. Figure 3.18 shows a schematic of this process.

Data is read from one array and placed in a second (temporary) array after working. This is done because as the program runs, the data point will be being smoothed using pre-worked data. This is deemed to be undesirable.

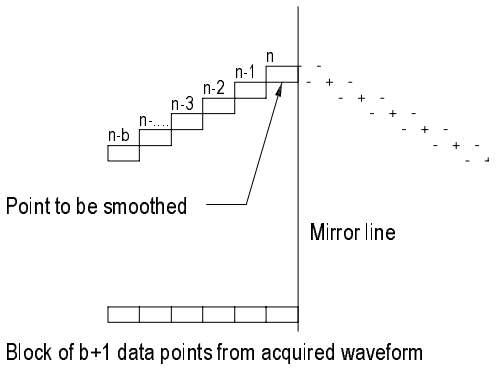

Figure 3.18 Schematic of smoothing process

The smoothing loop starts, not at 1, but at a number determined by the value of b(B%). This is done because when using outlying points for smoothing, the computer will give the value of zero for points lying outside the array, i.e. if B% was 5 and N% was started at 1, the value of WFTEMP!(-4) would be read giving a value of zero. The waveform data is insensitive to this part of the data since the scope is triggered at 10% of the waveform data, i.e. after 100 data points. The waveform is complete before the end of acquisition, so the remaining 5 points that remain unsmoothed are insignificant also.

It should be noted that smoothing the signal will modify the original data, by reducing maxima and minima in the manner of a low pass filter.

3.4.2 Waveform differentiation

The waveform is differentiated using a Taylor Series expansion, as described by Stone (1986) which incorporates 4th order terms and higher.

$$f'(a_n) = \frac{\left(f(a_{n-2}) - 8f(a_{n-1}) + 8f(a_{n+1}) - f(a_{n+2})\right)}{12h}$$

This *four point finite difference scheme* results in a reduction in noise carried over.

```
RDIFF:
      I% = 3
      DO WHILE I% < (WFPOINTS% - 3)
            DVDT!(I%) = (WFTEMP!(I% - 2) - 8 * WFTEMP!(I% - 1) + 8 *
WFTEMP!(I% + 1) - WFTEMP!(I% + 2)) / (12 * (XINCR!))
            I% = I% + 1
      LOOP
      FOR I% = 1 TO WFPOINTS%
            WFTEMP!(I%) = DVDT!(I%)
      NEXT I%
RETURN
```

3.4.3 Application to acquired data

As discussed above, differentiating experimental data can be disastrous, no signal is free of noise, and more importantly, a digitised signal is limited by the resolution of its analogue to digital conversion. The associated spikes and steps can lead to very steep gradients. It is possible to smooth the signal, both before and after differentiation, but this risks losing data.

The smoothing method discussed above is the *(1+2b)* method, where *b* is chosen as the minimum value to maintain the original data points with minimum noise.

The area of interest is the shallow rise in voltage after breakdown, as shown in Figure 3.19, this set of data, the first acquisition from a 2bar 20 m/s flow through a 90 degree J type electrode, has been smoothed and differentiated using both pre and post smoothing and different values of *b*. The waveforms, Figure 3.20 to Figure 3.28, can be compared in the region of interest. Figure 3.29 shows the effect of pre-smoothing.

It can be seen that the more a signal is smoothed, the lower the amplitude of the peaks becomes. This is most definitely a loss of data, but if this loss does not occur in the region of interest, the result does not affect the analysis.

A reasonable approach would be to pre-smooth the data then smooth the differential. This is what has been done in Figure 3.28. The pre-smoothed waveform has not lost any important information and is therefore suitable for differentiation. This is the procedure that will be adopted for this study.

The following figures use arbitrary units, but all scales are identical.

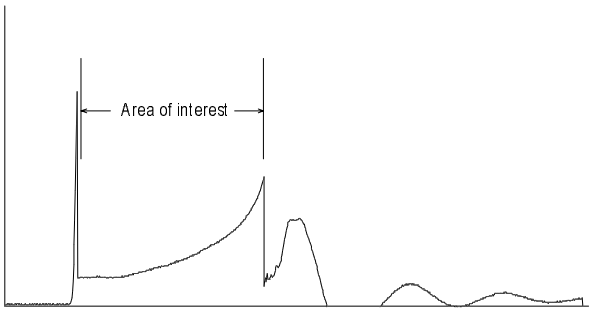

Figure 3.19 Raw data

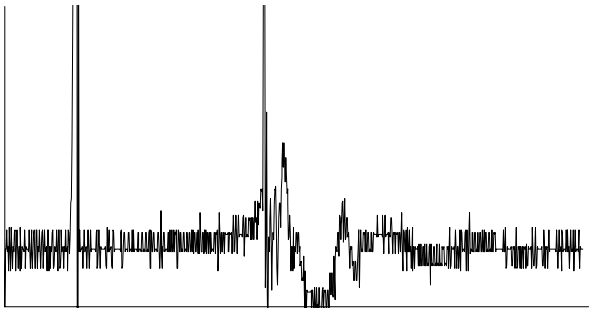

Figure 3.20 Differentiated raw data

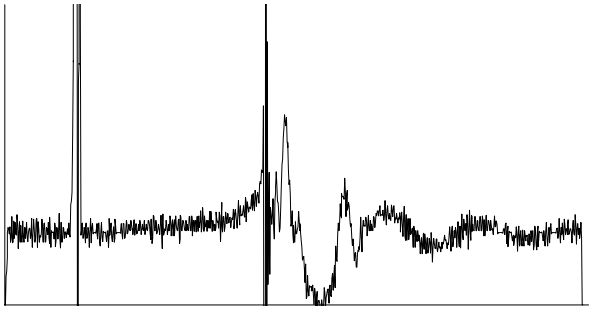

Figure 3.21 Differentiated raw data (5 point smoothed)

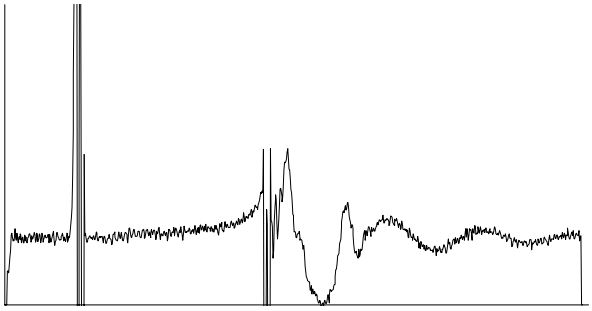

Figure 3.22 Differentiated raw data (11 point smoothed)

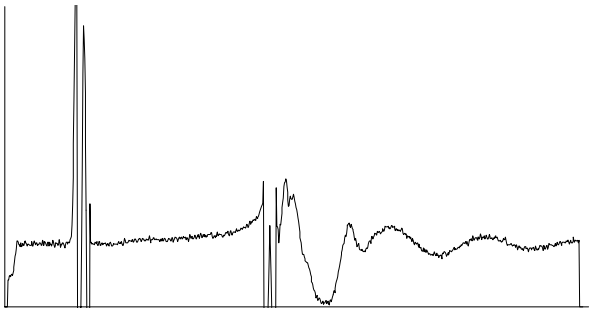

Figure 3.23 Differentiated raw data (21 point smoothed)

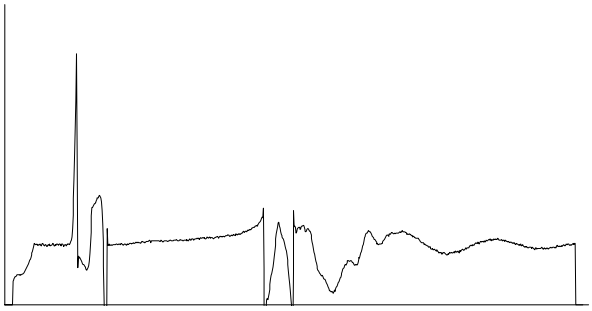

Figure 3.24 Differentiated raw data (51 point smoothed)

Figure 3.25 Differentiated raw data (101 point smoothed)

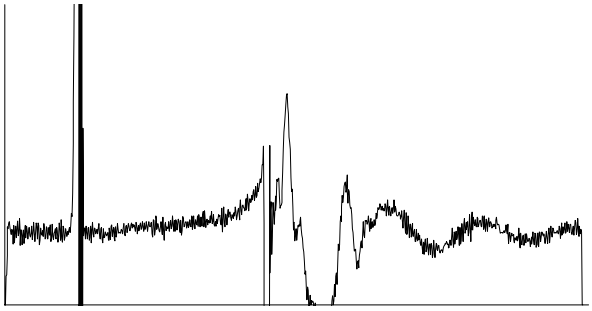

Figure 3.26 Differentiated raw data (5 point pre-smoothed 5 point post-smoothed)

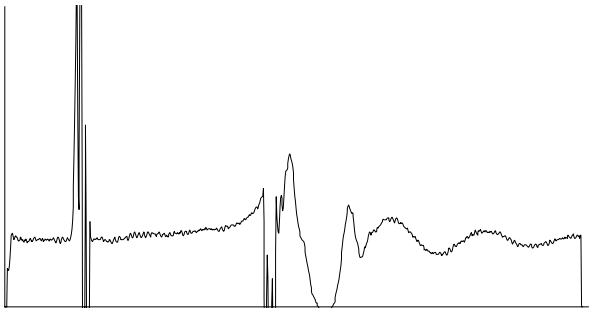

Figure 3.27 Differentiated raw data (11 point pre-smoothed 11 point post-smoothed)

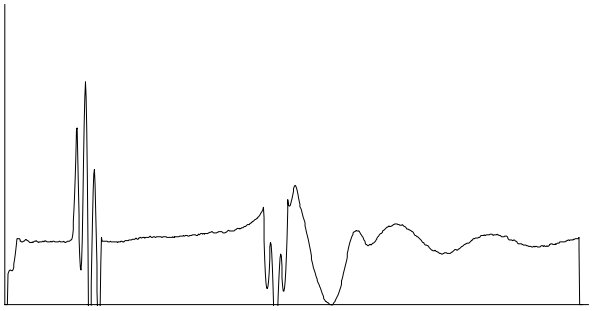

Figure 3.28 Differentiated raw data (21 point pre-smoothed 21 post-smoothed)

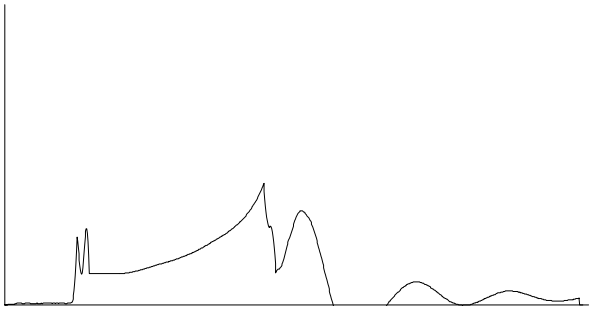

Figure 3.29 Raw data (21 point pre-smoothed)

4. Engine testing

4.1 Experimental apparatus

The engine used in this study was the Oxford University Rover K4 single cylinder, optical access, research engine, shown in Figure 4.1 with the specifications given in Table 4-1. Based upon the Rover K series 1400cc four cylinder automotive engine, it represents modern designs of combustion and gas exchange systems. The engine is composed of a purpose built crankcase with primary and secondary balance shafts to minimise vibration whilst using optical combustion analysis methods, such as high speed photography and laser diagnostics.
The single water cooled cylinder has the facility for the use of a synthetic quartz annulus just below the combustion face for viewing the early stages of combustion. The aluminium alloy piston is of an extended variety with open slots in the skirt, an angled mirror is placed through

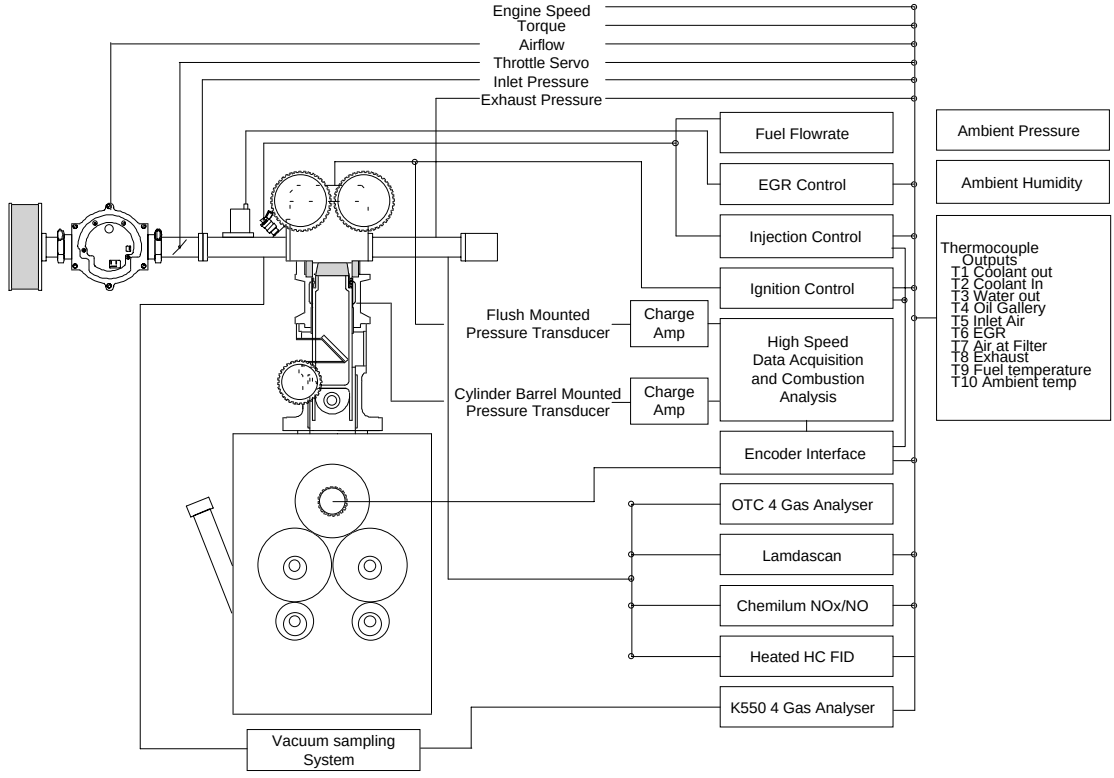

Figure 4.1 Schematic of Rover K4 engine and associated instrumentation

the slots and bolted to the upper cylinder block, this is used to view the combustion process through a synthetic quartz piston crown. The quartz window is held in position by an aluminium collar which screws onto the extended piston, sealing is achieved using viton rings. The optical components, in the piston crown and the annulus at the top of the barrel, were replaced with aluminium components, and the mirror removed, to reduce the risk of damage during extended test periods when optical access was not required. Three piston rings were used, the middle ring used was made from Zircon Z43, a modified crystalline polyether, the outer two, used to maintain the location of the piston, were made from Luytex C324, a fibre glass impregnated composite material. The cylinder head had been adapted from the multi-cylinder Rover K4 engine, the width had been reduced by two and a half cylinders from the opposite end to the cam drive, to leave two cam journal pairs, the head was then sealed at the severed end by a 20mm alloy plate. The cam journals were lubricated by a grease nipple since there was no oil provision in the upper cylinder. Initially valve springs of lower rate than the

production engine were used, but these were later changed as part of a study to maximise repeatability (Pashley 1997).

Main Specification	
Bore	80.0 mm
Stroke	89.0 mm
Con rod length (ctr-to-ctr)	160.0 mm
Compression ratio	10:1
Spark plug	Champion (C9YC)
Gap	0.8mm
Cam Timing	
IVO	12° BTDC
IVC	52° ABDC
Peak lift inlet	8.8 mm @ 70° BBDC
EVO	52° BBDC
EVC	12° ATDC
Peak lift exhaust	8.8 mm @ 70° ABDC
Cylinder head	
Type	Rover K16 1.4 MPI
No. valves per cylinder	4
Pent Angle	45°

Table 4-1- Rover K4 Specification.

The spark plug was installed in the cylinder head with a cross-flow orientation, i.e. the gap was exposed to the direction of flow. This arrangement is shown in Figure 4.2.

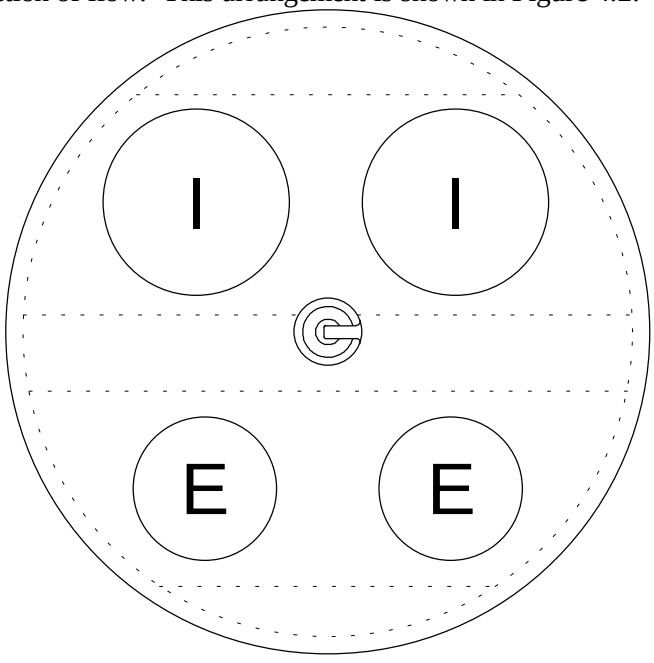

Figure 4.2 Schematic of cylinder head showing spark plug location and orientation in relation to the inlet valves

A water cooled AVL QC32C-E piezoelectric pressure transducer was installed in the cylinder head and was connected to a Kistler type 5006Y4 charge amplifier. The transducer and charge amplifier were calibrated together by means of a dead weight tester. A second pressure transducer was mounted in the cylinder barrel, a Kistler piezo-resistive 4075A10, and was used to measure absolute pressure whilst the piston was near to BDC. The barrel pressure transducer and charge amplifier outputs were fed to a 12 bit data acquisition card in a Personal Computer (PC). Readings were taken every degree crank angle, in response to the output from a Leine and Linde type 63 incremental crankshaft encoder. The encoder also generated a once per revolution flag, this was passed through a pulse extension circuit before being recorded by the data acquisition card. A sample size of 1MB was used, as this enabled the pressure data analysis to be carried out on over 300 consecutive cycles. The combustion analysis was undertaken with the PACE, COBRA and MEANBURN software (Ball 1997) which for the mass fraction burned analysis relied upon the methods of Rassweiler and Withrow (1938).

The engine was fuelled by two separate fuel injectors, one connected to a plenum for gaseous fuels (selection notes can be found in Appendix H) and the other, which was not used in this study, was connected through a pump to a liquid fuel tank. The gaseous fuel system consisted of a high pressure cylinder of methane, the flowrate from which was measured with two Rotameter type flowmeters. The air-fuel ratio was controlled by varying the injector pulse width duration, with a system designed by Oxford University, the controller was calibrated (although an output was available to view the pulse width on an oscilloscope).

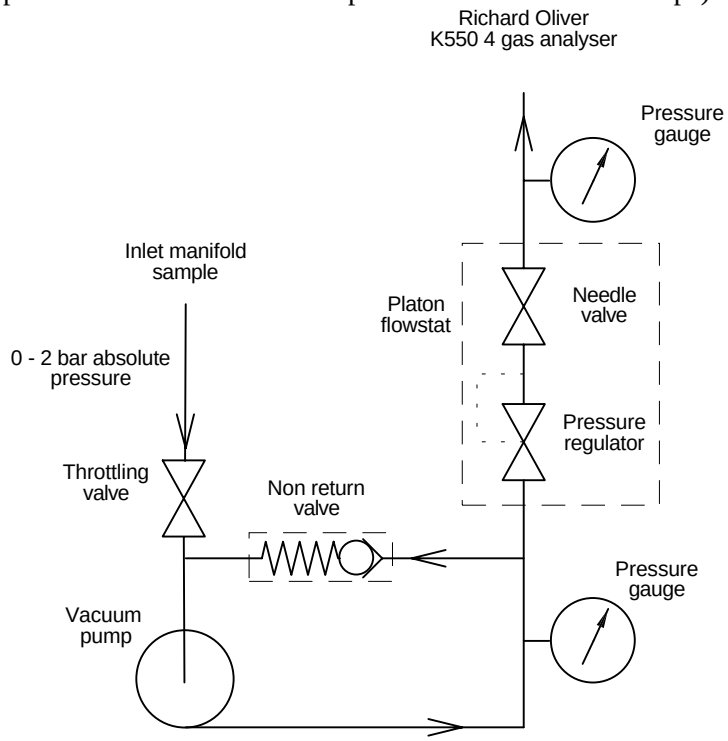

Figure 4.3 System diagram for sampling from inlet manifold with Richard Oliver K550

A Roots type positive displacement air flow meter driving a shaft encoder was used to measure the air consumption, the encoder output was connected to a rate meter which was calibrated in litres per second, instrumentation for which is shown in Appendix I. Ignition timing and coil charging time were controlled by a Lucas Dial-a-Time system which utilised a purpose built interface circuit enabling pulses to be used from the crankshaft encoder. An infra red cam flag signal was used to determine the point on the engine cycle where ignition should occur. The exhaust gas recirculation (EGR) level was controlled by an AC Rochester solenoid operated poppet type EGR valve, supplied by Delphi. The valve was interfaced to a controller designed

and built at Oxford University which used pulse width modulation to command the poppet position. This combination was found to be unstable at some operating points, so a manual valve was used, in series with the poppet valve, to control EGR flow.

An OTC 4 gas analyser, utilising a non dispersive infra-red (NDIR) system and a Teledyne Oxygen sensor was used for measuring the CO, CO_2 and O_2 in the exhaust, and a Rotork analysis flame ionisation detector (FID), calibrated as ppm CH_4, was used for measuring unburned hydrocarbons. An additional Richard Oliver K550 4 gas analyser was used to measure CO_2 levels in the inlet system when conducting tests with EGR, this used a sampling system which is shown in Figure 4.3. A vacuum pump was used to draw a sample from the inlet of the engine through the Platon Flostat, which ensured constant pressure, slightly above ambient, at the entry to the analyser. Pressure immediately downstream of the vacuum pump was controlled to approximately 0.3 bar gauge by the non-return valve. This allowed a certain amount of recycling of the sample to take place, results were only recorded after the analyser had stabilised and therefore the results were believed to be insensitive to this effect. If transient testing were to have been carried out, a time constant for the system would have to be evaluated and applied to all results. Air-fuel ratio and lambda were calculated using the CO, CO_2, O_2 measured from the OTC 4 gas analyser and FID measured HCs using methods described in Appendix J. The 4 gas analysers were both self calibrating after initial factory calibration, but were checked with span gases, the FID was calibrated in the normal manner, all analysers using certified gas mixtures containing methane, carbon monoxide, carbon dioxide and nitrogen.

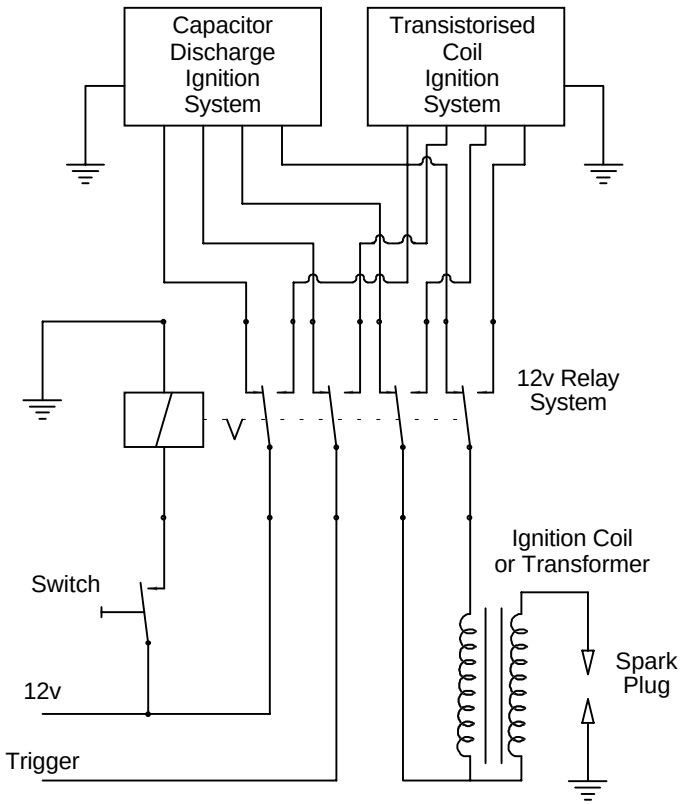

Figure 4.4 Method of changing between ignition systems

The speed and load of the engine were governed by a Control Techniques M155R four quadrant controller and Mawdsley DC dynamometer. The engine speed was measured from this system with a 60 tooth wheel with an inductive pickup supplying a digital panel meter on

the control panel. A relay system was used to connect the 12V supply and LT outputs from the ignition system to the coil, this arrangement is shown in Figure 4.4. When changing from one system to the other, minimal disturbance was made to the engine, with at most, one mis-firing cycle.

Electrical measurements were obtained using techniques described in Chapter 2, the measurement apparatus being shown in Figure 4.5.

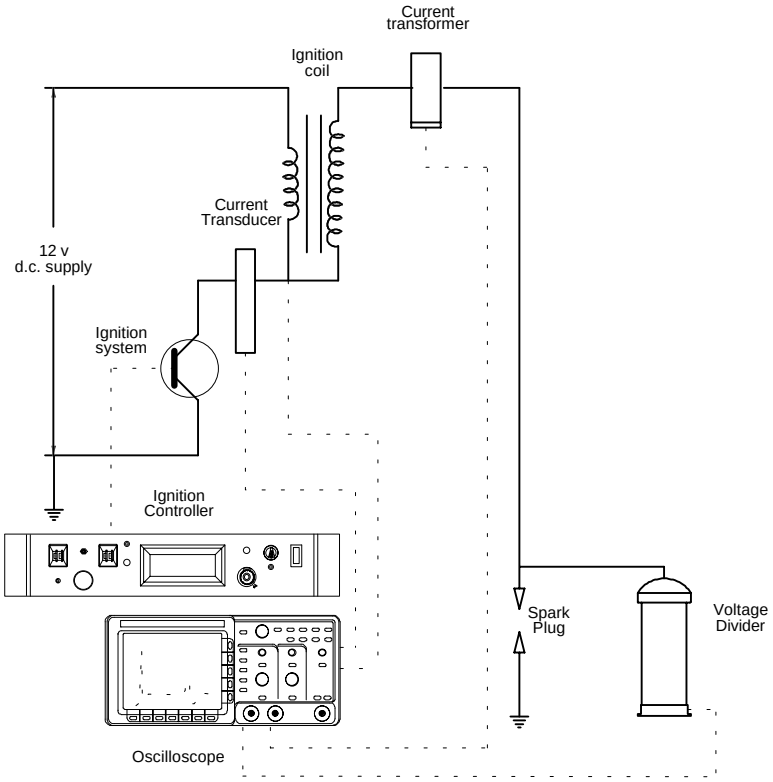

Figure 4.5 Experimental apparatus (on engine tests)

4.2 Method of investigation

In order to vary the engine operation as much as possible, three operating points were chosen and are shown in Table 4-2. These operating points covered different mixtures (at all test sites), different speeds, different loads and the use of EGR (at site 3).

Describing the operating points in BMEP terms would have been meaningless. Due to the greater friction loadings of the single cylinder engine design, the BMEP figures would be artificially low and bear no relation to those from the four cylinder variant. The ignition timing was fixed at 25° BTDC, this represented MBT at stoichiometric for the 1000 revs/min tests. The decision to maintain a fixed timing was made because of the difficulty in determining peak torque. This difficulty can be attributed to the engine being a single cylinder running at a condition where cycle-by-cycle variations in combustion were prominent, and a data logging system that required a complicated method of post processing to calculate IMEP. A more satisfactory method would be to use an on line IMEP meter, operating from a high speed data acquisition system which measures the cylinder pressure and calculates an average over a certain number of cycles. This should be readily achievable using a data acquisition system with integral software such as LabView.

Test site	Speed	Air flow rate	IMEP at λ=1
	r/min	L/sec	bar
1	1000	1	1.75
2	2000	2	2.25
3	1000	2	4.25

Table 4-2 - Engine operating points

Using the ignition timing discussed above, the two ignition systems were tested using a relay system to connect the 12V supply and LT outputs from the ignition system to the coil, as discussed in 4.1. High speed data acquisitions were made of two channels; the cylinder pressure and the crankshaft encoder flag. When the engine was at a satisfactory operating point, it was allowed to settle for a few minutes before 1MB of data was acquired. When the acquisition was complete, the data was saved to disk before another 1MB of data was acquired. After five separate acquisitions, the ignition system or energy level was changed, the engine allowed to settle and the process repeated. When all the system and energy configurations had been tested at that operating point, the mixture was changed, the engine allowed to settle and the process repeated.

At test point 3, the EGR was controlled by a manual valve, after the instability of the control system and pulsed valve was discovered. The Richard Oliver K550 was used to sample the inlet gases, the CO_2 level being compared to that in the exhaust, which was measured with the OTC analyser. The EGR level was calculated from:

$$\text{EGR\%} = \frac{\%CO_2 \text{ inlet}}{\%CO_2 \text{ exhaust}}$$

Careful valve adjustment was made to achieve the desired level. As the EGR level increased, inlet air was displaced and to maintain a constant air-fuel ratio the fuelling was reduced. No corrections for condensed water vapour were made, but this was believed to be small since the recycled exhaust gas external pipework was heated by the engine cooling water.

4.2.1 Combustion analysis

Ignition parameters have the most pronounced effect on the early stage of combustion, which is often termed the *ignition delay period* or the *flame development period* (Heywood 1988), it is this phase which is most critical when considering the combustion repeatability or cycle-by-cycle variance. The most applicable combustion parameters were therefore the 0-10% burn duration, and the coefficient of variance (COV) of IMEP. The COV of IMEP is a more robust calculation and is of direct relevance to driveability. With the 0-10% burn duration, the results have some dependence upon the calculation method used. The COV was measured by evaluating the average COV of five batches of 300 cycles. A mean cycle was used to obtain the 0-10% burn duration for each batch of 300 cycles and an average calculated for the 5 batches, this method was deemed to be accurate for this purpose by Ball (1997).

4.2.2 Influence of atmospheric conditions

Throughout the tests, the author was conscious that atmospheric conditions would have an effect on the acquired data. Tests were therefore always carried out against a benchmark ignition system and increases or decreases in engine performance were considered to be purely relative; the absolute values being meaningless without a complex correction. The necessary correction factors do not exist to the author's knowledge, and would require a test facility with

the ability to vary ambient humidity, temperature and pressure. Engine 'condition' may also influence results from day to day, examples of this may be piston ring wear and combustion deposit build-up. The aim of this study is therefore to suggest which ignition strategies are better in certain situations.

4.2.3 Energy storage

The TCI system differs from the CDI system in the way that the energy is stored. The TCI system uses an inductor, the primary winding of the ignition coil, as the storage device, the energy being stored in the magnetic field which is created by a current flow. The CDI system uses a capacitor as the storage device, energy being stored in the electric field which is created by a voltage source.

4.2.4 Calculation of stored energy

All energies quoted are stored energies and are calculated as follows:

For the TCI system:

(4-1

$$E = \tfrac{1}{2} LI^2$$

For the CDI system:

(4-2

$$E = \tfrac{1}{2} CV^2$$

The stored energies will differ considerably from the energy in the gap, which will again differ considerably from the energy deposited in the mixture. Nominal stored energies were calculated to be 60mJ for the CDI system and 100mJ for the TCI system.

4.2.5 Producing the spark

A spark or conduction path is achieved by ionising the medium in the spark plug gap, this is done by exciting the electrons, by inducing a very large potential difference, typically of around 1kV and above; but depending upon the gap length, temperature, pressure and medium. These high potential differences are generated by, in the case of the TCI system, the collapse of the magnetic field, inducing a voltage in the primary winding (up to 300V) which induces a voltage in the secondary winding through a turns ratio of approximately 66:1 (Tranter 1993), and hence an available voltage of up to 20kV. With the CDI system, the secondary voltage is induced by discharging the capacitor, which is charged to around 350V, through a transformer (similar to an ignition coil, but of lower primary inductance and resistance).

4.3 Discussion of results

4.3.1 Effects of reduction in energy (test site 1)

4.3.1.1 Electrical effects

With the TCI system, a reduction in stored energy results in a shorter spark duration, this effect can be seen in Figure 4.6, Figure 4.7 and Figure 4.8. The end of the discharge is signified by no current flow and a voltage 'ringing' in the HT lead, spark durations being 1.7, 1.2 and 0.5ms for the 100, 50 and 25% energy levels. It should be noted that the spark discharges for the TCI system differed from one to the next. Reducing the energy of the CDI system results in a lower peak current and a shorter spark duration, shown in Figure 4.9, Figure 4.10, and Figure 4.11. Reducing the energy further in a CDI system prevents breakdown occurring, the current and voltage measured is that of oscillations in the HT cable and coil. The shorter spark duration from the lowered energy in the CDI system is due to less energy being stored in the coil as the capacitor discharges through the primary winding. This energy is dissipated when the capacitor has fully discharged and the spark has collapsed. A new spark is initiated with the opposite polarity, and the breakdown voltage is small due to the abundance of ionised species in the plug gap. Spark durations for the CDI system were measured to be 0.15 and 0.12ms for the 100 and 50% energy levels.

4.3.1.2 Combustion effects

Figure 4.12 shows how ignition parameters have very little effect on the IMEP. Figure 4.13 shows that a reduction in energy on the TCI system gives less combustion stability with leaner mixtures, the watershed for this effect is at around lambda 1.4. Ignition effectiveness is at a maximum when using the full energy of the TCI system, at the extreme of lambda 1.7, the 50% test shows results not dissimilar to that of the 100% test, whereas the 25% test shows a marked reduction in stability. The CD system however, when using the Lucas coil, shows combustion improvements, over the TCI system, in the leaner regions.
Figure 4.15 and Figure 4.16 show the lack of effect on IMEP and cycle-by-cycle variation with an increase and decrease in energy of the CD system when used with the Lucas coil. When changing the energy, no increase or decrease in ignition effectiveness can be seen, we can conclude from this that as long as there is enough energy in the capacitor to break the plug gap, the higher powered spark is more beneficial for combustion initiation than a longer lower powered spark. The results of COV are backed up by Figure 4.14 and Figure 4.17, showing that long burn duration and high COV of IMEP correspond to one another.

4.3.2 Effects of different ignition transformer (test site 1)

4.3.2.1 Electrical effects

Capacitor discharge systems are designed to work with ignition transformers as opposed to ignition coils. As discussed previously, the ignition coil utilises a high primary inductance to enable a magnetic field to be produced for the purpose of energy storage. An ignition transformer primary winding is of very low inductance and resistance, so low that the winding is very fragile and can be damaged if too much power is dissipated through it, for instance if the transformer was mistakenly connected to a transistorised ignition system.
Reducing the primary winding resistance and inductance results in a much faster primary current rise, and hence a faster secondary voltage rise, which is one attraction of a CD system. The lower inductance of the ignition transformer results in less energy being stored in the

magnetic field and hence a smaller energy dissipated across the gap on the collapse of the magnetic field; this shortens the spark duration. With an ignition coil, not only does the coil act as an ignition transformer, albeit with a longer secondary voltage rise time, it also acts as a second energy storage device. When the spark is formed on the building of the magnetic field, some energy is stored in the primary winding, and this is dissipated when the first spark collapses.

Figure 4.18 shows the effects of different ignition transformers on the voltage rise time in a rig at ambient pressure. The breakdown voltage appears to be higher with the ignition transformer, this is most probably due to a poor choice of data. However, it is possible that the slower voltage rise time of the ignition coil allows a longer residence time for the medium between the gap, and therefore could allow conduction to occur from a lower breakdown voltage. It can be seen that a glow phase (seen as a phase of higher voltage and lower current) develops when using an ignition coil; this is due to the slower discharge of energy through the higher resistance of the secondary winding (coil specifications can be found in Appendix F). The ignition transformer allows only the arc phase to exist. When considering the current in the early part of the discharge, shown in Figure 4.19, the glow and arc phases can be seen as low and high levels of current respectively. Figure 4.20 and Figure 4.21 show the complete discharge. The use of an ignition transformer shortens the duration by 30%, the ignition coil discharge having a duration of approximately 0.15ms and the ignition transformer a duration of approximately 0.1ms. The peak current with an ignition transformer is approximately 0.4amps (neglecting the breakdown phase), this is reduced to 0.15amps with the ignition coil.

4.3.2.2 Combustion effects

Although the IMEP remains unperturbed (Figure 4.22), Figure 4.23 shows that the use of an ignition transformer with a CD system has a detrimental effect on engine performance at lower energy levels, when compared with the use of an ignition coil, as the mixture is made leaner. Reducing the energy of the CD system reduces the ignition effectiveness to a greater extent that that exhibited with the ignition coil (Figure 4.16). Figure 4.24 shows the corresponding burn duration lengthening as the COV increases. Conclusions from these tests are that the mixture is ignited more reliably by a longer spark, which is achieved by *throttling* the voltage rise time and storing some of the energy to be released on the collapse of the spark. It can be postulated that a glow discharge, induced by the ignition coil, is more effective at ignition than an arc discharge which is induced by the ignition transformer.

4.3.3 Effects of higher engine speeds (test site 2)

Higher speed tests show that ignition parameters are more critical. Whereas it was shown, at 1000 rpm, that a discharge from the CDI system with the Lucas ignition coil was beneficial to combustion compared to the TCI system regardless of the stored energy, Figure 4.25 and Figure 4.26 show that this is not the case at higher speeds. Higher speed operation is more stable with the TCI system with 50% or 100% of the stored energy, or the CDI system with 100% of the stored energy. Both the 50% CDI and 25% TCI have a very poor performance at anything leaner than stoichiometric and this is echoed in the IMEP characteristics shown in Figure 4.25. Figure 4.27 shows the leanest results of the 100% and 50% TCI and the 100% CDI on a more suitable scale. They show that marginally better stability can be obtained from the highest energy TCI system, the burn duration, shown in Figure 4.28 emphasises these results. It should also be noted that the lean mixture limit is closer to stoichiometric, at the lower engine speed a COV of 50% was encountered at λ=1.7 when using the most beneficial ignition system. This level is reached at λ=1.6 when running at 2000 rpm. We can conclude that the engine requires more energy input for higher speed low load operation. It should be remembered that higher engine speeds result in less time available for the coil (or capacitors) to

charge, although in this study these constraints will not apply due to there being only one cylinder operating at a relatively low speed.

4.3.4 Effects of higher IMEPs (test site 3)

4.3.4.1 Electrical effects

Higher loads are possible with a higher volumetric efficiency, this in turn leads to a higher pressure at the point of ignition. This higher pressure will demand a higher breakdown voltage, and will therefore redistribute the ignition energy shortening the spark duration, or in the case of the lower energy CD system, the higher pressure may demand more energy than is stored, and hence breakdown may not occur.

4.3.4.2 Combustion effects

Figure 4.29 and Figure 4.30 show that at higher loads, the mixture is not readily ignitable by either the 25% energy TCI or the 50% energy CDI systems. As the mixture is weakened, the 100% CDI and the 50% and 100% TCI systems show similar ignitability, although it would seem that the higher energy TCI system has the best performance. Figure 4.31 shows that the poor performance of the lower energy systems is not apparent when considering the burn duration. This is believed to be a consequence of the calculation method and is discussed in section 4.3.5.

4.3.5 Effects of EGR (test site 3)

EGR is used as a diluent to reduce part load pumping losses, and also to reduce engine-out NOx emissions, which is most useful before catalyst light-off. The recycled exhaust gas was transported from the exhaust pipe by a heated pipe and introduced into the inlet pipe, downstream of the throttle. When using EGR, albeit at the higher load, lower speed condition, the effects of the different ignition systems are more pronounced. The lowest energy TCI system is unsatisfactory as ignition is unreliable with more than about 10% EGR, this can be seen in terms of IMEP (Figure 4.32) and COV (Figure 4.33), additional data was not acquired due to continous misfire and therefore only one data point supports this claim. The apparent 0-10% burn duration (Figure 4.34), however, shows that the burn duration is lowest with the 25% TCI and 50% CDI even though the COVs are relatively high for both these systems. This anomaly is due to the calculation method. The Rassweiler and Withrow (1938) method assumes the total charge burned per cycle analysed to be 100%, i.e. complete combustion occurs; the algorithm does not detect misfires or partial burns, hence 10% of the total charge burned will oxidise in a shorter period than 10% of the total charge present.

4.4 General discussion

The results have shown that different operating conditions place different demands on the ignition system. At the low speed, low load condition, the CDI system outperforms the TCI system, even with 30% of the energy (30mJ compared to 100mJ) of the inductive system, and a spark duration an order of magnitude shorter. The same system, at the higher load, performs very poorly, this is mainly due to insufficient energy to cause reliable breakdown at the increased cylinder pressure at the time of ignition.

For the same operating point, as the mixture becomes leaner, the pressure at the time of ignition increases. This is due to an increasing ratio of specific heats (κ). The ratio of specific heats for air, a mainly diatomic mixture, is 1.4, whereas for methane, with five atoms, it is 1.19 (at

450K). The higher the ratio of specific heats, the higher the pressure increase for the same increase in volume (ideal gas undergoing an isentropic process). This effect is also present when using EGR, the recycled exhaust gas has a ratio of specific heats of approximately 1.3, most of the oxygen being used to form carbon dioxide (κ=1.19 at 450K)) and water (κ=1.24 at 450K) in the combustion process. As the EGR level increases, κ reduces and hence the pressure at ignition reduces also. The pressure at ignition is also reduced by a decrease in volumetric efficiency since the EGR is inducted by the engine at a higher temperature than ambient, reducing the density of the charge. Reductions in κ result in lower breakdown voltages, this allows more energy to be dissipated in the later stages of the discharge, which for an inductive ignition system will result in a longer spark duration.

It has been shown that the maximum energy available from an ignition system is not always required. Higher ignition energies are normally associated with decreased electrode life, it is therefore prudent to use the minimum energy needed to ensure reliable flame initiation. A variable energy or perhaps a dual strategy system is therefore desirable.

When the COV is high, the 0-10% burn duration is also long provided there is no partial burn. There will always be a minimum 0-10% burn time for a given engine and operating point. As ignition becomes unreliable, perhaps due to eroded spark plugs, there will be certain cycles where the early flame development period increases, this will then increase the average 0-10% burn duration. This increases the COV of IMEP because the flame kernel is subject to more disturbance before the transition to fully turbulent combustion.

It is interesting to note that the use of an ignition coil, as opposed to an ignition transformer, with the CDI system was beneficial for lower stored energies (although no back to back testing was carried out). The higher inductance of the coil resulted in energy storage as the capacitor discharged through the primary winding and as the magnetic field collapsed, a further EMF was produced in the secondary winding and hence more current to flow through the electrode gap. The higher inductance and resistance of the ignition coil resulted in an early transition from the arc mode to the glow mode, whereas the use of the ignition transformer resulted in an arc discharge only.

4.5 Chapter conclusions

Table 4-3 shows the relative effectiveness of each ignition system at each operating point. The results show that the best compromise for an ignition system is the TCI, this the most suitable for all but one operating point. The trend displayed can be extrapolated to assume that a high load condition would be best ignited by a TCI system also. The CDI system shows good results at the lowest load and speed condition, this contradicts the findings of other workers, although no publications which have been found show a direct comparison of the effects of ignition systems at a number of different operating conditions.

Test site	**Speed**	**Load**	**TCI 100% (100mJ)**	**TCI 50% (50mJ)**	**TCI 25% (25mJ)**	**CDI 100% (60mJ)**	**CDI 50% (30mJ)**
1	low	low	4	3	1	5	5
2	med	low	5	4	0	4	1
3	low	med	5	4	0	4	0
EGR	low	med	5	5	0	4	3

Table 4-3 - Ignition system suitability to engine operating point (5=best, 0 =worst)

The choice of ignition transformer for the CD ignition system was found to have a marked effect on combustion at lower energy levels, using an ignition coil resulted in a glow discharge, but the lower resistance and inductance of an ignition transformer resulted in no glow phase, an arc phase occurring instead. It was found that the ignition transformer induced a discharge of around 66% as long as that of the ignition coil, and combustion was seen to suffer slightly even though more energy is likely to be deposited in the gap due to less resistive losses. The ignition effectiveness, with the ignition transformer, was reduced further when the stored energy was halved, this effect was more pronounced than for the same case with the ignition coil, although this is a relative comment and no direct back to back testing was carried out.

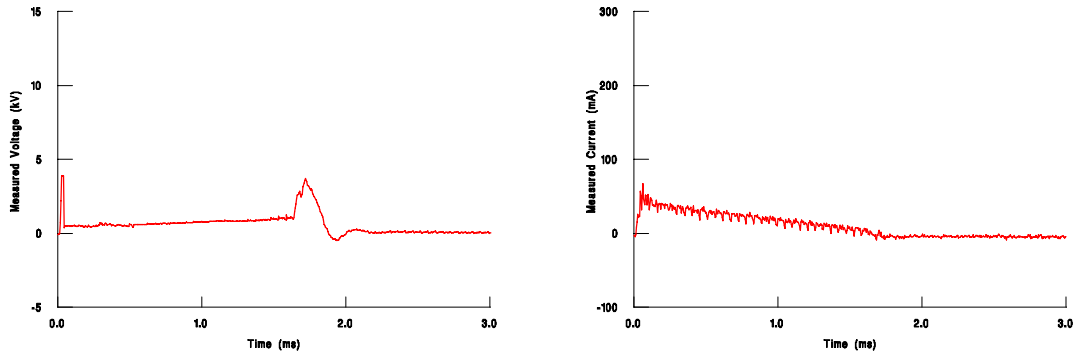

Figure 4.6 Transistorised Coil Ignition System - Lucas Coil - 100mJ stored energy

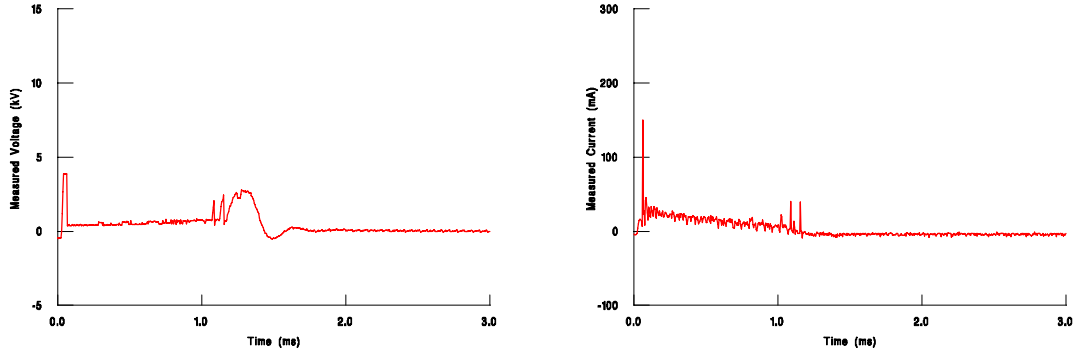

Figure 4.7 Transistorised Coil Ignition System - Lucas Coil - 50mJ stored energy

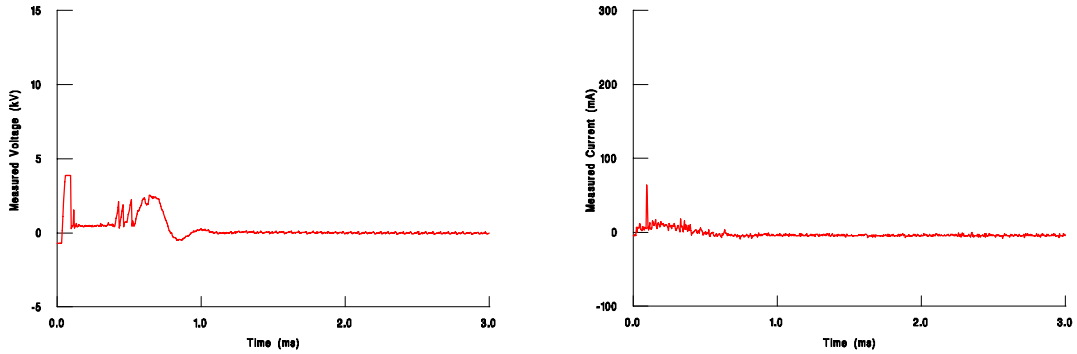

Figure 4.8 Transistorised Coil Ignition System - Lucas Coil - 25mJ stored energy

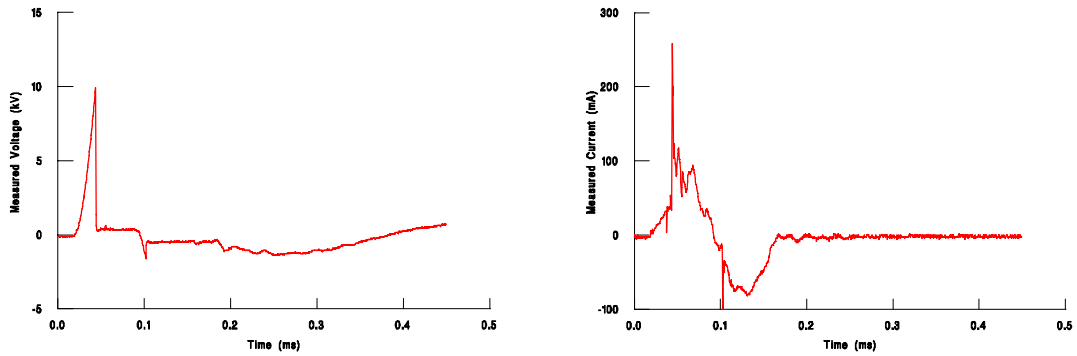

Figure 4.9 Capacitor Discharge Ignition System - Lucas Coil - 60mJ stored energy

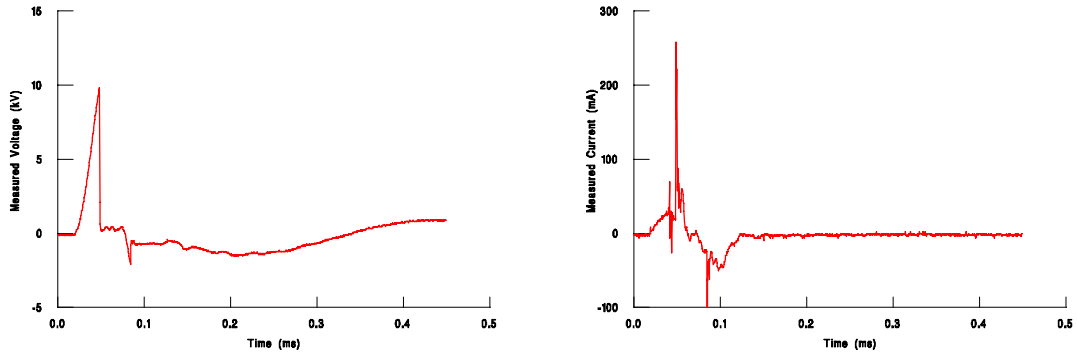

Figure 4.10 Capacitor Discharge Ignition System - Lucas Coil - 30mJ stored energy

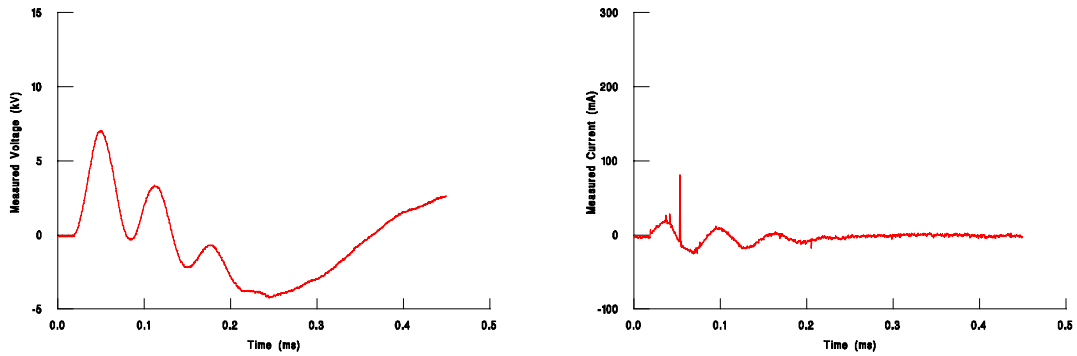

Figure 4.11 Capacitor Discharge Ignition System - Lucas Coil - 15mJ stored energy

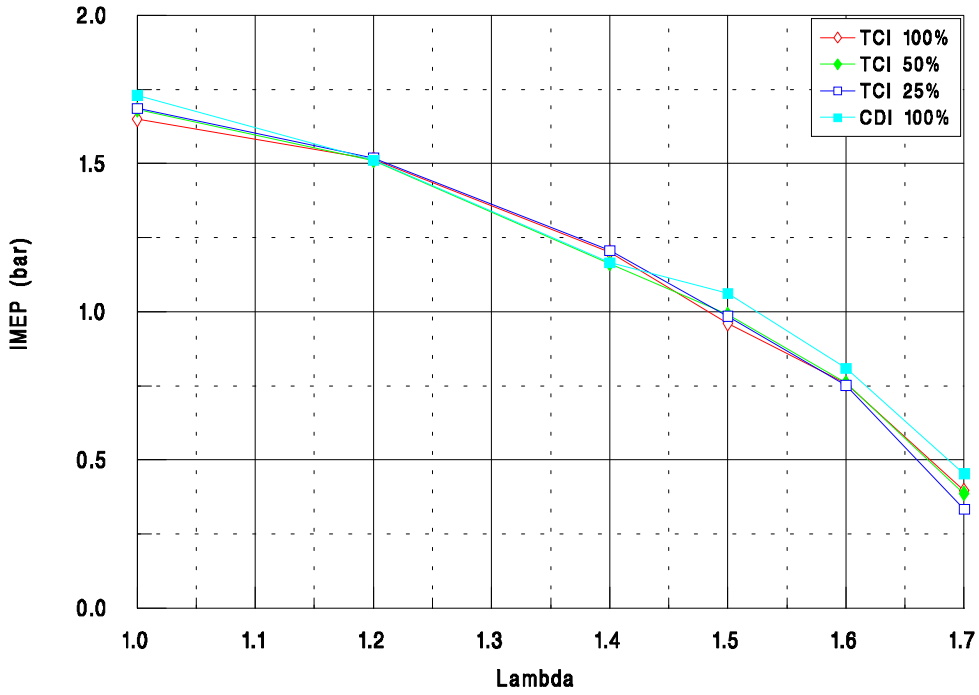

Figure 4.12 **Relationship between lambda and IMEP for transistorised ignition, with reduction in energy, and capacitor discharge ignition at 1000 rpm and 1 L/s air consumption**

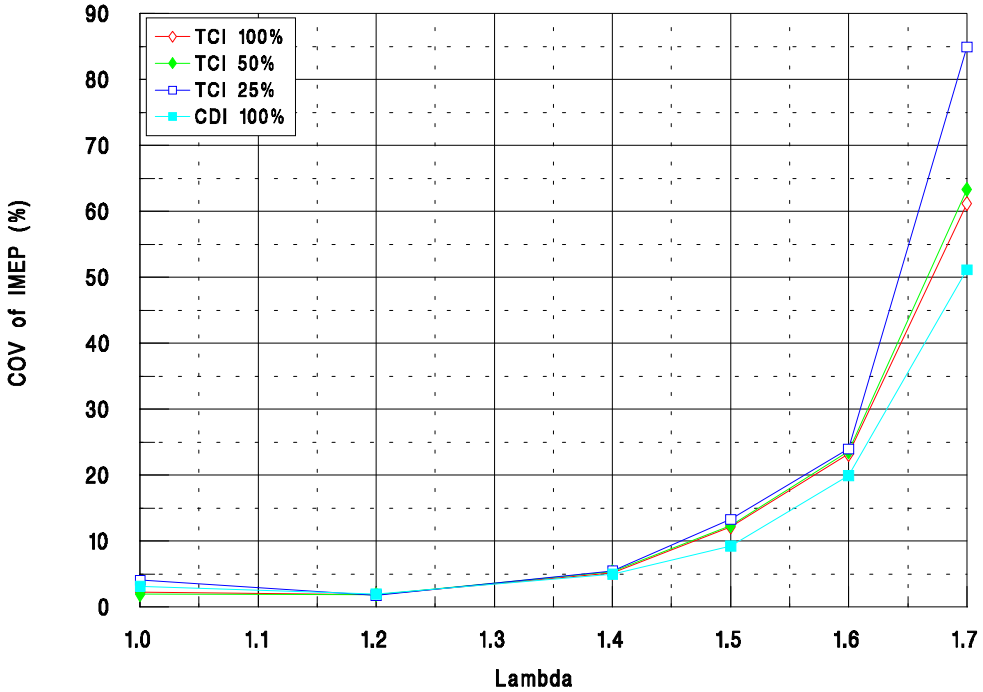

Figure 4.13 **Relationship between lambda and COV of IMEP for transistorised ignition, with reduction in energy, and capacitor discharge ignition at 1000 rpm and 1 L/s air consumption**

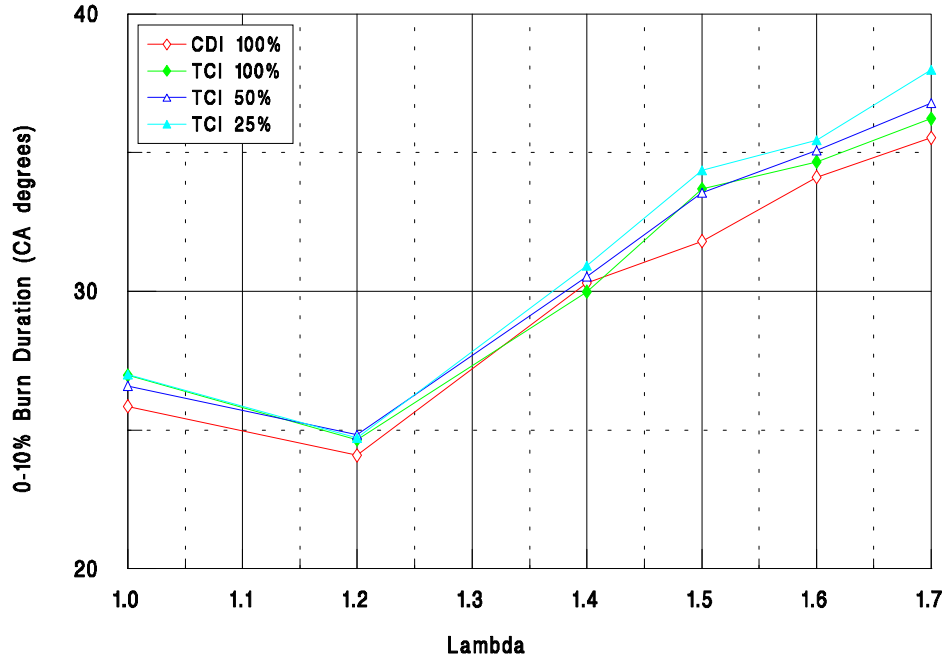

Figure 4.14 **Relationship between lambda and 0-10% burn duration for transistorised ignition, with reduction in energy, and capacitor discharge ignition at 1000 rpm and 1 L/s air consumption**

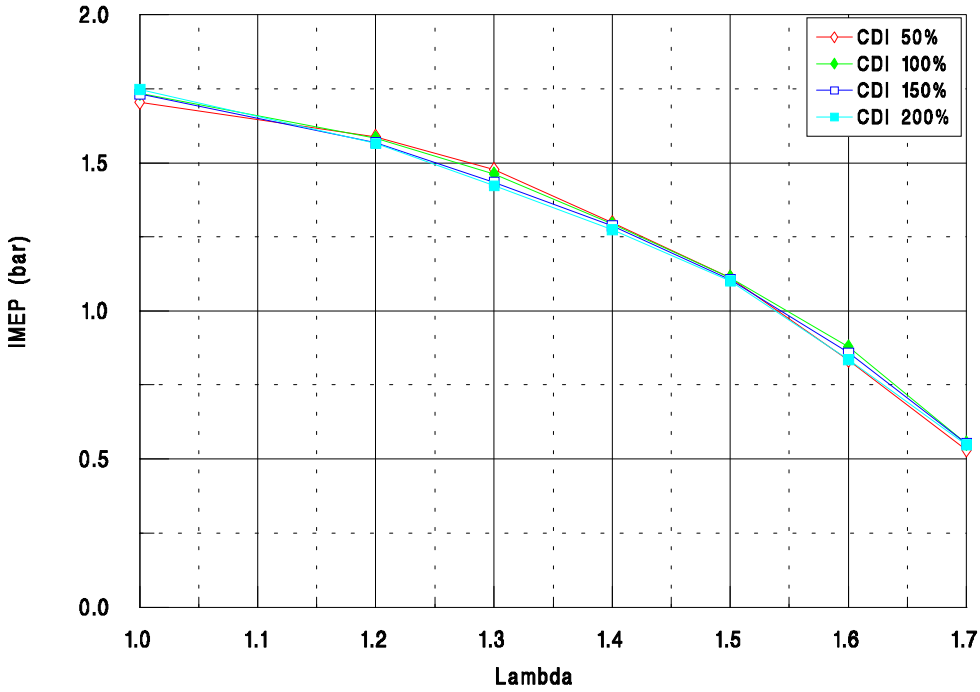

Figure 4.15 **Relationship between lambda and IMEP for capacitor discharge ignition with change in energy at 1000 rpm and 1 L/s air consumption**

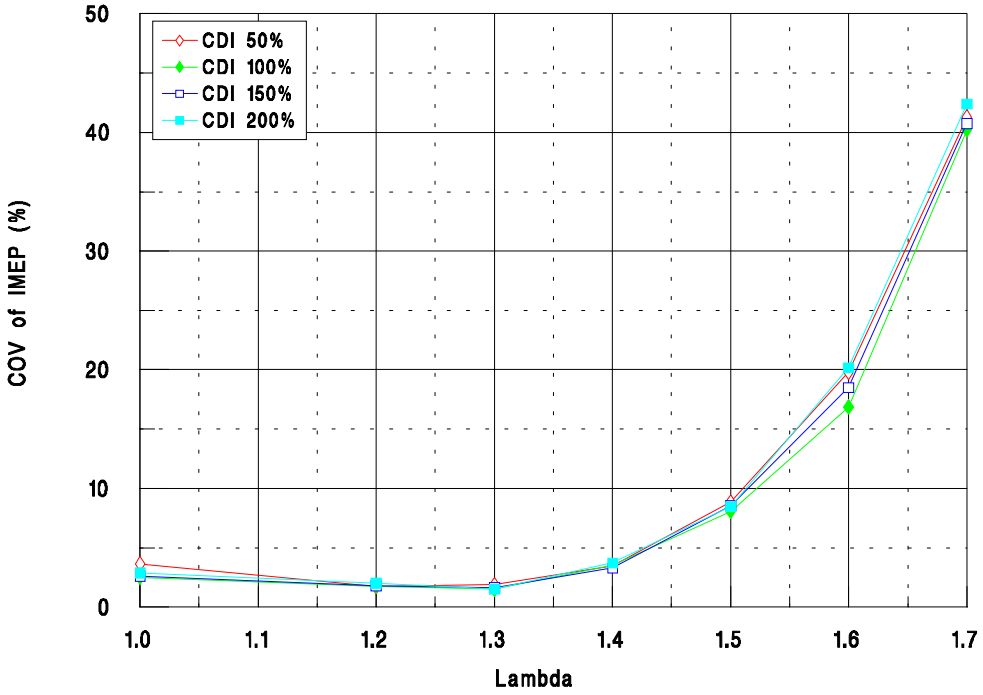

Figure 4.16 **Relationship between lambda and COV of IMEP for capacitor discharge ignition with change in energy at 1000 rpm and 1 L/s air consumption**

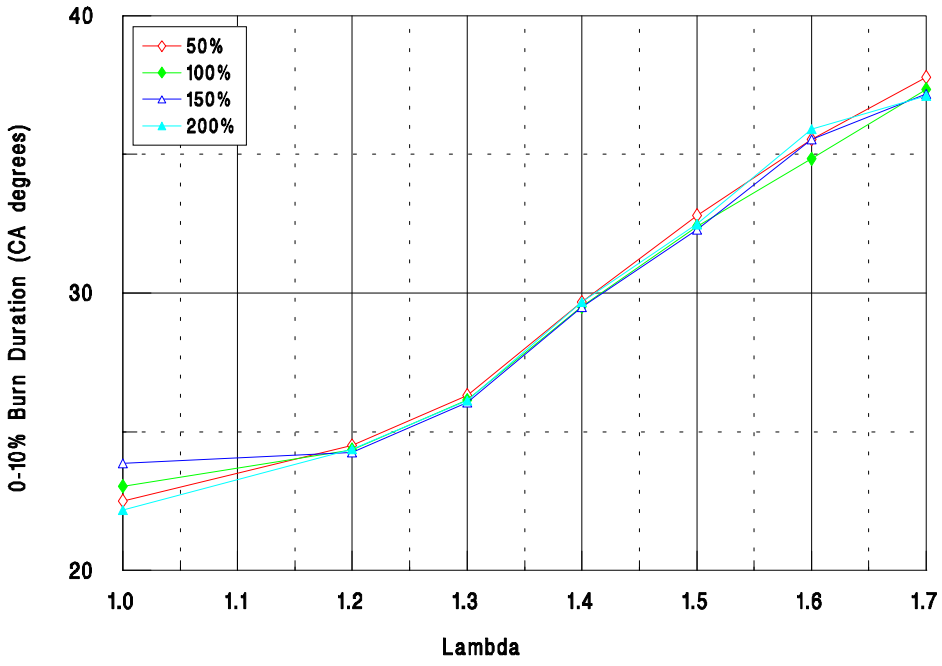

Figure 4.17 **Relationship between lambda and 0-10% burn duration for capacitor discharge ignition with change in energy at 1000 rpm and 1 L/s air consumption**

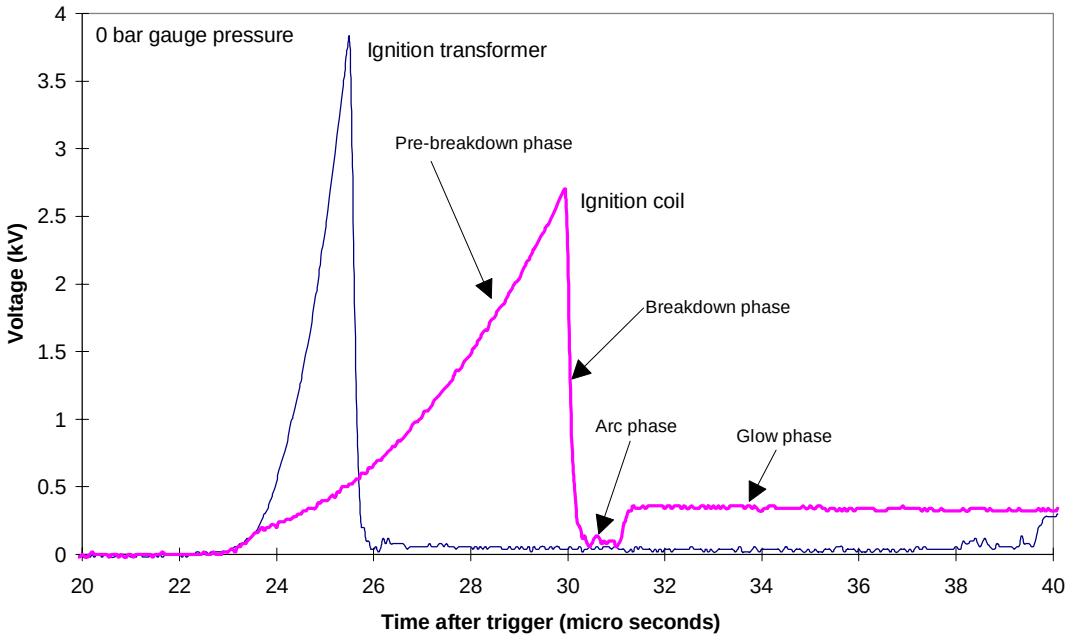

Figure 4.18 **Relationship between voltage and time for CDI system with ignition transformer and ignition coil during the early part of the discharge**

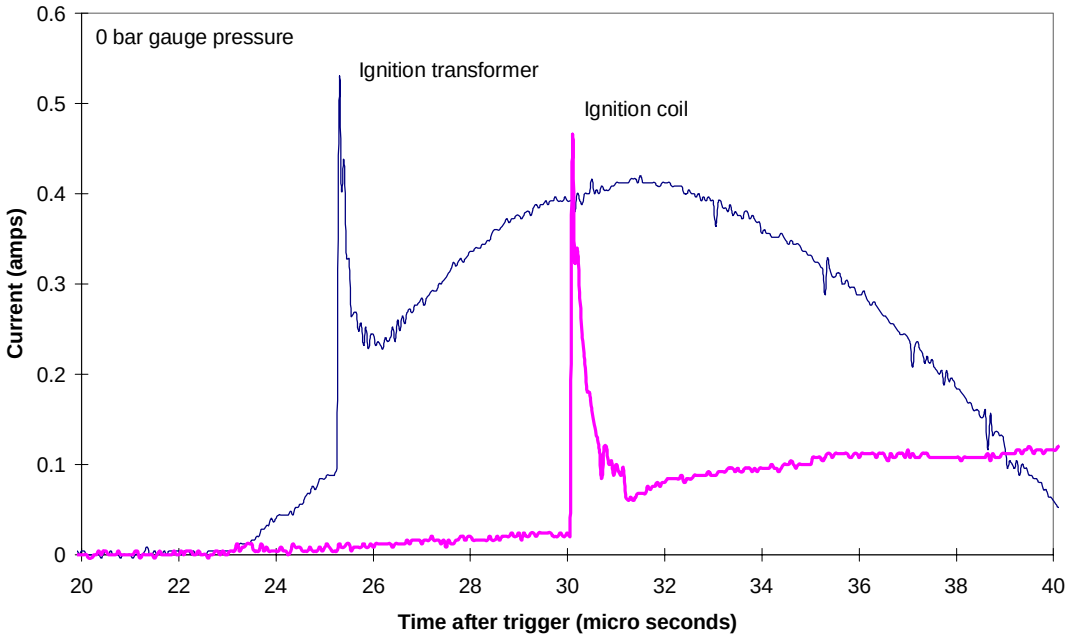

Figure 4.19 **Relationship between current and time for CDI system with ignition transformer and ignition coil during the early part of the discharge**

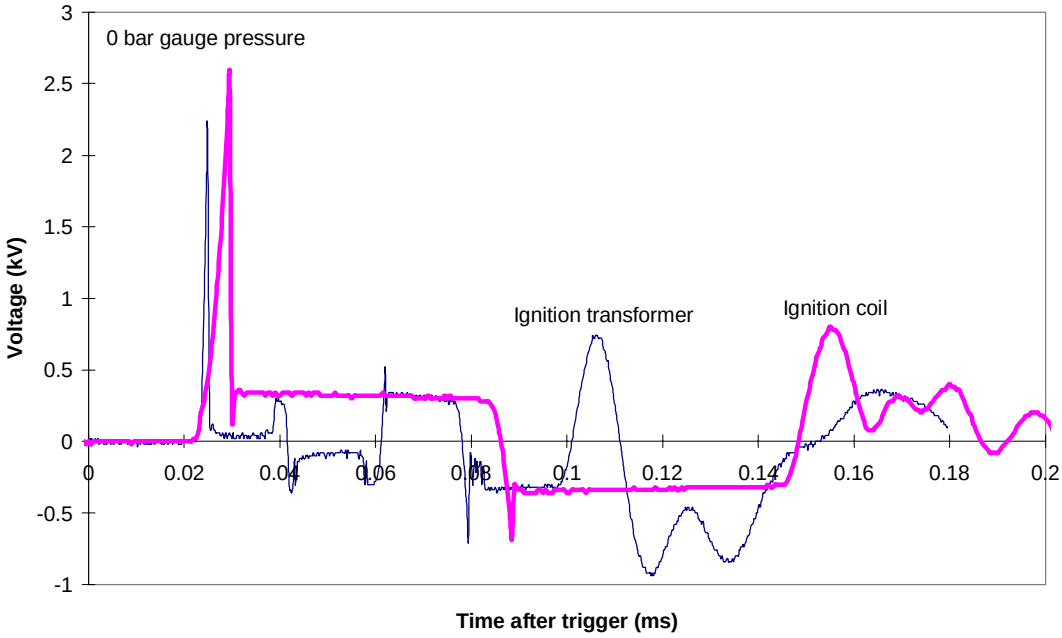

Figure 4.20 **Relationship between voltage and time for CDI system with ignition transformer and ignition coil during the complete discharge**

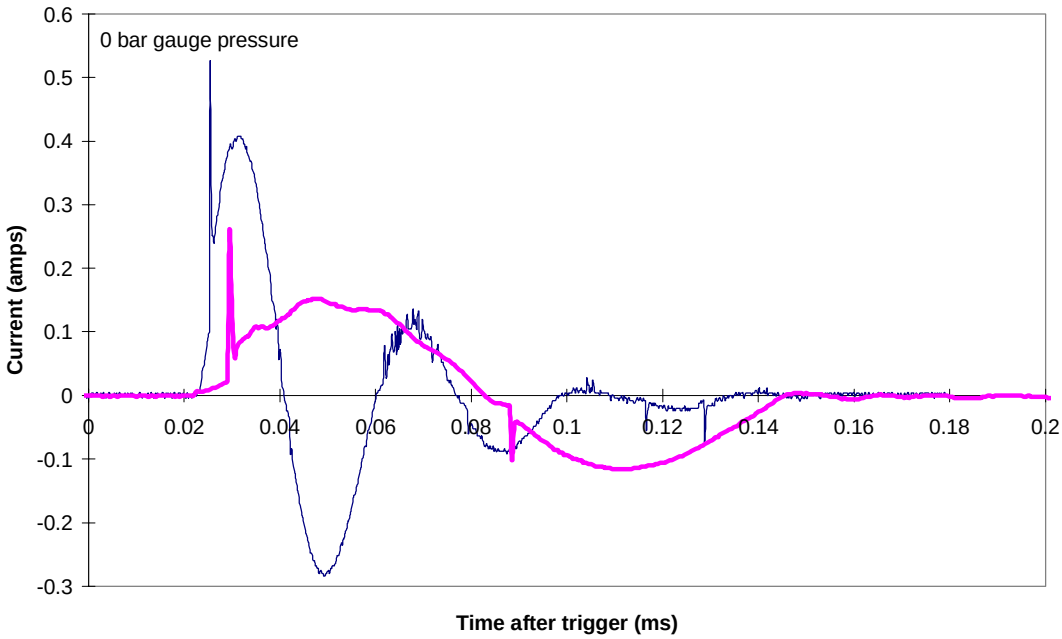

Figure 4.21 **Relationship between current and time for CDI system with ignition transformer and ignition coil during the complete discharge**

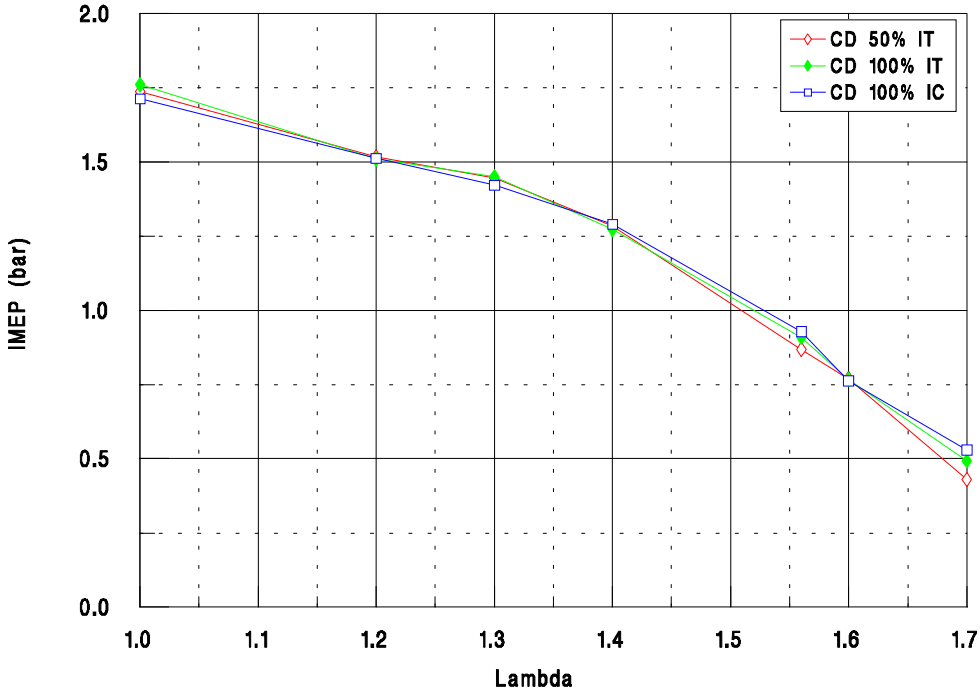

Figure 4.22 **Relationship between lambda and IMEP for capacitor discharge ignition, with ignition transformer (IT) and ignition coil (IC) with reduction in energy for the IT at 1000 rpm and 1 L/s air consumption**

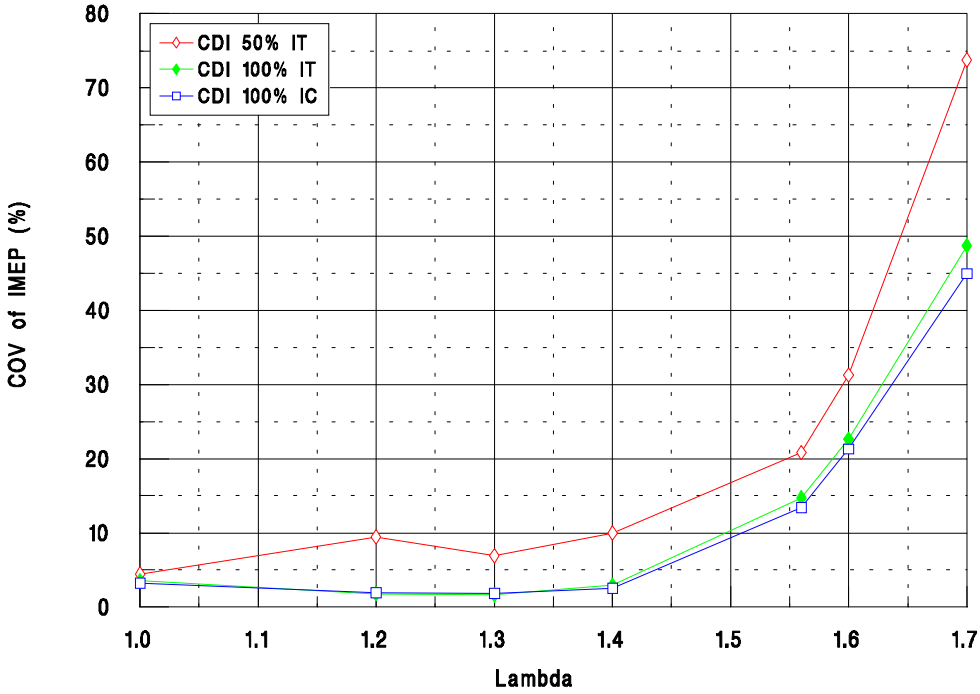

Figure 4.23 **Relationship between lambda and COV of IMEP for capacitor discharge ignition, with ignition transformer (IT) and ignition coil (IC) with reduction in energy for the IT at 1000 rpm and 1 L/s air consumption**

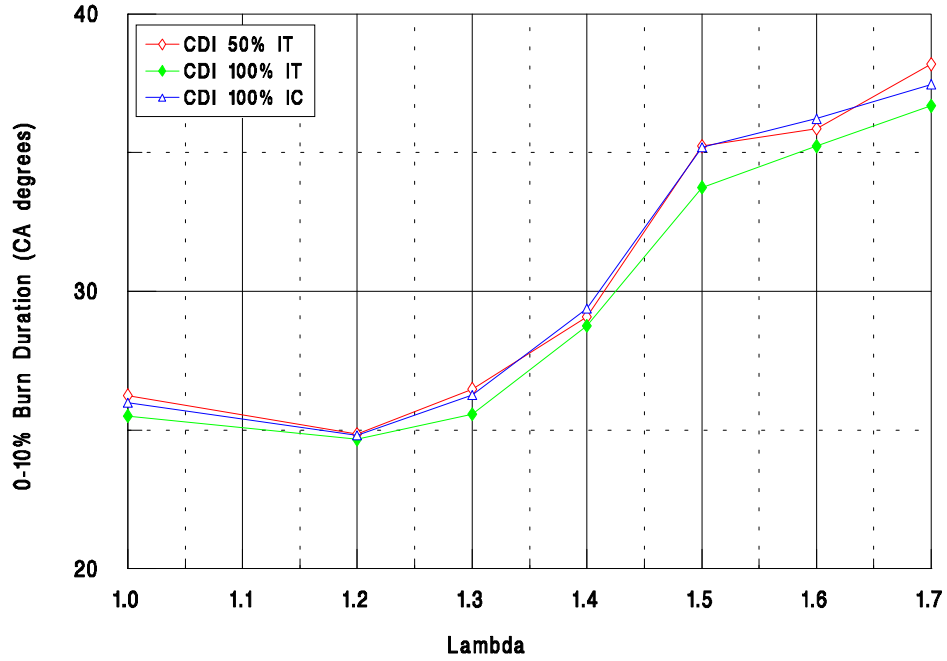

Figure 4.24 **Relationship between lambda and 0-10% burn duration for capacitor discharge ignition, with ignition transformer (IT) and ignition coil (IC) with reduction in energy for the IT at 1000 rpm and 1 L/s air consumption**

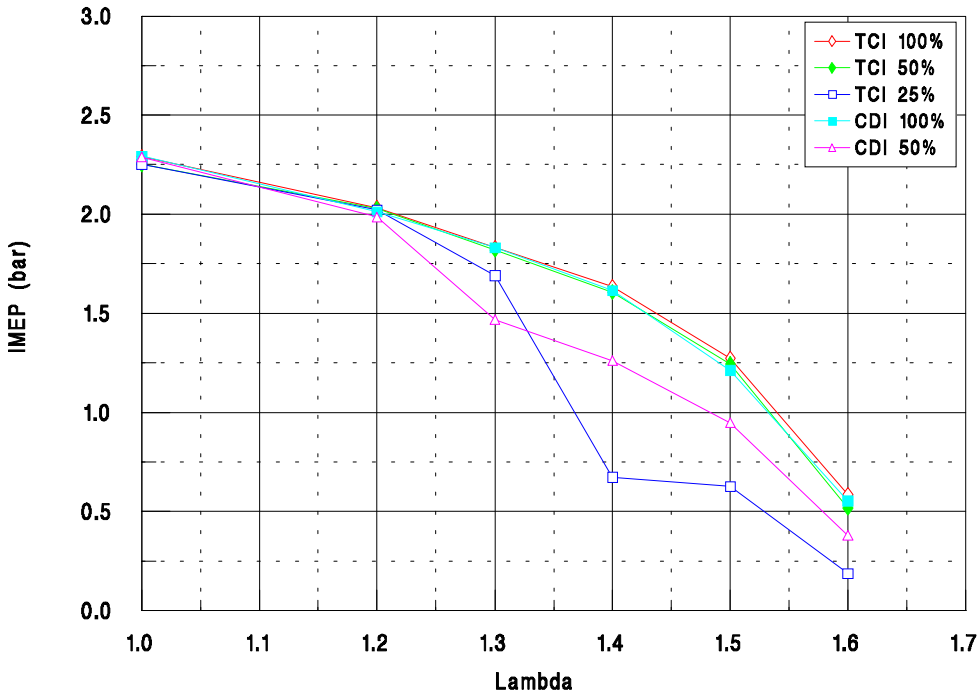

Figure 4.25 **Relationship between lambda and IMEP for transistorised and capacitor discharge ignition with reduction in energy at 2000 rpm and 2 L/s air consumption**

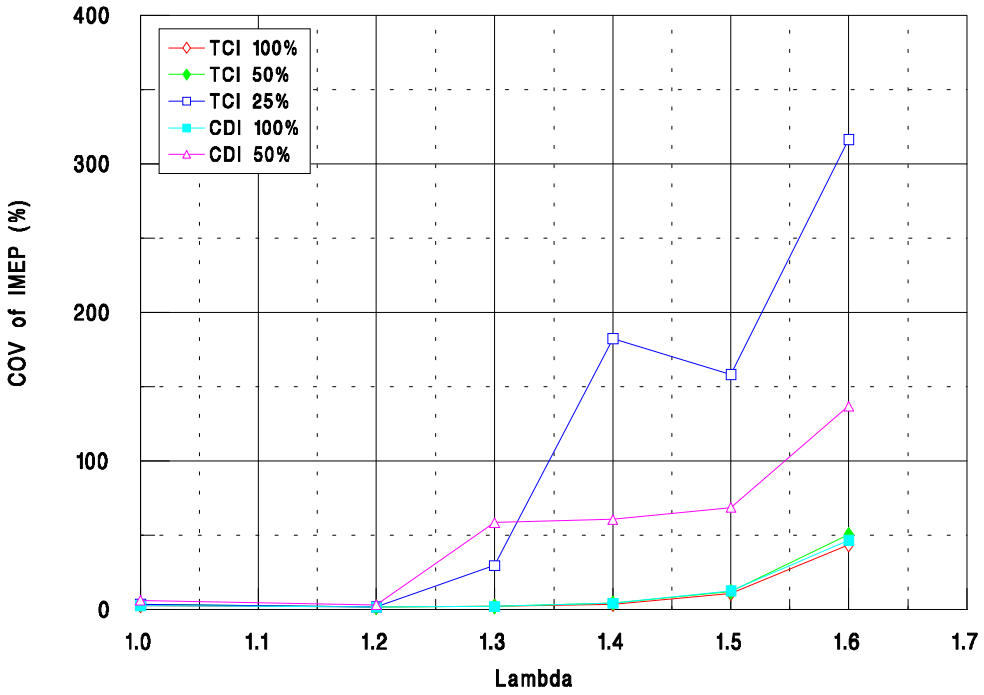

Figure 4.26 **Relationship between lambda and COV of IMEP for transistorised and capacitor discharge ignition with reduction in energy at 2000 rpm and 2 L/s air consumption**

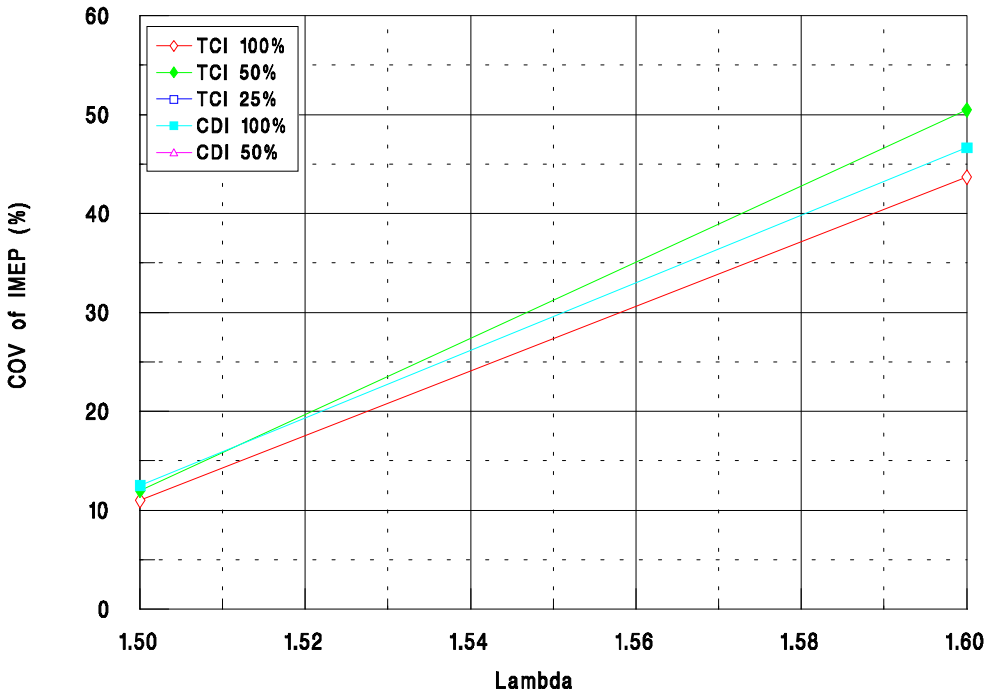

Figure 4.27 **Relationship between lambda and COV of IMEP for transistorised and capacitor discharge ignition with reduction in energy at 2000 rpm and 2 L/s air consumption (re-scaled)**

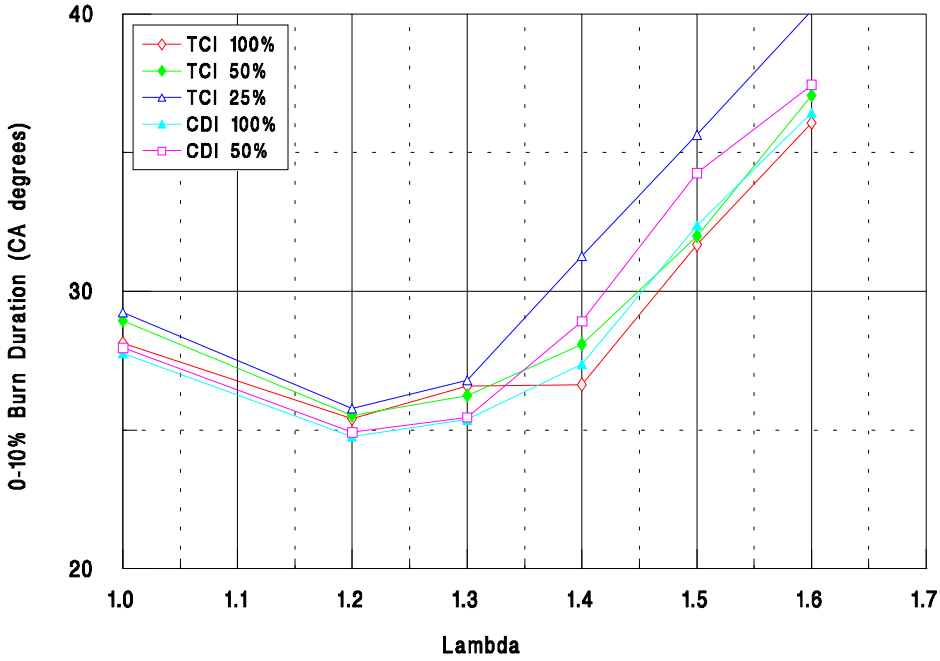

Figure 4.28 **Relationship between lambda and 0-10% burn duration for transistorised and capacitor discharge ignition with reduction in energy at 2000 rpm and 2 L/s air consumption**

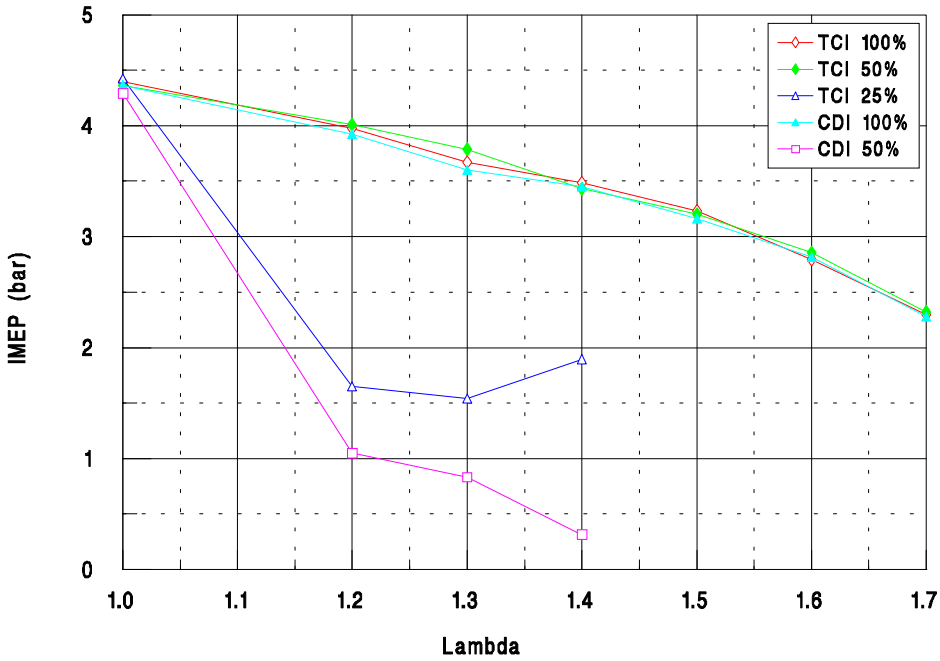

Figure 4.29 **Relationship between lambda and IMEP for transistorised and capacitor discharge ignition with reduction in energy at 1000 rpm and 2 L/s air consumption**

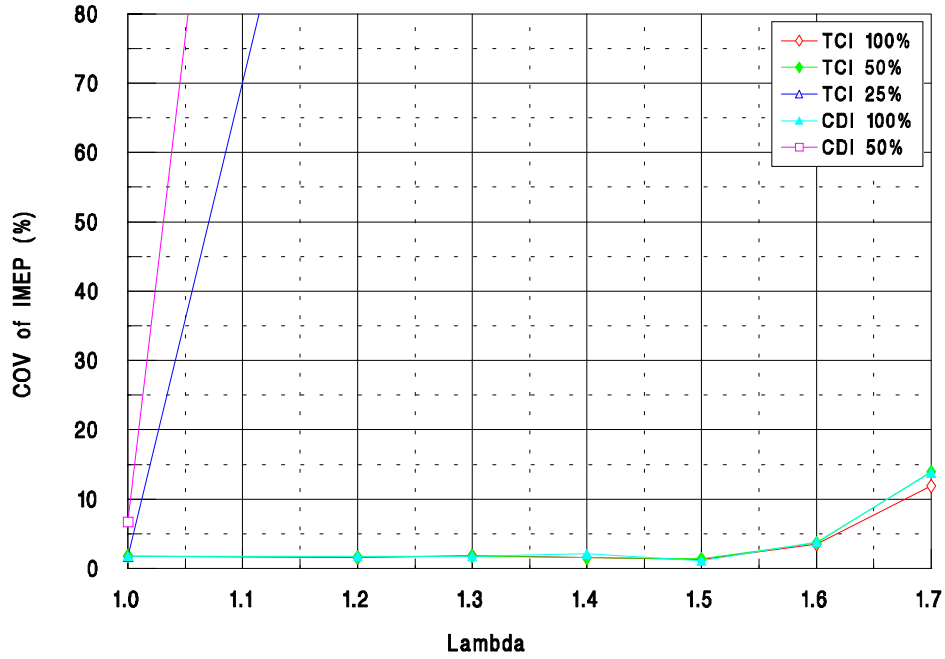

Figure 4.30 **Relationship between lambda and COV of IMEP for transistorised and capacitor discharge ignition with reduction in energy at 1000 rpm and 2 L/s air consumption**

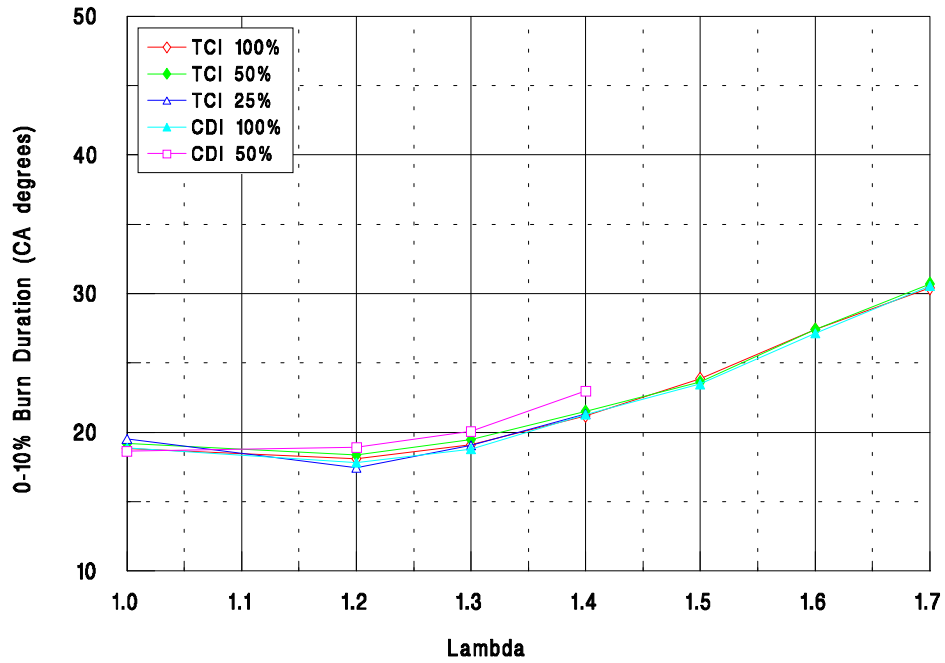

Figure 4.31 **Relationship between lambda and 0-10% burn duration for transistorised and capacitor discharge ignition with reduction in energy at 1000 rpm and 2 L/s air consumption**

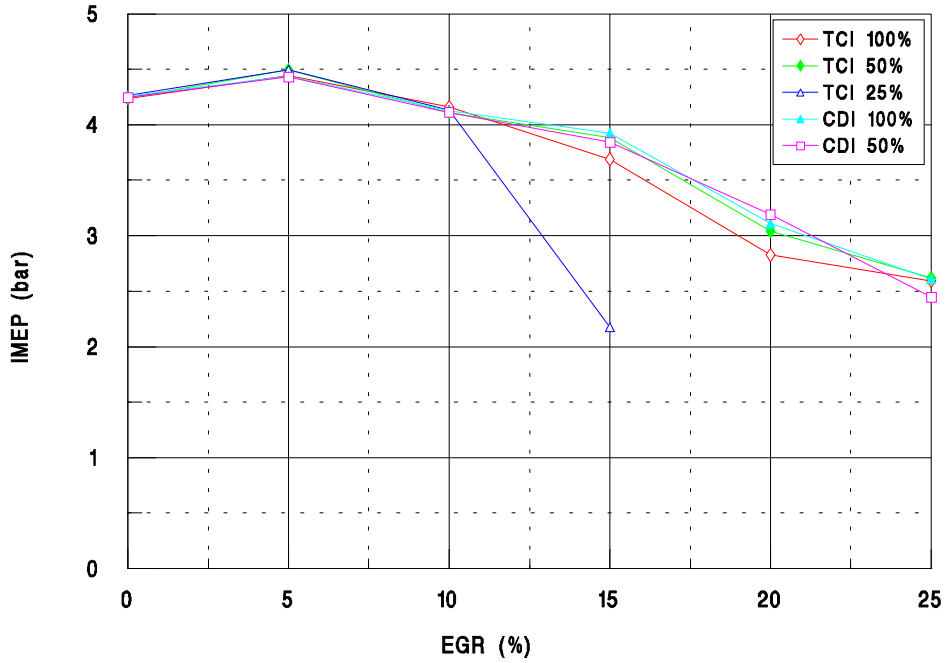

Figure 4.32 **Relationship between EGR and IMEP for transistorised and capacitor discharge ignition with reduction in energy at 1000 rpm and 2 L/s air consumption**

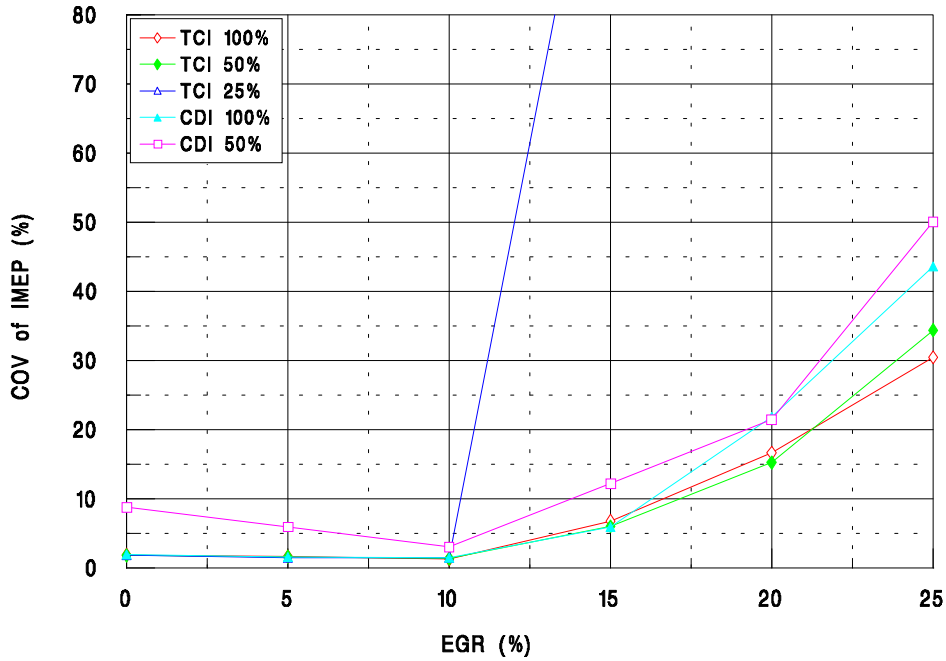

Figure 4.33 **Relationship between EGR and COV of IMEP for transistorised and capacitor discharge ignition with reduction in energy at 1000 rpm and 2 L/s air consumption**

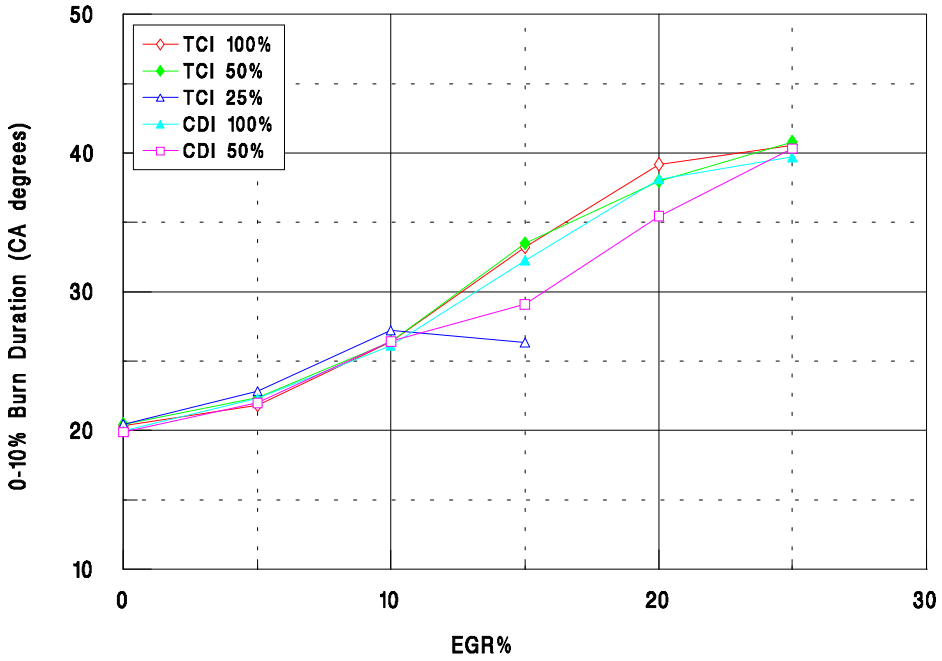

Figure 4.34 **Relationship between EGR and 0-10% burn duration for transistorised and capacitor discharge ignition with reduction in energy at 1000 rpm and 2 L/s air consumption**

5. Non-flow rig testing

5.1 Heated pressure vessel testing

A heated pressure vessel was constructed to replicate non flow conditions, so as to investigate the effects of: gas composition, increased temperature and pressure on the spark discharge parameters.

The vessel was constructed from stainless steel, chosen for its high heat capacity and mechanical properties at elevated temperatures, with provision for four cartridge heaters. A spark plug thread was machined at one end of the vessel, and a small bore tee piece, chosen to minimise heat losses, fitted to the other end. The tee piece linked the supply gas to the vessel and the pressure gauge. The vessel was mounted on four thin stainless steel legs to reduce the heat losses.

It was intended to carry out tests at up to 400 °C and pressures of 30 bar to replicate a worst case, where an engine with an 11:1 compression ratio achieves 100% volumetric efficiency and

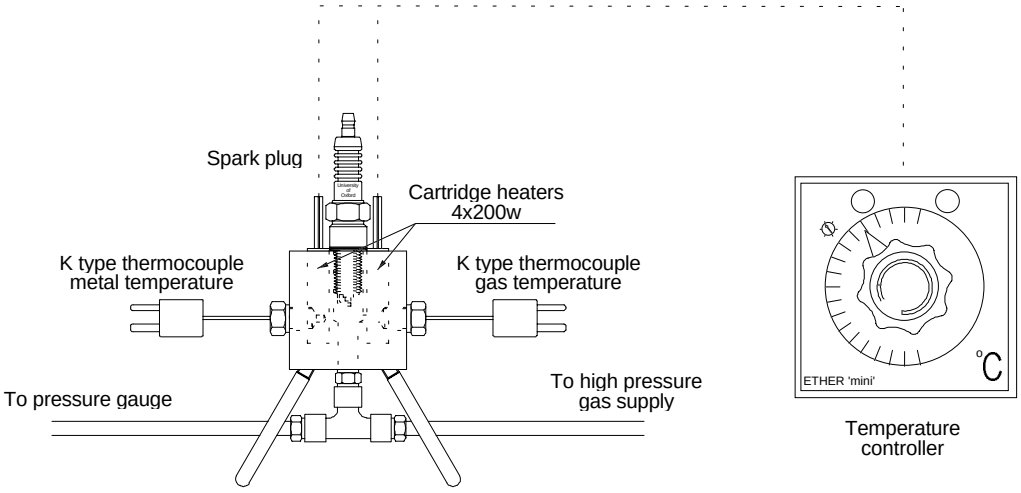

Figure 5.1 Heated pressure vessel

initiates ignition at TDC, with little heat being lost to the engine structure on mixture compression. Four cartridge heaters (RS catalogue number 731-259) of 200 watts power each were used to heat the vessel, these were connected in parallel to a Pye mini temperature closed loop controller. Two thermocouples were employed to measure the metal and gas temperatures, the thermocouple measuring metal temperature was used as part of the feedback loop for the temperature controller. The system resulted in stable temperatures within 5°C of that desired.

5.2 Results

5.2.1 Effects of increasing the pressure and temperature on the breakdown process

Figure 5.2 shows that an increase in pressure results in a higher breakdown voltage. This is also detailed in Paschen's law (Cobine 1958).

$$V_B = \frac{Bd_g P}{\ln\left(\frac{Ad_g P}{\ln\left(1+\frac{1}{\gamma}\right)}\right)} \quad \textbf{(5-1}$$

where V_B is the breakdown voltage, in volts
P is the pressure, in mmHg
d_g is the spark gap, in cm and
A, B and γ are constants depending upon mixture and electrode material

It can be seen that increasing the medium temperature reduces the breakdown voltage, this is due to a reduction in density for the same pressure. Cobine argues that Paschen's law should use a density term as opposed to the pressure term, and that this will cater for temperature effects. The temperature increase produced by the heated pressure vessel will also increase the electrode temperature, although these effects are assumed to be negligible, since the cathode fall is only reduced when cathode hot spots are formed (Cobine 1958), and this happens at a much greater temperature than those used in this study. In an engine, the breakdown voltage is reduced since the charge undergoes heating in the polytropic compression process, and once firing, the engine structure will provide additional heat input to the incoming charge.

Considering a proportionality between breakdown voltage and gas temperature, from the ideal gas law:

$$\rho = \frac{P}{RT}$$

and for constant density:

$$\frac{P_1}{RT_1} = \frac{P_2}{RT_2}$$

therefore the pressure at which the breakdown voltage will remain the same as that at initial conditions can be calculated from:

$$P_2 = \frac{P_1 T_2}{T_1}$$

With initial conditions of 0.5mm gap, 4 bar (gauge) and 293K, the breakdown voltage is measured to be 10kV. At 573K, for the same breakdown voltage, the pressure can be increased to 8.78 bar (gauge). This value is very similar to the interpolated value of approximately 10 bar (gauge) for the 300 °C case with the 10kV breakdown voltage as seen in Figure 5.2. Reasons for this discrepancy of about 10% may be experimental error or electrode effects.

The cold gas and electrode conditions can be compared to a cold start on a car, where external breakdown can often occur, preventing firing on cylinders where the high tension insulation is borderline.

5.2.2 Effects of increasing electrode gap on the breakdown process

Increasing the electrode spacing results in an increase in required breakdown voltage. Figure 5.2, Figure 5.3 and Figure 5.4 show that at a constant pressure and temperature of 200 °C and 8 bar, the breakdown voltage is 11, 13 and 17kV for an electrode spacing of 0.5, 1.0 and 1.5mm respectively. It can also be seen throughout these figures that an increase in electrode gap results in a greater effect from increasing pressure.

5.2.2.1 Effects of different gases on the breakdown process

Tests have shown that helium and argon do not require such high breakdown voltages (Figure 5.5 and Figure 5.6), although these gases are not relevant, it could suggest that rich mixtures have slightly different breakdown characteristics to lean mixtures.

This elevated temperature and pressure data can be used to estimate electrode temperature in a running engine, the pressure being measured by a cylinder pressure transducer. The results may be correlated with thermocoupled plugs, although this will give an average electrode (or more correctly, the insulator) temperature over the complete 4 stroke cycle, whereas the breakdown voltage analysis is more concerned with the conditions at the point of ignition. Additionally, this data could be useful for pre-ignition studies.

5.2.3 Effects of increasing the pressure and temperature on the glow discharge

Figure 5.8 shows the effects of increased temperature on the glow discharge. It can be seen that the glow discharge characteristics for each temperature are very similar apart from the 200°C case, which can be considered as a rogue piece of data. The characteristics of the 100 and 20°C cases deviate towards the end of the phase, this is due to there being less energy available for the later stages of the discharge because of the higher breakdown voltage needed at these temperatures. It is apparent that the glow discharge is insensitive to medium (and electrode) temperature for the range tested.

The effect of pressure upon the glow discharge is shown in Figure 5.9. The discharges all lie in order of pressure, with the lowest pressure case resulting in the lowest voltage gradient. These effects are caused by the relocation of energy during the breakdown process, resulting in less energy being available for the later stages of discharge. These results show that the glow discharge is sensitive to increases in medium pressure.

5.2.4 The validity of Paschen's Law

It was discussed in section 5.2.1 that Paschen's Law takes no account of temperature. Figure 5.10 compares the results of Paschen's Law to experimental results, with a 0.5mm gap, at ambient pressure and elevated temperatures. Cobine suggests the use of 14.6, 365 and 0.036 for A, B and γ respectively for nickel electrodes in air, using units of volts, cm and mmHg. At pressures of 4bar gauge and below, Paschen's Law gives good agreement with the experimental results, above 4bar the Paschen model over-predicts.

Figure 5.11 compares Paschen's Law with experimental results for different electrode gaps. Above a gap of 0.5mm, the Paschen model over-predicts, even though the results obtained were between the constraints, outlined by Cobine, for which the chosen constants were valid.

5.2.5 A linear fit for voltage prediction

For a constant electrode material in air, the breakdown voltage depends upon pressure, temperature and electrode gap, this suggests a dependency on the mass (or density) of medium between the electrodes.

A linear equation was used to fit the experimental data using the least squares method:

$$V = A + B\frac{P}{T} + Cd_g\frac{P}{T}$$

where A, B and C are constants
P is the pressure in bar absolute
T is the temperature in Kelvin
d_g is the electrode gap dimension in mm

For a conventional spark plug, the constants were found to be:

A=4.3
B=136
C=324

This relationship gives good predictions of breakdown voltage at all temperatures, as shown in Figure 5.12. The linear equation gives good agreement for changes in gap also, Figure 5.13 shows these results. The constants and the linear equation can be considered to be valid for nickel electrodes on air over the gaps and temperatures tested.

5.3 Heated Rig Summary

The use of the heated pressure vessel has shown that the required breakdown voltage in a given gas is increased by:

1. Increase in electrode gap
2. Increase in pressure
3. Decrease in gas and electrode temperature

An increase in the required breakdown voltage can induce higher electrical stresses on components, namely the coil or ignition transformer, the spark plug leads, the connector to the coil or ignition transformer, and the plug cap and connector. These increased stresses can result in discharge paths being formed where electrical insulation is lower, these discharge paths can allow the circuit to earth, over time, without the use of the spark plug, and lead to a misfire in the engine cylinder. Obviously, this misfire will increase fuel consumption and increase unburned hydrocarbon emissions.

Additionally, higher breakdown voltages can lead to a shortening of the spark duration because more of the stored energy is required in the first part of the discharge. The reduced spark duration can lead to a reduced ignition probability when conditions are marginal e.g. high excess oxygen or high EGR.

Paschen's Law was investigated and predicted results were plotted against experimental results. Correlation was found to be poor and a linear equation was developed which modelled the experimental data more accurately, taking into account the temperature, pressure and gap.

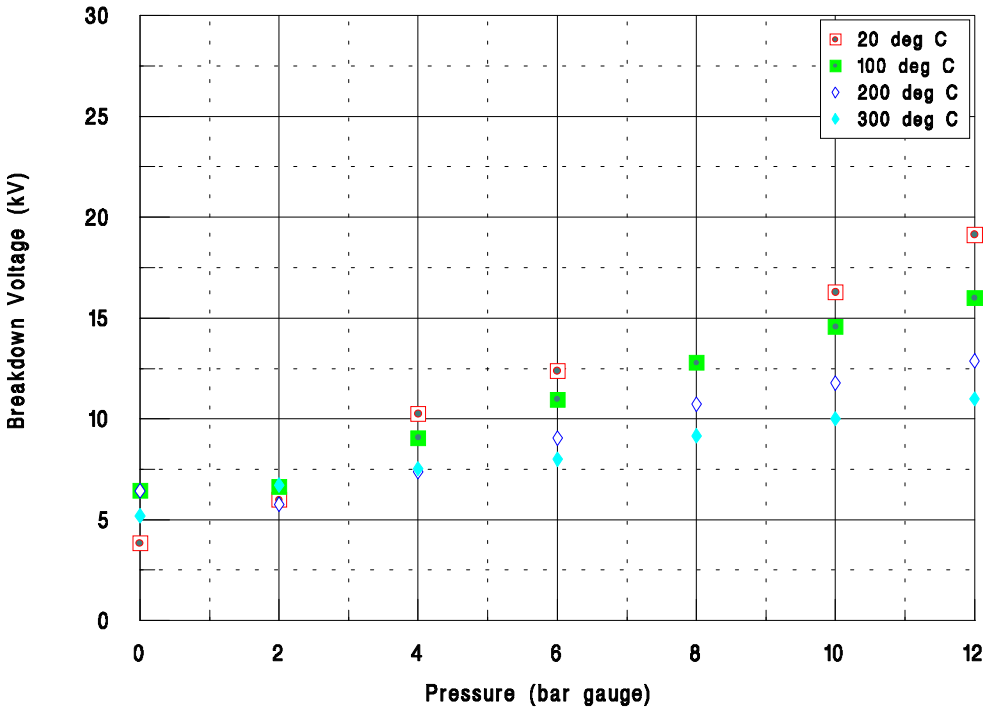

Figure 5.2 **Variation of breakdown voltage with increases in gauge pressure and temperature with Air (0.5 mm gap)**

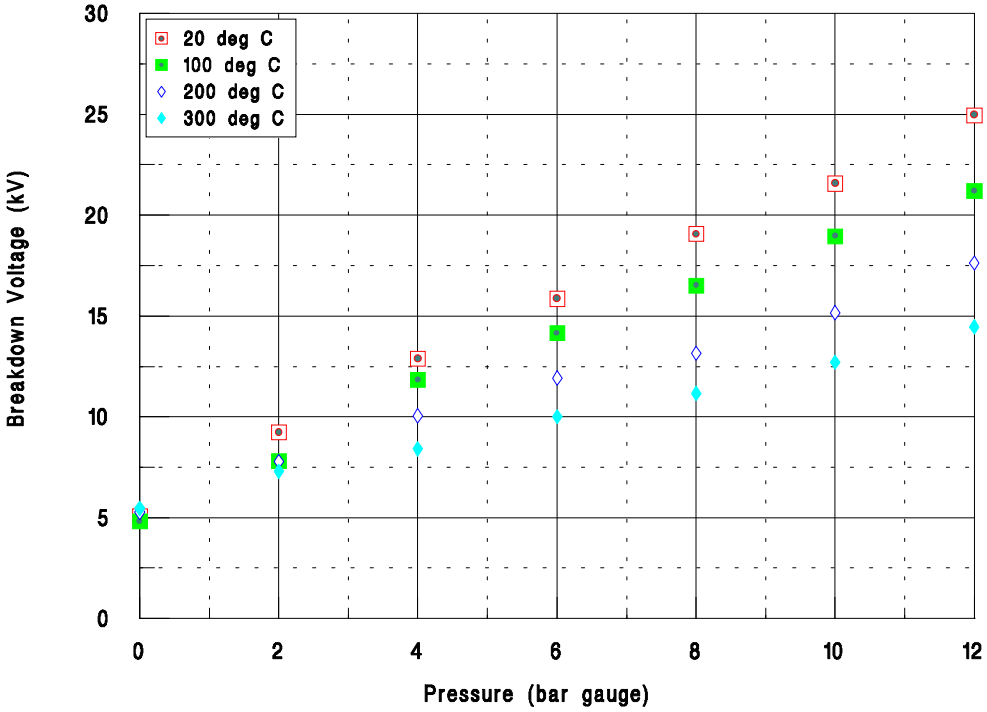

Figure 5.3 **Variation of breakdown voltage with increases in gauge pressure and temperature with Air (1 mm gap)**

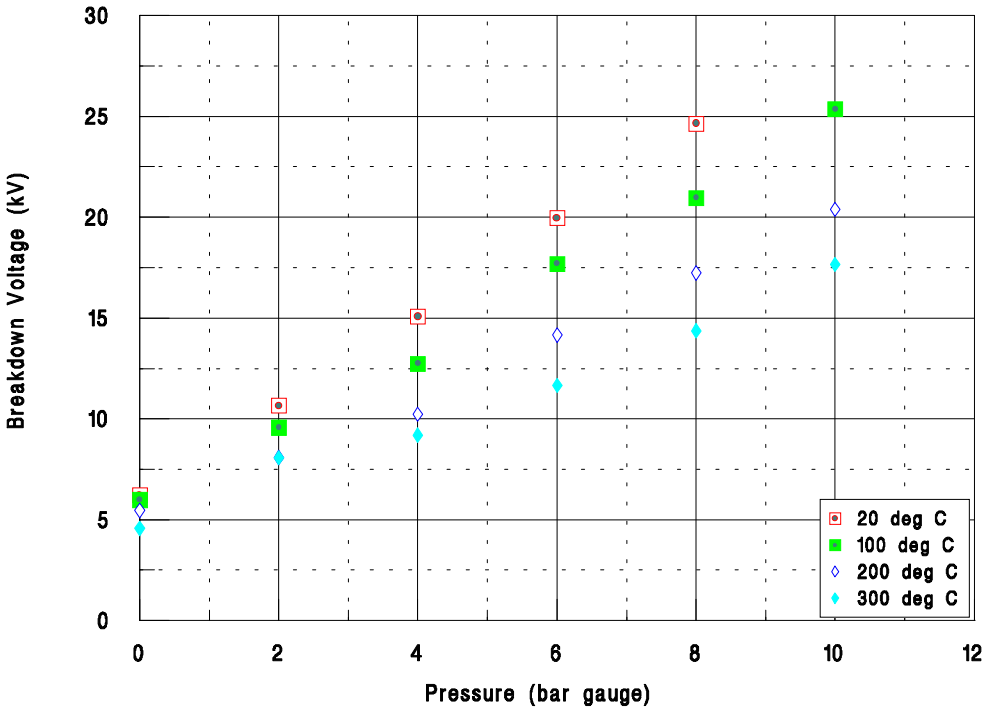

Figure 5.4 **Variation of breakdown voltage with increases in gauge pressure and temperature with Air (1.5 mm gap)**

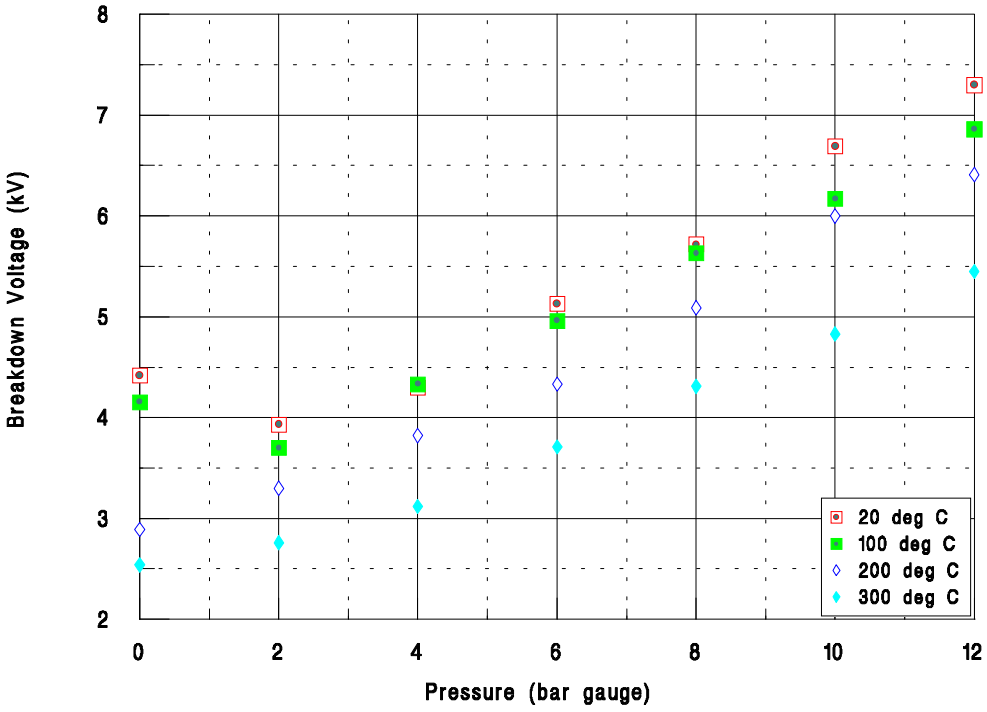

Figure 5.5 **Variation of breakdown voltage with increases in gauge pressure and temperature with Argon (1mm gap)**

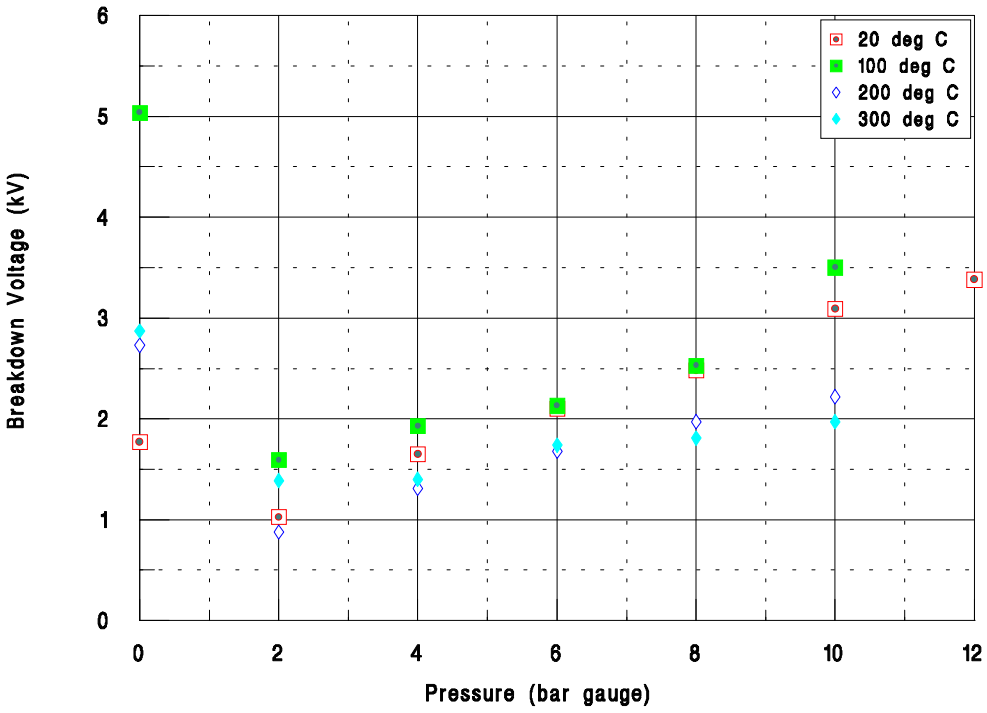

Figure 5.6 **Variation of breakdown voltage with increases in gauge pressure and temperature with Helium (1mm gap)**

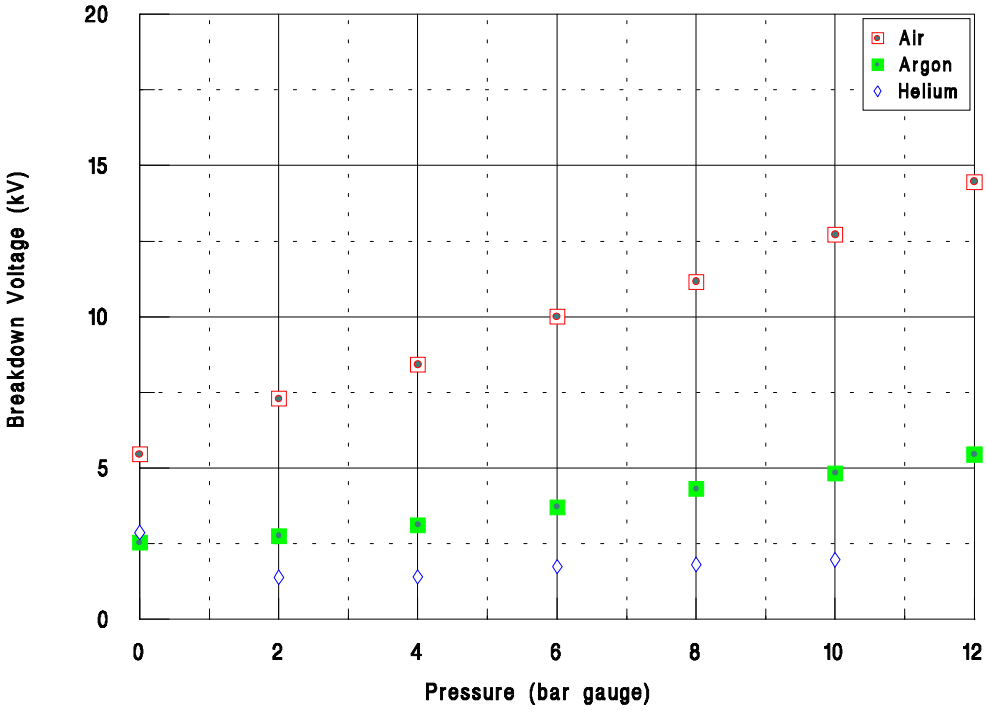

Figure 5.7 **Effects of different gases on the breakdown voltage at elevated pressures (1mm gap 300 °C)**

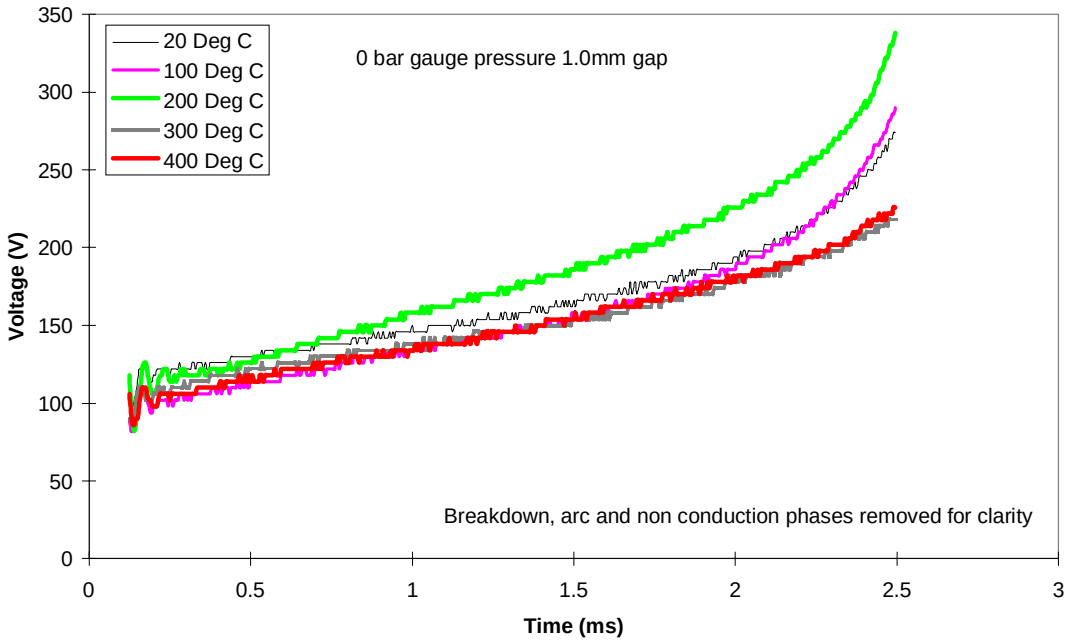

Figure 5.8 Variation of glow voltage with increases in temperature with air at 1 bar gauge and 1mm gap

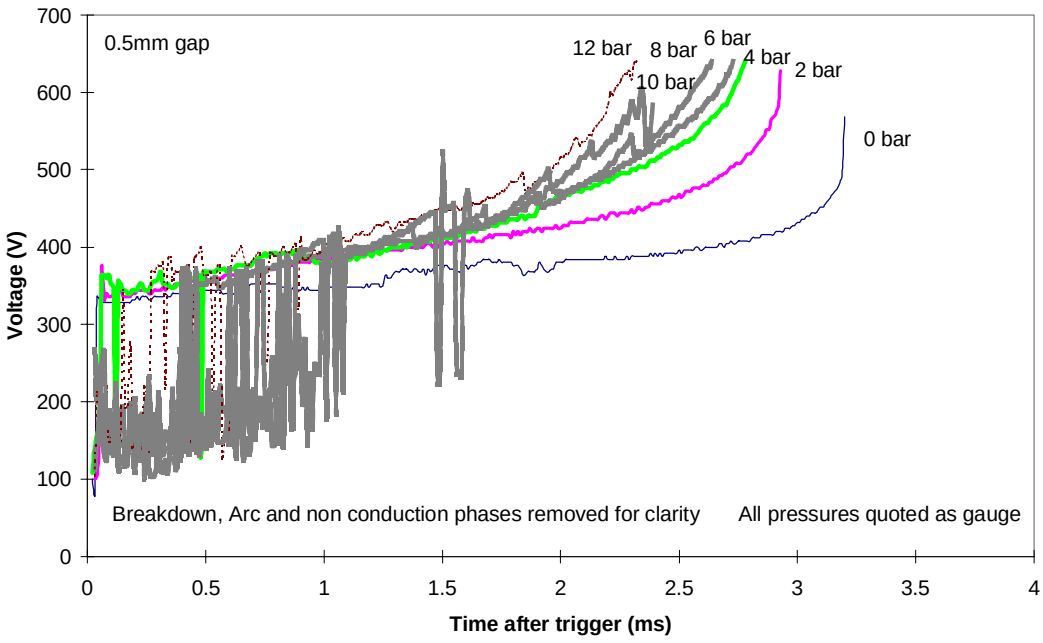

Figure 5.9 Variation of glow voltage with increases in pressure with air at 20°C gauge and 0.5 mm gap

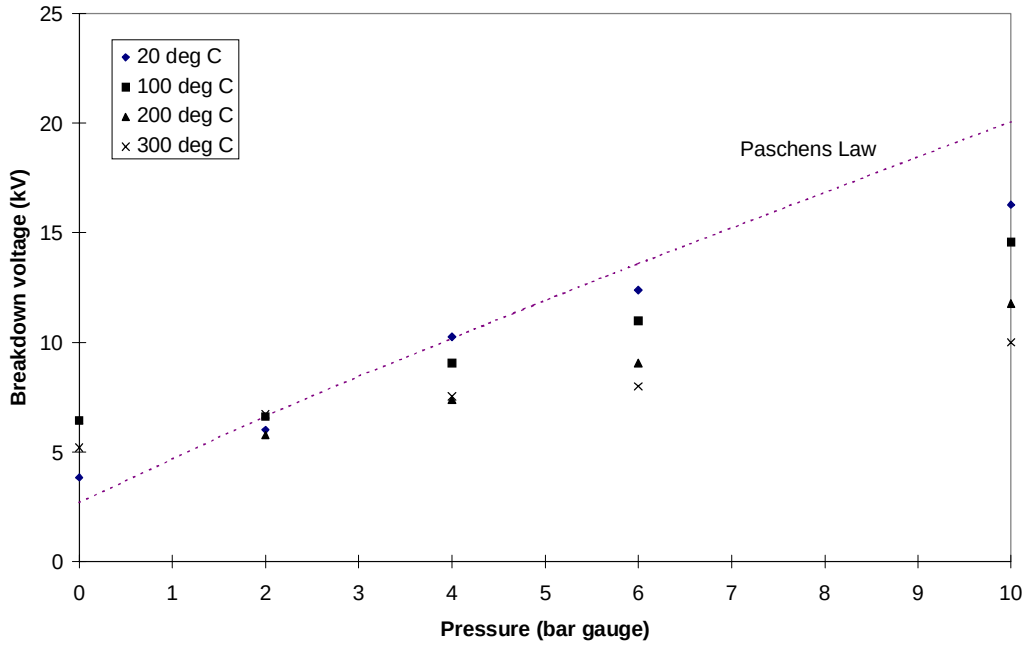

Figure 5.10 **Comparison of Paschen's Law with experimental data at elevated pressures and temperatures**

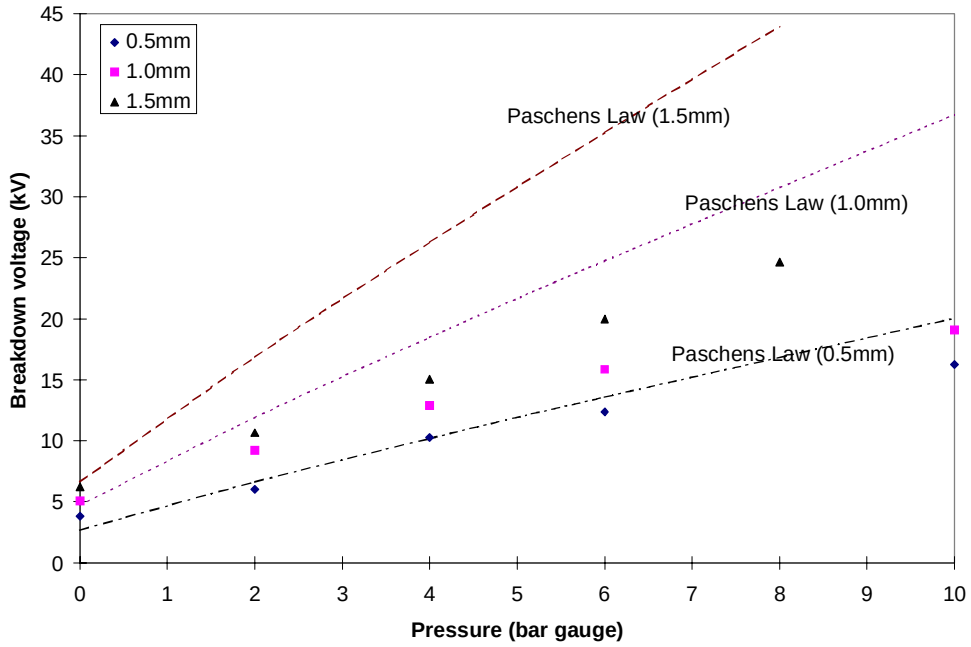

Figure 5.11 **Comparison of Paschen's Law with experimental data at elevated pressures and different electrode gaps**

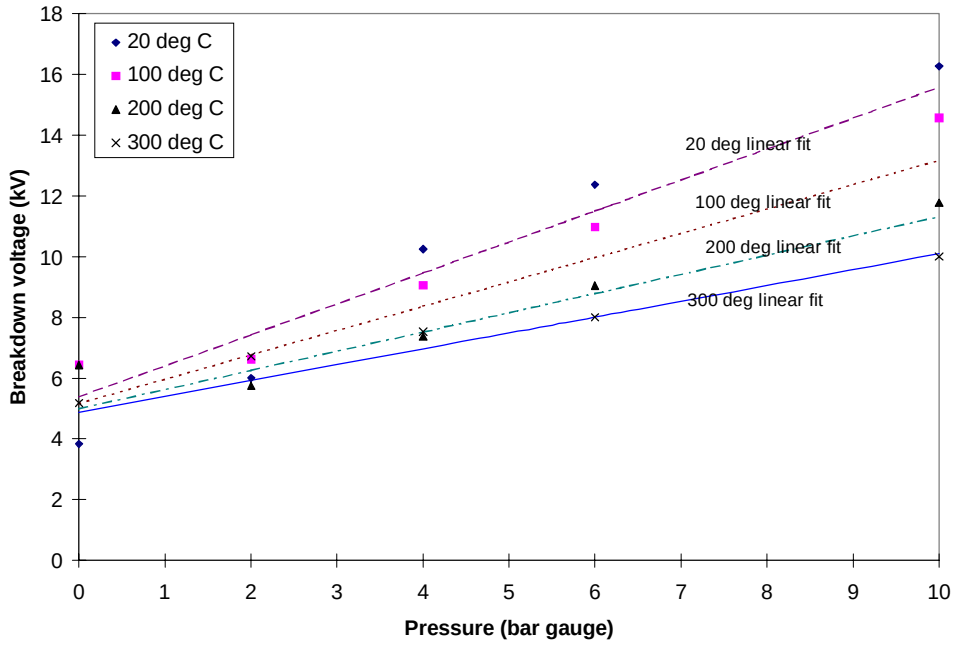

Figure 5.12 Comparison of linear fit with experimental data at elevated pressures and temperatures

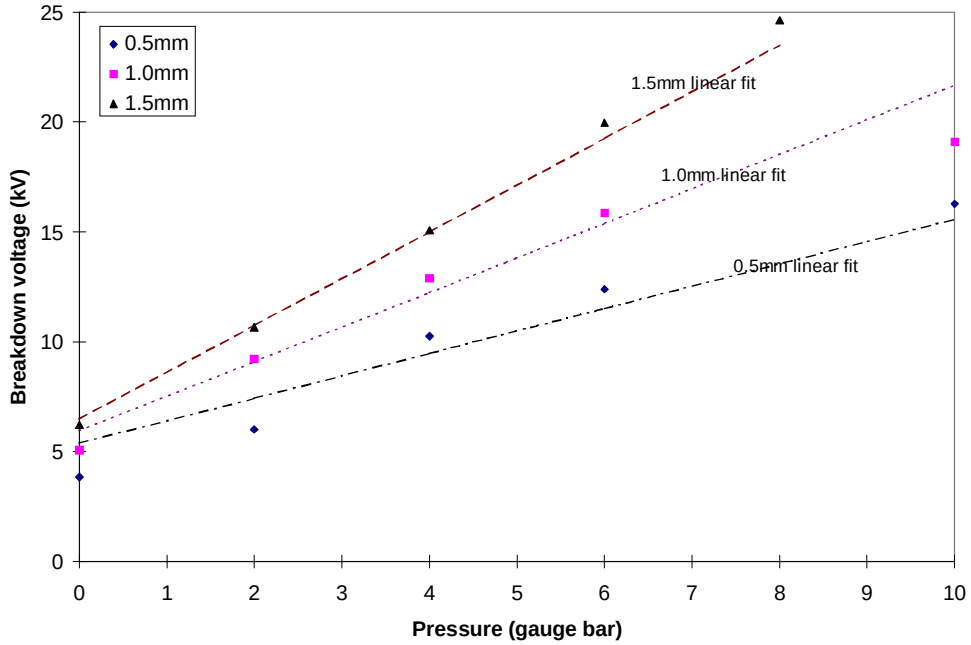

Figure 5.13 Comparison of linear fit with experimental data at elevated pressures and different electrode gaps

5.4 Erosion testing

5.4.1 Introduction

The effects of erosion can be seen as excessive plug gap widening, and this needs an increased breakdown voltage. As the gap widens, a limit can be reached, where the breakdown voltage needed to create a conductive path between an external part of the circuit to earth is lower than that required to cause conduction in the plug gap. This situation is known as external breakdown. The voltage required to cause external breakdown can be reduced substantially by dirty or damaged plug leads, poor internal coil insulation and damp conditions. The erosion of spark plug electrodes can occur from two sources, chemical corrosion and electrical erosion. Chemical corrosion is caused by the interaction of the fuel (and air) with the electrode material at very high temperatures. The only way to reduce this effect is to reduce the spark plug temperature or to change the fuel type. The erosion of a pair of electrodes can be measured by three methods: required breakdown voltage, loss of electrode mass or electrode gap growth. Each method has its merits and drawbacks.

5.4.2 Required breakdown voltage

The increase in required breakdown voltage is the most relevant measurement of spark plug erosion since the ignition HT current will follow the path of least resistance. As electrodes erode and the gap grows, the resistance across the gap grows also. If the resistance increases beyond that of the resistance of the lowest system insulation, e.g. the insulation between windings of the coil or the rubber boots that cover the ignition terminals, the current will not flow through the spark plug electrodes and combustion will not be initiated. Eroded spark plugs result in higher required breakdown voltages, which means that measuring the breakdown voltage is probably the best method to use to infer electrode condition. The drawbacks are that, as noted in section 5.1, the required breakdown voltage is sensitive to: temperature, pressure and gas composition, in addition to electrode gap. Further to these sensitivities, it has been seen that the breakdown voltage does vary between discharges. This is due to the non-repetitive nature of the discharge path; the path taken is always the one of least resistance, the resistance being reduced by sharp edges (promoting a high electric field) and the abundance of higher temperature ionised gas (perhaps from previous discharges). The sharp edges on the electrode surface are constantly being eroded during the discharge.

5.4.3 Loss of electrode mass

The loss of electrode mass is a good measure of erosion, although it cannot be directly related to ignition performance since the required breakdown voltage depends heavily upon the electrode gap, which the loss of mass method cannot predict accurately. However, the lost mass method is useful for comparing different ignition system erosion performance in the laboratory. The major drawback is that the lost mass is very small, and hence the electrodes must be quite small to enable a balance of the required sensitivity to be used, this rules out the use of automotive spark plugs which weigh in the region of 100g compared to a lost mass of around 100μg. A specially designed rig could be used with small removable electrodes, these electrodes must be handled carefully when being weighed since any contamination will result in an addition of mass. The addition of mass can also occur from oxidation of the electrodes, the experiments therefore need to be done in an inert atmosphere, but not a closed environment, since the inert atmosphere would quickly become ionised.

5.4.4 Electrode gap growth

The measurement of electrode gap growth is the most widely used method to assess spark plug life, and is usually carried out with a set of feeler gauges. At best this can measure the peak to peak distance, and is dependent upon the perceived fit of the gauges in the electrode gap. A more accurate method is to use a shadowgraph which projects a 2D scaled up image of the electrodes, and enables measurements as small as 1µm to be made. With this method we are faced with measuring the peak to peak dimension, or an average gap measurement, at the discretion of the user. Again, the problem of oxidation is present which can actually appear to make the gap smaller when oxides build up at the edge of the electrodes. Measuring the gap width is not a perfect method of measuring erosion. The discharge path emanates from areas of high electrical field, these are found at sharp edges or points of low surface area. With this fact in mind, the discharge will probably not occur across the shortest path, but between points of the highest electrical field. These points will not necessarily be on the faces of the electrodes, hence the shortest distance between the electrode surfaces may be misleading.

5.4.5 Method of investigation

5.4.5.1 Automotive spark plug in ambient conditions

A spark plug of conventional design, and standard nickel based alloy electrodes, was subjected, in ambient air, to 50 million discharges, equating to 28000 miles at 50 mph and 3000 revs/min. A counter was used to count the number of trigger signals sent to the ignition driver. The average (of 25 discharges) breakdown voltage was recorded every ten thousand discharges.

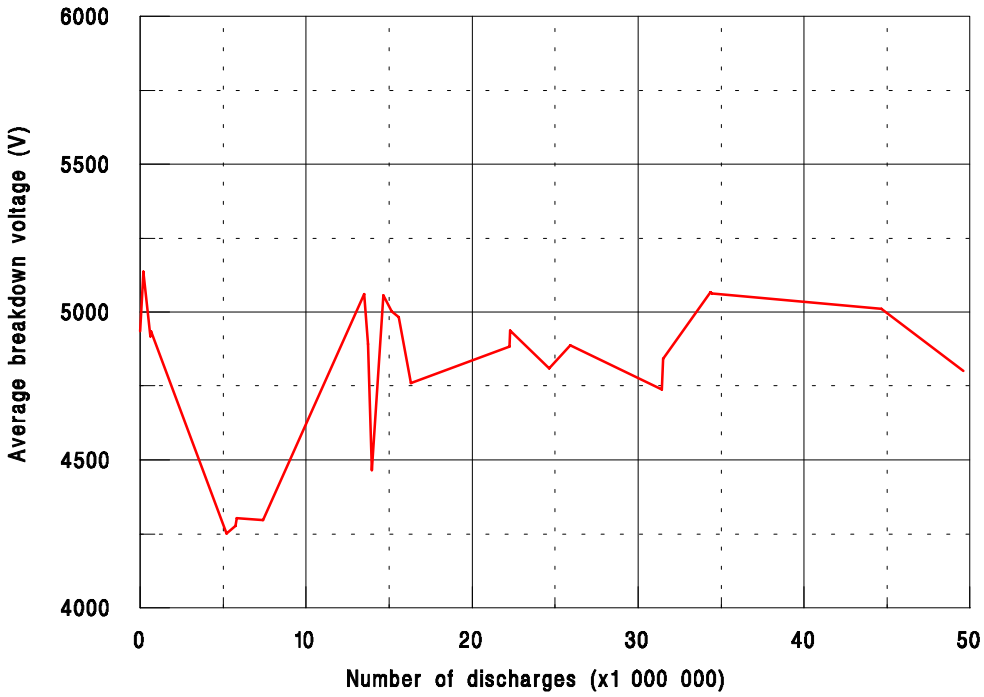

Figure 5.14 Average breakdown voltage v's number of discharges for L82YCC spark plug at ambient conditions

After the test, the plug was inspected and measured using feeler gauges, the original gap length had not been increased by a measurable amount, although the surface of the electrodes was noticeably distorted. Figure 5.14 shows the breakdown voltage versus number of discharges, it can be seen that the required breakdown voltage reduced dramatically over the first 5 million discharges returning to its approximate initial value over time, although not increasing beyond this level. When the electrode gap was exposed to the atmosphere and subjected to repeated discharges, it was found that electrical erosion was very slow. It was believed that this was due to the temperature at which the tests were being carried out and that chemical corrosion was not present. The erosion rate, when being measured on a gap length basis, was very slow with the large area electrodes.

5.4.5.2 The use of thin electrodes in a slowly flowing medium

After attempting to erode the electrodes of an automotive spark plug in ambient conditions, it was believed that a lower surface area was required to enable measurements to be taken in an acceptable period of time. A rig was designed to hold two electrodes of a material of low erosion resistance and much reduced cross sectional area in a stream of flowing gas, this is shown in Figure 5.15. The electrodes were produced from tinned copper wire. Although this is not representative of a spark plug electrode material, as long as the material was maintained for all the tests, a relative order of erosion could be determined for each ignition system in an acceptable period of time. The material chosen for the body of the rig, shown in Figure 5.16, was perspex for its electrical insulation properties, ease of production and optical characteristics. Two electrode clamps were fitted to each side of the rig, to which lengths of copper wire were inserted. A mock spark plug insulator is fitted to the cathode clamp which

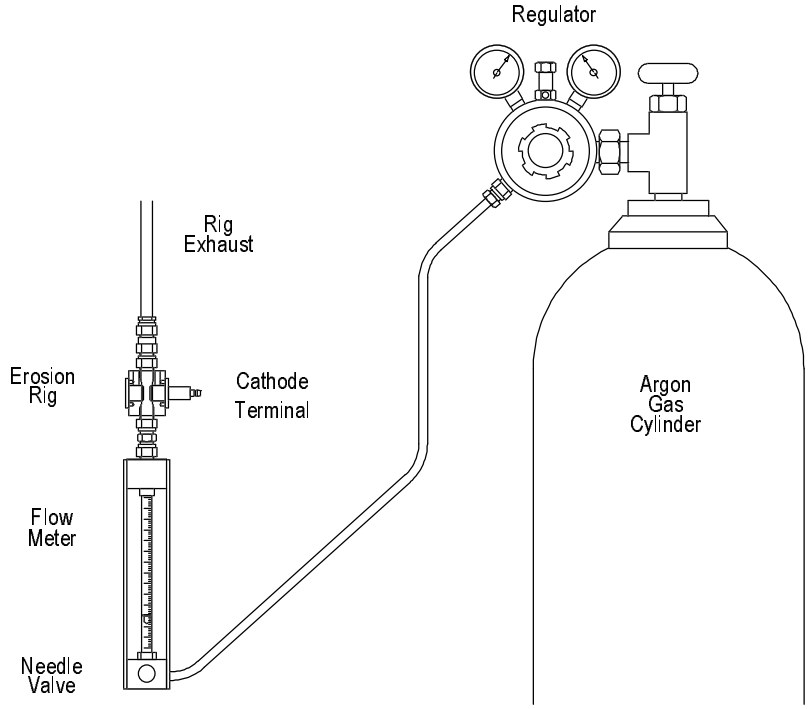

Figure 5.15 - Erosion testing apparatus

allows a normal spark plug type terminal to be connected, the anode is connected to a common earth. The rig was designed to allow a flow of gas through the gap so that ionised medium could be replaced by fresh lower temperature gas.

When inserting new electrodes. an approximate length of wire was inserted into the electrode collar and a length spacer placed over the protruding wire. The wire was cut to length with a pair of side cutters and the faces filed flat using a needle file. The electrode gap was then kept reasonably repeatable. The gas used was air from the lab air supply, this was fed through at a flowrate of 10 cm^3/min.

Electrode gap growth was measured using a shadowgraph. An attempt was made to measure breakdown voltage increase, but the breakdown characteristic was found to be very erratic from discharge to discharge. This resulted in varying average breakdown voltages which did not seem to follow a trend. It was found that it was difficult, if not impossible to measure an increase in breakdown voltage. On measuring the gap, it was found that the electrodes were oxidising and this obscured the image on the shadowgraph. Discharging in air resulted in oxide formation on the electrodes which resulted in imprecise growth measurements with the shadowgraph.

5.4.5.3 The use of thin electrodes in a slowly flowing inert medium

The fluid flowing through the rig was changed to Argon to reduce if not eliminate foreign compounds from forming or depositing themselves on the electrodes. This flowrate was small enough to not cause a great deal of disruption to the arc, certainly resulting in no discernible increase in glow voltage, yet large enough to maintain a flow of fresh gas through the electrode gap. A flowmeter was positioned upstream of the rig to allow the gas flowrate to be measured and kept constant throughout the tests. Tests showed encouraging results, although erosion rates were slow. A deficiency in some of the apparatus was also highlighted. The counter was prone to interference from the breakdown process, or more correctly, the arc phase and the high current associated with it.

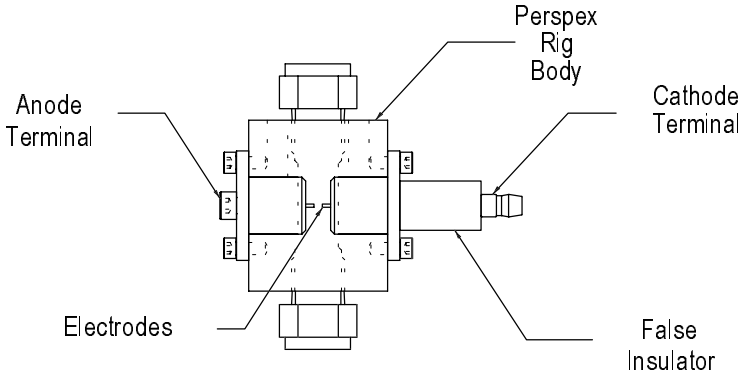

Figure 5.16 - Erosion testing rig body and electrodes

The counter was replaced with a stopwatch which was started when the power was turned on to the ignition system, using the trigger frequency and the recorded time, the number of discharges could be calculated to an accuracy of better than plus or minus 150 discharges. After a period of time, it was found that interference was causing disruption of the signal generator display and increasing the noise from the discharge. The cause was believed to be the ingress of air into the vessel caused by the loss of Argon after heating in the arc. Increasing the flow rate of the Argon to above 40cm^3/min improved matters as far as the ingress of air was concerned, but caused the arc to bow. An extension to the exhaust of the rig was made which resulted in the Argon cooling sufficiently enough before reaching the atmosphere and prevented air from entering the system.

The experiment was allowed to run for 100 hours and the results for required voltage plotted in Figure 5.17. Both the average voltage and the maximum voltage over 50 discharges are plotted

for every hour of testing. We would expect to see a rise in breakdown voltage as the gap grows due to the greater length of the discharge path and the loss of sharp edges which promote high electric fields, but in actual fact we see a fall. In these tests, the average breakdown voltage did not increase in a manner similar to the gap growth, it is possible that a maximum breakdown voltage of a group of discharges should be used. The gap growth was measured using a shadowgraph, sample results can be seen in Figure 5.18 and Figure 5.19; the corresponding measurements of electrode gap growth can be seen in Figure 5.20. As time progressed, oxidation did start to appear on the electrode surfaces, this obscured the measurements being taken on the shadowgraph. It was possible that the copper being used was not 'oxygen free' and that there was a certain amount of porosity that allowed small quantities into the electrode gap.

5.5 Discussion

It was concluded that for measuring erosion at room temperature and pressure, small diameter electrodes were needed, the copper electrodes used were believed to contain oxygen which resulted in contamination which obscured the measuring process. It was also found that the required voltage method is unsuitable. The use of Argon reduced the energy needed in the breakdown phase and hence lengthened the arc, this required a lower trigger frequency (reduced from 150Hz to 70Hz) to ensure that the discharge was complete before recharging the coil.

5.6 Erosion summary

It was shown from section 5.4.5.1 that the erosion rates experienced in atmospheric conditions were not as high as those seen in the combustion chamber of a firing engine. This lower rate of erosion can be attributed to three effects;

lower temperature
lower pressure
no combustion reactants or products

It was not possible to carry out increased pressure or temperature testing due to a steady increase in ionisation in the vessel. The erosion of electrodes in an ignitable medium would present problems since an exhaust flow would be needed to maintain a low degree of ionisation in the erosion apparatus, this would be costly and potentially dangerous for obvious reasons.

In summary, lab based testing for electrode erosion has proved to be very difficult due to the low erosion rates witnessed. The negative observations reported here can be used to guide further work. The only foolproof method would be to use engine tests, even then, the engine operating history and spark plug operation would need to be known.

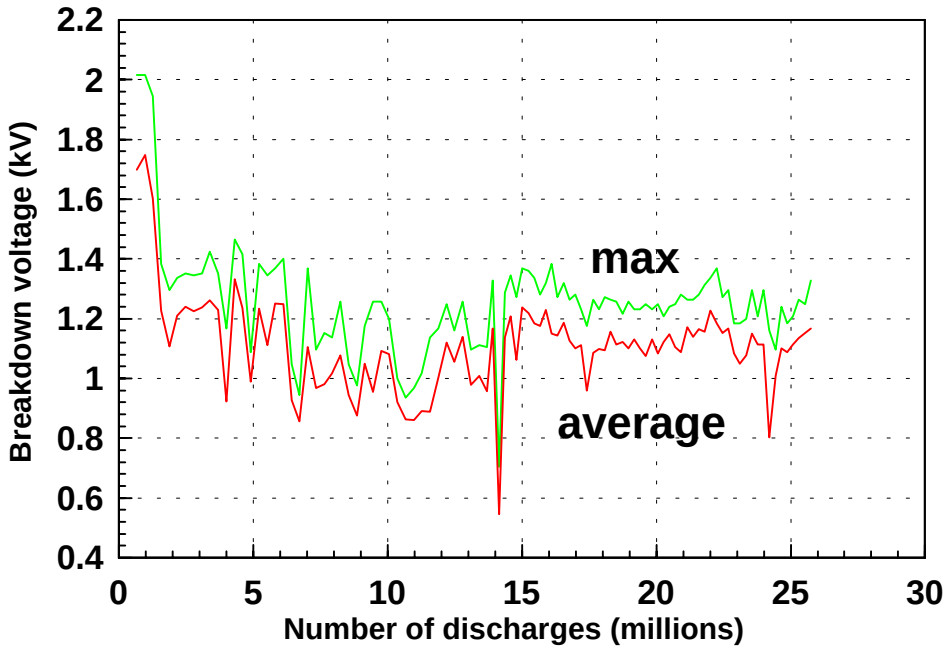

Figure 5.17 **Relationship between required voltage and number of discharges in Argon**

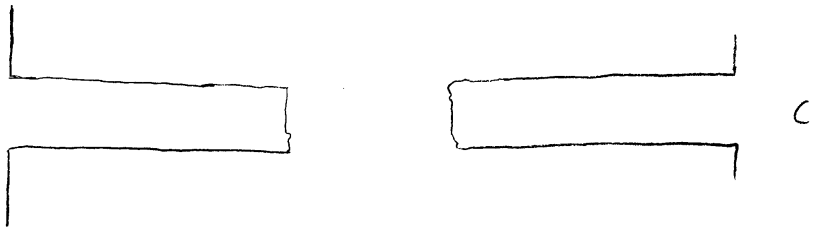

Figure 5.18 **Electrode surface shape as viewed at start of test**

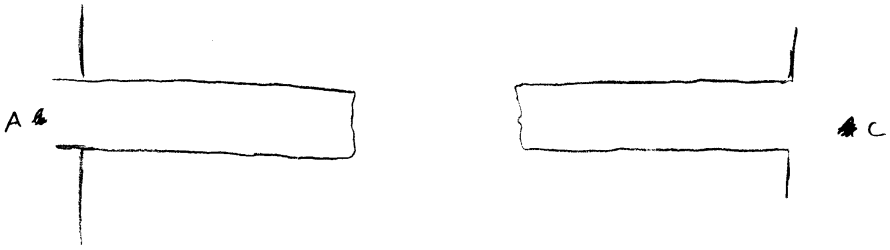

Figure 5.19 **Electrode surface shape after 14 683 200 discharges**

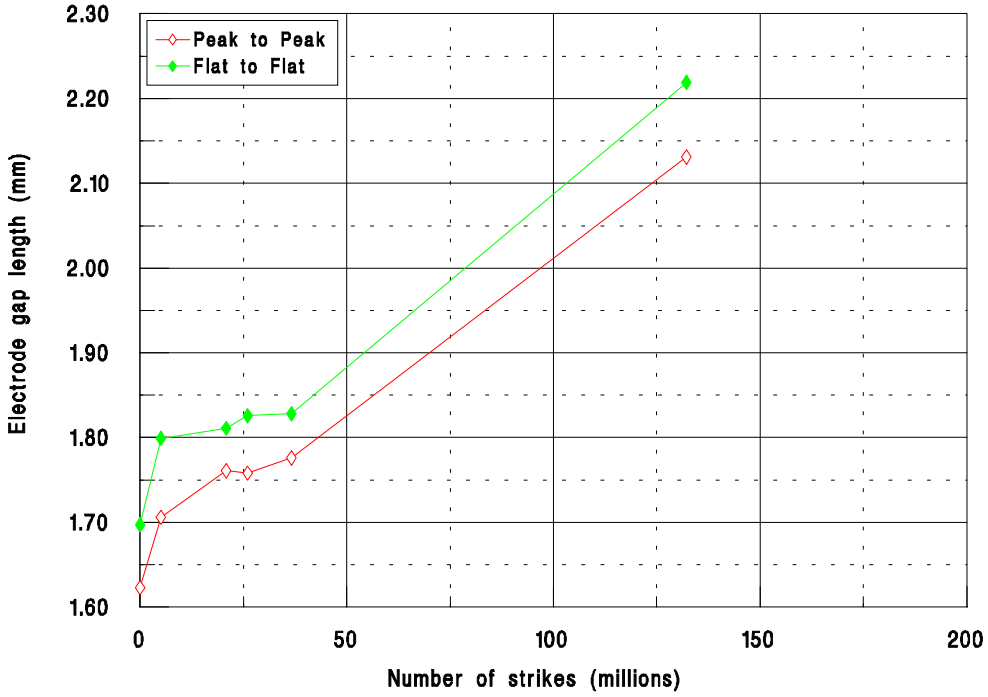

Figure 5.20 Gap length versus number of strikes for TCI system

6. Flow rig testing

The flowrig was used to produce a high pressure, high velocity flow field in the spark gap, replicating the conditions in an engine with high mean flow. This would be typical of gas engines converted from compression ignition engines and some spark ignition combustion systems, e.g. the Honda VTEC engine at part load (Horie and Nishizawa 1992).

6.1 Apparatus

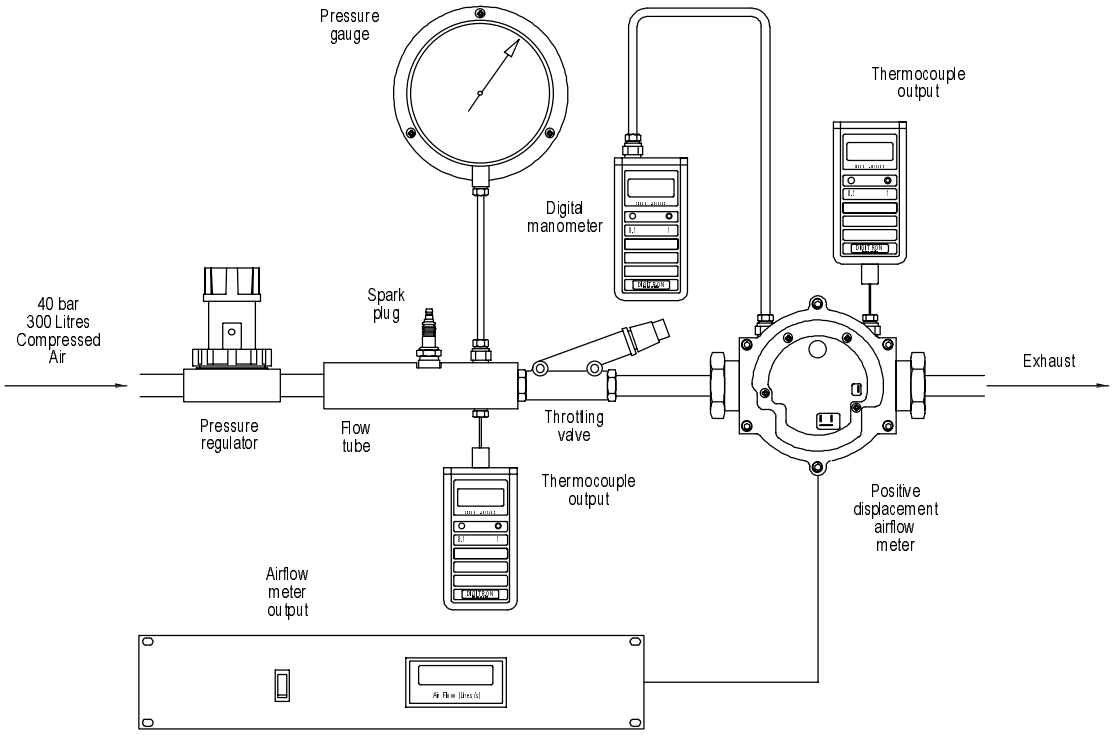

Figure 6.1 Flow rig and measuring apparatus for producing mean flow velocity at spark plug electrodes

A Reavall CSA4 air compressor was used to pressurise a 40 litre cylinder receiver to 40 bar. A primary regulator reduced this pressure to 20 bar, with a secondary regulator reducing the pressure to 0 to 10 bar, that was needed for the test programme. A wire mesh screen was positioned between the second regulator and the measuring tube to act as a flow conditioner and reduce the turbulence effects induced from the exit of the regulator mechanism. The flow tube contained the spark plug and tappings for pressure and temperature, the spark plug was positioned 10 diameters downstream of the tube entrance, i.e. much too short for fully developed flow. A bourdon gauge was used to measure the pressure in this section, with a K type thermocouple being used for temperature measurement. The spark plug electrode orientation was adjusted by placing thin washers, cut from shim material, between the mating surfaces of the spark plug shell and flow tube. The flow velocity was controlled by a throttling valve and the flowrate was measured using a positive displacement (Roots type) flowmeter (this flowmeter was also used in the engine study for measuring air consumption). A shaft encoder was mounted on the rear of the flowmeter and was interfaced to a counter which was calibrated in litres/second. Pressure and temperature were measured at the meter, using a

manometer and K type thermocouple, and enabled the flow velocity to be calculated using the Ideal Gas Relationship. Once pressurised, the air used was of lower humidity than that of ambient conditions and could also be considered to be of a constant humidity from day to day. During pressurising of the receiver, a condensate drain ensured that the maximum amount of water was removed from the air prior to reaching the receiver. The receiver also had a drain which was used to remove any water which had managed to get past the condensate drain. No effort was made to remove oil particles from the air, although it was though that since the air would have been stagnant in the receiver for a matter of minutes, any oil vapour would have separated out by the time the air was used. On inspection of the sparking plugs and measuring tube after extensive testing, no corrosion or contamination by oil was found.

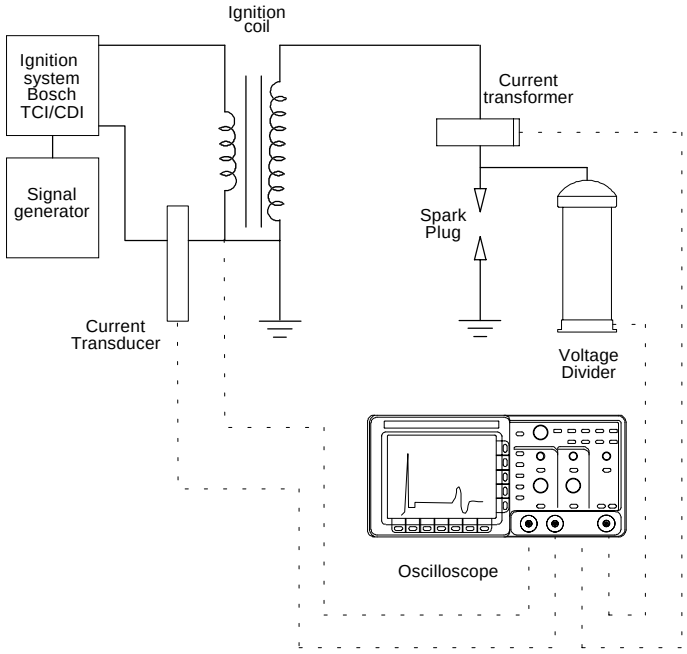

Figure 6.2 Experimental apparatus for flow rig tests - electrical measurements

6.1.1 Blockage caused by spark plug protrusion

When the spark plug was fitted to the rig, the electrode, insulator and plug shell caused a reduction in flow area. This reduction in area has been calculated by drawing the electrode shape and plug protrusion into the measuring tube using a CAD package, and using the area measurement facility. These factors were used when calculating the air flowrate throughout the system.

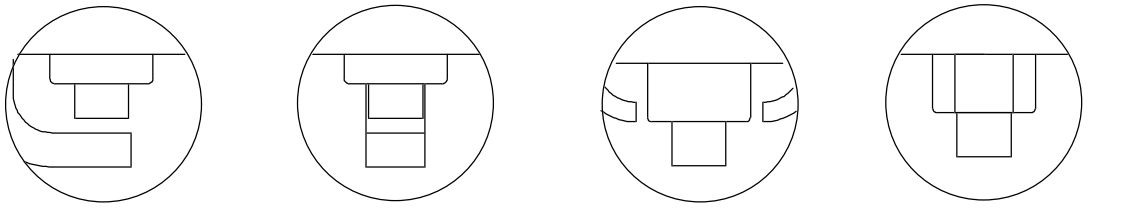

J type electrode 90 degree orientation	J type electrode 0 or 180 degree orientation	Double electrode 90 degree orientation	Double electrode 0 or 180 degree orientation
48.76% flow factor	55.49% flow factor	55.60% flow factor	60.36% flow factor

Figure 6.3 Examples of obstruction to flow tube caused by spark plug electrode and insulator

6.2 The effects of flow on an electrical discharge

A spark is merely a column of ionised gas which is able to conduct electricity. Forces do exist which hold the molecules in the column together, but these molecules may still be displaced by a flowing gas. Many modern engines employ some sort of turbulence or mixture motion mechanisms to promote faster burning of the charge, the object of this part of the study is to look closely at what this does to the spark process.

6.2.1 Factors to consider

Important parameters to consider are:
Pressure
Velocity of gas in gap
Electrode type
Orientation

6.2.1.1 Pressure

Experiments in chapter 5 have shown that increased pressures do have an effect on the required breakdown voltage.

6.2.1.2 Velocity of gas flowing through the gap

The velocity of the gas flowing through the gap will have an effect on the displacement of the ionised particles.

6.2.1.3 Electrode type

The type and shape of electrode will determine how the flow acts around the electrode gap, for instance, a triple electrode plug has three paths for the spark to take and each gap will have a different flow characteristic due to the position in relation to the flow direction.

6.2.1.4 Orientation

As with the electrode type, the orientation is important. Electrodes may shield discharges from the flow or cause flow effects which may interact with the column of ionised gas.

6.3 Flow effects on an inductive ignition system

Figure 6.7 and Figure 6.9 show the voltage characteristics for an inductive ignition system under no flow and high flow conditions. A normal J type electrode plug was used, orientated at 90 degrees to a flow velocity of 25 m/s, with a gap of 0.5mm. It can be seen that the effects of flow reduce the discharge duration by almost 85%, the no flow case having a duration of around 2.8ms and the high flow case having a duration of approximately 0.5ms. Figure 6.9 shows the restriking effects, which are additional breakdown phases occurring when the discharge is broken or has become sufficiently long to cause a higher voltage drop than would be needed to re-establish a discharge column. Figure 6.8 and Figure 6.10 show the current characteristic which can also be used to measure the discharge duration, i.e. when the current ceases to flow. The shortened discharge duration can reduce ignition probability, just as a lower energy discharge was found to be detrimental to engine performance in chapter 4.

6.4 Flow effects on a capacitive ignition system

The discharge from a capacitive ignition system is very short compared to that of an inductive ignition system, typically less than 10% of the duration. The shorter duration makes the arc less susceptible to being affected by the flow field. Figure 6.11 and Figure 6.13 show the voltage characteristics for a capacitive system under the influence of a pressure of 6 bar gauge, and a flow velocity through the electrode gap of 0 and 25 metres/sec respectively, the spark plug used was of J type electrode, with a gap of 0.5mm and orientated at 90 degrees to the flow. The spark duration is not shortened although a slightly higher secondary breakdown voltage can be seen from the 25 m/s case, which is accompanied by a slightly higher arc voltage. The secondary breakdown, caused by the release of energy which is stored in the coil during the first discharge, is always lower than the first since there is an abundance of ionised species available to promote conduction. The higher secondary breakdown with the high flow case is caused by the loss of some ionised species due to the flow. The current characteristics, shown in Figure 6.12 and Figure 6.14, show little difference. Peak values are very hard to detect, since there is a dependency on response time of the instruments, although the second peak, (corresponding to the second breakdown) does appear to last for a slightly longer period. It should be remembered that discharges do vary quite considerably from one event to the next and hence the reader should not draw too many conclusions from these results of single discharges.

6.5 Effects of electrode type and orientation on inductive ignition performance

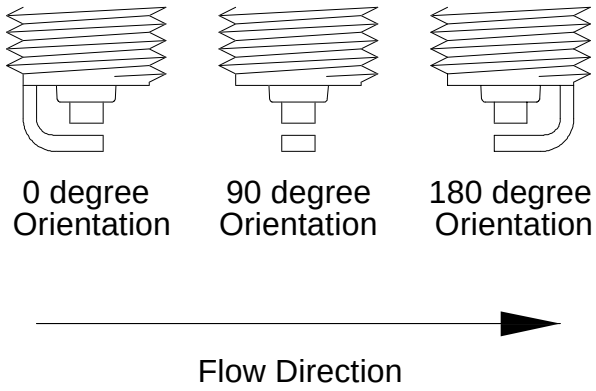

Figure 6.4 Orientation of the J type electrode plug

6.5.1 J type electrode

Under a flow of 15m/s, the J type electrode was positioned in three orientations, the results of which are shown in Figure 6.25 to Figure 6.30. The 0 degree orientation has a spark duration of between 2 and 2.5ms, this is up to twice as long as the duration of the 90 and 180 degree orientated electrodes. The longer discharge of the 0 degree case is due to the sheltering of the column from the flow by the earth electrode.

6.5.2 Double electrode

The results for the double electrode case are shown in Figure 6.15 to Figure 6.18. Both orientations show a similar spark duration, approximately 0.6ms. This is a shorter duration than any orientation of the J type electrode. Both orientations of the double electrode plug are of the same duration, yet the voltage characteristic differs considerably, this could be due to the choice of data, since all discharges differ. The reason that the durations are short compared to

the J type case could be because of the electrode design and the difficulty of ensuring an electrode gap of desired size. Appendix J suggests an equivalent electrode gap for all non J type electrodes plugs tested.

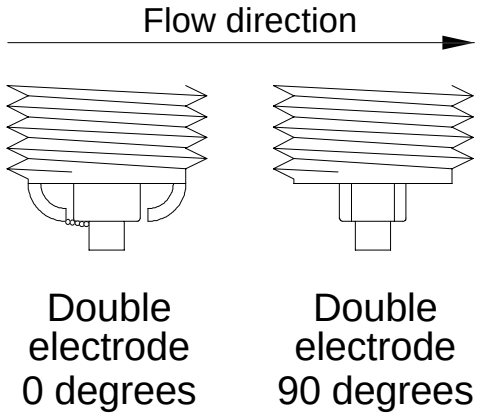

Figure 6.5 Orientation of the double electrode plug

Figure 6.5 shows the electrode arrangement and how the discharge is not shielded by the earth electrode in the 0 degree orientation, but by the centre electrode or cathode (assuming the discharge is between the downstream electrodes). The measurement of the electrode gap is complicated by the assumed path of the discharge (although an estimate of this may be made through careful measurement of the breakdown voltage, see Appendix J). From the results however, it is assumed that the discharge is not fully shielded from flow, and hence the durations are the same for both orientations. Since the speed of electrons is much greater than the velocity of the flow, it is assumed that the electric field is not distorted, hence the discharge path is not necessarily the most sheltered one.

6.5.3 Triple electrode

With triple electrode plugs it will be more difficult to predict the behaviour of the discharge (the electrode arrangement for which is shown in Figure 6.3). The breakdown will occur across the path of least resistance and this will not be influenced by the flow. Since the earth electrode provides the discharge with a horizontal path, in the 0 degree orientation, the discharge (assuming the gas prefers to break over in sheltered conditions) may be shielded by the earth electrode, in the 60 degree orientation, the discharge may be shielded by the centre electrode although as discussed above, the flow should have no bearing on where the breakdown occurs. The results, shown in Figure 6.19 to Figure 6.22 show similar spark duration and voltage characteristics. The similarity could be because both discharges have taken place in sheltered conditions as discussed above, or that they occurred between other electrodes for which the gaps were not shielded from the flow. The duration for both was approximately 1.2ms, which is slightly longer than that of the J type electrode in the 90 and 180 degree orientations.

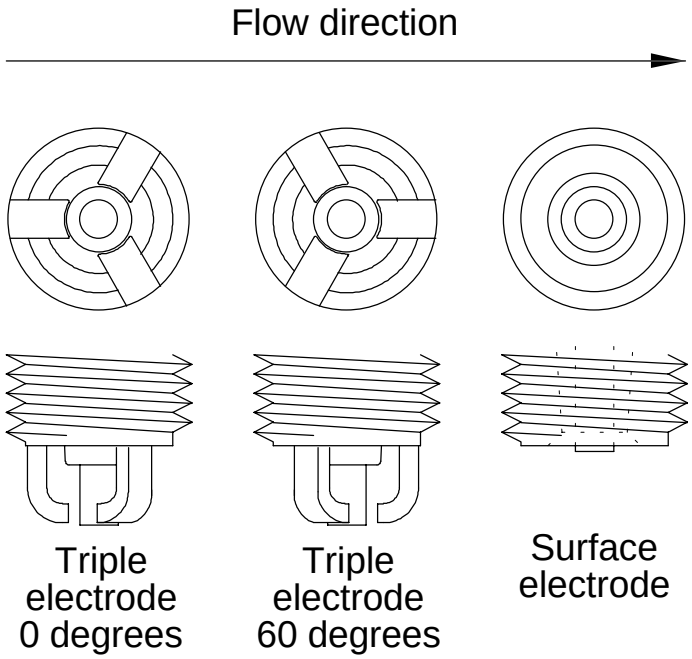

Figure 6.6 Orientations of triple electrode and surface discharge plugs

6.5.4 Surface discharge

The surface discharge plug provides little shelter for the spark although it is assumed that the discharge path can move around the earth electrode since inspection of the plug after use showed discolouration of the electrode (anode) surface downstream in the direction of the flow. If the discharge occurred below the electrode surfaces, in the trough above the insulator, vortices shed by the interaction of the flow with the slight protrusion of the centre electrode could disrupt the discharge. Figure 6.23 and Figure 6.24 show the voltage and current characteristics for this type of plug in a 15m/s flow at 6 bar gauge pressure. The discharge duration is approximately 1.7ms long, and is the longest duration with the exception of the J type electrode at 0 degrees to the flow. This is made all the more remarkable because the surface discharge has a larger effective electrode gap (appendix J) than the J type electrode plug.

6.6 Conclusions

It has been seen that the influence of flow on the discharge from an inductive ignition can dramatically shorten its duration. This shortened duration can reduce the ignition reliability, since it was shown in chapter 4 that the reduction of energy results in a higher COV of IMEP, this reduction in energy has been seen to shorten the duration also.

Electrode orientation and design has been shown to preserve the arc under high flow conditions, although in the case of multiple electrode plugs, the breakdown and formation of the discharge occurs across the path of least resistance and is insensitive to flow during this early period. The electrode design which gives greatest shelter is that of the J configuration in the 0° orientation. The surface discharge plug allows a similar spark duration under the same flow conditions, and the further advantage of this electrode design is that the orientation is not important. The shortest duration was achieved using the 90° orientation of the J type electrode, the gap being open to the direction of flow.

When installed in an engine, it would be near enough impossible to ensure that the spark plug electrode is orientated in the chosen direction since there is no control over how the threads are machined in the cylinder head, and the threads on the plug shell are machined in such a way that the electrode can be in one of six positions relative to the thread start. An additional, and perhaps most important factor is the plug sealing washer, once the plug is being tightened, the washer deforms and even with careful management of the torque applied, the degree of crush is not repeatable since the condition of the threads themselves will have a more dominant effect. However, if the electrode orientation is important (as may be the case in direct injection gasoline engines) then great care will be needed.

The CD ignition system has been shown to be insensitive to flow regardless of the electrode design or orientation. This system has also been shown, in chapter 4, to be comparable in performance to the TCI system.

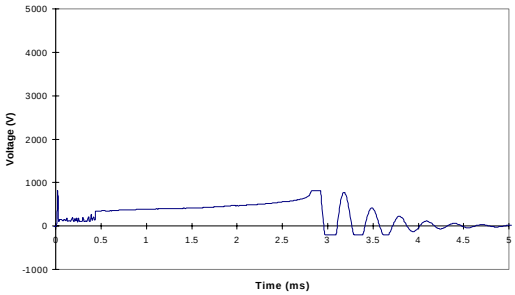

Figure 6.7 Voltage characteristic for an inductive ignition system with no flow

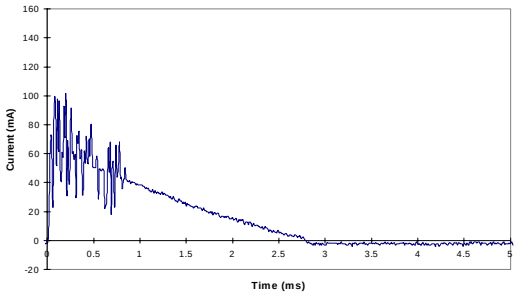

Figure 6.8 Current characteristic for an inductive ignition system with no flow

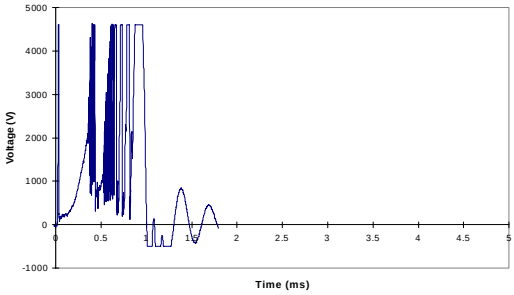

Figure 6.9 Voltage characteristic for an inductive ignition system in a flow of 25m/s

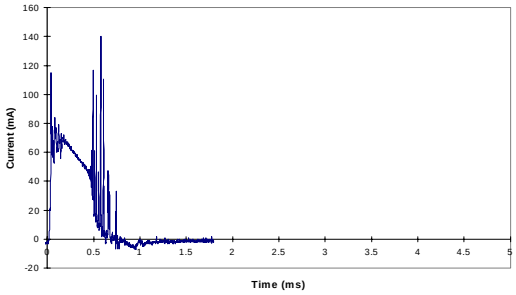

Figure 6.10 Current characteristic for an inductive ignition system in a flow of 25m/s

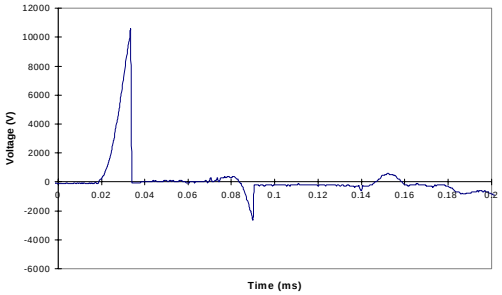

Figure 6.11 Voltage characteristic for a capacitive ignition system with no flow

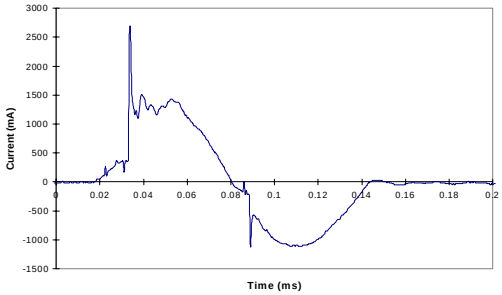

Figure 6.12 Current characteristic for a capacitive ignition system with no flow

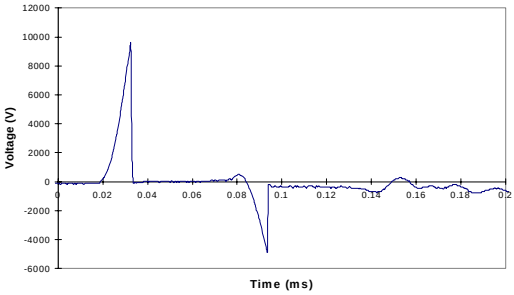

Figure 6.13 Voltage characteristic for a capacitive ignition system in a flow of 25m/s

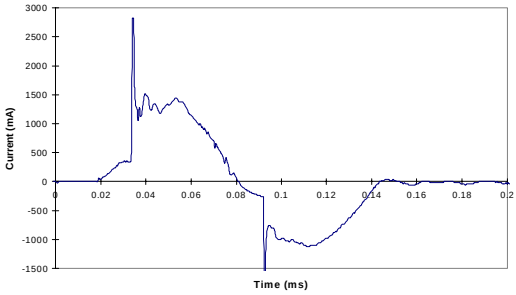

Figure 6.14 Current characteristic for a capacitive ignition system in a flow of 25m/s

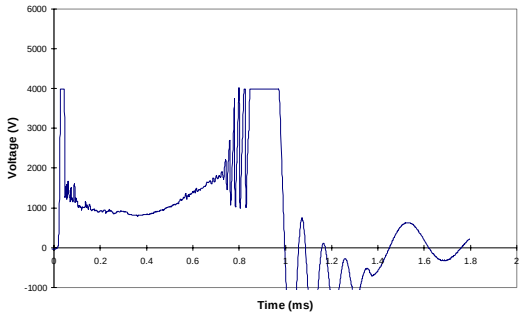

Figure 6.15 Voltage characteristic for an inductive ignition system with double electrodes at 0 degrees to flow direction

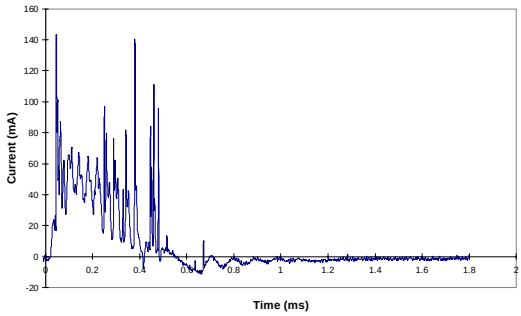

Figure 6.16 Current characteristic for an inductive ignition system with double electrodes at 0 degrees to flow direction

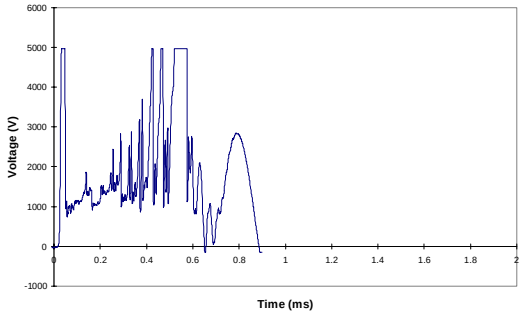

Figure 6.17 Voltage characteristic for an inductive ignition system with double electrodes at 90 degrees to flow direction

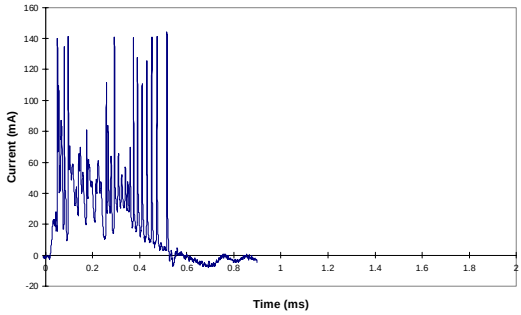

Figure 6.18 Current characteristic for an inductive ignition system with double electrodes at 90 degrees to flow direction

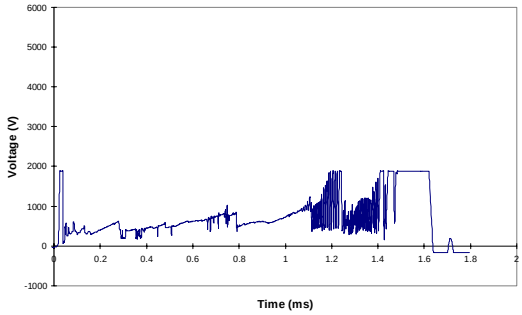

Figure 6.19 Voltage characteristic for an inductive ignition system with triple electrodes at 0 degrees to flow direction

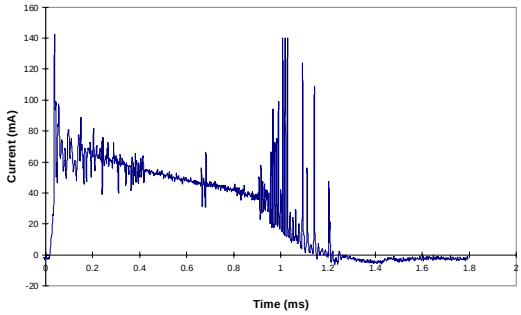

Figure 6.20 Current characteristic for an inductive ignition system with triple electrodes at 0 degrees to flow direction

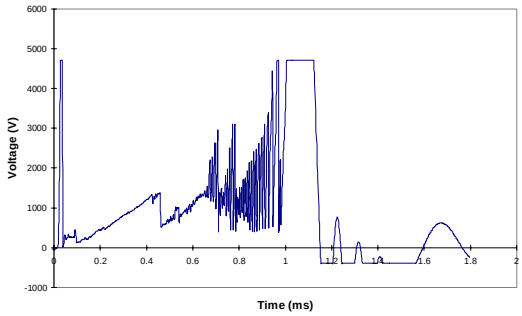

Figure 6.21 Voltage characteristic for an inductive ignition system with triple electrodes at 60 degrees to flow direction

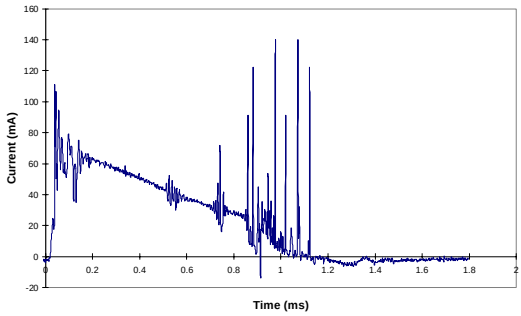

Figure 6.22 current characteristic for an inductive ignition system with triple electrodes at 60 degrees to flow direction

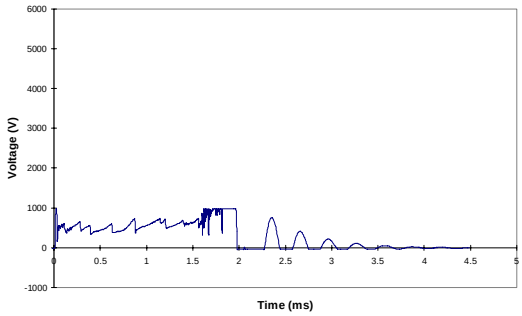

Figure 6.23 Voltage characteristic for an inductive ignition system with surface discharge plug

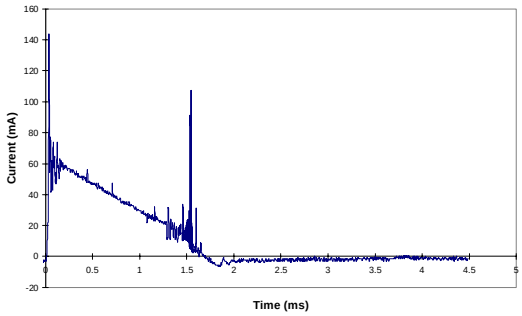

Figure 6.24 Current characteristic for an inductive ignition system with surface discharge plug

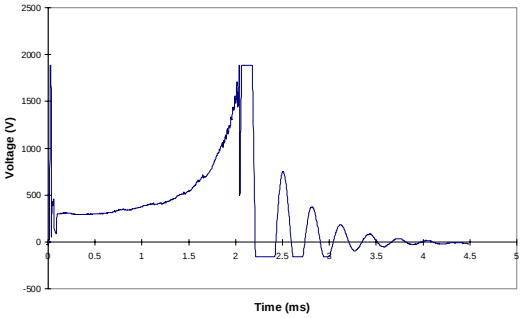

Figure 6.25 Voltage characteristic for an inductive ignition system with J type electrode at 0 degrees to flow direction

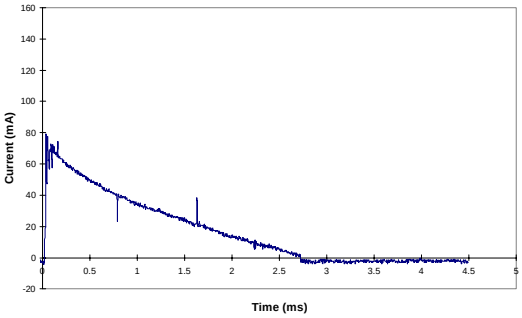

Figure 6.26 Current characteristic for an inductive ignition system with J type electrode at 0 degrees to flow direction

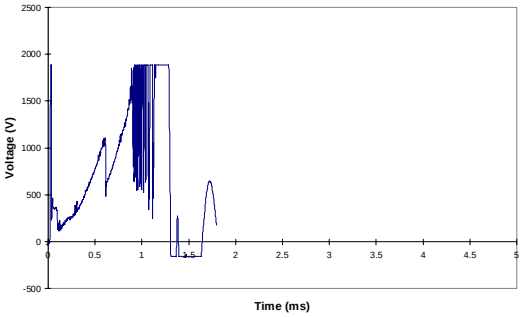

Figure 6.27 Voltage characteristic for an inductive ignition system with J type electrode at 90 degrees to flow direction

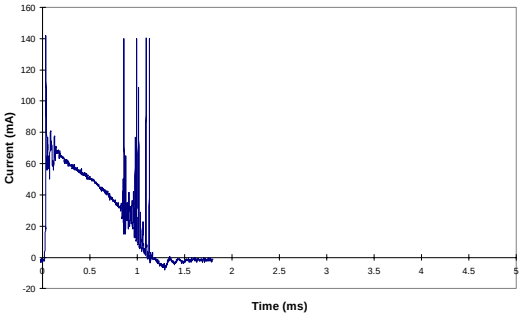

Figure 6.28 Current characteristic for an inductive ignition system with J type electrode at 90 degrees to flow direction

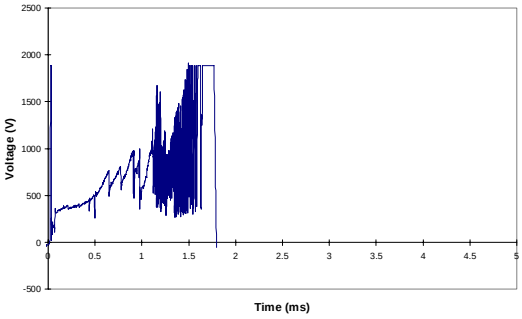

Figure 6.29 Voltage characteristic for an inductive ignition system with J type electrode at 180 degrees to flow direction

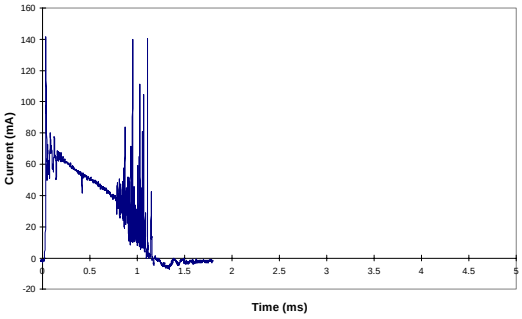

Figure 6.30 Current characteristic for an inductive ignition system with J type electrode at 180 degrees to flow direction

6.7 Flow velocity determination

Under the action of a flow field the discharge path, between a pair of electrodes, is elongated. This elongation increases the resistance of the discharge and results in a rise in voltage. The rate of the rise of voltage can be used to estimate the velocity of the gas travelling through the gap. Analysis such as this concentrates on the glow discharge regime since this has the longest duration.

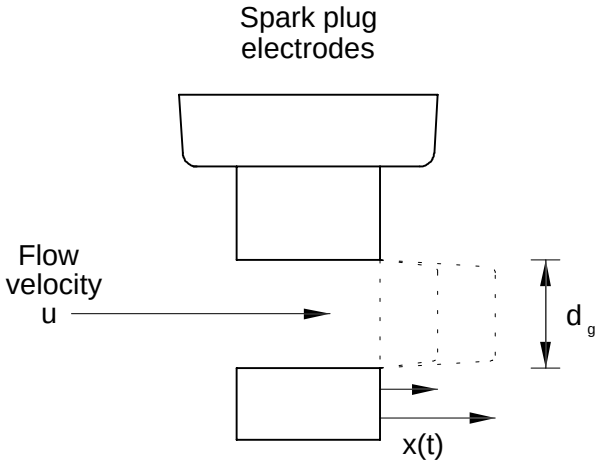

Figure 6.31 Effects of flow velocity on the discharge path between a pair of electrodes

Figure 6.31 shows what is thought to happen to the discharge path under the influence of a mean flow component. Since the electrodes are short in the x direction, the boundary layer is considered to be thin and this assumption allows the discharge to be modelled as a piece-wise rectangle, and therefore the length of the discharge at any instant can be calculated from;

$$L = 2x + d_g \qquad \textbf{(6-1}$$

rearranging gives:

$$x = \frac{L - d_g}{2} \qquad \textbf{(6-2}$$

and the velocity can be calculated from:

$$\frac{dx}{dt} = \frac{1}{2}\frac{dL}{dt} \qquad \textbf{(6-3}$$

With knowledge of the electric field within the gap, and the other voltage drops associated with the electrodes, the discharge length can be estimated. There are three main voltage drops across the spark plug (Cobine 1958), these are the cathode fall (or drop), the positive column fall and the anode fall. With a resistive spark plug, the voltage measuring system would also measure a further voltage drop induced by the plug's internal resistance.

For the cathode fall in a normal glow discharge:

$$V_c = \frac{3B}{A} \ln\left(1 + \frac{1}{\gamma}\right) \quad \textbf{(6-4}$$

where V_c is the cathode fall (volts)
B is a constant dependent upon the gas (volts/cm/mmHg)
A is a constant dependent upon the gas (volts/cm/mmHg), and
γ is the electron emission constant (dependent upon gas and electrode material)

For air and nickel electrodes in the normal glow discharge;
A=14.6
B=365
γ=0.036

this results in a cathode fall of 252 volts.

The anode fall in a normal glow discharge is similar to that in the arc phase; no relationships could be found by the author, although an estimate by Cobine places the value between 2 and 10 volts (although not documented for nickel electrodes, this value is similar for copper, carbon and iron electrodes), and in any case, this is very much smaller than the cathode fall.

Anderson and Kim (1995) used a different relationship for calculating the anode fall, referencing Cobine (1958), the relationship below was adopted:

$$V_a = V_1 + \phi \quad \textbf{(6-5}$$

where V_1 is a constant (13.6V), and
ϕ is the work function of the electrode material

The positive column voltage is calculated by subtracting the cathode and anode falls from the measured voltage drop across the plug. The anode and cathode falls are considered to be constant throughout the glow discharge phase, this yields the following equation:

$$V_{pc} = V - (V_a + V_c) \quad \textbf{(6-6}$$

or for nickel electrodes in air

$$V_{pc} = V - 262 \quad \textbf{(6-7}$$

The column field strength can be calculated from:

$$E = \frac{V_{pc}}{L} \quad \textbf{(6-8}$$

and hence from equation (6-3, the velocity can be calculated as:

$$u = \frac{\partial V / \partial t}{2E} \quad \textbf{(6-9}$$

This is only an approximation, since over an electrode gap the electric field will vary with distance, and at some point within the gap the field will be zero. To simplify matters, the field strength is assumed to be uniform throughout the gap. For calculation purposes the column

field strength, at any point in the discharge, is believed to be a function of time, current, temperature and pressure.

6.8 Column field sensitivity

6.8.1 Column field strength as function of measuring time and current for a conventional coil ignition system

A conventional inductive ignition system was used to produce ignition discharges with a conventional spark plug of 0.5mm gap, the results of which are shown in Figure 6.32. The coil-on-time, and hence stored energy, was progressively reduced to make current levels occur earlier, albeit with the loss of peak current. Each point on the graph signifies an average of 25 values. The results of Maly (1983), shown in Figure 6.31, look somewhat different to those reported here, but further investigation showed that it was possible to obtain similar results by using a resistor spark plug; Maly's work does not reference the type of plug used. Maly's results show a higher field at an earlier time, and it is believed that this is due to a higher voltage drop across the plugs internal resistance.
Figure 6.34 shows the effect of coil-on-time on the glow phase. Neglecting the shortest two discharges, the rate of rise of voltage appears to be the same for each energy level, and only deviates when the current ceases to flow and resonance occurs (which has been removed for clarity). Figure 6.35 shows the corresponding current traces, it can be seen that up to six different voltage values can be obtained for the same current value.

6.8.2 Column strength as a function of pressure

The column field strength can be seen to rise with an increase in pressure. Figure 6.36 shows this effect for a non resistive plug, with data from three points in the same discharge. Again, each point refers to an average of 25 data sets. Figure 6.37 shows the effects of increased pressure on a resistive plug, and a comparison with Figure 6.33 supports the hypothesis that they used a resistive spark plug.

At elevated pressures, the glow voltage exhibits what could be described as noise, since rapid fluctuations in current and deviations in the voltage characteristics are present; Figure 6.38 and Figure 6.39 show these effects. The plug used was a non resistor type, and it was thought that a resistive type would result in the eradication of this noise.

Testing with a resistive spark plug, Figure 6.43, gave similar results, although a negative overall gradient of voltage with time was apparent, compared to the non resistive plug's positive overall gradient. It was therefore thought that the suspected noise was in fact a switching between arc and glow discharge modes. It is common thought that glow discharges only occur at very low pressures, these tests were carried out at higher pressures with cold electrodes. The deviance was accompanied by a severe drop in voltage; this occurs because the cathode fall is so much lower in magnitude for the arc discharge regime. When considering the resistive plug, the negative dV/dt characteristic can be explained, since a higher voltage drop across the plug resistance would be expected with a higher current, since the resistance of the non-resistive plug is very close to zero and therefore the voltage drop is insignificant compared to that of the gap.

Referring to the work of Weyl (1993), this effect of switching between discharge regimes was not noted, the most probable reason for this being the gain of the data acquisition system being optimised to capture the initial breakdown magnitude. In actual fact, the glow discharge was

never considered to be of importance, instead attention was paid to the discharge duration and the successive discharges occurring due to the interaction of the flow with the ionised gas column.

6.8.3 Column strength as a function of temperature

Figure 6.40 shows the effects of temperature on the column field strength at three different points in the discharge. The tests were conducted in the heated pressure vessel where 25 data sets were averaged to obtain one data point. Maly's results are shown in Figure 6.41, the conclusions for which were that the glow regime was insensitive to temperature differences. The results reported here could also be interpreted in that manner.

6.8.4 The calculation of column field strength at any point in a discharge

Cobine (1958) gives the following relationship between positive column voltage, gap and current at constant pressure and no flow.

$$V_p = Bd_g I^{-n} \qquad \textbf{(6-10}$$

where B is a constant
I is current
d_g is distance between the electrodes

After performing similar tests to those detailed above, Anderson and Kim (1995) adapted the above relationship to determine the positive column voltage at any point in time with a change in pressure and mean flow velocity:

$$V_p(t) = 40.46\, d_g I^{-0.32} p^{0.51}\left(1 + \frac{2ut}{d_g}\right) \qquad \textbf{(6-11}$$

where p is pressure (bar)
u is mean flow velocity (mm/s)
t is time (s)

6.8.5 The graphical user interface (GUI) for data analysis

Experimental data is notorious for its unrepeatability and susceptibility to interference and signal corruption. The data acquired from ignition systems is no different. After frustrated attempts to characterise the discharge, so as to enable a computer code to recognise areas of interest, it was decided to implement a GUI technique. Visual Basic was chosen for its flexibility and compatibility with the acquisition file format.

Figure 6.44 shows the data analysis window, and in this version of the program, the user can view all acquired discharges. Facilities are included for selecting and exporting ASCII data to spreadsheets, for calculating the electric field at any given time, and for the calculation and display of the voltage gradient between two user selected points.

6.8.6 Curve fitting

Anderson and Kim believe the positive column voltage is a function of current and pressure:

$$V_p = f(I) \times f(P) \times C \qquad \textbf{(6-12}$$

Cobine gives the following relationship:

$$V_p = B \times d_g \times I^n \qquad \textbf{(6-13}$$

and including a pressure term, this becomes:

$$V_p = B \times d_g \times I^n \times P^m \qquad \textbf{(6-14}$$

Combining B and d_g to form one constant, and taking logs to make the equation suitable for least squares fitting gives and equation of the form:

$$y = a + bx + cz \qquad \textbf{(6-15}$$

where:

y is ln V_p
a is ln B + ln d_g
b is n
x is ln I
z is ln P, and
c is m

Using the methods described in Appendix L to obtain a, b and c,

$$B \times d_g = \exp(a)$$
$$n = b$$
$$m = c$$

using experimental data at pressures between 0 and 12 bar gauge, the following constants were evaluated:

$$B \times d_g = 396.480$$

and with d_g = 0.5mm,

$$B = 792.96$$
$$n = -0.415$$
$$m = 0.182$$

so for the non resistive J type electrode spark plug, the voltage of the positive column can be evaluated with:

$$V_p = 396.480 \times d_g \times I^{-0.415} \times P^{0.182} \qquad \textbf{(6-16}$$

where I is in mA
P is in Bar absolute, and
d_g is in mm

This differs slightly from the results of Anderson and Kim, and is probably due to the plug type used.

With the stretching of the discharge channel due to the interaction of the flow, the effective spark gap grows. Anderson and Kim assumed a picewise continuous rectangular shaped discharge, with the depth being equal to the electrode gap, and the lengths of the connecting limbs being a function of the time and velocity of the flowing gas. The length of the discharge is therefore

$$L = \left(d_g + 2ut\right) \qquad \textbf{(6-17}$$

where u, the velocity is in mm/s
L, the discharge length is in mm, and
t, the time is in seconds
so, at any point in a discharge in a flowing gas, the positive column voltage can be calculated from:

$$V_p = 396.480 \times d_g \times I^{-0.415} \times P^{0.182}\left(1 + \frac{2ut}{d_g}\right) \qquad \textbf{(6-18}$$

where P, the pressure is in bar
I, the current is in mA, and
t, the time is in seconds
the electric field, equation (6-8 can be calculated (in V/mm)a in a similar manner and is assumed to depend upon the current and pressure only:

$$E = 396.480 \times I^{-0.415} \times P^{0.182} \qquad \textbf{(6-19}$$

6.9 Estimates of the flow velocity in the pressurised flow rig for the glow voltage

Using the pressurised flow rig, Figure 6.1, described in section 6.1, a series of discharges were captured at a range of velocities and two pressures. In order to test equation (6-18, use can be made of the data from the flow rig, in which the pressure and velocity are known

The method for calculating the flow velocity was:
1. Pick two points on the rise in the glow regime to represent voltage rise rate
2. Calculate E at both points
3. Calculate the voltage gradient between the two points
4. Calculate the velocity from equation (6-9
5. Repeat for all discharges
6. Calculate mean and standard deviation

The results plotted in Figure 6.45 and Figure 6.46 are the averages, with the error bars showing the standard deviation of the samples. Both sets of results show that the velocity measured by the spark plug is about 20% lower than that measured by the air flow meter. The results by Anderson and Kim (1995) showed errors of up to 30% and the results obtained were at ambient pressure, the higher pressures investigated in this study are more representative of in-cylinder conditions at the point of ignition.

As mentioned earlier in this chapter (in section 6.5.2), no two discharges are the same. When analysing each trace for the purposes of measuring velocity, the voltage rise rate differed considerably, the plotted results being an average of 25 discharges. Some of the discharges showed a non linear rise in voltage, in these cases, the rate towards the end of the rise, before a restrike occurred, was used for the analysis. This decision was made since the connecting legs of the discharge (see Figure 6.31) are at a near maximum length and hence the errors would be at a minimum. Anderson and Kim (1995) noted that *poor selection of E and dV/dt was found to cause a variation of the predicted velocity of up to 30%*. With this comment in mind, a better correlation would be obtained if discharges with low values of velocity were rejected.

6.10 Application to engine measurements

Applying the methods described above to an engine will enable the velocity at the spark plug gap to be determined. The experimental cylinder pressure data were used to provide pressure data for the prediction of the electric field by assuming a linear variation with time. Least squares fitting is shown in Figure 6.47 for the three engine conditions used in chapter 4. The results of this are shown below:

Speed (revs/min)	Mean piston speed (m/s)	Air consumption (l/s)	Velocity at ignition (m/s)	Standard deviation
1000	2.97	1	1.872	1.725
1000	2.97	2	3.6772	3.319
2000	5.94	2	7.018	6.605

It is thought that the mean flow in the cylinder should be of a similar order of magnitude to the mean piston speed, and should scale with it. The 1l/s case at 1000rpm is slightly less than the mean piston speed and both the 2l/s cases are slightly higher. The values of standard deviation are high compared to the predicted velocity. It is suggested that these values represent the turbulence intensity at the spark plug gap.

6.11 Conclusions

It has been shown that velocity can be measured from a spark plug, although many assumptions are made and errors are sizeable, the trends are as expected for the pressures tested and a correction factor can be applied. This method can be used in both a motored and firing engine

No mean flow and turbulence data are available from Rover at the spark plug location, but LDA measurements at Imperial College have been made in a plane 10mm below the cylinder head (i.e. 8.5mm below the spark plug gap). For an air flow rate of about 1.5L/s at 1000rpm the turbulence intensity is about half the mean piston speed at 45° BTDC, and this level might be expected to rise with the collapse of the tumble vortex. Mean flow measurements are only available up to 75° BTDC and these results would suggest that the mean flow is of the same order of magnitude as the mean piston speed (Arcoumanis et al. 1997)

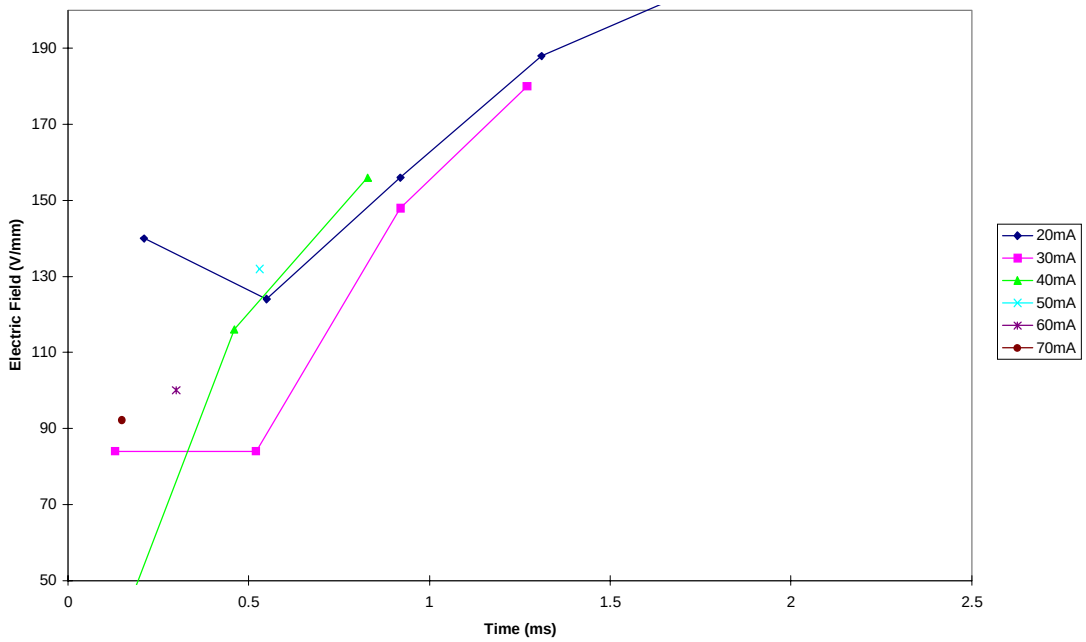

Figure 6.32 **Column field strength as function of measuring time and current for a conventional coil ignition system**

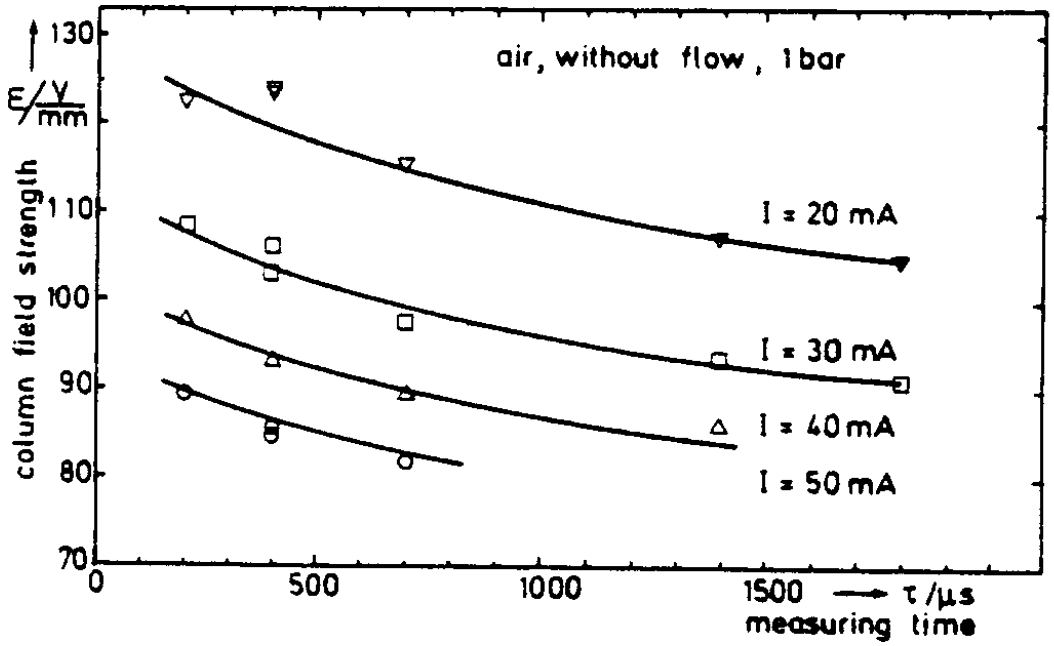

Figure 6.33 **Column field strength as function of measuring time and current for a conventional coil ignition system (Maly 1988)**

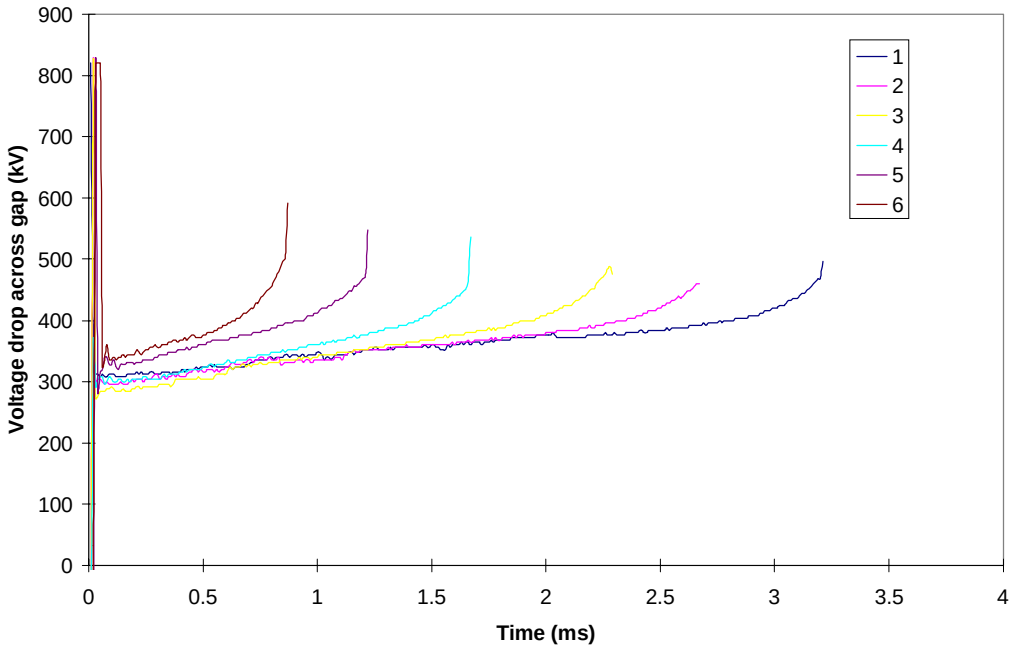

Figure 6.34 Relationship between voltage and time for various stored energies

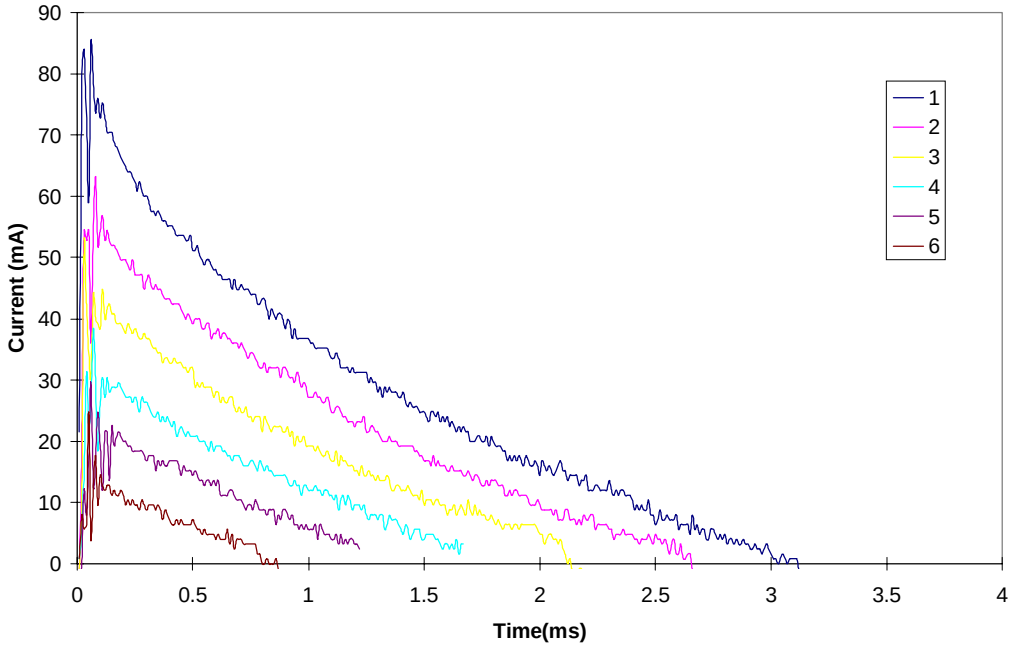

Figure 6.35 Relationship between current and time for various stored energies

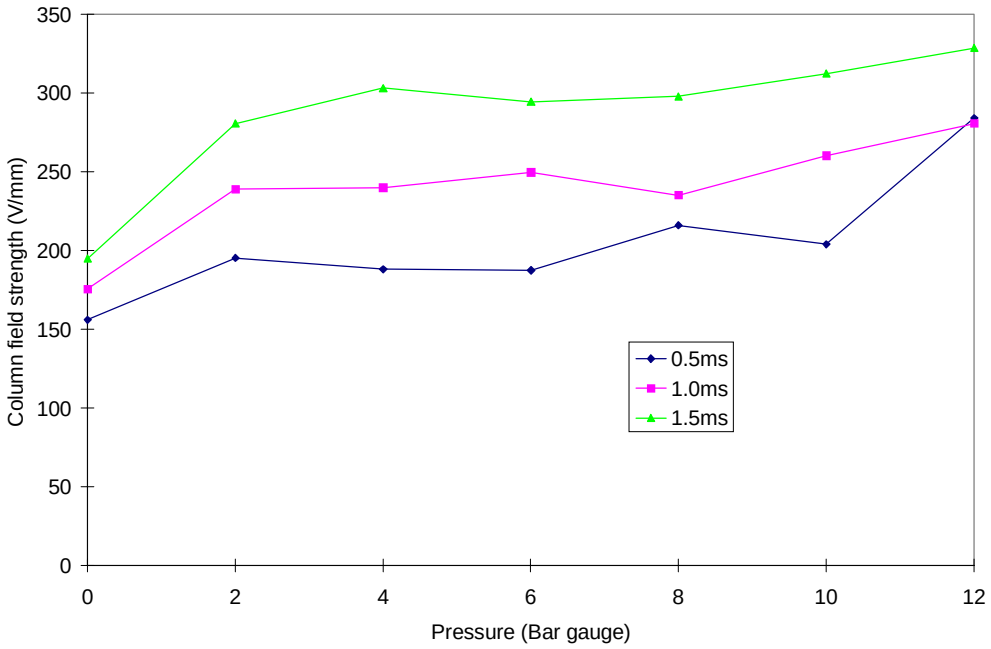

Figure 6.36 **Relationship between column field strength and pressure at various points in the discharge (non resistor plug)**

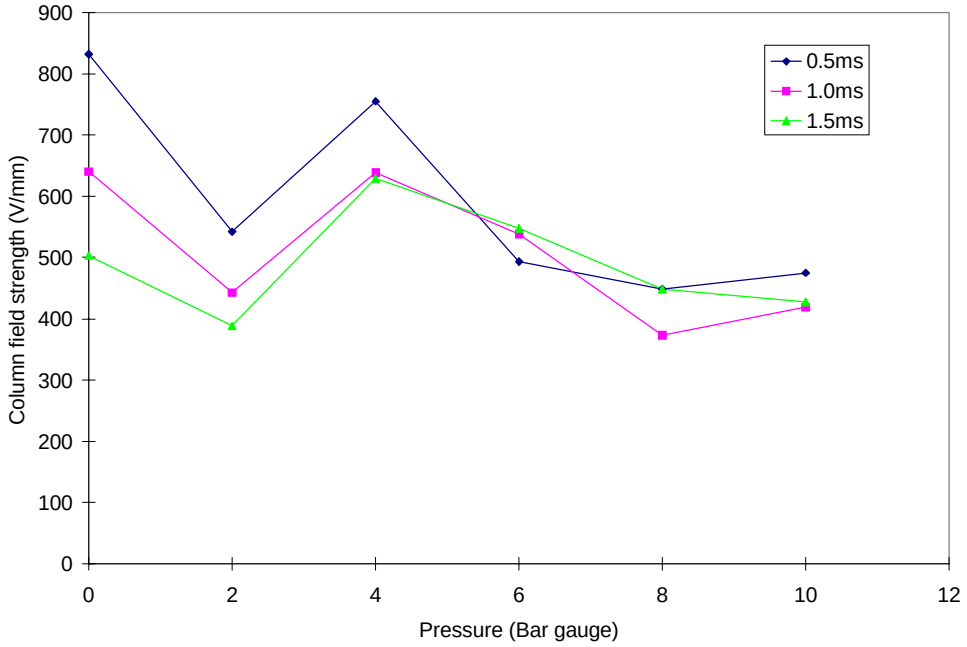

Figure 6.37 **Relationship between column strength and pressure at various points in the discharge (resistive plug)**

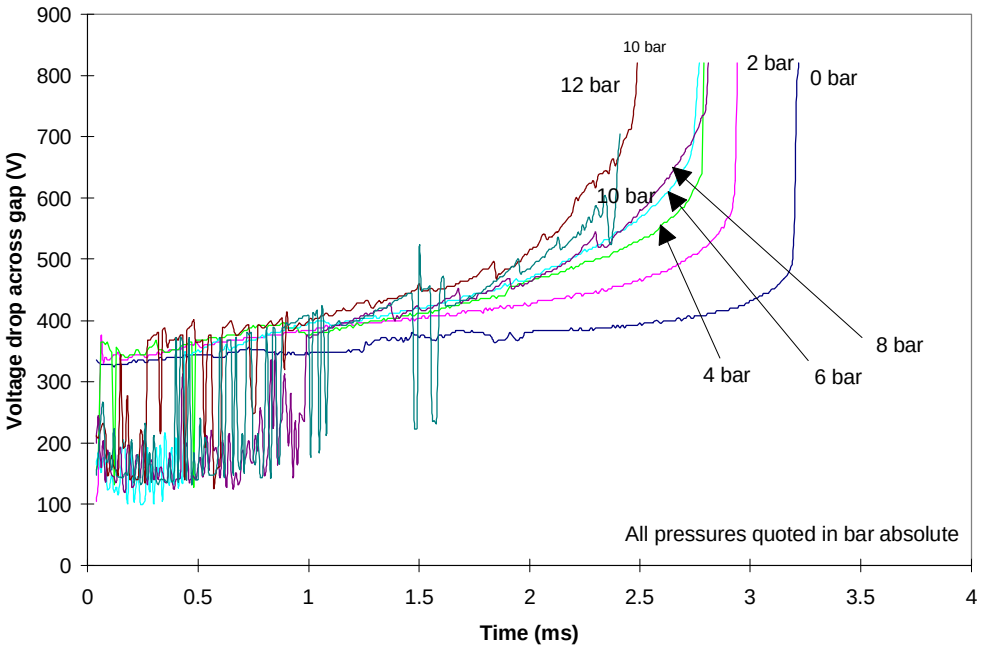

Figure 6.38 **Glow voltage for 0.5mm gap and increase in pressure for non-resistive spark plug**

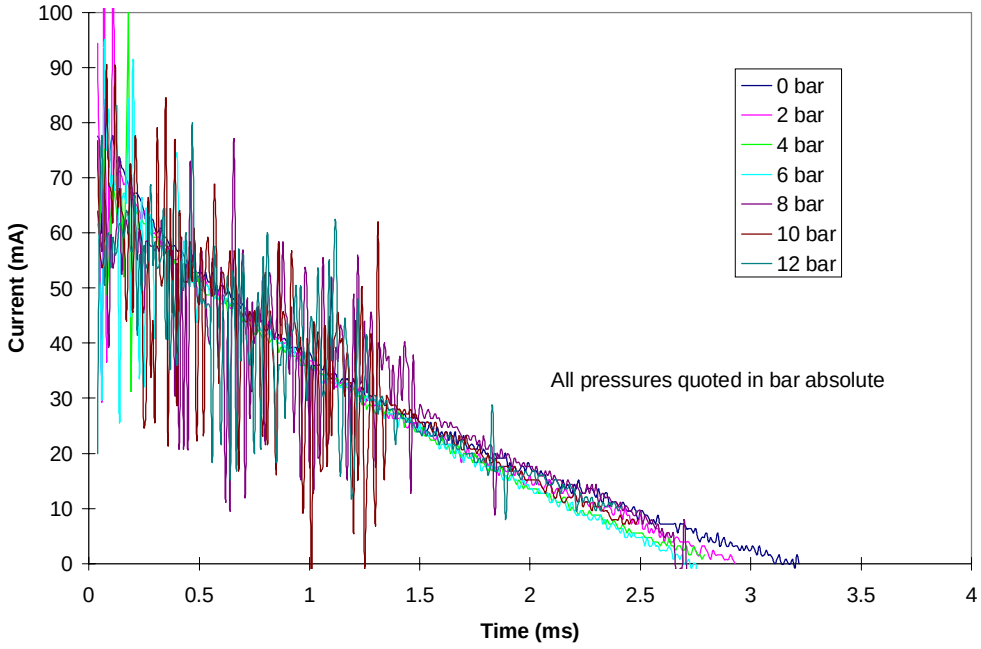

Figure 6.39 **Glow current for 0.5mm gap and increase in pressure for non-resistive spark plug**

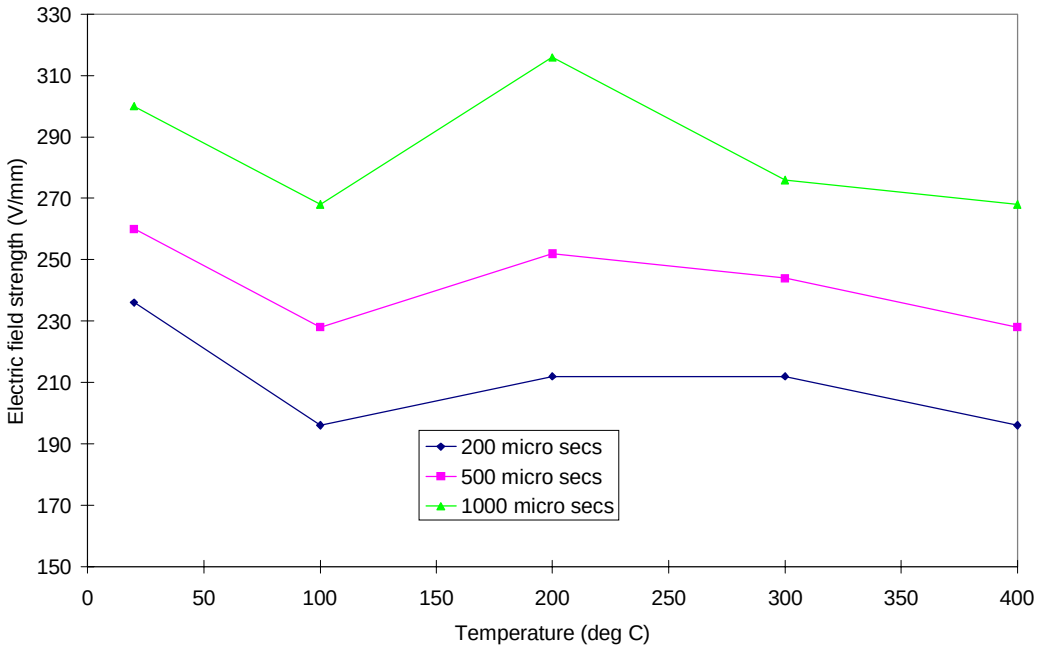

Figure 6.40 **Column field strength as function of measuring time and temperature for a conventional coil ignition system**

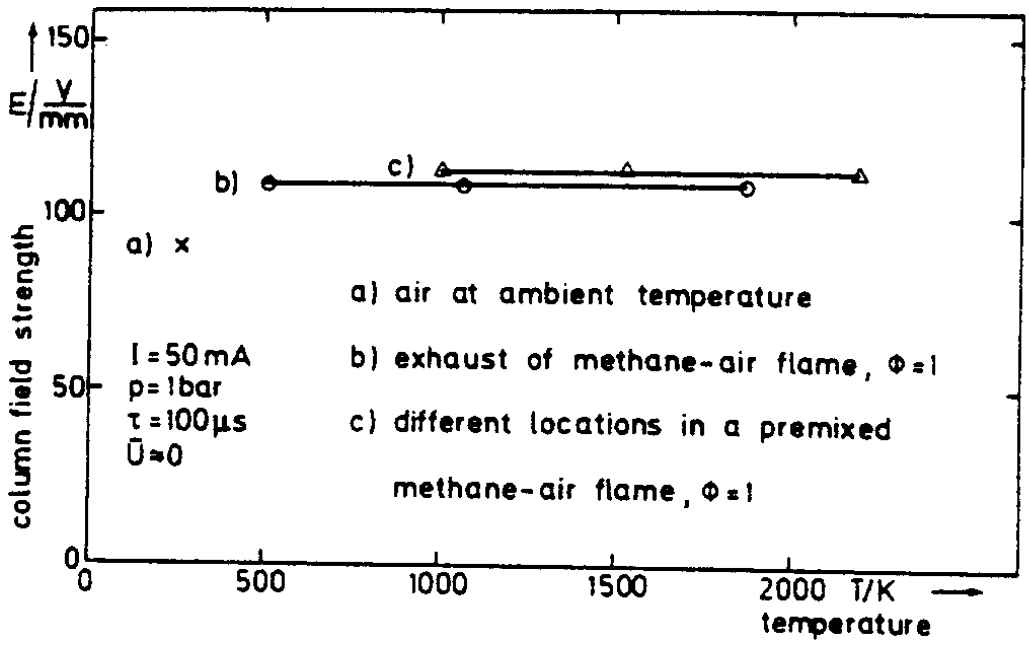

Figure 6.41 **Column field strength as function of measuring time and temperature for a conventional coil ignition system (Maly 1988)**

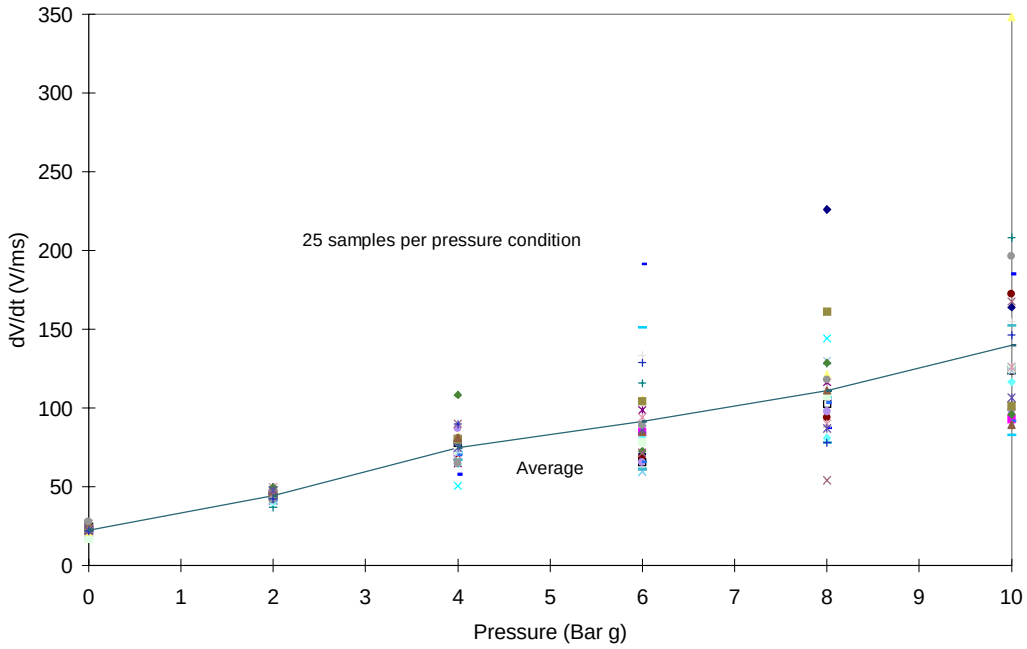

Figure 6.42 Relationship between pressure and voltage rise rate for non resistor plug

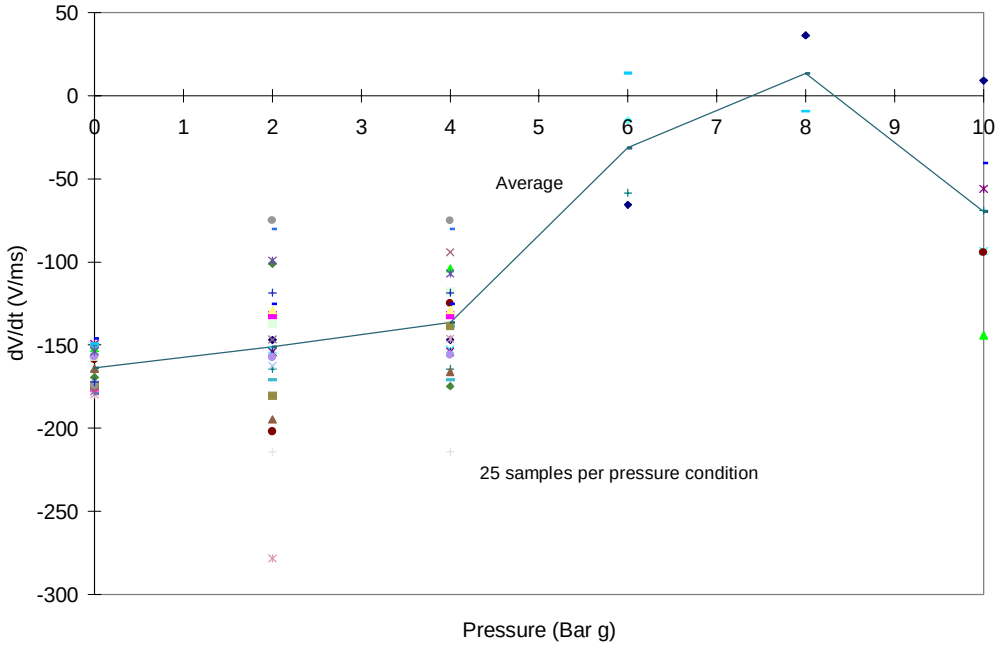

Figure 6.43 Relationship between pressure and voltage rise rate for resistor plug

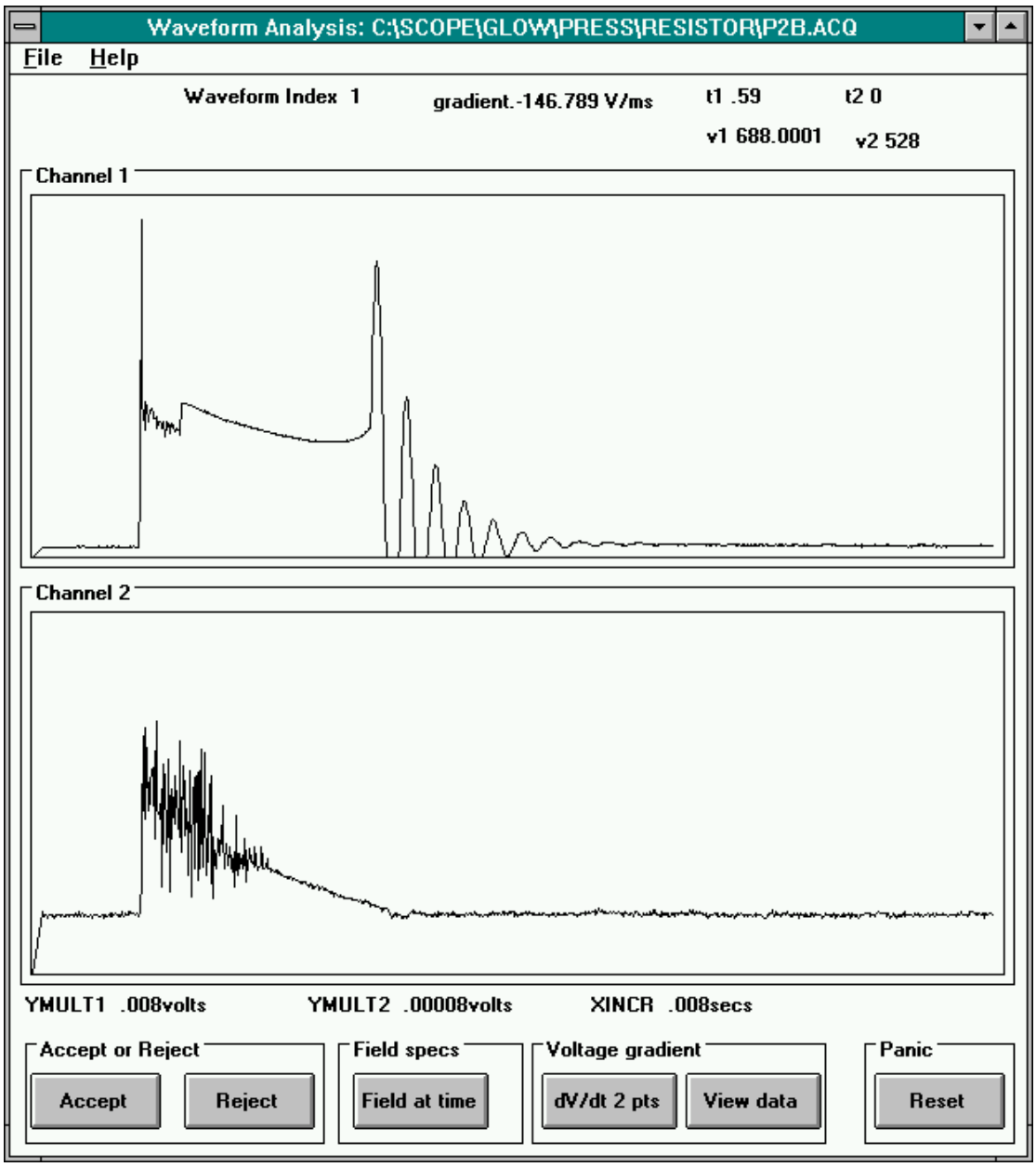

Figure 6.44 Graphical user interface developed to allow analysis of data

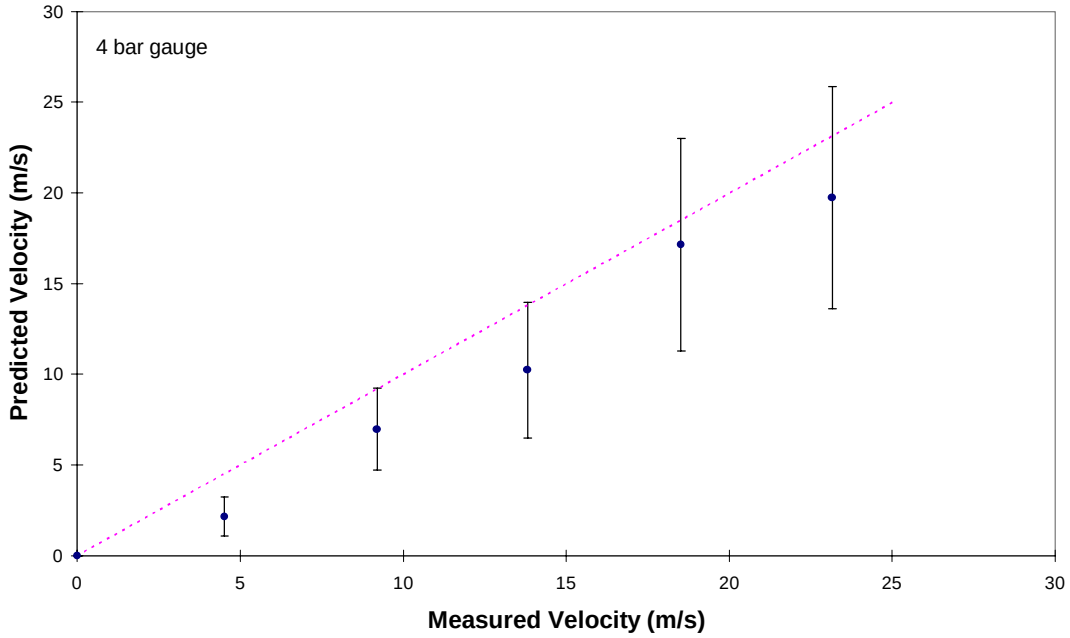

Figure 6.45 Velocity measured by increase in discharge length against actual velocity for a pressure of 4 bar gauge

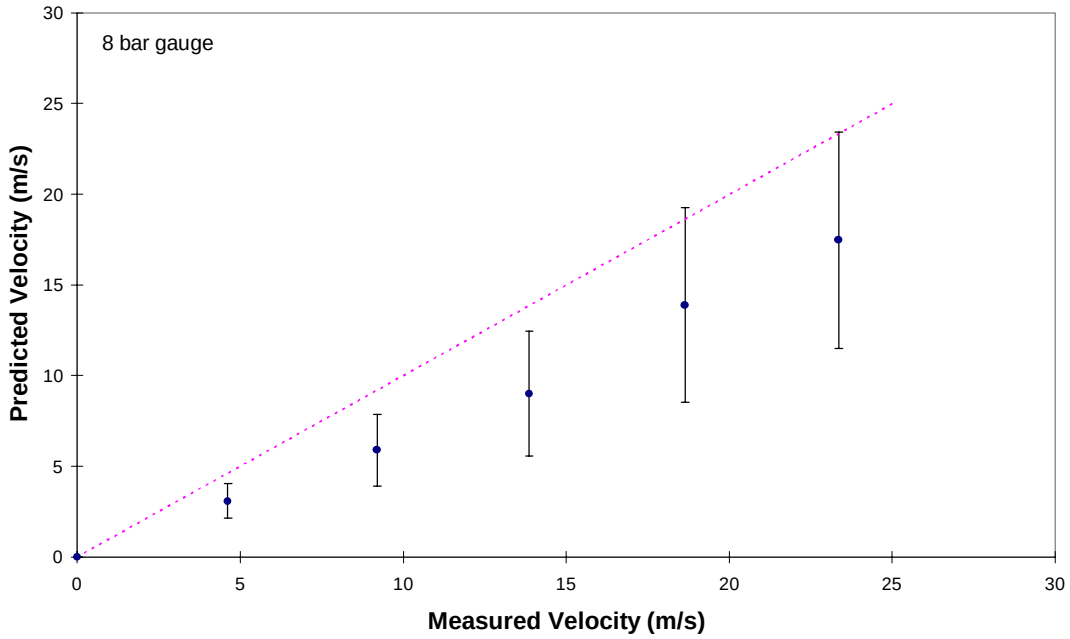

Figure 6.46 Velocity measured by increase in discharge length against actual velocity for a pressure of 8 bar gauge

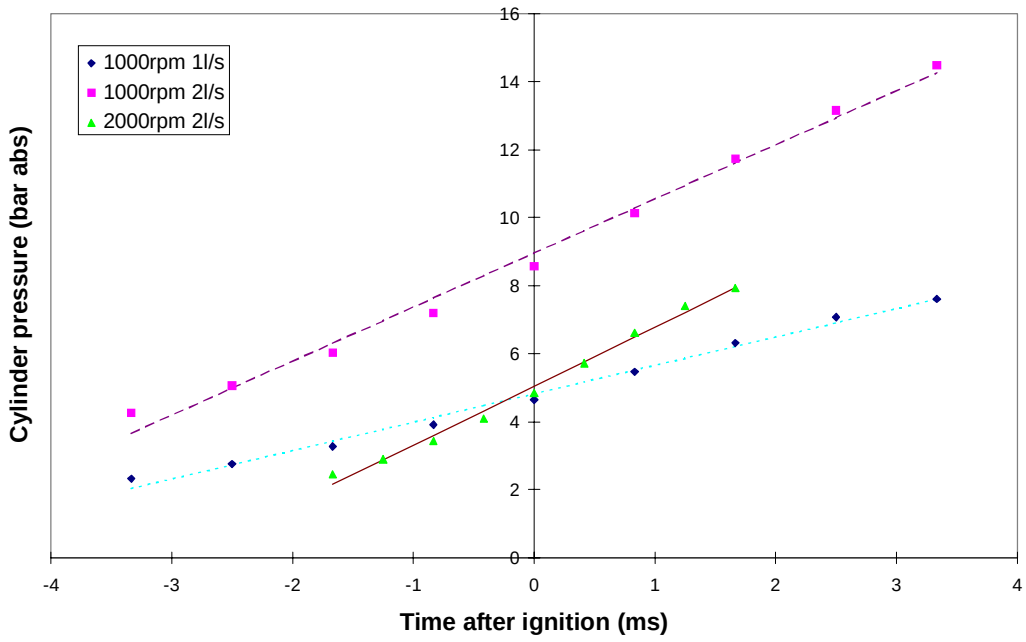

Figure 6.47 **Mean cycle cylinder pressure as a function of time for different speed and load points with linear fit**

7. Conclusions and recommendations for further work

7.1 Review of goals

The desired outcome of this project was to rate different types of ignition systems, at a range of different energy levels, for performance in ignitability and erosion testing. It was also intended that the spark discharge should be investigated in a flow field of varying velocity.

7.1.1 Ignitability experiments

A Rover K4 single cylinder research engine was used to test inductive and capacitive ignition systems at a range of energy levels. It was found that the optimum ignition system, and minimum energy level, for combustion stability varied with the engine operating point. The CDI system was best suited to the low speed, low load condition (30% of full load at 1000rpm), and out performed the TCI system, for which the discharge duration was up to ten times longer, and the stored energy up to 200% greater. At higher speeds and loads (60% full load at 1000rpm and 30% full load at 2000rpm) and with EGR (60% full load at 1000rpm), the TCI system gave better engine performance than the CDI system.

A comparison, indirectly in the case of the lower stored energy, was made between different ignition transformers for the CDI system. It was found that the use of an ignition coil, of higher inductance and resistance than a dedicated ignition transformer, was beneficial to engine performance when used in conjunction with a lower energy level. The higher primary and secondary resistance resulted in a glow discharge, whereas with the ignition transformer, the discharge was in the arc mode (signified by higher currents and lower voltages).

7.1.2 Erosion Experiments

Attempts were made to test the erosion rate of a pair of electrodes with inductive and capacitive ignition systems for a range of energy levels at ambient conditions. An automotive spark plug was used initially, although it was found that the growth rate of the electrode gap was too small to allow tests to be carried out in a reasonable amount of time. A rig was designed and developed to allow much thinner electrodes, of a less erosion resistant material, to be used in an inert environment. Two methods of erosion characterisation were investigated, the required voltage method and the gap growth method, which was measured using a shadowgraph. The required voltage method was found to be unreliable due to fluctuations caused by the non-repeatability of the discharge process.
The electrodes were eroded in an inert atmosphere, but it was found that a layer of oxide developed over time, and it was postulated that this could be caused by the porosity of the electrode material, which may contain small quantities of oxygen. These layers of oxide made measurements using the shadowgraph void. Tests were carried out with the two different ignition systems, but gap growth was slow and the results were inconclusive.

7.1.3 Flow rig testing

Spark discharges were subjected to pressurised flow fields to represent the conditions in an engine with an active combustion system. Results were obtained for different ignition systems, electrode configurations and orientations, and were considered qualitatively. It was found that the influence of the flow could shorten the duration of an inductive discharge by up to 75% due to the stretching of the discharge channel. The orientation of the plug was found to be important also and this effect was found to reduce the duration by up to 50% at the same mean

flow conditions. The results showed that electrode configuration was important. It was found that a surface discharge plug was able to sustain a discharge as long as a J type plug, orientated in a manner where the electrode was sheltered. It was argued that a shorter discharge could result in a reduced ignition probability. The effects of flow upon a capacitive discharge were found to be minimal since the discharge is very short in duration.

A model was developed, based upon the findings reported here and in the literature, and it was used to predict the electric field in the electrode gap of an automotive spark plug at any point in a glow discharge. Dividing the measured voltage by the predicted electric field enabled the discharge length to be calculated, and by calculating this at two points, a known time-step apart, the velocity of the flow field in the gap could be calculated. The pressurised flow rig was used to validate the model, and predictions of velocity were found to have an accuracy of better than 15% at elevated pressures. This model was used to predict the charge velocity in the Rover K4 engine during normal operation. Velocity measurements using this method were compared to experimental results, which had been carried out on a similar engine at another institution. The results were found to be similar.

The electric field was modelled by;

$$E = 396.480 \times I^{-0.415} \times P^{0.182}$$

where E is electric field in V/mm,
P is the absolute pressure in bar, and
I is the current in mA.

The velocity is calculated from;

$$u = \frac{\partial V / \partial t}{2E}$$

where u is the velocity in m/s,
t is the time in seconds.

7.1.4 Effects of ambient conditions upon the spark discharge process

Results have shown that increasing the gas (and electrode) temperature reduced the breakdown voltage, this is predominantly due to a reduction in density at a given pressure. The glow discharge mode (the longest part of the discharge) was found to be insensitive to increases in temperature, although for a given pressure, the mode is actually lengthened due to less of the available energy manifesting itself in the breakdown phase. Increasing the gas pressure leads to a higher breakdown voltage due to an increase in the density. This effect reduces the amount of energy available in the glow regime and hence shortens the spark duration. Increases in pressure have also been shown to result in a slightly higher voltage needed to sustain the glow discharge. It was shown that the use of argon and helium as the medium resulted in lower required breakdown voltages.

Paschen's law, a model for the breakdown voltage, was investigated and was found to be unsatisfactory for spark gaps larger than 0.5mm and temperatures higher than 20°C. A linear model was developed to include the effects of pressure, gap and temperature. This model was found to be accurate, for nickel electrode plugs in air, over the range tested, and was used to predict the electrode gaps of plugs where gap measurement was difficult. The model is shown below:

$$V = 4.3 + 136\frac{P}{T} + 324\frac{P}{T}d_g$$

where: V is the breakdown voltage in kV,
P is the absolute pressure in Bar,
T is the temperature in Kelvin, and
d_g is the electrode gap in mm.

7.2 Suggestions for further work

7.2.1 Erosion testing

This work has shown that bench testing for electrode erosion is very difficult. It is suggested that erosion testing is carried out using the ignition systems tested, but with a running engine. A CHP unit, or a gas engine undergoing endurance testing would be an ideal subject, since dedicated testing for erosion would lead to very high fuel costs and is hence discouraged.

7.2.2 Engine testing - Electrode orientation and electrode type

This study has been concerned with engine testing for ignition system suitability, and all engine tests were carried out using one spark plug, at one orientation. Daniels and Scilzo (1996) investigated electrode orientation effects on a running engine, although ignition parameters remained constant. It would be interesting to note the effects of orientation on erosion and the effects on combustion induced by ignition parameters.

7.2.3 Further velocity predictions in a running engine

Although the flow field velocity was predicted for a running engine, it was only undertaken at one ignition timing. An ignition timing sweep would allow the velocity through the plug gap to be predicted for the whole engine cycle whilst motoring. The limits for a firing engine would be the onset of knock, and the maximum retarded timing where combustion would still occur. However, for representative combustion to occur, the measurements will have to be taken very close to MBT timing, which is the period of most interest when considering conditions at or close to the point of ignition.

8. References and bibliography

Adler, J., *Laser ignition of a combustible gas: A composite layer steady-state model*, Presented at 24th symposium (Int.) on combustion, the combustion institute, 1992, pp 1769-1776

Amann, C.A., *Power to burn - a history of the spark ignition engine*, Mechanical Engineering, April 1990, pp 46 - 54

Anbarasu, M., Abata, D.L., *Sensitivity of pressure rise to spark energy and flame travel velocity in a spark ignition engine*, SAE paper 960071, 1996

Anderson, R.W., *The effect of ignition system power fast burn engine combustion*, SAE paper, 870549, 1987

Anderson, R.W., and Asik, J.R., *Ignite-ability experiments in a fast burn, lean burn engine*, SAE paper, 830477, 1983

Anderson, R.W., and Kim, J., *Spark anemometry of bulk gas velocity at the plug of a firing engine*, SAE paper, 952459, 1995

Annand, W.J.D., *The estimation of flame propagation rates in routine computer synthesis of spark-ignition engine combustion*, IMechE paper C48/83, 1983

Arcoumanis, C., *Personal communication*, 26th November 1997

Arcoumanis, C., and Bae, C.S., *Correlation between spark ignition characteristics and flame development in a constant volume combustion chamber*, SAE paper, 920413, SAE Trans., 1992, Vol. 101, pp 556-570

Arcoumanis, C., and Bae, C.S., *Visualisation of flow/flame interaction in a constant-volume combustion chamber*, SAE paper 930868, 1993

Arcoumanis, C., Gold, M.R., Whitelaw, J.H., Xu, H.M., *Mixture preparation in a Rover optical engine – progress presentation*, Imperial College Department of Mechanical Engineering, 22nd July 1997

Arkless, S., *Principles of racecar engineering - the design, manufacture and application of spark plugs for race engines*, Racecar Engineering, Vol. 2, No. 5, 1992, pp 70-71

Asik, J.R., and Bates, B.(1976), *The ferroresonant capacitor discharge ignition (FCDI) system - a multiple firing CD ignition with spark discharge sustaining between firings*, SAE paper, 760226, 1976

Asik, J.R., Piatkowski, P., Foucher, M.J., Rado, W.G., *Design of a plasma jet ignition system for automotive application*, SAE paper 770355, 1977

Ask, T.O., Almas, T., Valland, H., Paulsen, H., *Study of the initial flame growth in a spark ignition engine*, presented at Measurement and Observation Analysis of Combustion in Engines, IMechE, London, 22nd March 1994

Azzoni, P., Marseguerra, M., *Assesment of the potential of a Wiener-Hilbert filter for automatic diagnosis of spark ignition engine faults*, Mechanical Systems and Signal Processing (!995) **9**(2) 199-128, 1995

Ball, J.K., *Combustion Burn Rate Analysis User Manual*
Oxford Internal Combustion Engine Group, Dept. of Engineering Science, University of Oxford, 1997.

Bamsey, I. (ed.), *Champion - turbo lessons*, Racecar Engineering, Vol. 1, No. 3, 1991, p37

Barrie, C., *Spark plug control runs lean-burn engines smoothly*, Techscan, Motor Industry, The Engineer, 20th November 1986

Bell, A.G., (1993), *Four-stroke performance tuning*, Haynes, 1993

Bell, A.G., (1983), *Performance tuning in theory and practise - two-strokes*, Haynes, 1983

Black, R.L., *Comment*, 25th Champion Ignition and Engine performance conference, Dearborn Michigan, 1986

Blair, D.T.A., *Electrical breakdown in gases*, Meek, J.M. and Craggs, J.D. (eds.), John Wiley, New York, 1978, p. 533

Blauhaut, R.B., Horton, M.J., and Wilkinson, A.C.N., *A knock detection system using spark plug ionisation current*, IEE 4th ann. conf. automotive electronics, London, 1983

Borgato, A., Mauceri, A., Wilson, P.S., *Power semiconductor device technologies developed for automotive applications*, Presented at the IEE Sixth International Conference on Automotive Electronics, London, 12-15 October 1987

Bosch (1976), *Electronic battery ignition systems*, Technical Instruction, 1st Ed., Delta Press Ltd, 1976

Bosch (1985), *Spark plugs*, Technical Instruction, 1st Ed., Delta Press Ltd, 1985

Bosch (1987), *Battery ignition*, Technical Instruction, 1st Ed., Delta Press Ltd, 1987

Bosch (1988), *Automotive electric / electronic systems*, 1st Ed., Delta Press Ltd, 1988

Cetegen, B., Teichman, K.Y., Weinberg, F.J., Oppenheim, A.K., *Performance of a plasma jet igniter*, SAE paper 800042, 1980

Champion (1995a), *Personal communication - David Latham / Chris Middlemass*, Upton, Merseyside, 11th January 1994

Champion (1995b), *Presentation to British Gas*, Gas Research Centre, Loughborough, Leicester, 26th January 1994

Champion (1995c), *From racing to modern multivalve engines - evolutions of the ignition coils and spark plugs for high performance engines*, 2nd Int Seminar on High Performance Spark Ignition Engines for Passenger Cars, November 23-34, 1995

Champion, *Industrial spark plug application guide and service manual*, publication number 98036, Champion Spark Plug Co, Toledo, Ohio

Champion (1994), *Champion Spark Plug Catalogue 1994*, Champion Spark Plug Co., Upton, Merseyside.

Cherry, M.A., Morrisset, R.J., Beck, N.J., *Extending lean limit with mass-timed compression ignition using a catalytic plasma torch*, SAE paper 921556, 1992

Cho, Y.S., Santavicca, D.A., and Sonntag, R.M., *The effect of spark power on spark-ignited flame kernel growth*, SAE paper, 922168, presented at International Fuels and Lubricants Meeting and Exposition, San Francisco, CA, Oct. 19 -22, 1992

Cobine, J.D., *Gaseous conductors*, Dover Publications Inc, New York, Dover Edition, 1958

Collings, N., Dinsdale, S. and Hands, T., *Plug fouling investigations on a running engine - an application of a novel multi-purpose diagnostic system based on the spark plug*, SAE paper, 912318, presented at Fuels and lubricants meeting and exposition, Toronto, Canada, October 7th - 10th, 1991

Colvin, A.D., Gierczak, C.A., Siegl, W.O., Butler, J.W., *A software program for carrying out multi-purpose exhaust composition calculations*, SAE paper 970749, 1997

Crane, M.E., King, S.R., *Emission reductions through precombustion chamber design in a natural, lean burn gas engine*, ASME paper, Transactions of the ASME, Vol. 114, p466, July 1992

Curtess, A., *Lightning strikes twice*, The Works, Motor, July 9th, 1988

Dale, J.D., and Oppenheim, A.K. (1981), *Enhanced ignition for I.C. engines with premixed gases*, SAE paper, 810146, presented at the International congress and exposition, Detroit, Michigan, Feb. 23-27, 1981

Dale, J.D., Smy, P.R., Clements, R.M. (1978), *Laser ignited internal combustion engine - an experimental study*, SAE paper 780329, 1978

Daniels, C.F., Scilzo, B.M., *The effects of electrode design on mixture ignitability*, SAE paper 960606, 1996

Dawe, J.R., Smy, P.R., Haley, R.F., Dale, J.D., Bardon, M.F., and Gardiner, D.P., *Plasma jet ignition of methanol at sub-zero temperatures*, IMechE Proceedings, Part D, Journal of Automobile Engineering, 1994, Vol.
208, No. D3, pp153-159

Day, J., *Engines - the search for power*, Hamlyn, London, 1980

Dearden, J., *Spark gaps*, Wireless World, November 1980

Decker, H., *Evolution of ignition systems*, IMechE paper C217/85, 1985

Dellis, E.A., *Lean-burn ignition systems*, Automotive Engineering, Vol. 97, No. 2, February 1989

De Sote, G.C., *Propagation behaviour of spark ignited flames in early stages*, IMechE paper C59/83, 1983

D'Orsay, E., Guipaud, S., Ordines, J.P., *New components and recent developments in ignition systems*, Presented at the IEE Sixth International Conference on Automotive Electronics, London, 12-15 October 1987

Eureka, *Electronic gasket provides perfect spark*, Eureka on campus, Autumn 1993, Vol. 6, No. 1, p15

Fisher, P.D., Ridley, J.D., Pitt, P.L., and Clements, R.M., *An investigation of puff-jet ignition in an internal combustion engine fuelled by natural gas*, SAE paper, 860538, presented at the International Congress and Exposition, Detroit, Michigan, Feb. 24-28, 1986

Gallacher, G.J., *Laser ignition*, BEng final year project report, Department of Mechanical Engineering, Heriot-Watt University, Edinburgh, April 1991

George, M., *Electronic ignition*, Electronic Projects for the Car, pp69-75, Newnes Technical Books, 1979

Gidlow, M.L., Wilkinson, G.A., *Electronic ignition - a vehicle manufacturer's development and operating experience*, Presented at the IEE Sixth International Conference on Automotive Electronics, London, 12-15 October 1987

Granlund, O., *Comment - Champion Ignition Conference*, 25th Ignition and engine performance conference, Dearborn, Michigan, 1986

Hacohen, J., Belmont, M.R., Thurley, R.F.W., Thomas, J.C., Morris, E.L., and Buckingham, D.J., *Electrohydrodynamic ignition system for S.I. engines*, SAE paper, 922236, presented at International fuels and lubricants meeting and exposition, San Francisco, California, October 19th - 22nd, 1992

Hacohen, J., Belmont, M.R., Thurley, R.F.W., Thomas, J.C., Morris, E.L., and Buckingham, D.J., *Experimental and theoretical analysis of flame development and misfire phenomena in a spark ignition engine*, SAE paper 920415, 1992

Halldin, C., *Velocity and turbulence measurements close to a spark plug*, SAE paper, 920154, Presented at the International Congress and Exposition, Detroit, Michigan, Feb. 24-28, 1992

Han, S.B., Choi, K.H., Ra, S.O., Lee, S.J., Lee, J.T., *Ignitability and combustion characteristics of the multi spark capacitor discharge igniter for a lean burn engine*, SAE paper 952396, 1995

Hancock, M.S., Buckingham, D.J., Belmont, M.R., *The influence of arc parameters on combustion in a spark ignition engine*, SAE paper 860321, 1986

Harrington, J.A., Shishu, R.C., and Asik, J.R., *A study of ignition system effects on power, emissions, lean misfire limit, and EGR tolerance of a single-cylinder engine - multiple spark versus conventional single spark ignition*, SAE paper, 740188, 1974

Hart, W., *A versatile ignition module for automotive application*, Presented at the IEE Sixth International Conference on Automotive Electronics, London, 12-15 October 1987

Hattori, T., Goto, K., Ohigashi, S., *Study of spark ignition in flowing lean mixtures*, IMechE paper C101/79, 1979

Hawdel, S., *A dictionary of electronics*, Penguin, 1967

Herweg, R., Begleris, P.H., Zettlitz, A., Ziegler, G.F.W., *Flow field effects on flame kernel formation in a spark ignition engine*, SAE paper 881639, 1988

Heywood, J.B., *Internal combustion engine fundamentals*, McGraw Hill, 1988

Hickling, R., Smith, W.R., *Combustion bomb tests of laser ignition*, SAE paper 740114, 1974

Hills, P.C., Zhang, D.K., Samson, P.J., and Wall, T.F., *Laser ignition of combustible gases by radiative heating of small particles*, Combustion and flame, 91, pp 399 - 412, 1992

Ho, C.M., Santavicca, D.A., *Turbulence effects on early flame kernel growth*, SAE paper 872100, 1987

Holmes, M., *Adaptive ignition control*, Presented at the IEE Sixth International Conference on Automotive Electronics, London, 12-15 October 1987

Hood, S., *The V grooved electrode spark plug*, SAE paper, 901535, 1990

Hori, O., and Nishizawa, K., *An analysis on the voltage requirement of spark plug and its effect on electro-magnetic interference*, JSAE Review, July 1981

Horie, K., and Nishizawa, K., *Development of a high fuel economy and high performance four-valve lean burn engine*, IMechE paper C448/014, 1992

Houston, B., *Improving cold-start, overrun and engine efficiency with multiple spark ignition*, Automotive Engineer, April/May 1994

Howson, P. A.,(1992) *Bulk photoconductive high voltage switching techniques*, Phd Thesis, Power Engineering Research Unit, Department of Electrical and Electronic Engineering, University of Brighton, September 1992

Howson, P., DeWit, D.,(1990a) *Distributorless ignition system*, Patent Specification, CSPESA CASE No 170, No 9014561.6, June 29, 1990

Howson, P.A., Miller, R., Ryder, D.M.,(1990b) *Photoconductive switch design and applications*, IEEE paper, presented at IEEE International Symposium on Electrical Insulation, Toronto, Canada, June 3-6, 1990

Howson, P.A., Zhang, Y., Miller, R., Ryder, D.M.,(1990c) *Fundamental design of power photoconductive switches*, Presented at UPEC 90, 1990

Howson, P.A., Miller, R., Black, I.A., Ryder, D.M.,(1989) *Bulk photoconductive high voltage switching techniques*, Presented at UPEC 89, 1989

Howson, P.A., Vu, N.T., Miller, R., Lazzerrini, F., Rajkovic, M.,(1991) *A novel distributorless variable spark energy I.C. engine ignition system*, Presented at the 8th International Conference on Automotive Electronics, 28-31 October 1991

Igashira, T., Kawai, H., Yoshinaga, T., Nakamura, N., *Evaluation of a spark plug by the pre-ignition simulator*, SAE paper 880692, 1988

Jacoel, R., Maioglio, M., *Evolution of electronic ignition on motor cars*, IMechE paper C167/78, 1978

Johansson, B., *Influence of the velocity near the spark plug on early flame development*, SAE paper 930481, 1993

Jost, K., *The continuing evolution of the spark plug*, pp 72-77, Automotive Engineering, Vol. 104, No. 2, February 1996

Junichi, K., Kato, H., *Development of small spark plug (M8x1)*, SAE paper 891760, 1989

Kagawa, J., and Kato, H., *Development of a small spark plug (M8x1)*, SAE paper, 891760, Presented at the small engine technology conference, Milwaukee, Wisconsin, Sept. 11-13, 1989

Kalghatgi, G.T., *Improvement in the ignition ability of glow discharges brought about by deposits of potassium sulphate on the electrodes*, IMechE paper, C50/88, 1988

Karim, G.A., *The dual fuel engine of the compression ignition type - prospects, problems and solutions - a review*, SAE paper, 831073, 1983

Kennedy, R., *The book of the motor car*, Caxton, London, 1913

Khassaf, F.H., *Cyclic dispersion in gas engines*, Ph.D. Thesis, 1972, Department of Mechanical Engineering, UMIST

Kim, J., Anderson, R.W., *Spark anemometry of bulk gas velocity at the plug gap of a firing engine*, SAE Paper No., 952429, 1995

Kingston Jones, M.G. and Heaton, D.H., *Nebula combustion system for lean burn spark ignited gas engines*, SAE paper, 890211, 1989

Klimstra, J., and Overmars, F., *Monitoring the spark-plug gap of natural-gas-fuelled stationary engines*, SAE paper, 912361, 1991

Ko, Y., Anderson, R.W., *Electrode heat transfer during spark ignition*, SAE paper 892083, 1989

Kono, M., Niu, K., Tsukamoto, T., Ujiie, Y. (1988), *Mechanism of flame kernel formation produced by short duration sparks*, presented at 22nd Symposium (International) on Combustion, The Combustion Institute, 1988, pp1643-1649

Kono, M., Hatori, K., Hnuma, K., *Investigation of ignition ability of composite sparks in flowing mixtures*, presented at 20th Symposium (International) on Combustion, The Combustion Institute, 1984, pp133-140

Kravchik, T., Sher, E., *Numerical modelling of spark ignition and flame initiation in a quiescent methane-air mixture*, Combustion and Flame 99:635-643, 1994

Krylov, O.V., Mamedov, A. Kh., and Mirzabekova, *Catalytic oxidation of hydrocarbons and alcohols by carbon dioxide on oxide catalysts*, Industrial engineering chemistry research, Vol. 34, 1995, pp 474-482

Kuo, K.K., *Principles of combustion*, John Wiley and Sons Inc., New York, 1986

Kupe, J., Wilhemi, H. and Adams, W., *Operational characteristics of a lean burn SI-engine: comparison between plasma-jet and conventional ignition system*, SAE paper, 870608, 1987

Kuroda, H., Nakajima, Y., Sugihara, K., Takagi, Y., and Muranaka, S., *The fast burn with heavy EGR, new approach for low NOx and improved fuel economy*, SAE paper, 780006, 1976

Lenk, M., Podiak, R.S., *Copper cored ground electrode spark plug design*, SAE paper, 881777, 1977

Lentz, L.R., Miller, R.D., Cadmus, T.E., *Trends in the design and performance of spark plugs as related to engine exhaust emissions*, IMechE paper C89/72, 1972

Lewis, B. and Von Elbe, G., *Combustion, flames and explosions of gases*, Academic press, New York, 1961

Lichty, L.C., *Combustion engine processes*, McGraw Hill, 1967

Longstaff, K., *Ignition and timing systems*, Presented at the IEE Sixth International Conference on Automotive Electronics, London, 12-15 October 1987

Lord, D.L., Anderson, R.W., Brehob, D.D., Kim, Y., *The effects of charge motion on early flame kernel development*, SAE paper 930463

Lucas, D., Cavolowsky, J.A., Breber, P.R., Oppenheim, A.K., *Pulsed plasma jet igniters: species measurements in methane combustion*, presented at 22nd Symposium (International) on Combustion, The Combustion Institute, 1988, pp 1661-1667

Lynch, D., Smith, W.J., *Comparison of AFR calculation methods using gas analysis and mass flow measurement*, SAE paper 971013, 1997

Magnetti Marelli, *Plug top type ignition coil - BAE 700*, Technical data sheet

Maly, R., and Vogel, M., (1978) *Initiation and propagation of flame fronts in lean CH_4 - air mixtures by the three modes of the ignition spark*, 17th symposium (international) on combustion, 1978

Maly, R., Meinel, H., and Wagner, E., (1983a) *Novel method for determining general flow parameters from conventional spark discharges*, IMechE paper, Presented at combustion in engines conference, 11th - 14th April, 1983

Maly, R., (1984) *Spark ignition - its physics and effect on the internal combustion engine*, Chapter 3, Fuel economy: road vehicles powered by spark ignition engines, Hilliard, J.C. and Springer, G.S. (Eds.), Plenum press, 1984

Manger, H., *Development trends for battery ignition systems*, International Conference on Automobile Electronics, 6-9 July 1976

Mantel, T., *Three dimensional study of flame kernel formation around a spark plug*, SAE paper 920587, 1992

Markus, J., *Sourcebook of electronic circuits*, Chapter 7, pp65-71, McGraw-Hill, 1968

Mavinahally, N.S., Assanis, D.N., Govinda Mallan, K.R., Gopalakrishnan, K.V., *Torch ignition: ideal for lean burn premixed charge engines*, Transactions of the ASME, Vol. 116, p794, October 1994

Maxson, J.A., Oppenheim, A.K., *Pulsed jet combustion - key to a refinement of the stratified charge concept*, Presented at 23rd symposium (Int.) on combustion, the combustion institute, 1990, pp 1041-1046

Mears, T. and Oxley, S.J. (1989), *An advanced racing ignition system*, IMechE paper C391/062, Proc. IMechE, presented at the seventh international conference on automotive electronics, 9-13th Oct. 1989, Olympia, London

Meyer, R.C., Meyers, D.P., King, S.R., and Liss, W.E. (1992), *Effects of spark plug number and location in natural gas engines*, Journal of Engineering for Gas Turbines and Power, Transactions of the ASME, July 1992, Vol. 114, pp475-479

Meyer, R., Kubesh, J.T., and Shahed, S.M. (1993), *Simultaneous application of optical spark plug probe and head gasket ionisation probe to a production engine*, SAE paper, 930464, Presented at International congress and exposition, Detroit, Michigan, March 1st - 5th, 1993

Miyata, S., Ito, Y., and Shimasaki, Y., *Flame ion density measurement using spark plug voltage analysis*, SAE paper, 930462, Presented at International congress and exposition, Detroit, Michigan, March 1st - 5th, 1993

Modian, R.M., Checkel, M.D., and Dale, J.D., *The effect of enhanced ignition systems on early flame development in quiescent and turbulent conditions*, SAE paper, 910564, presented at the International congress and exposition, Detroit, Michigan, Feb. 25 - Mar 1, 1991

Mogi, K., Ohno, E. and Nakamura, N., *Spark plug fouling: behaviour and countermeasure*, SAE paper, 922093, presented at World-wide passenger car conference and exposition, Dearborn, Michigan, September 28th - October 1st, 1992

Nakai, M., Nakagawa, Y., Hamai, K., and Sone, M., *Stabilised combustion in a spark ignited engine through a long spark duration*, SAE paper, 850075, 1975

Nakamura, N., Baika, T., and Shibata, Y., *Multipoint spark ignition for lean combustion*, SAE paper, 852092, 1985

NGK, *Engineering manual for spark plugs*, NGK Spark Plug Co. Ltd, OP-0076-9105

NGK, *NGK Spark Plugs 1991-1992*, OP-0071-9102, NGK Spark Plug Co. Ltd., Nagoya, Japan

Nishio, K., Oshima, T., and Ogura, H., *A study on spark plug electrode shape*, Int. J. of Vehicle Design, Vol. 15, Nos. 1/2, pp. 119-130, 1993

Nishio, K., Suzuki, T., Sugino, K., *Study on spark discharge current for noise suppression*, JSAE Review, July 1981

Nishio, K., Yoshida, M., *Suppression methods of radio frequency interference for motorcycles*, IMechE paper C143/78, 1978

Ofurum, A.U., *The assessment of the effect of a spark enhancement unit on petrol engine performance*, Final year project report, Department of Mechanical Engineering, UMIST, June 1993

Ohanian, H.C., *Physics*, 2nd Edition
Norton, 1989

Oppenheim, A.K., *Quest for controlled combustion engines*, SAE paper 880572, 1988

Padgitt, K.W., *Distributorless electronic ignition timing*, Presented at the IEE Sixth International Conference on Automotive Electronics, London, 12-15 October 1987

Pashley, N.C (1996)., *Ignition systems for lean burn gas engines - Ignition HT current measuring systems - A critical study*, Internal report, Department of Engineering Science, University of Oxford, 20th March 1996

Pashley, N.C (1997)., *On-engine testing with the Rover K4 engine - A study to maximise repeatability*, Internal report, Department of Engineering Science, University of Oxford, 22nd July 1997

Pearson (a), *Wide band current monitors, high voltage pulse transformers, capacitive voltage dividers*
Pearson electronics, Inc.

Pearson (b), *Application notes for current monitors manufactured by Pearson electronics, Inc.*
Pearson electronics, Inc.

Pearson (1991), *Selecting a Pearson current monitor.*
Pearson electronics, Inc., 1991

Pearson (1994), *Standard current monitors.*
Pearson electronics, Inc., 1994

Performance Tuning, *Hot stuff*, Performance tuning, Jan 1989, pp40-41

Pickworth, G., *The spark that gave radio to the world*, Electronics and Wireless World, November 1993

Pischinger, S., and Heywood, J.B. (1988), *A study of flame development and engine performance with breakdown ignition systems in a visualisation engine*, SAE paper, 880518, presented at International Congress and Exposition, Detroit, Feb. 29th - March 4th, 1988

Pischinger S., and Heywood, J.B. (1990a), *How heat losses to the spark plug electrodes affect early flame kernel development in an SI engine*, SAE paper, 900021, 1990

Pischinger S., and Heywood, J.B. (1990b), *A model for flame kernel development in an SI engine*, The combustion institute, 1990

Quarrell, A.P., *An outline history of the oil engine and its lubrication*, Shell, 1961

Ricardo, H.R. and Glyde, H.S., *The high-speed internal-combustion engine*, Blackie and Son Ltd., 1941

Richiardi, P., *A leaner, cleaner engine*, University of Melbourne Gazette, p21, April 1994

Robson, J.V.B., *Meeting the spark plug requirements of European engines*, Proc. IMechE, Vol. 182, Part 2A, No. 1, 1967-1968

Ryu, H., Chtsu, A., Asanuma, T., *Effect of torch direction on combustion and performance of a prechamber spark ignition engine*, SAE paper 870167, 1987

SAAB, *Press information - SAAB's new ignition system ready for series production*, Press and public relations dept, SAAB GB ltd, Bucks, 1988

SAE (1995), *Ignition system measurements procedure*, SAE J973a, March 1995
SAE Recommended practice, 1996 SAE Handbook

SAE, *Ignition system nomenclature and terminology*, SAE J139 JUN90
SAE recommended practice.

Sakurai, T., Iko, M., Okamoto, K., and Shoji, F., *Basic research on combustion chambers for lean burn gas engines*, SAE paper, 932710, 1993

Salvat, O.P., Checng, A.S., Cheng, W.K., Heywood, J.B., *Flame shape determination using an optical-fibre spark plug and a head-gasket ionization probe*, SAE paper 941987, 1994

Schmieder, R.W., *Laser spark ignition and extinction of a methane-air diffusion flame*, American Institute of Physics, J.Appl.Phys. 52(4), April 1981

Schroeder, C., *Advanced techniques for performance measurements and computer simulations of racing ignition systems*, SAE paper 962549, 1996

Schwarz, H.(1979), *Ignition systems for lean burn engines*, IMechE paper C95/79, 1979

Schwarz, H.(1987), *Features and facilities of a digital electronic spark advance system and its advantages compared with mechanical systems*, Presented at the IEE Sixth International Conference on Automotive Electronics, London, 12-15 October 1987

Setright, L.J.K., *Electrical and ignition systems*, Anatomy of the motor car, Ward, I. (Ed.), MacDonald and Co., London, 1988

Seymour, J., *Physical electronics*
Pitman 1972

Shen, H., Jiang, D., *Investigation on the flame initiation and early development in a spark ignition engine*, SAE paper 922239, 1992

Sher, E., Keck, J.C., (1986), *Spark ignition of combustible gas mixtures*, Combustion and Flame 66: 17-25, 1986

Sher, E., Heywood, J.B. and Hacohen, J. (1991), *Heat transfer to the electrodes a possible explanation of misfire in SI engines*, Short communication, Combustion science and technology, Vol. 83, pp.323-325, 1991

Sher, E., Ben-Ya'ish, J., Pokryvailo, A., and Spector, Y. (1992), *A corona spark plug system for spark-ignition engines*, SAE paper, 920810, Presented at International congress and exposition, Detroit, Michigan, Feb. 24th - 28th, 1992

Sher, E., Ben-Ya'ish, J., Kravchik, T., *On the birth of spark channels*, Combustion and Flame, 89:186-194 (1992), 1992

Shimasaki, Y., Kanehiro, M., Baba, S., Maruyama, S., Hisaki, T., and Miyata, S., *Spark plug voltage analysis for monitoring combustion in an internal combustion engine*, SAE paper, 930461, Presented at International congress and exposition, Detroit, Michigan, March 1st - 5th, 1993

Silvis, W.M., *An algorithm for calculating the air-fuel ratio from exhaust emissions*, SAE paper 970514, 1997

Sloane, T.M., *Numerical simulation of electric spark ignition in methane-air mixtures at pressures above one atmosphere*, Combustion Sci. and Tech., 1992, Vol. 86, pp 121-133, 1992

Smy, P.R., Clements, R.M., Dale, J.D., Simeoni, D. and Topham, D.R. (1983), *Efficiency and erosion characteristics of plasma jet igniters*, J. Phys., D:Appl.Phys., Vol. 16, pp783 - 791, 1983

Snyder, W.E., Dexter, S.G., *Looking into a lean burn spark ignited gas engine*, Fuel Injection and Combustion, presented at 13th Annual Energy Sources Technology Conference and Exhibition, New Orleans, Louisinia, January 14-18, 1990

Stone, C.R., *Introduction to internal combustion engines*, second edition, Macmillan Press Ltd, 1994

Stone, C.R., and Steele, A.B., *Measurement and modelling of ignition system energy and its effect on engine performance*, Proc. IMechE, Vol. 203, Part D, 1989, pp 277-286

Taylor, C.F., *The internal combustion engine in theory and practice*, Volume 2, MIT press, 1985

Teasel, R.C. and Miller, R.D. (1967), *Characteristics of new ignition systems to improve engine performance*, Proc. IMechE, Vol. 182, Part 2A, No.1, 1967-1968

Teets, R.E., and Sell, J.A., *Calorimetry of ignition sparks*, SAE paper, 880204, Presented at International congress and exposition, Detroit, Michigan, Feb. 29th - March 4th, 1988

Tektronix, *AM503 current measurement systems*.
Tektronix, Inc., 5/94 WSS 10M 51W-7955-2

Tozzi, L. and Dabora, E.K. (1982), *Plasma jet ignition in a lean-burn CFR engine*, Nineteenth symposium (International) on combustion, The combustion institute, Pittsburgh, pp. 1467-1474, 1982

Tranter, T., *Motorcycle electrical manual*, 2nd Ed., Haynes Publishing, 1993

Ujiie, Y., *Spark ignition properties of combustible mixtures under high-turbulence-intensity conditions*, JSME Int. Journal, Series B, Vol. 37, No. 3, 1994, pp 611 - 617

VanDuyne, E., Porreca, P., *Performance improvement from dual energy ignition on a methanol injected cosworth engine*, SAE paper 940150, 1994

Walker, D., *Bright spark*, Cars and Car Conversions, February 1995, pp 14 - 19

Warburton, A., *Acquisition and analysis of hot wire anemometer data from the combustion chamber of a motored single cylinder research engine*, IMechE paper C78/83, 1983

Ward, M.A.V.(1989), *A new spark ignition system for lean mixtures based on a new approach to spark ignition*, SAE paper 890475, 1989

Ward, M.A.V.(1986), *Science and technology - the spark plug that could save forests*, The Economist, July 5th, 1986

Watkinson, J.R., *Electronic ignition techniques - current methods applied to engines*, pp216-219, Wireless World, July 1974

Wattam, M., Sinah, S.K., and Johnson, D., *Operating experience and design process cooperate in the RK270 spark ignition engine development*, IMechE paper, presented at Gas engines for co-generation seminar, London, 17th June 1993

Weber (1994), *Personal communication - Paul Birch*, Weber Concessionaires, Sunbury, 8th November 1994

Weinberg, F.J. (ed.) (1986), *Advanced combustion methods*, Academic press, 1986

Weinberg, F.J.(1971), *A preliminary investigation of the use of focussed laser beams for minimum ignition energy studies*, Proc. Roy. Soc. Lond., A.321, 41-52, 1971

Weyl, N., *The effect of pressure and flow on spark plug discharge*, Internal project report, Department of Manufacturing and Engineering Systems, Brunel University, 1993

Werson, M.J., Stafford, E.M., *Self-adaptive ignition timing system*, Presented at the IEE Sixth International Conference on Automotive Electronics, London, 12-15 October 1987

Willi, M.L., *Design and development of a direct injected, glow plug ignition assisted natural gas engine*, Journal of Engineering for Gas Turbines and Power, Transactions of the ASME, Vol. 117, p799, October 1995

Wilkinson, B., *Electronic Ignition system*, Electronics Today International, p10, April 1975

Yo, A.H., Moynihan, A., *A distributorless engine management system*, Presented at the IEE Sixth International Conference on Automotive Electronics, London, 12-15 October 1987

Yosesefi, D., Belmont, M.R., Thurley, R., Thomas, J.C., Hacohen, J., *A coupled experimental-theoretical model of flame kernel development in a spark ignition engine*, SAE paper 932716, 1993

Young, C., *Penguin dictionary of electronics*
Penguin, 1979

Young, C.T., and Grimes, D.A., *Erosion mechanisms of automotive spark plug electrodes*, SAE paper, 780330, Presented at International Congress and Exposition, Detroit, Michigan, Feb 27th - Mar 3rd, 1978

Zeigler G. F. W., Schaudt, Herweg (1986), *Influence of spark plug orientation on flame kernel formation in flowing mixtures*, SAE paper, 860531, Presented at FISITA, 1986

Ziegler, G. F. W., Maly R. R., Wagner, E. P. (1983), *Effect of ignition system design on flammability requirements in ultra lean turbulent mixtures*, IMechE paper, Presented at combustion in engines conference, 11th - 14th April, 1983

Ziel, A., Solid state physical electronics
Macmillan, 1958

Zytec (1994), *Personal communication - Andrew Todd*, Zytec Racing, Birmingham, 9th November 1994

Appendix A Equivalent circuit for automotive ignition system

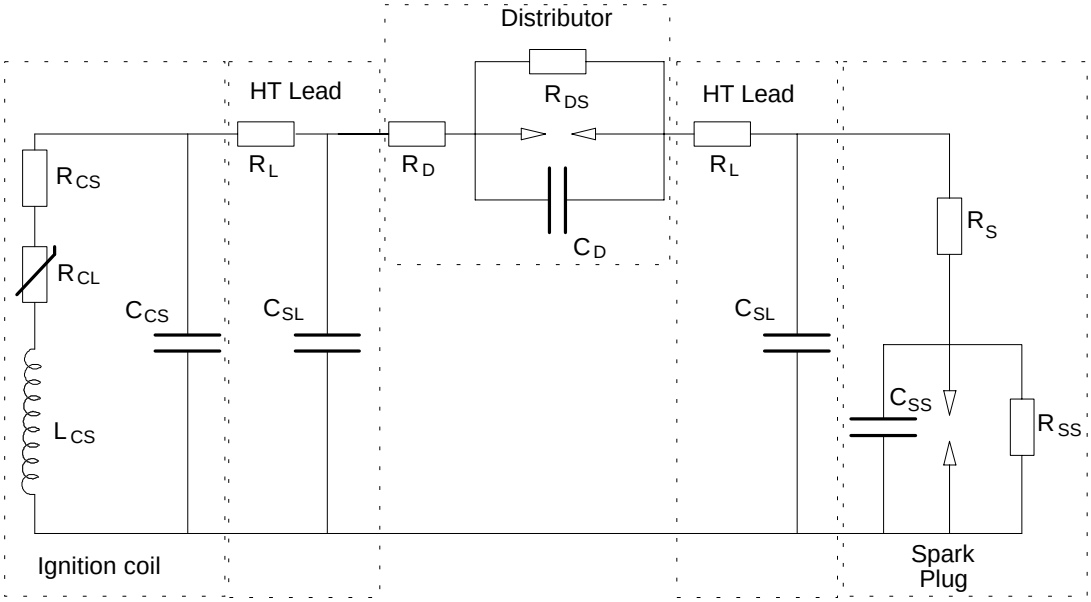

Figure A.1 Equivalent circuit

Script	Subscript	
C	CS	Capacitance of coil secondary
C	D	Capacitance of distributor
C	SL	Stray capacitance of HT lead
C	SS	Stray capacitance of spark plug
L	CS	Inductance of coil secondary
R	CS	Resistance of coil secondary
R	CL	Equivalent resistance of coil losses
R	D	Resistance of distributor
R	DS	Shunt resistance of distributor
R	L	Resistance of HT lead
R	S	Resistance of spark plug
R	SS	Shunt resistance of spark plug

Table A.1 Key to equivalent circuit

Appendix B Current measuring system specifications

Property	**Resistor RS 100Ω**	**Tektronix TM502A**	**Pearson 410**	**Pearson 411**	**Pearson 4100**
Output V/A	1/R	1mA - 5A per div	0.1	0.1	1
Max I	*	50A	5000	5000	5000
Droop (%/μsec)	None	None	0.06	0.0009	0.09
Risetime (ns)	*	7	10	20	20
Low (Hz)	*	DC	120	1	140
High (MHz)	*	50	20	20	35
Cost (£)	0.05	2825	600	600	600

Table B.1 Current measuring specifications

*] Oscilloscope dependent

Appendix C Ignition system specifications

Engine testing

Type	:	TCI
Manufacturer	:	
Switch	:	Bosch
Coil	:	Nippondenso
Model number	:	
Switch	:	0 227 100 118
Coil	:	5-029700-745
Triggering	:	Falling edge of TTL pulse
Coil specs :		
Primary resistance	:	0.8Ω
Primary inductance	:	6.246mH
Secondary resistance	:	9140Ω
Secondary inductance	:	48.3H

Rig testing

TCI system

Manufacturer	:	
Switch	:	Bosch
Coil	:	Bosch
Model number	:	
Switch	:	1 227 022 008
Coil	:	1 227 020 009
Triggering	:	Falling edge of TTL pulse
Coil specs :		
Primary resistance	:	0.9Ω
Primary inductance	:	3.82mH
Secondary resistance	:	8040Ω
Secondary inductance	:	28.5H

CDI system

Manufacturer	:	Bosch
Model number	:	
CDS unit	:	0 227 300 004
Transformer	:	0 221 121 001
Triggering	:	Falling edge going negative (see figs D.1 and D.2)
Transformer specs :		
Primary resistance	:	0.6Ω
Primary inductance	:	165.7µH
Secondary resistance	:	665Ω
Secondary inductance	:	923.4mH

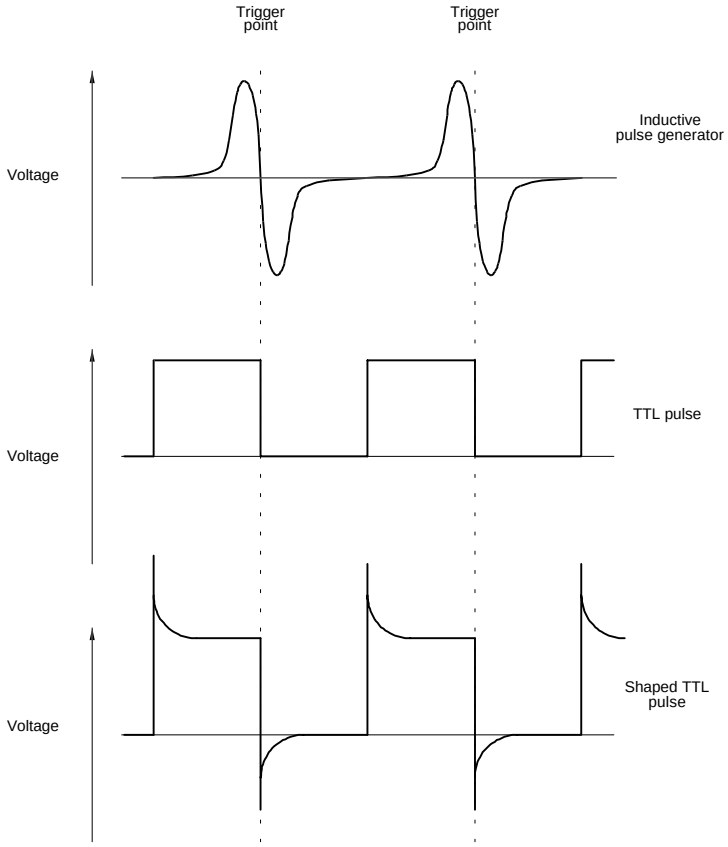

Figure C.1 Pulse signals used for ignition triggering

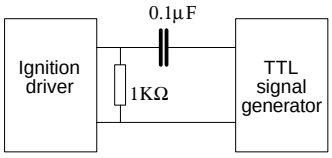

Figure C.2 Additional circuitry for pulse shaping

Appendix D Additional results with discussion (chapter 3)

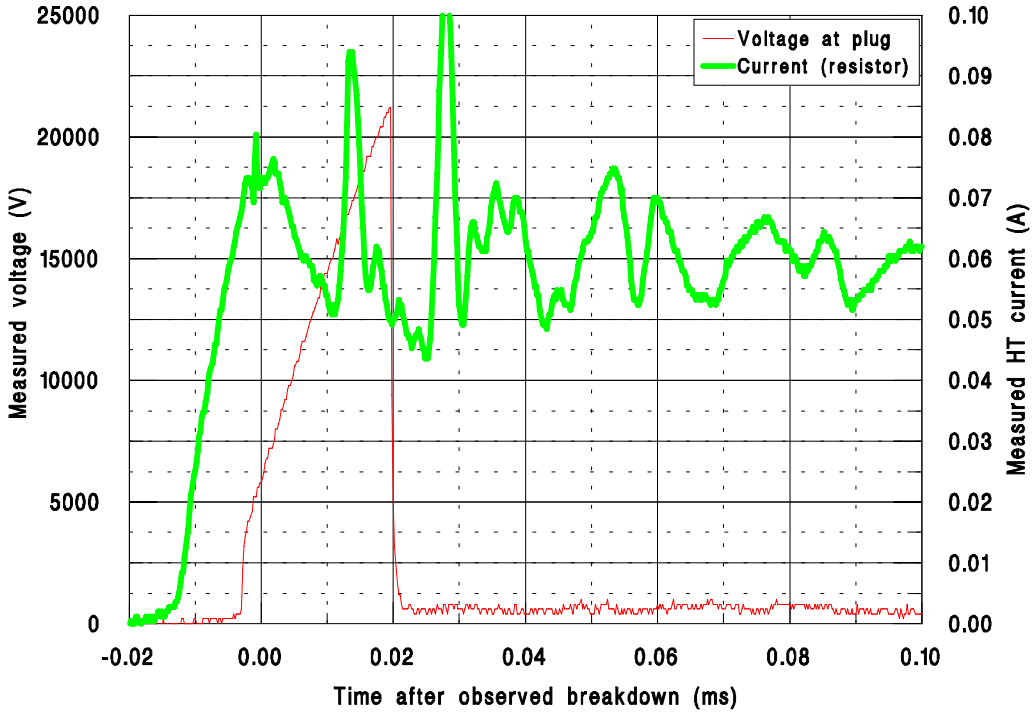

Figure D.1 Measured voltage and current events for early stages of single discharge

The figure shows the effect of measuring the current close to the coil and the voltage at the spark plug. In reality, the current rises rapidly as breakdown occurs, the voltage results therefore lag the measured current by over 30 µs. The lagging is caused by the capacitance effects of the ignition lead and the effects of a series gap, i.e. the distributor, which needs to be broken down before current can reach the plug gap. When the capacitance has been charged to a voltage which is high enough to ionise the gas in the spark plug gap, the stored energy discharges through the plug inducing momentarily high currents. The rise in current is too fast for the current measuring equipment to catch at the sampling rate used.

When calculating energy in the spark discharge, it is very important to measure the voltage and current as close to each other as possible. It is also important to measure the voltage as close to the electrodes as possible to eliminate the inclusion of losses in the HT lead.

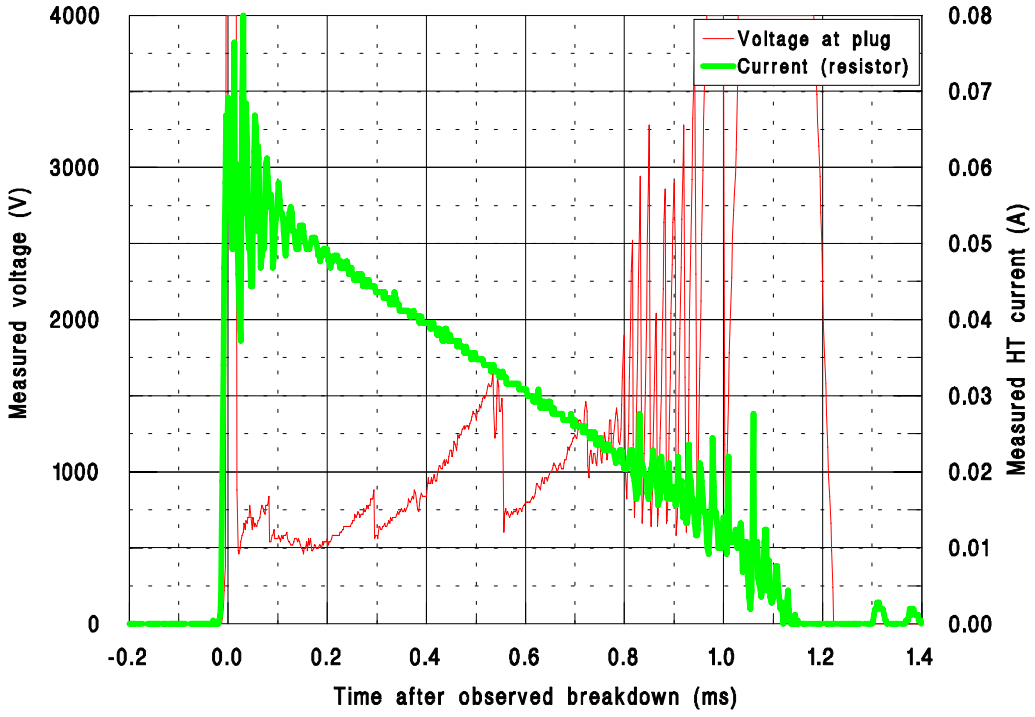

Figure D.2 Measured voltage and current events for complete duration of single discharge

The active combustion chamber of the Rover engine is characterised by the restriking effects during the glow discharge, this is an effect of the arc being stretched and blown away.

The velocity of the bulk gas flow could be inferred from the gradient of the voltage waveforms and perhaps the number of re-strikes (Anderson and Kim 1995, Maly et al. 1983, Weyl, 1993).

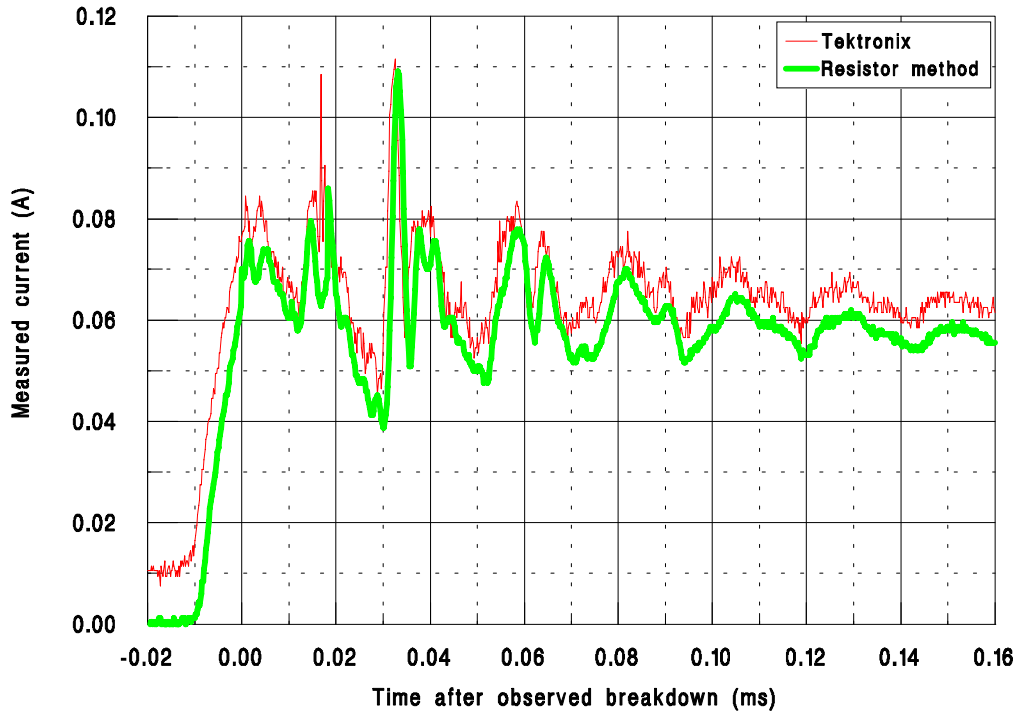

Figure D.3 Comparison of current measuring performance between Tektronix and resistor method for early stages of single discharge

The Tektronix TM502A current probe is noticeably noisier than the resistor method although these effects will not be significant when integrating over the discharge to calculate energy dissipation. The Tektronix suffers from a DC offset, although still following the trend of the resistive method.

The DC offset could be corrected in software by zeroing the current at the start of the discharge, although it is uncertain if the DC offset varies during the discharge.

The increased noise is due to the low volts/division that the system uses on the scope for impedance matching.

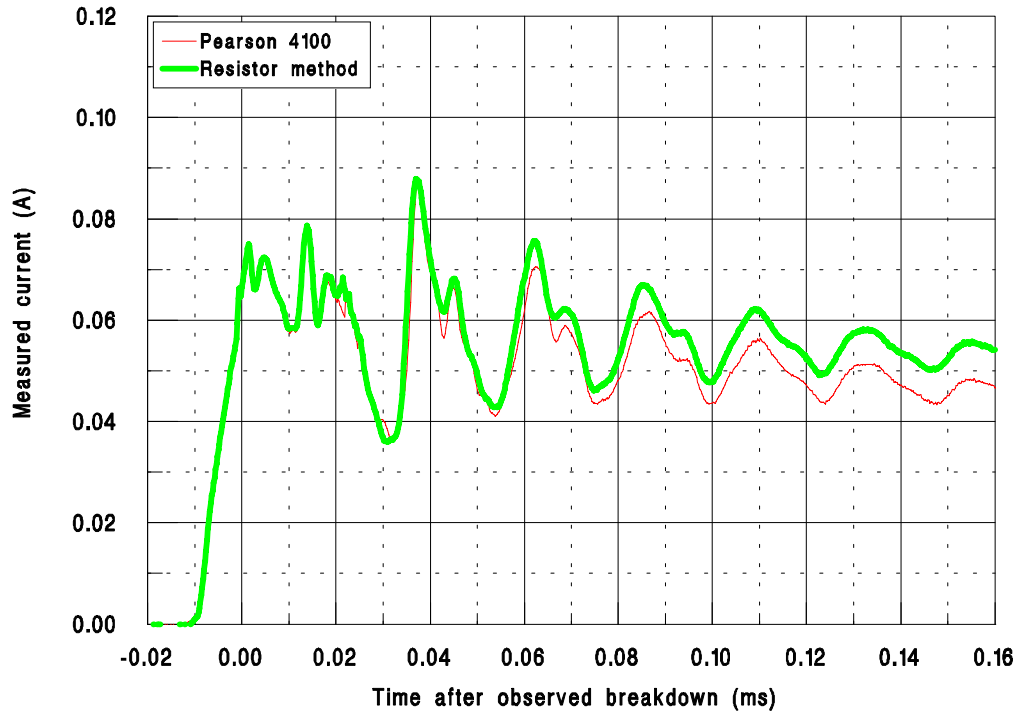

Figure D.4 Comparison of current measuring performance between Pearson 410 and resistor method for early stages of single discharge

During the early period of the discharge, the Pearson 4100 follows the resistor characteristic. Although as the discharge time increases, the Pearson output begins to fall away from that of the resistor. This is a consequence of the droop characteristic of the transducer and is linked to the useable frequency range. Electrical noise is low due to the high gain of the transformer.

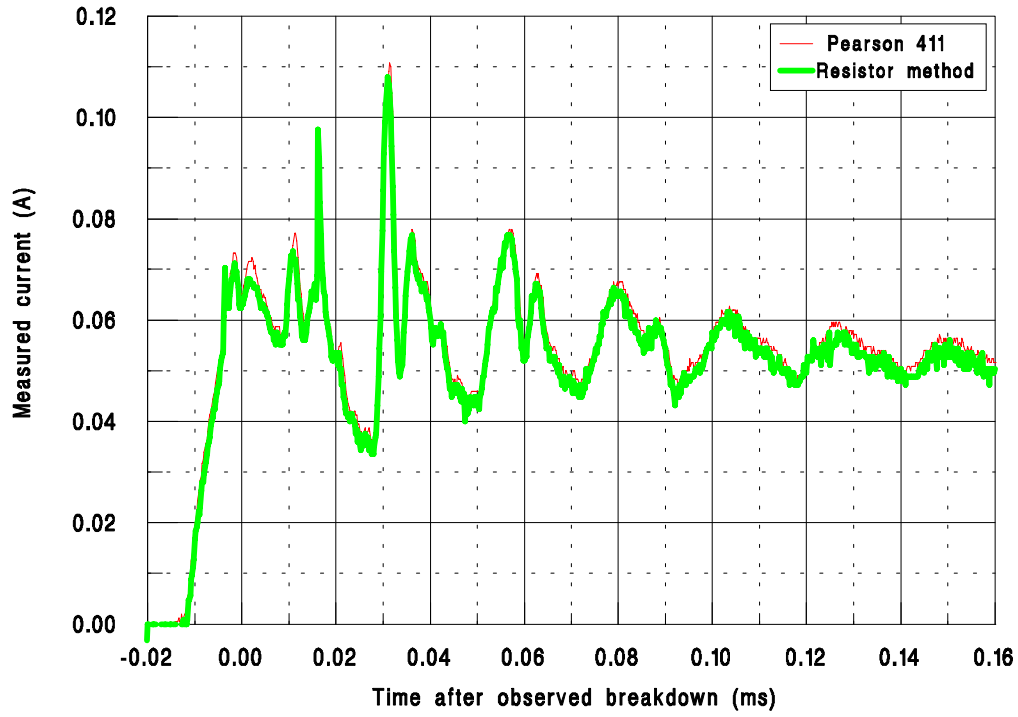

Figure D.5 Comparison of current measuring performance between Pearson 411 and resistor method for early stages of single discharge

The Pearson 411 transformer gives results very similar to those obtained by the resistor method although the lower gain (0.1V per amp) renders the device susceptible to noise.

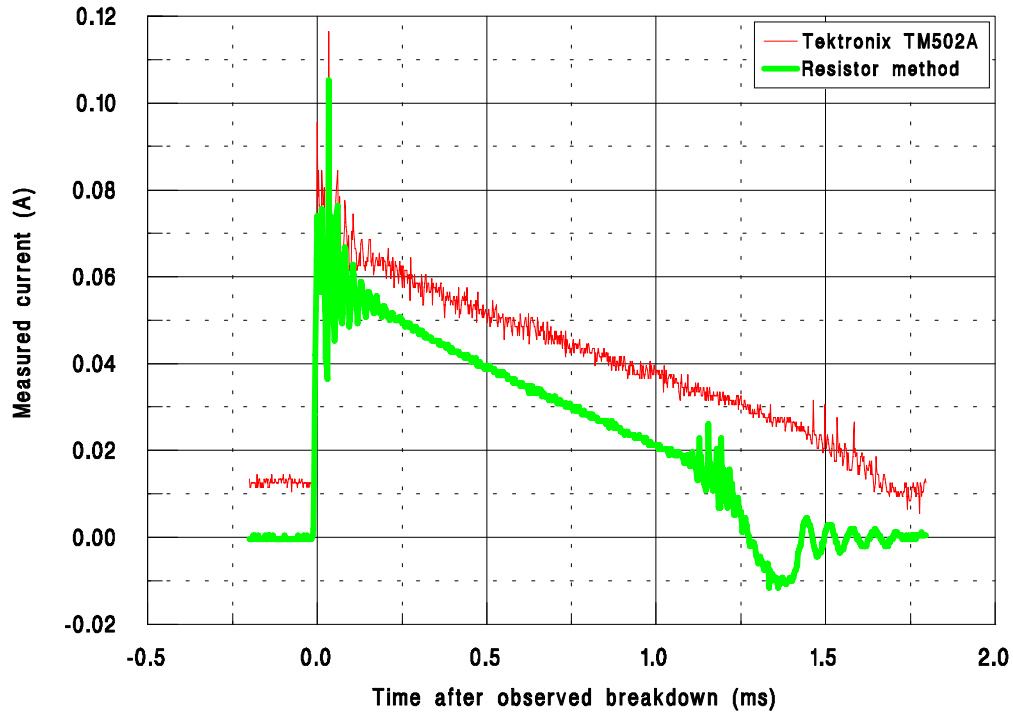

Figure D.6 Comparison of current measuring performance between Tektronix TM502A and resistor method for complete single discharge

The Tektronix system exhibits a DC offset and higher noise when compared to the resistor method. The ringing at the end of the resistor characteristic does not seem to be duplicated by the Tektronix even though both sets of results are from the same discharge. When viewing the traces on the oscilloscope screen, the Tektronix normally shows good correlation with the resistor although there is an evident DC offset problem for some discharges.

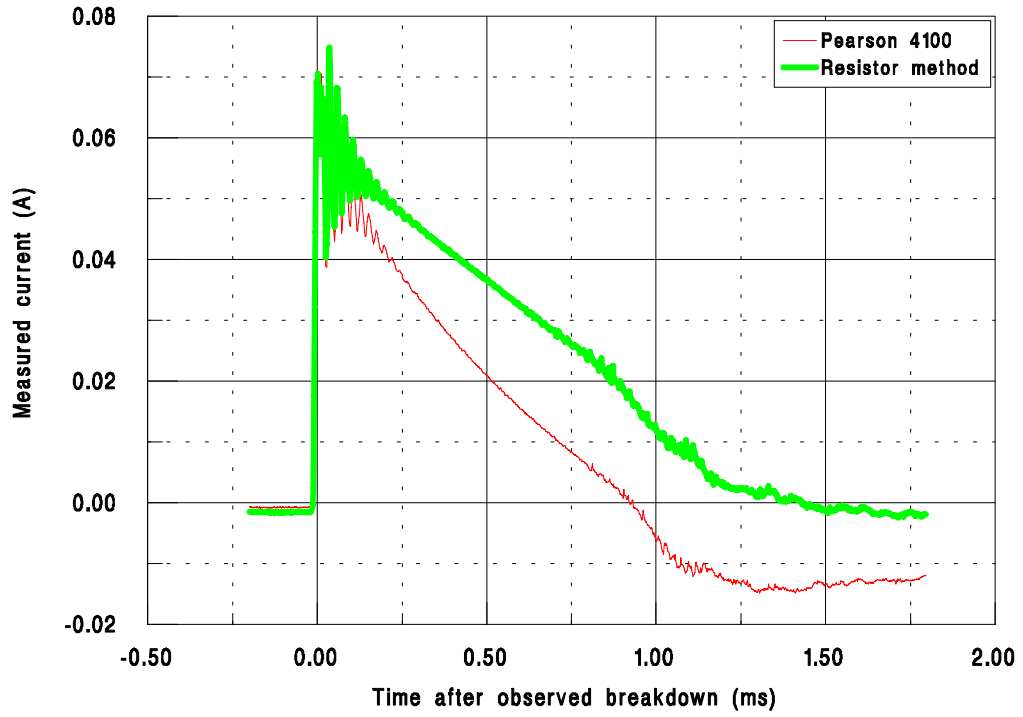

Figure D.7 Comparison of current measuring performance between Pearson 4100 and resistor method for complete single discharge

The Pearson 4100 can be seen to fall much more rapidly than the resistor case. This is a function of the poor low frequency response which results in a droop of the output. The droop is specified as a % per unit time, the longer the discharge, the larger the error.

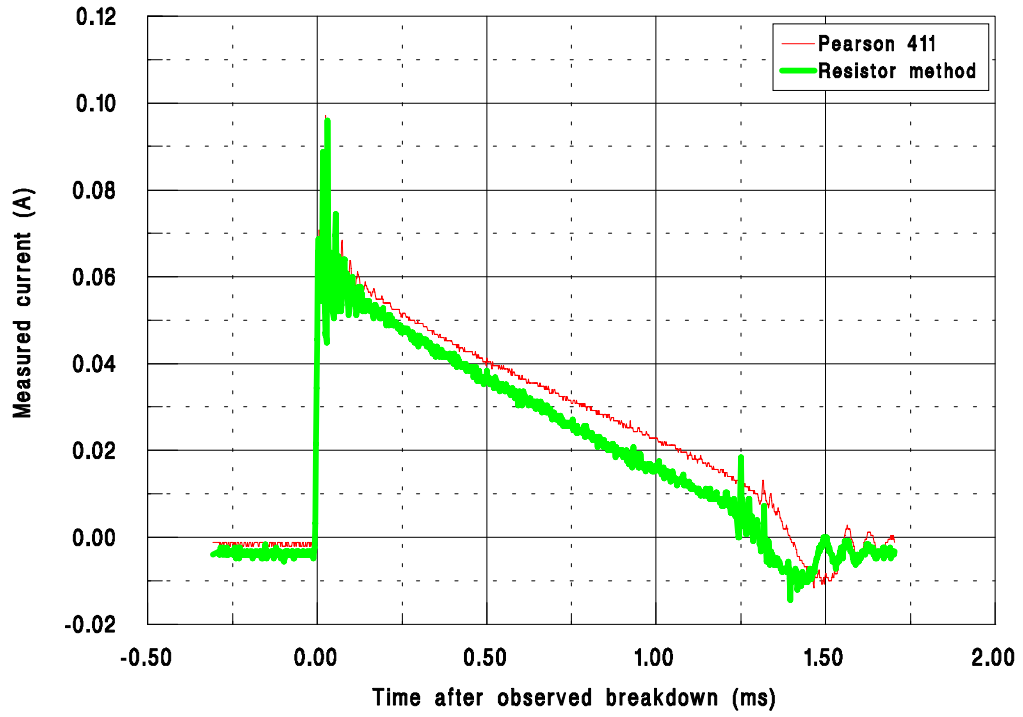

Figure D.8 Comparison of current measuring performance between Pearson 411 and resistor method for complete single discharge

The Pearson 411 has a droop rate of approximately one hundredth of that of the Pearson 4100 allowing longer pulses to be examined. The lower droop rate , a consequence of an improved lower frequency response, is at the expense of high frequency operation and response time to pulses.

A small DC offset exists, due to what is thought to be, a calibration error on the oscilloscope, the scope is used on a very low volts/division scale to enable the low gain of the current monitor to be used. This offset error becomes large with the scaling factors used, but can be eliminated by software when downloading data from the scope.

When viewed on the scope, the resistor and Pearson 411 gave very similar results and were indistinguishable from each other, although the Pearson 411 does exhibit slightly more noise due to the amplification of the scope compensating for the lower gain of the transducer.

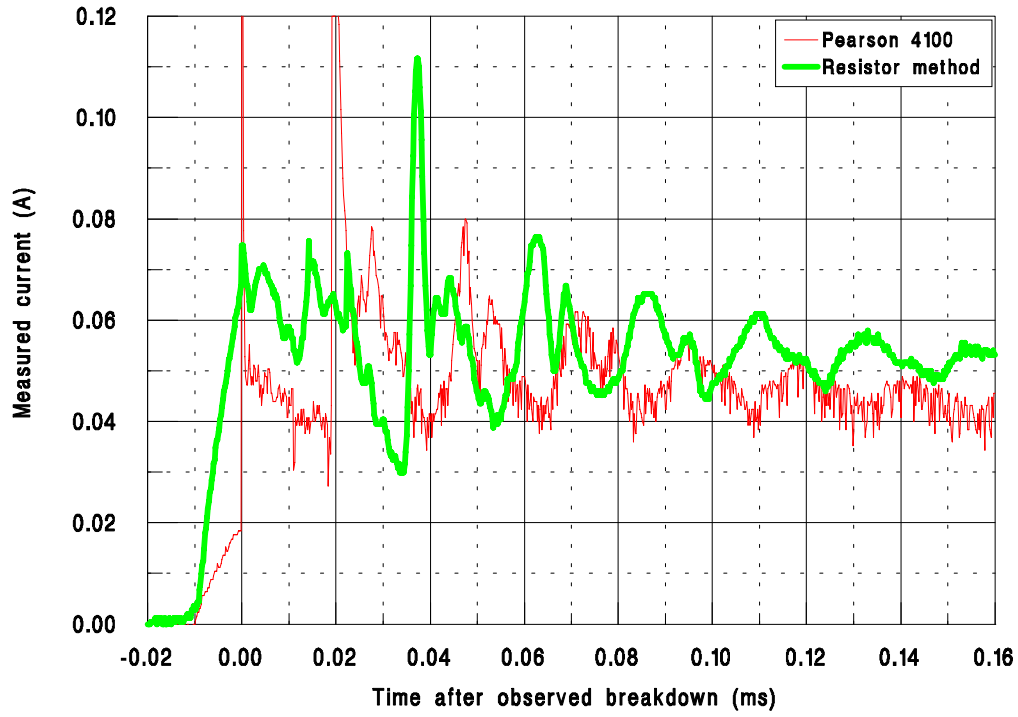

Figure D.9 Comparison of current measuring performance between Pearson 4100 and resistor method for breakdown of single discharge (revised position)

When the Pearson 4100 transducer is positioned along the HT lead, the current characteristic changes dramatically when compared to measurements made closer to the coil. This effect is caused by capacitance effects in the HT lead, distributor and the plug itself.

Errors in calculated energy could occur, highlighting the importance of measuring the current as close to the point of voltage measurement as possible.

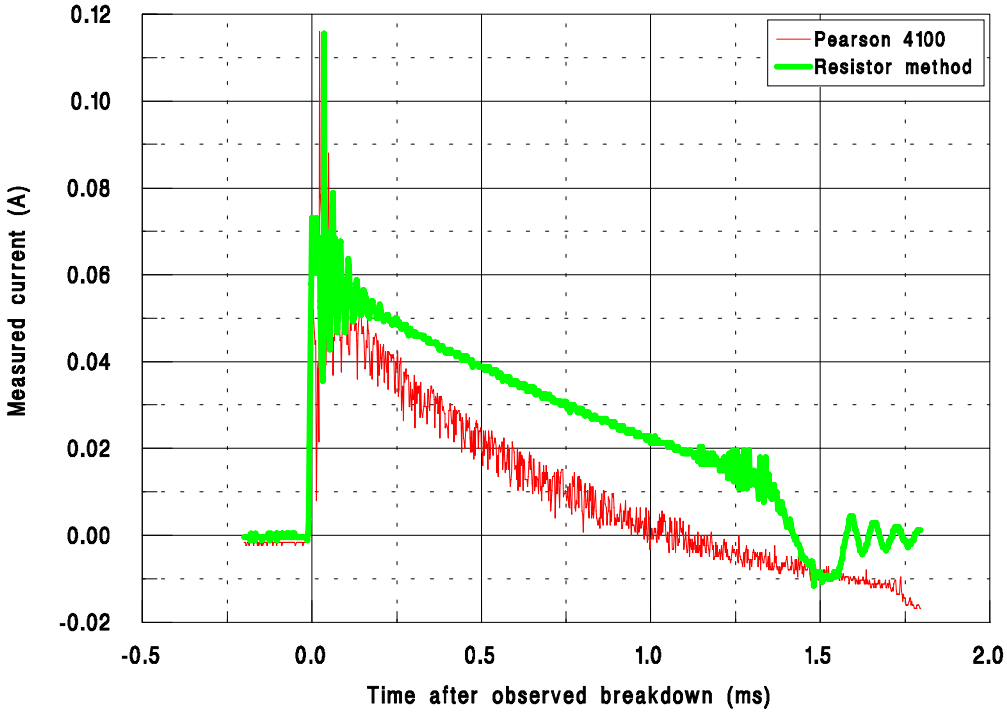

Figure D.10 Comparison of current measuring performance between Pearson 4100 and resistor method for single complete discharge (revised position)

The Pearson 4100 shows the same droop characteristic as that seen in figure D.7 although more noise can be seen. This noise is thought to be the consequence of local electric fields, since in this position, the current transformer is closer to the distributor where an open electrical discharge exists.

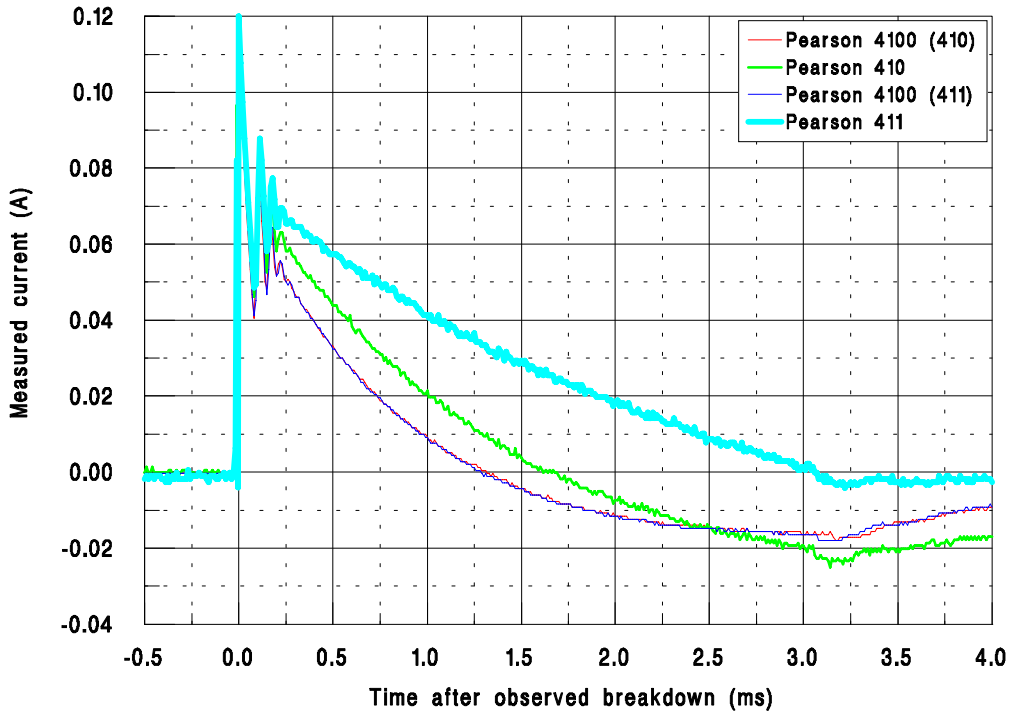

Figure D.11 Comparison of current measuring performance between Pearson 4100, Pearson 410 and Pearson 411 for complete single discharge (Bosch TCI system

This figure shows the effects of droop on the measured current from a standard coil where the primary and secondary windings are joined. The three suitably sized Pearson current transducers are all compared. Both the 410 and 411 were compared to the 4100, for this reason both the corresponding 4100 traces are shown and the repeatability of the complete discharge current can be seen clearly.

When discharging at low pressure, the spark duration is longer (more energy dissipated in the glow phase), this presents a greater problem to the inductive current transformers since the droop will be higher.

These waveforms should not be considered to have come from the same discharge.

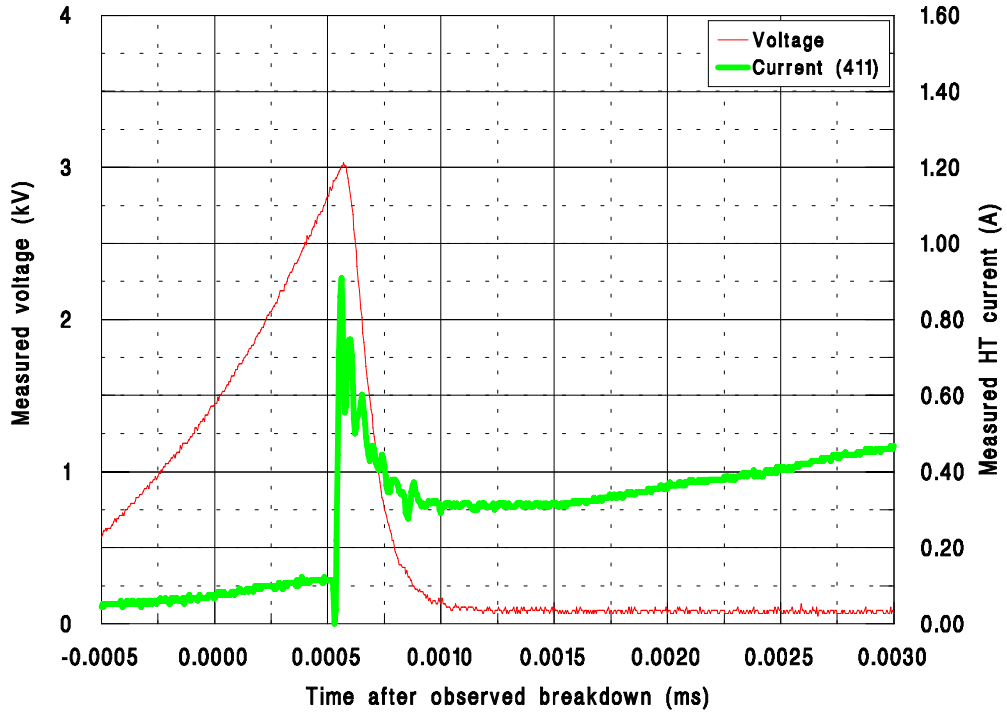

Figure D.12 Measured voltage and current events for early stages of single discharge (Bosch CDI system)

The current and voltage have been measured as close to each other as possible. When breakdown occurs, a sudden rise in current, from the discharge of circuit capacitance follows.

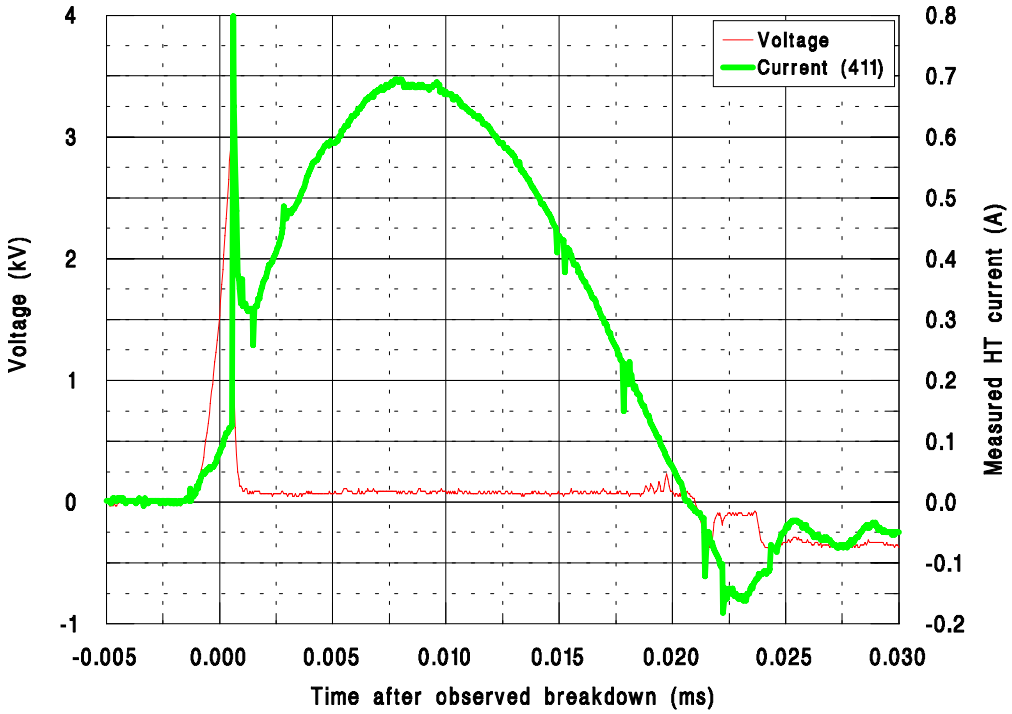

Figure D.13 Measured voltage and current events for complete single discharge (Bosch CDI system)

The complete discharge shows the higher currents associated with CD ignition systems, up to ten times as high as TCI ignition systems.

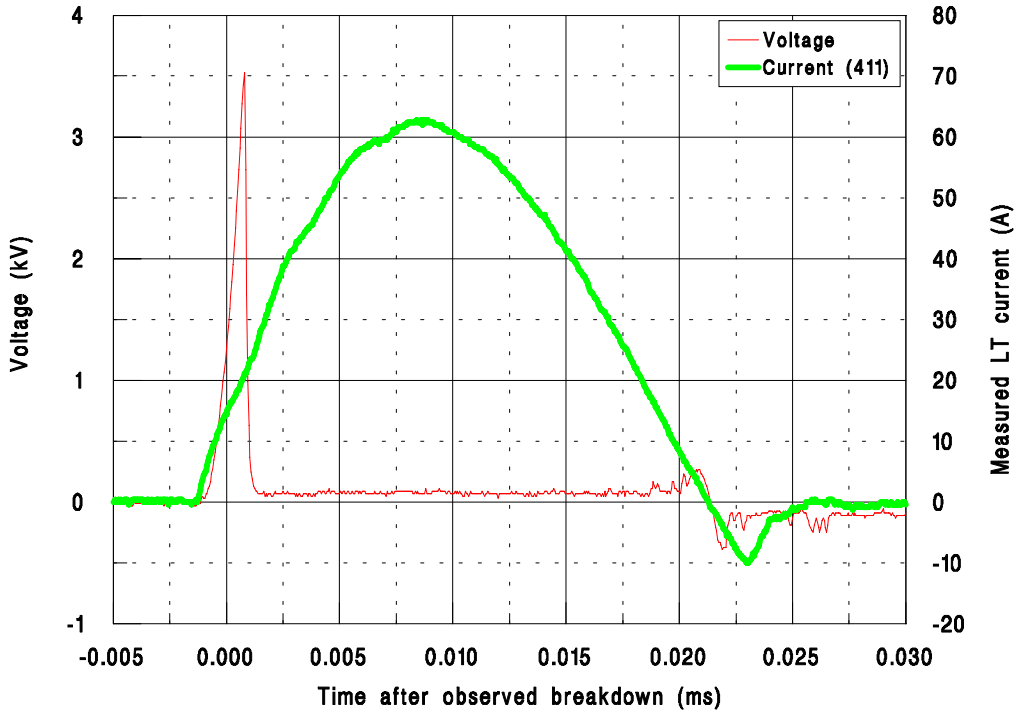

Figure D.14 Measured voltage and LT current events for complete single discharge (Bosch CDI system)

The LT current for the CD ignition system can rise up to 65 amps, the flow lasting for as long as the discharge duration.

CD ignition transformers are normally wound with a ratio of 100:1, this is confirmed by the peak current ratio of 65:0.7.

Appendix E CD Ignition Sources

Type	Source	Comments
Bosch CDS	Porsche 911 1969-1978	3 pin system. Contact breaker triggered.
Bosch CDS	Porsche 911 1978-1983	6 pin system. Inductive triggering.
Wilkinson	Electronics Today Intnl, April and May 1975	Used for project. Has rev limit and rev counter circuits built in. PCB design included.
EDA Sparkrite	Radio and Electronics World, July 1982	Three in one ignition system. Can be switched between CDI, TCI and BCI modes. Circuit diagram of commercial system. PCB Design included.
Cooper	Wireless World, March 1982	Simple circuit, PCB design included.
RCA	RCA Designers handbook - Solid State Power Circuits, SP52, 1971, RCA Corporation, Somerville, N.J., USA	Simple circuit
SAAB	SAAB 9000 1988-1991	Part of engine managment system. Uses separate coils and has multistriking at low rpm for idle stabilisation

Although a majority of Japanese motorcycles use CD ignition systems they require a magneto system for charging and triggering. In this case, they are unsuitable for direct fitting and testing on research or commercial engines.

Appendix F Coils used for experiments

Manufacturer	Primary Inductance μH	Secondary Inductance H	Primary Resistance Ω	Secondary Resistance Ω
Lucas DLB102	4288	44.63	1.5	7300
Bosch 0 221 121 001 CDI 4 cyl	165.7	0.9234	0.6	665

Other coils for which experimental results are not reported here

Ford	6246	48.3	0.8	1373
Kawasaki	151.6	1.768	0.4	9.14
Bosch 0 221 122 008 TCI 6-cyl (?)	7872	23.06	1.3	7010
Bosch 1 227 020 009 TCI 4 cyl (Yel)	3820	28.5	0.9	8400/10680
Bosch 0 221 122 349 TCI 4 cyl (Grn)	6022	15.52	0.9	3050

Appendix G Pin connections for ignition systems used

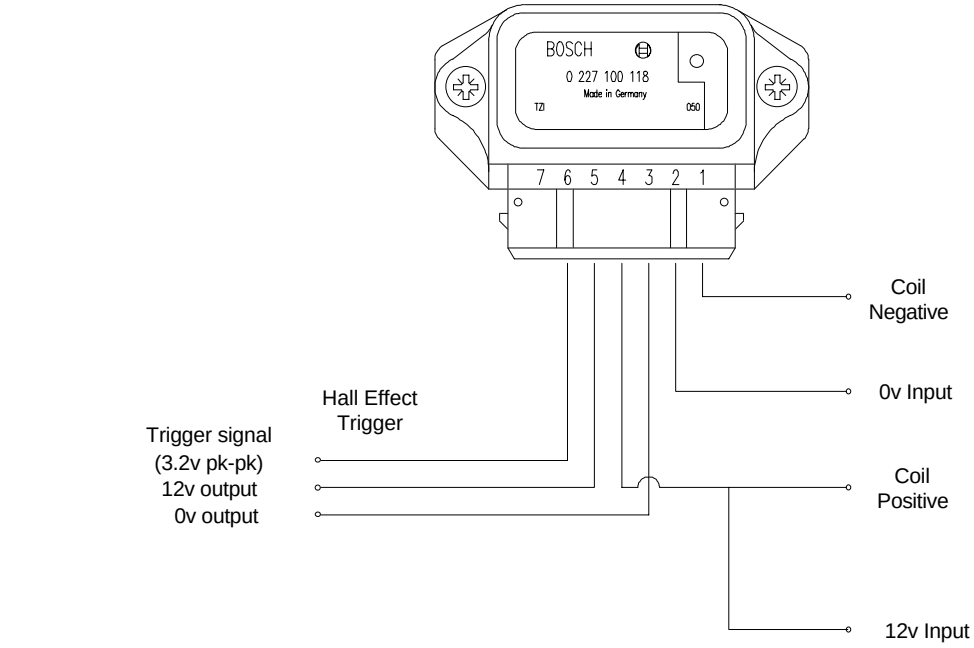

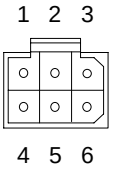

1. Black - Earth
2. Black/White - Coil -ve
3. White - 12v in/Coil +ve
4. Black - Hall sender earth
5. Green - Hall sender signal
6. Red - Hall sender +ve

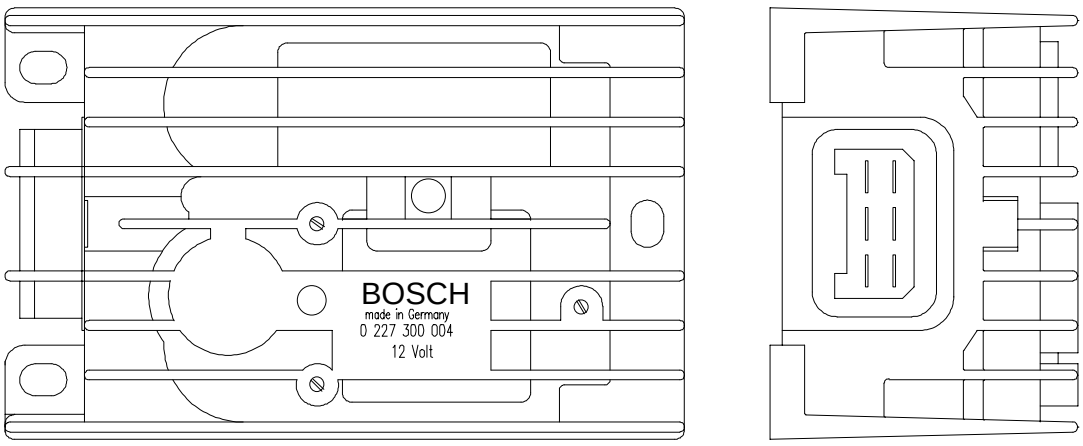

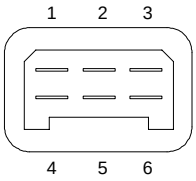

1. Inductive sensor (0v)
2. Tachometer drive
3. Main 0v input
4. Ignition output (approx 400v)
5. Main 12v input
6. Inductive sensor (+v)

Appendix H Fuel injector technical note

Accepted for publication in Proceedings of IMechE

Predictions of liquid fuel injector performance with gaseous fuels

Nick Pashley, BEng, MSc, **Richard Stone**, MA, DPhil, MSAE, FIMechE
Department of Engineering Science, University of Oxford, Oxford

A method to predict the maximum flowrate of a liquid fuel injector when operating with gaseous fuels has been developed. Three injectors were tested for flow capability with four gases of varying molecular mass and ratio of specific heats. Compressible flow theory has been used to non-dimensionalise the results, and predictions have been made for performance with other gases and mixtures.

1 INTRODUCTION

Pulsed fuel injectors are used to a great extent in spark ignition engines where liquid fuels are used, but there are a number of reasons why their use might extend to gaseous fuels. Natural gas is increasingly being used for automotive and stationary engines. In automotive applications natural gas has inherently low emissions of carbon dioxide, nitrogen oxides (NOx) and atmospherically reactive hydrocarbons. In stationary applications, natural gas is a readily available and economical fuel. However, in both applications, it is necessary to have good control of the air fuel ratio, if the conflicting aims of high fuel economy and lower emissions are to be achieved. Other notable gaseous fuels are LPG (Liquefied Petroleum Gases, such as propane and butane), and these too are used in engines; for examples taxis and fork lift trucks.

Pulsed injectors allow the fuelling to be tailored to the engine operating condition, measured by external sensors, measuring parameters such as speed, load and Lambda. An electronic control unit can provide a mapped behaviour pattern for the fuelling, and ignition, which is based on experimental results, an adaptive controller can compensate for the condition of the engine and ancillaries by matching the fuelling and ignition to emissions legislation or power criteria.

As mentioned above, the majority of pulsed injectors are used with liquid fuels, the performance of which are measured in volume of liquid per unit time. These figures are not readily applicable to gases since at injection pressures, liquids are effectively incompressible, the maximum flowrate

through a restriction being a function of upstream pressure, fluid density and orifice dimensions, and also to a small extent the Reynolds number.

The maximum mass flow rate of gas through a restriction is obtained during a choked flow condition, i.e. when the gas reaches the speed of sound, for that particular medium. This occurs at the smallest area in the system, the point usually referred to as the throat.

With an electronic system, a constant fuel pressure is maintained at the injector. An electronic control unit (ECU) supplies pulses to the injector to energise a solenoid. The solenoid causes a needle valve to open, allowing fuel to flow. The fuel flow can be controlled by the pulse width to the injector.

2 THEORY

This work compares the flow through an injector nozzle with that through a convergent divergent duct. The choked flow theory assumes an adiabatic, isentropic process which is, in reality, impossible. In the injector, heat transfer will occur to or from the fluid, and fluid friction and sudden increases in flow area will cause irreversibility. However, these effects are likely to be relatively small and therefore can be neglected for the purposes of analysis.

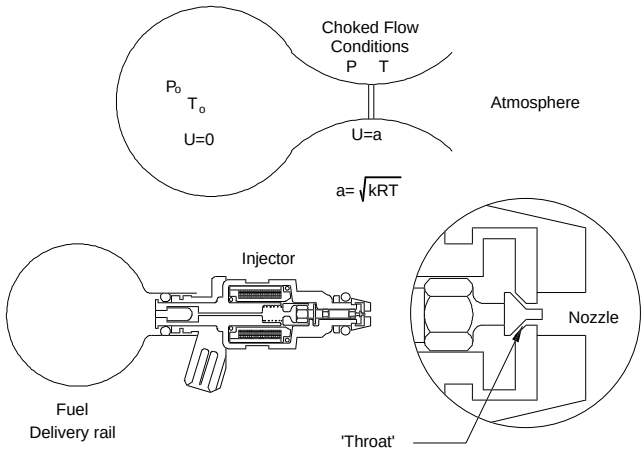

Figure 1 Comparison between flow through the injector and a nozzle

With an adiabatic process in which there is no work exchange, the steady flow energy equation can be used to link the reservoir temperature with the temperature anywhere along the system. The maximum massflow occurs during choked flow at the throat, i.e. the velocity equals the speed of sound. Assuming perfect gas behaviour, and that the process is reversible (i.e. ignoring fluid friction) then the standard compressible flow equations can be used to determine the mass flow rate through the injector {1} :

$$\dot{m} = \frac{Ap_o}{\sqrt{RT_o}} \sqrt{\kappa} \left(\frac{2}{\kappa + 1} \right)^{(\kappa+1)/2(\kappa-1)} \qquad \{1\}$$

Where : A is the area in (m^2)

p_o is the stagnation pressure (Pa)

R is the specific gas constant (J/K)

T_o is the stagnation temperature (K)

κ is the ratio of specific heats

Considering the injector nozzle to be the throat and the fuel rail to be the reservoir, the mass flow rate at the sonic (or choked) condition can be evaluated from reservoir conditions and gas properties.

In practise the geometric throat area, A, is not identical to the effective flow area, A_e, and a discharge coefficient, C_d, is defined in order to obtain agreement between the above analysis and geometric area.

$$A_e = A \times C_d \qquad \{2\}$$

3 EXPERIMENTAL SYSTEM PROCEDURE

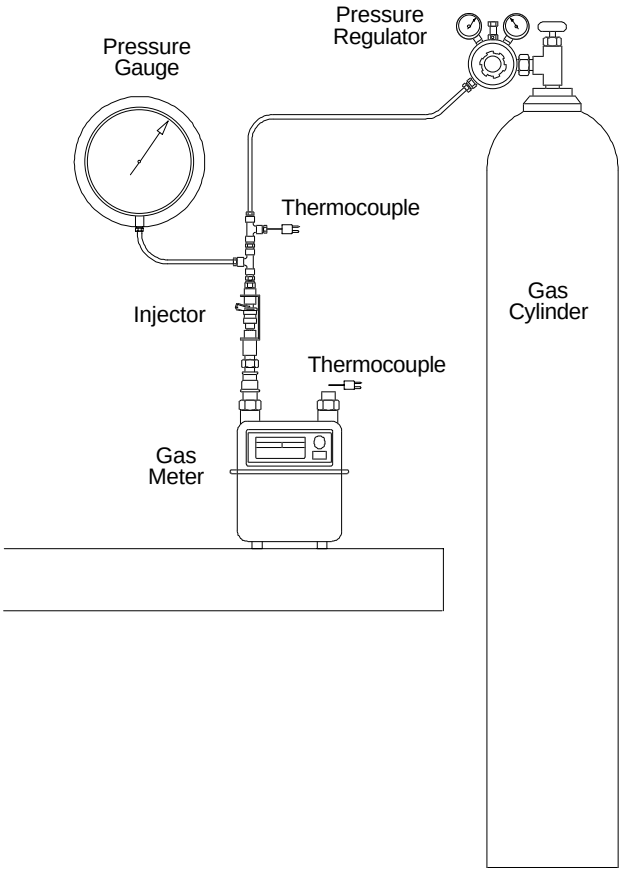

Figure 2 Experimental apparatus

The apparatus was assembled as shown in figure 2. Two tee pieces upstream of the injector allowed the measurement of temperature and pressure using a K type thermocouple and Budenberg

Reference pressure gauge respectively. The pressure gauge was calibrated using a dead weight tester. The thermocouple welded junction was allowed to protrude into the centre of the flow.

Gas was supplied from standard cylinders, through a two stage regulator connected to the injector by nylon pipe. A positive displacement gas meter, with calibration traceable to NAMAS, was used to measure volume flow rate with the temperature being measured at the meter outlet.

Three fuel injectors were tested, two large capacity Weber gasoline injectors (IW031 and IW058) and a Bosch methanol injector (B 280 412 912/3 V3641). The injectors were energised using a DC power supply at 12V, at which a current of approximately 0.75 amps was required. Four gases were used for flow evaluation, air (zero grade), carbon dioxide (N4.5), helium (N5.0) and nitrogen (N4.8).

The pressure regulator was adjusted to give the required upstream injector pressure. The volumetric flow rate was then evaluated by timing the discharge of 10 litres of gas.

Line pressure and temperature were measured at the beginning and end of each test, the average value being used in all calculations. The pressure measured in the line was assumed to be representative of the static pressure, the reservoir pressure was back calculated using both compressible and incompressible relations. The difference between the calculated reservoir pressure and the static pressure was found to be negligible, even when using helium as the working fluid.

The exit pressure from the injector was assumed to be atmospheric which was realistic since the pressure drop across the meter, even at maximum flow, was in the region of $100N/m^2$, which is negligible compared to atmospheric pressure of $100kN/m^2$. Large pipe fittings were used directly downstream of the injector nozzle to reduce the Reynolds number and therefore minimise pressure losses.

The flow meter exit temperature was measured, using a second K-type thermocouple, and this was used to determine the working fluid density in the meter. The flow rate measurement had an accuracy better than 0.5%, and the temperature measurements had an accuracy of 0.15%. The pressure measurement had an accuracy of ±0.03 bar. Thus in the mid pressure range the evaluation of the effective area has an accuracy no worse than 1.2% (0.5 + 0.15/2 + 0.6) or a root mean square error of 0.8%.

4 DISCUSSION

The highest volumetric flow rate was recorded when using helium, with approximately three times as much flow as that obtained when using carbon dioxide; see figure 3. The flow rates for air and nitrogen are very similar, which is to be expected since nitrogen is the major constituent of air. The results for carbon dioxide are approximately 20% lower than those of air and nitrogen.

Figure 3 shows the maximum mass flow rate with any upstream pressure, is achieved using carbon dioxide as the working fluid, with over 350% of that obtained when using helium.

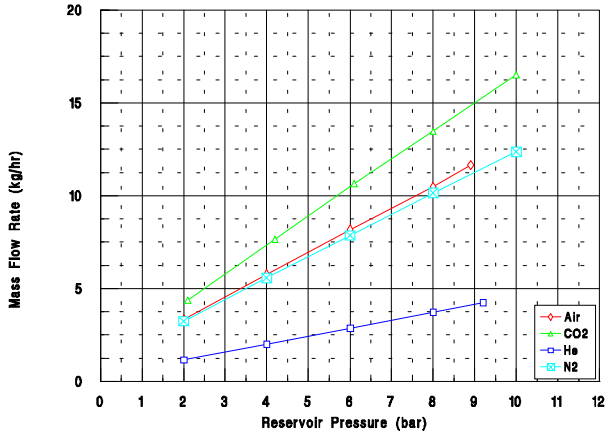

Figure 3 Bosch mass flow rate characteristics

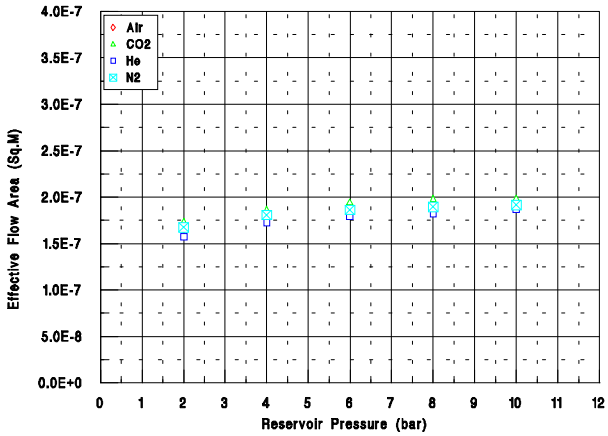

Figure 4 Calculated effective flow area as a function of reservoir pressure for the Weber IW031 injector

Figure 3 suggests a linear relationship between the mass flowrate of a gas and it upstream pressure, and this implies that the compressible flow equations are applicable. Combining and rearranging equations 1 and 2 gives :

$$A_e = AC_d = \dot{m}\frac{\sqrt{RT_o}}{P_o\sqrt{\kappa}}\left(\frac{\kappa+1}{2}\right)^{(\kappa+1)/2(\kappa-1)} \quad \{3\}$$

If the compressible flow theory is valid, then the effective flow area will be independent of the gas and its reservoir pressure.

When the mass flow rates are used to calculate an effective throat area from the equations of compressible flow, the results are very similar, (see figs 4, 5 and 6), and are generally within four percent at each pressure.

It is clear that the effective flow area is almost independent of upstream injector pressure. The most probable reason for this deviation is due to a slight dependence on Reynolds number.

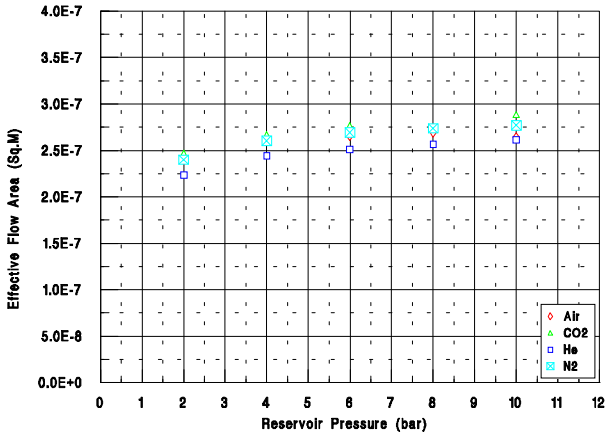

Figure 5 Calculated effective flow area as a function of reservoir pressure for the Weber IW058 injector

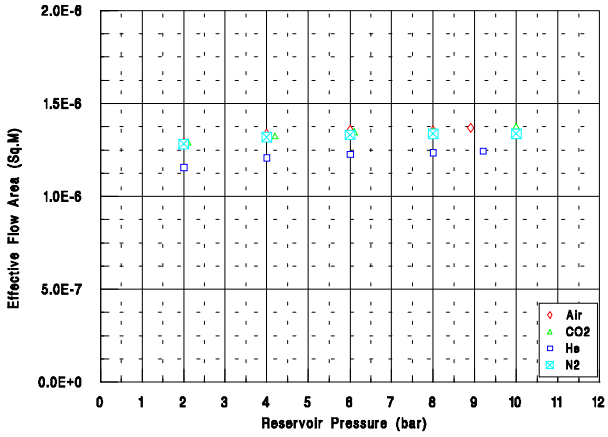

Figure 6 Calculated effective flow area as a function of reservoir pressure for the Bosch injector

The effective flow area, the quantity appears to reduce with decreasing molar mass. The largest deviation from the mean effective flow area is obtained when using helium, which has the highest volumetric flow rates and velocities. This will increase frictional losses within the injector therefore leading to a lower effective area.

5 PERFORMANCE PREDICTIONS

With the effective area known for a range of upstream pressures, it is possible to predict the mass flow rate through the injector when using other gases. For stationary and automotive use, the most promising fuel is natural gas, which is predominantly methane. The performance for other gases may

be predicted (not necessarily fuels) for engineering applications where a precisely metered amount of the fluid is needed.

For mass flow rate prediction, the only parameters needed for the gas are the stagnation temperature, stagnation pressure, molar mass and the ratio of specific heats.

Values of the molar mass and ratio of specific heats for various gases are included in appendix A.

The equation for predicting the mass flow rate is a rearrangement of equation {3} :

$$\dot{m} = \frac{A_e p_o}{\sqrt{RT_o}} \sqrt{\kappa} \left(\frac{2}{\kappa + 1} \right)^{(\kappa+1)/2(\kappa-1)} \qquad \{4\}$$

Figures 7 to 10 give performance predictions when using hydrogen, methane, ethane and propane.

With regards to use as an automotive fuel injector for gaseous fuels, the Bosch injector is the most suitable. A 500cc cylinder swept volume engine, running at 3000 rpm and an air-fuel ratio of 9:1, will consume about 1 g/s (3.6 kg/hr) of methane gas. It is clear from the predicted curves in figure 8 that this flow rate can only be achieved, at a convenient pressure, by the Bosch injector. Two Weber IW058 injectors could be used to supply such an engine, with a reservoir pressure of approximately 6 bar.

Figure 10 shows predicted mass flow rates for propane when using the three injectors. It must be noted however that propane liquefies at 7.58 bar at a temperature of 294K. However with propane there are advantages in operating with higher pressures, so as to be able to use liquid injection.

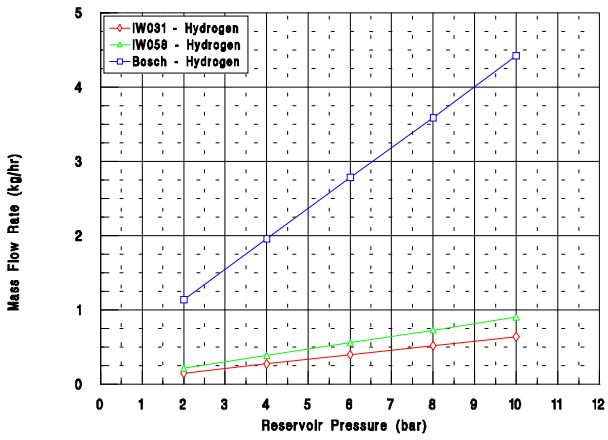

Figure 7 Predicted injector mass flow rate performance using Hydrogen as the working fluid

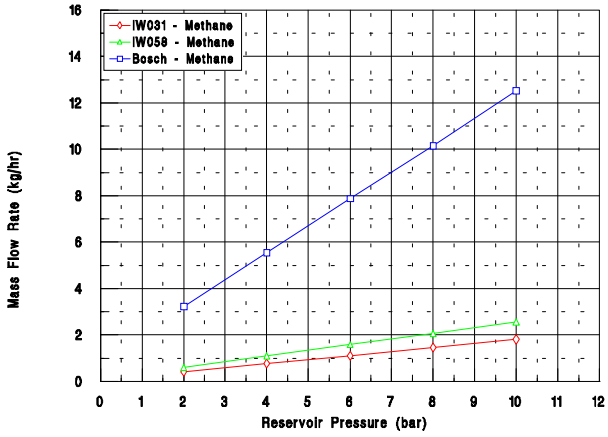

Figure 8 **Predicted injector mass flow rate performance using Methane as the working fluid**

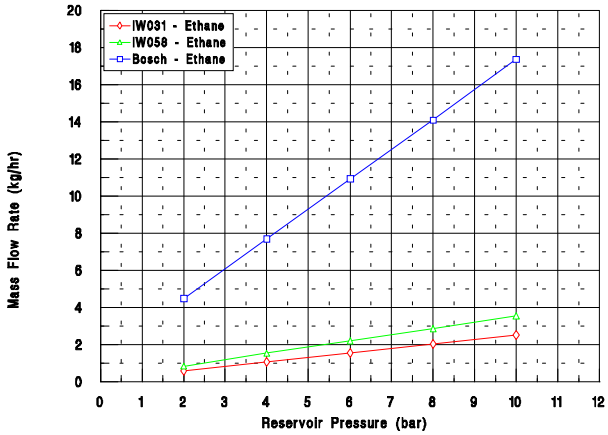

Figure 9 **Predicted injector mass flow rate performance using Ethane as the working fluid**

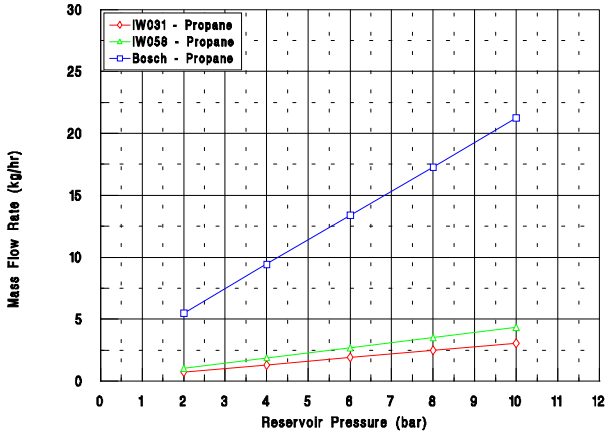

Figure 10 **Predicted injector mass flow rate performance using Propane as the working fluid**

For gas mixtures such as natural gas or LPG, the Gibbs-Dalton law may be applied to the gas properties. The ratio of specific heats may not be evaluated by a straight mass weighting method, as the specific heats must be obtained separately.

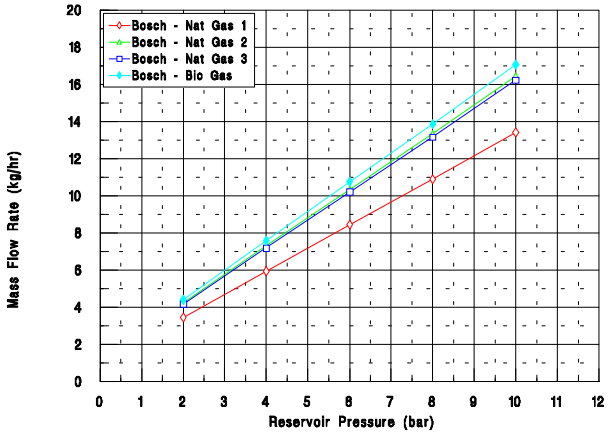

Figure 11 Predicted Bosch injector mass flow rate performance using gas mixtures

All relevant gas properties are presented in appendix A.

Figure 11 shows the predicted performance of the Bosch injector with blends of natural gas and bio-gas using the methods described above, properties of which are described in appendix B.

It should be noted that maximum mass flow performance can be reduced by as much as 25% when changing the natural gas composition.

6 CONCLUSIONS

Three automotive type fuel injectors were tested with a view to their use for fuelling natural gas engines. Two injectors were supplied by Weber Concessionaires, and were designed to be used with petrol. The third injector, manufactured by Bosch, was designed to be used with methanol.

The injectors were tested for flow capability with four gases of differing molar masses and ratios of specific heats. The gases were air, nitrogen, carbon dioxide and helium. With the results obtained, an effective injector valve flow area was calculated using compressible flow theory. The calculated effective areas were found to be virtually the same for all four gases at all delivery pressures. These data can be used to calculate the flow characteristics with any gas. This has been done for hydrogen, methane, ethane and some gas mixtures.

REFERENCES

1. **White, F.M.**, *Fluid mechanics*, 2nd Edition, McGraw-Hill, 1986
2. **The Matheson Co. Inc.**, *Matheson gas data book*, 4th Edition, Matheson of Canada Ltd, Ontario

3. **Charlton, S.J., Tawfig, M.E. and Shooshtarian, A.,** *The response of an open-chamber natural gas engine to gas composition*, IMechE paper, presented at Gas Engines for Co-Generation seminar, 17th June 1993
4. **Raine, R.R., Zhang, G. and Pflug, A.,** *Comparison of emissions from Natural Gas fuelled engines - Total hydrocarbon and Methane emissions and Exhaust Gas Recirculation effects*, SAE paper, 970743, SAE Congress and Exposition, Detroit, Feb 1997

ACKNOWLEDGEMENTS

The authors wish to thank Paul Birch of Weber Concessionaires for the loan of the two gasoline injectors, Shang-you Duan, formerly of BG plc, for the loan of the Bosch methanol injector and Dr Rachel Palmer for valuable input, and BG plc for funding the work.

APPENDIX

A Gas properties [2]

Gas	Molar mass (kg/kmol)	Spec. gas const. (J/kg K)	Specific heat ratio κ
Air	28.96	287	1.40
Carbon Dioxide	44.01	189	1.30
Helium	4.003	2077	1.66
Nitrogen	28.02	297	1.40
Methane	16.04	518	1.307
Ethane	30.07	276	1.192
Propane	44.10	189	1.131
Butane	58.12	143	1.096
Hydrogen	2.016	4124	1.41
Argon	39.944	208	1.67

B Specifications of Gas Compositions used in performance predictions (based on [3] and [4])

Gas	Nat Gas 1 (UK field)	Nat Gas 2 (Algerian field)	Nat Gas 3 (New Zealand field)	Bio Gas
Methane	89.9	56.6	83.3	60.0
Ethane	5.1	22.2	6.8	
Propane	1.6	12.2	2.5	
Butane	0.5	5.0	0.8	
Pentane	0.1	2.0	0.13	
Hexane		0.5	0.02	
Hydrogen				
Nitrogen	0.2		2.2	
Carbon Dioxide	2.6	1.5	4.2	40.0
Carbon Monoxide				
Water Vapour				

Appendix I Instrumentation for airflow meter

The airflow meter was fitted with a shaft encoder (RS Miniature Speed and Position Transducer 341-597) of 500 pulses per rev. This rotates at the rotor speed, therefore one pulse per 0.00063 litres. Two options exist for the encoded output, the first is a rate meter which is fed by the digital signal and counts pulses over a fixed period of 1 second, the second is a frequency to voltage conversion circuit.

The rate meter displays a pseudo average flowrate and supplies the encoder with the five volts needed for operation. This average fluctuates since the speed of rotor rotation is not constant.

The frequency to voltage converter is based around the LM2917-8 integrated cicuit which is fast enough to enable time resolved measurements of airflow to be made. The circuit, shown in Figure I.1 has been designed for an output of 1V per 2kHz with a maximum output voltage of slightly over 5V, the component values to achieve this are shown in Table I.1. This gives a maximum measurable flowrate of 6.3 litres/second, equivalent to a 2000 rpm wide open throttle condition.

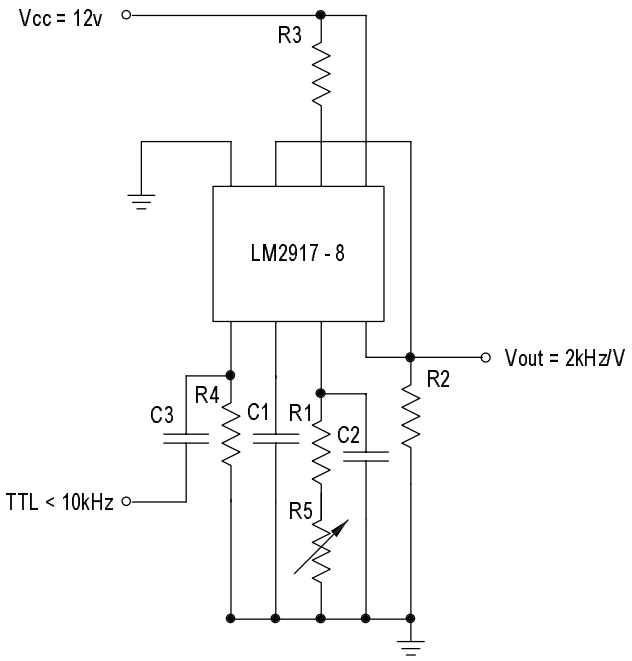

Figure I.1 Frequency to voltage conversion circuit

Component	Value
C1	680 pF
C2	1.0 μF
C3	10 nF
R1	91 kΩ
R2	10 kΩ
R3	470 Ω
R4	1 kΩ
R5	10 kΩ

Table I.1 Component values for frequency to voltage conversion circuit

The LM2917 requires an input to swing below zero volts, C3 and R4 are used to provide a voltage spike to achieve this.

Conversion factors

cubic feet	to	litres	multiply by	28.316 865 9
cubic feet per hour	to	litres per second	multiply by	0.007 865 8

Appendix J Calculations for air-fuel ratio

Calculation of Gravimetric Air-Fuel Ratio from Exhaust Gas Composition

Three methods of calculating the air-fuel ratio and lambda from exhaust gas composition are presented. These equations are designed for use with methane or natural gas fuelled engines. A sample code is included in MS Quick Basic.

Exhaust gas concentration measurement

CO	NDIR	(OTC analyser)
CO2	NDIR	(OTC analyser)
HC	FID	(Rotork analyser)
O2	Galvanic cell	(OTC analyser)

Method 1 use of all four components and assumed knowledge of HC ratio (n) for fuel

Method 2 use of all four components with no knowledge of HC ratio (n)

Method 3 use of first three components and assumed knowlege of HC ratio (n) for fuel

Combustion equation

$$C_xH_{nx} + z\left(O_2 + {}^{79}\!/\!_{21}\,N_2\right) \rightarrow aCO + bCO_2 + cCH_4 + dO_2 + eNO + fH_2 + wH_2O + (100 - a - b - c - d - e - f)N_2$$

Assumes all unburned hydrocarbons are methane and that the magnitudes of *x* and *z* give 100 kmols of dry products.

Method 1

Atom balances

Atom	Equation	Unknowns	Equation number
C:	$x = b + a + c$	none	{1}
H:	$nx = 4c + 2w + 2f$	w, f	{2}
O:	$2z = 2b + a + w + e + 2d$	z, w	{3}

N: $2 \times {}^{79}\!/_{21}\, z = 2(100 - a - b - c - d - e - f) + e$ z, f {4}

Water gas reaction

$$wg = \frac{aw}{bf}$$ w, f {5}

Procedure

Evaluate *x* from {1}

Get {5} in terms of *w* and substitute into {2} to yeild {6}

$$f = \frac{nx - 4c}{\left(\frac{2bwg}{a} + 2\right)}$$ {6}

Use {5} to find *w*

Use {3} to find *z*

$$AFR = \frac{z\left(32 + \frac{79}{21} \times 28\right)}{x(12 + n)}$$

$$Lambda = \frac{z}{\left(x + {}^{nx}\!/_{4}\right)}$$

Method 2

Atom balances

Atom	Equation	Unknowns	Equation number
C:	$x = b + a + c$	none	{1}
H:	$nx = 4c + 2w + 2f$	n, w, f	{2}
O:	$2z = 2b + a + w + e + 2d$	z, w	{3}
N:	$2 \times {}^{79}\!/_{21}\, z = 2(100 - a - b - c - d - e - f) + e$	z, f	{4}

Water gas reaction

$$wg = \frac{aw}{bf} \qquad \text{w, f} \qquad \{5\}$$

Procedure

Evaluate *x* from {1}

Get {5} in terms of *w* and substitute into {3} to yeild {7}

$$f = \frac{(2z - 2b - a - e - 2d)a)}{bwg} \qquad \{7\}$$

z is still unknown so get {4} in terms of *f* to yeild {8}

$$f = 200 - 2a - 2b - 2c - 2d - \frac{2 \times 79}{21} z \qquad \{8\}$$

Combine {7} and {8} to eliminate *f* and form {9}

$$z = \frac{1}{\frac{2 \times 79}{21} + \frac{2a}{bwg}} \left(200 - 2b - 2c - 2d + \frac{a}{bwg}(2b + a + e + 2d - 2) \right) \qquad \{9\}$$

Evaluate *w* from {3}

Evaluate *f* from {5}

Evaluate *n* from {2}

$$AFR = \frac{z\left(32 + \frac{79}{21} \times 28\right)}{x(12 + n)}$$

$$\text{Lambda} = \frac{z}{\left(x + nx/4\right)}$$

Method 3

Atom balances

Atom	Equation	Unknowns	Equation number
C:	$x = b + a + c$	none	{1}
H:	$nx = 4c + 2w + 2f$	w, f	{2}
O:	$2z = 2b + a + w + e + 2d$	d, z, w	{3}
N:	$2 \times {}^{79}\!/_{21}\, z = 2(100 - a - b - c - d - e - f) + e$	z, d, f	{4}

Water gas reaction

	$wg = \frac{aw}{bf}$	w, f	{5}

Procedure

Evaluate *x* from {1}

Solve {2} and {5} simultaneously to find *f* and *w*

Substitute {3} into {4} to get {10} and find *d*

$$d = \frac{\frac{21e + 42(100 - a - b - c - e - f)}{2 \times 79} - b - \frac{a + w + e}{2}}{1 + \frac{42}{2 \times 79}} \qquad \{10\}$$

Use {3} to find z

$$AFR = \frac{z\left(32 + \frac{79}{21} \times 28\right)}{x(12 + n)}$$

$$Lambda = \frac{z}{\left(x + {}^{nx}\!/_{4}\right)}$$

Sample code

```
INPUT " CO%=", a
INPUT " CO2%=", b
INPUT " HCppm(FID)=", hc
INPUT " O2%=", d
INPUT "H/C ratio 1:"; hcrat
c = hc / 10000
wg = 3.5

'******************     First calculation H/C ratio known       **********
n = hcrat
x = a + b + c
f = (n * x - 4 * c) / ((2 * b * wg / a) + 2)
w = b * f * wg / a
z = (2 * b + a + w + e + 2 * d) / 2
afr1 = (z * (32 + 79 / 21 * 28)) / (x * (12 + n))
lambda1 = z / (x + n * x / 4)
hcrat1 = n
equiv1 = 1 / lambda1
d1 = d
f1 = f
w1 = w
x1 = x
z1 = z

'******************     Second calculation H/C ratio unknown     **********
x = a + b + c
z = 1 / ((2 * 79 / 21) + ((2 * a) / (b * wg))) * (200 - 2 * b - 2 * c - 2 * d + (a / (b * wg) * (2 * b
+ a + e + 2 * d - 2)))
w = 2 * z - 2 * b - a - e - 2 * d
f = (a * w) / (b * wg)
n = (2 * w + 4 * c + 2 * f) / x
afr2 = (z * (32 + 79 / 21 * 28)) / (x * (12 + n))
lambda2 = z / (x + n * x / 4)
```

```
hcrat2 = n
equiv2 = 1 / lambda2
d2 = d
f2 = f
w2 = w
x2 = x
z2 = z

'******************     Third calculation Oxygen unknown        **************
n = hcrat
x = a + b + c
f = (n * x - 4 * c) / ((2 * b * wg / a) + 2)
w = b * f * wg / a
d = ((21 * e + 42 * (100 - a - b - c - e - f) / (2 * 79)) - b - (a + w + e) / 2) / (1 + 42 / (2 * 79))
z = (2 * b + a + w + e + 2 * d) / 2
afr3 = (z * (32 + 79 / 21 * 28)) / (x * (12 + n))
lambda3 = z / (x + n * x / 4)
hcrat3 = n
equiv3 = 1 / lambda3
d3 = d
f3 = f
w3 = w
x3 = x
z3 = z

PRINT , "Method 1", "Method 2", "Method 3"
PRINT "y/x",
PRINT USING "##.###        "; hcrat1; hcrat2; hcrat3
PRINT "AFR",
PRINT USING "##.###        "; afr1; afr2; afr3
PRINT "Equiv Ratio",
PRINT USING "##.###        "; equiv1; equiv2; equiv3
PRINT "Lambda",
PRINT USING "##.###        "; lambda1; lambda2; lambda3
PRINT "d  %O2",
```

```
PRINT USING "##.###       "; d1; d2; d3
PRINT "f  %H2",
PRINT USING "##.###       "; f1; f2; f3
PRINT "w  %H2O",
PRINT USING "##.###       "; w1; w2; w3
PRINT "x  %CH4",
PRINT USING "##.###       "; x1; x2; x3
PRINT "z  %AIR",
PRINT USING "##.###       "; z1; z2; z3
```

Sample operation

CO%=	0.06
CO2%=	7.3
HCppm(FID)=	3500
O2%=	7.73
H/C ratio 1:?	4

	Method 1	**Method 2**	**Method 3**
y/x	4.000	4.045	4.000
AFR	24.940	24.966	24.998
Equiv Ratio	0.688	0.690	0.687
Lambda	1.453	1.450	1.456
d %O2	7.730	7.730	7.782
f %H2	0.034	0.035	0.034
w %H2O	14.686	14.857	14.686
x %CH4	7.710	7.710	7.710
z %AIR	22.403	22.489	22.455

It should be noted that the value of *d* in the third method was back calculated giving an error of 0.67% which can be considered to be negligible. The difference in calculated lambda between the three methods is 0.006, which again shows good agreement from all methods.

Appendix K Equivalent electrode gaps for non J electrode plugs

The electrode gap on spark plugs, with complicated electrode designs, is difficult to measure. Designs such as the surface gap and the double electrode pose the biggest problems since the discharge path is not readily known. An alternative method is to use the required breakdown voltage and compare this to the tests in Chapter 5.

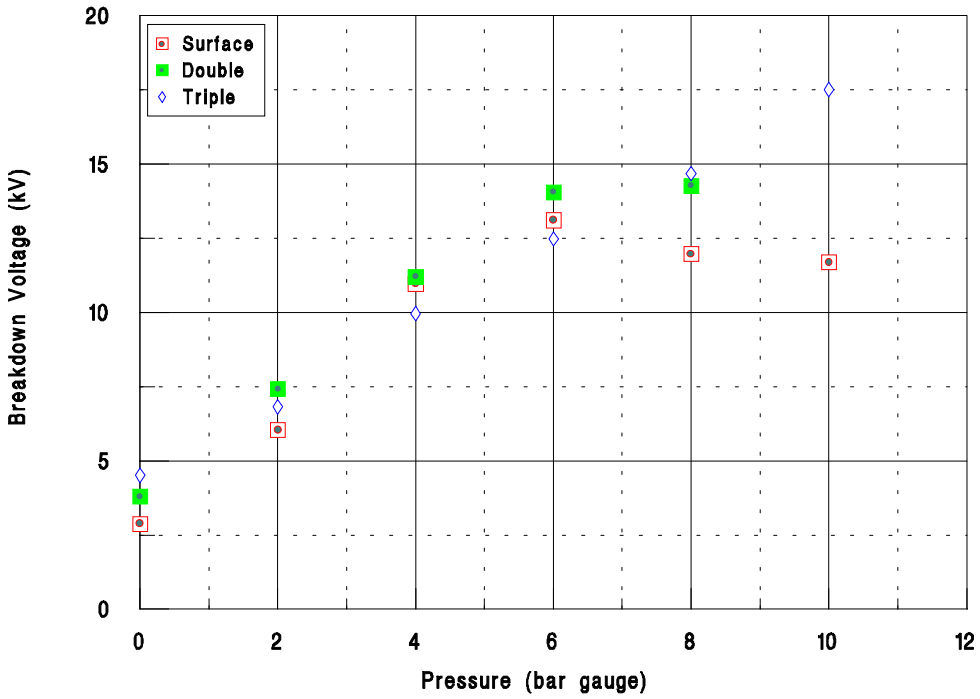

Figure K.1 Required breakdown voltage for spark plugs with alternative electrode designs

Using the linear model described in section 5.2.5, the gap can be estimated from :

$$d_g = \frac{T}{CP}\left(V - A - \frac{BP}{T}\right)$$

where A, B and C are constants

dg is the electrode gap, in mm

V is the breakdown voltage, in kV

P is the pressure, in bar absolute

T is the temperature, in Kelvin

For nickel electrodes in air, the following constants are suggested;

A=4.3

B=136

C=324

The effective electrode gaps, calculated from the experimental data shown above, are:

Electrode type	Equivalent gap (mm)
Surface C53VC	0.74
Double C9BMC	0.82
Triple C6BYC	0.62

Appendix L Calculation of air velocity for flow rig experiments

From the perfect gas law

$$PV = mRT$$

hence at two points, for a constant mass flow rate of gas at a fixed composition,

$$\frac{P_1\dot{V}_1}{T_1} = \frac{P_2\dot{V}_2}{T_2}$$

where P is pressure in pascals

V is volume in cubic metres

T is the temperature in kelvin

and

$$\dot{V}_1 = U_1 \times A_1$$

where U is the velocity in metres/second

A is the area in square metres

for the flow tube, the area can be calculated as :

$$A_1 = \frac{\pi d^2}{4}$$

and hence the velocity can be calculated from :

$$U_1 = \frac{P_2 V_2 T_1}{T_2 \frac{\pi d^2}{4} P_1}$$

taking the blockage factor (See chapter 6), fb, into account :

$$U_1 = \frac{P_2 V_2 T_1}{T_2 \frac{\pi d^2}{4} P_1 \, fb/100}$$

Appendix M Three Term Least Squares Fitting

For an equation of the form :

$$y = a + bx + cz$$

the error is :

$$q = \sum_{j=1}^{n} \left(y_j - a - bx_j - cz_j \right)^2$$

where n is the number of sets of data points and j is the set of data being considered.

The errors for each term are at a minimum when :

$$\frac{\partial q}{\partial a} = 0$$

$$\frac{\partial q}{\partial b} = 0$$

$$\frac{\partial q}{\partial c} = 0$$

so :

$$\frac{\partial q}{\partial a} = -2\sum_{j=1}^{n} \left(y_j - a - bx_j - cz_j \right) = 0$$

$$\frac{\partial q}{\partial b} = -2\sum_{j=1}^{n} x_j \left(y_j - a - bx_j - cz_j \right) = 0$$

$$\frac{\partial q}{\partial c} = -2\sum_{j=1}^{n} z_j \left(y_j - a - bx_j - cz_j \right) = 0$$

or :

$$\frac{\partial q}{\partial a} = \sum_{j=1}^{n} y_j - \sum_{j=1}^{n} a - \sum_{j=1}^{n} bx_j - \sum_{j=1}^{n} cz_j = 0$$

but

$$\sum_{j=1}^{n} a = na$$

giving

$$\frac{\partial q}{\partial a} = \sum_{j=1}^{n} y_j - na - b\sum_{j=1}^{n} x_j - c\sum_{j=1}^{n} z_j = 0 \qquad \{1\}$$

$$\frac{\partial q}{\partial b} = \sum_{j=1}^{n} x_j y_j - a\sum_{j=1}^{n} x_j - b\sum_{j=1}^{n} x_j^{\,2} - c\sum_{j=1}^{n} x_j z_j = 0 \qquad \{2\}$$

$$\frac{\partial q}{\partial c} = \sum_{j=1}^{n} z_j y_j - a\sum_{j=1}^{n} z_j - b\sum_{j=1}^{n} z_j x_j - c\sum_{j=1}^{n} z_j^{\,2} = 0 \qquad \{3\}$$

from 1

$$a = \frac{\sum_{j=1}^{n} y_j - b\sum_{j=1}^{n} x_j - c\sum_{j=1}^{n} z_j}{n} \qquad \{1a\}$$

from 2

$$a = \frac{\sum_{j=1}^{n} x_j y_j - b\sum_{j=1}^{n} x_j^{\,2} - c\sum_{j=1}^{n} x_j z_j}{\sum_{j=1}^{n} x_j} \qquad \{2a\}$$

from 3

$$a = \frac{\sum_{j=1}^{n} z_j y_j - b\sum_{j=1}^{n} x_j z_j - c\sum_{j=1}^{n} z_j^{\,2}}{\sum_{j=1}^{n} z_j} \qquad \{3a\}$$

combining {1a} and {2a}

$$\frac{\sum_{j=1}^{n} y_j - b\sum_{j=1}^{n} x_j - c\sum_{j=1}^{n} z_j}{n} = \frac{\sum_{j=1}^{n} x_j y_j - b\sum_{j=1}^{n} x_j^{\,2} - c\sum_{j=1}^{n} x_j z_j}{\sum_{j=1}^{n} x_j}$$

which gives :

$$b\left(\frac{\sum_{j=1}^{n} x_j^{\,2}}{\sum_{j=1}^{n} x_j} - \frac{\sum_{j=1}^{n} x_j}{n}\right) + c\left(\frac{\sum_{j=1}^{n} x_j z_j}{\sum_{j=1}^{n} x_j} - \frac{\sum_{j=1}^{n} z_j}{n}\right) = \left(\frac{\sum_{j=1}^{n} x_j y_j}{\sum_{j=1}^{n} x_j} - \frac{\sum_{j=1}^{n} y_j}{n}\right)$$

setting :

$$A1 = \left(\frac{\sum_{j=1}^{n} x_j^{\,2}}{\sum_{j=1}^{n} x_j} - \frac{\sum_{j=1}^{n} x_j}{n}\right)$$

$$A2 = \left(\frac{\sum_{j=1}^{n} x_j z_j}{\sum_{j=1}^{n} x_j} - \frac{\sum_{j=1}^{n} z_j}{n}\right)$$

$$A3 = \left(\frac{\sum_{j=1}^{n} x_j y_j}{\sum_{j=1}^{n} x_j} - \frac{\sum_{j=1}^{n} y_j}{n} \right)$$

gives :

$$bA1 + cA2 = A3 \qquad \{4\}$$

combining {3} and {1} :

$$\frac{\sum_{j=1}^{n} z_j y_j - b\sum_{j=1}^{n} x_j z_j - c\sum_{j=1}^{n} z_j^{\,2}}{\sum_{j=1}^{n} z_j} = \frac{\sum_{j=1}^{n} y_j - b\sum_{j=1}^{n} x_j - c\sum_{j=1}^{n} z_j}{n}$$

$$b\left(\frac{\sum_{j=1}^{n} x_j}{n} - \frac{\sum_{j=1}^{n} x_j z_j}{\sum_{j=1}^{n} z_j} \right) + c\left(\frac{\sum_{j=1}^{n} z_j}{n} - \frac{\sum_{j=1}^{n} z_j^{\,2}}{\sum_{j=1}^{n} z_j} \right) = \left(\frac{\sum_{j=1}^{n} y_j}{n} - \frac{\sum_{j=1}^{n} y_j z_j}{\sum_{j=1}^{n} z_j} \right)$$

and setting :

$$B1 = \left(\frac{\sum_{j=1}^{n} x_j}{n} - \frac{\sum_{j=1}^{n} x_j z_j}{\sum_{j=1}^{n} z_j} \right)$$

$$B2 = \left(\frac{\sum_{j=1}^{n} z_j}{n} - \frac{\sum_{j=1}^{n} z_j^{\,2}}{\sum_{j=1}^{n} z_j} \right)$$

$$B3 = \left(\frac{\sum_{j=1}^{n} y_j}{n} - \frac{\sum_{j=1}^{n} y_j z_j}{\sum_{j=1}^{n} z_j} \right)$$

$$bB1 + cB2 = B3 \qquad \{5\}$$

from {4}

$$b = \frac{A3 - A2c}{A1}$$

and from {5}

$$b = \frac{B3 - B2c}{B1}$$

combining {4} and {5}

$$\frac{A3 - A2c}{A1} = \frac{B3 - B2c}{B1}$$

$$c = \frac{\frac{B3}{B1} - \frac{A3}{A1}}{\frac{B2}{B1} - \frac{A2}{A1}}$$

c is evaluated and is used in {4} to evaluate b then c and b are used in {1a} to evaluate a.